ESTCP

FINAL REPORT

Evaluating and Applying Site-Specific NAPL Dissolution Rates During Remediation

Lloyd “Bo” Stewart
Praxis Environmental Technologies, Inc.

Mark Widdowson
Virginia Tech

Julie Chambon
Rula Deeb
Mike Kavanaugh
Jennifer Nyman
Geosyntec Consultants

January 2023

ESTCP Project ER19-5223

REPORT DOCUMENTATION PAGE

Form Approved
OMB No. 0704-0188

1. REPORT DATE *(DD-MM-YYYY)*	**2. REPORT TYPE**	**3. DATES COVERED** *(From - To)*
31/01/2023	ESTCP Final Report	5/13/2019 - 5/12/2023

4. TITLE AND SUBTITLE

Evaluating and Applying Site-Specific NAPL Dissolution Rates During Remediation

5a. CONTRACT NUMBER
19-C-0026

5b. GRANT NUMBER

5c. PROGRAM ELEMENT NUMBER

6. AUTHOR(S)
Lloyd "Bo" Stewart
Praxis Environmental Technologies, Inc.

Mark Widdowson
Virginia Tech

Julie Chambon, Rula Deeb, Mike Kavanaugh, Jennifer Nyman
Geosyntec Consultants

5d. PROJECT NUMBER
ER19-5223

5e. TASK NUMBER

5f. WORK UNIT NUMBER

7. PERFORMING ORGANIZATION NAME(S) AND ADDRESS(ES)
Praxis Environmental Technologies, Inc.
1440 Rollins Road
Burlingame, CA 94010

8. PERFORMING ORGANIZATION REPORT NUMBER
ER19-5223

9. SPONSORING/MONITORING AGENCY NAME(S) AND ADDRESS(ES)
Environmental Security Technology Certification Program
4800 Mark Center Drive, Suite 16F16
Alexandria, VA 22350-3605

10. SPONSOR/MONITOR'S ACRONYM(S)
ESTCP

11. SPONSOR/MONITOR'S REPORT NUMBER(S)
ER19-5223

12. DISTRIBUTION/AVAILABILITY STATEMENT
DISTRIBUTION STATEMENT A. Approved for public release: distribution unlimited.

13. SUPPLEMENTARY NOTES

14. ABSTRACT
Remediation of nonaqueous phase liquid (NAPL)-impacted sites is difficult and costly. Even with enhancements (e.g., thermal, chemical), mass transfer constraints of NAPL dissolution govern control of sources and the attainment of cleanup goals. To better manage expenditures, the Department of Defense needs a scientifically-based, process-centric method to evaluate source control provided by past NAPL remediation and the potential benefit of future treatment. Current approaches to predict the impact of remediation include (1) screening models, which are simplistic, and (2) numerical transport models, which are complex and costly. The objective of this project was to establish a practical and cost-effective method to assess source control at NAPL sites using site- and technology-specific NAPL dissolution rates in a volume-averaged source zone.

15. SUBJECT TERMS
Non-aqueous phase liquid, NAPL Dissolution Rates, Remediation

16. SECURITY CLASSIFICATION OF:			**17. LIMITATION OF ABSTRACT**	**18. NUMBER OF PAGES**	**19a. NAME OF RESPONSIBLE PERSON**
a. REPORT	**b. ABSTRACT**	**c. THIS PAGE**			Lloyd Stewart
UNCLASS	UNCLASS	UNCLASS	UNCLASS	251	**19b. TELEPHONE NUMBER** *(Include area code)* 650-548-9288

FINAL REPORT
Project: ER19-5223

TABLE OF CONTENTS

Page

TABLE OF CONTENTS (Continued)

Page

TABLE OF CONTENTS (Continued)

Page

LIST OF FIGURES

Page

LIST OF FIGURES

Page

LIST OF FIGURES

Page

LIST OF TABLES

Page

LIST OF TABLES

Page

ACRONYMS AND ABBREVIATIONS

µg/L	micrograms per liter
AFB	Air Force Base
BECOS	BRAC Environmental Construction and Optimization Services
bgs	below ground surface
BRAC	Base Realignment and Closure
CHP	catalyzed hydrogen peroxide
CSM	conceptual site model
cVOC	chlorinated volatile organic compounds
CZ	cobble zone
DCE	cis-1,2-dichloroethene
DNAPL	dense nonaqueous phase liquid
DoD	Department of Defense
DPT	direct-push technology
EPA	US Environmental Protection Agency
ESTCP	Environmental Security Technology Certification Program
FOSM	first-order second-moment
GTP	ganglia-to-pool
ISCO	in situ chemical oxidation
JP-4	Jet Propulsion Fuel No. 4
LPZ	low permeability zone
LRV	light reflection visualization
LSZ	lower saturated zone
m3	cubic meter
MCL	maximum contaminant level
mg/L	milligrams per liter
mL	milliliters
MNA	monitored natural attenuation
MODFLOW	modular finite-difference flow model
NAPL	nonaqueous phase liquid
NAS	natural attenuation software
NOD	natural oxidant demand
NRC	National Resource Council

NSB	Naval Submarine Base
ODE	order differential equation
PCE	tetrachloroethylene
PDF	probability density function
PLM	power law model
PV	pore volumes
RMSE	root mean square error
ROD	Record of Decision
RPMs	remedial project managers
RT3D	Reactive Transport in 3-Dimensions
RUVR	relative parameter uncertainty variance reduction
SCARPÉ	Source Control and Remedial Performance Evaluation
SEAM3D	Sequential Electron Acceptor Model, 3D
SEE	steam enhanced extraction
SERDP	Strategic Environmental Research and Development Program
SSM	Site Selection Memorandum
SVE	soil vapor extraction
TCE	trichloroethylene
TCM	trichloromethane
TEE	thermal enhanced extraction
TOUGH	transport of unsaturated groundwater and heat
USGS	United States Geological Survey
UTCHEM	University of Texas Chemical Transport
UWBZ	upper water bearing zone
VC	vinyl chloride
VOC	volatile organic compound
WAFB	Williams Air Force Base

ACKNOWLEDGMENTS

We wish to thank Michael Singletary for providing access to site data and information as part of the demonstration for Site 11. We wish to thank team members of the Arizona Department of Environmental Quality who oversee the cleanup of Site ST012 for their review and comments on the demonstration results, in particular Wayne Miller, Natalie Romanoff, Daniel Sola and Steve Willis. We wish to thank Michael Brooks of EPA for providing a thorough and encouraging review of an early version of the modeling approach. We wish to thank the US Air Force for providing detailed data regarding past and present characterization and remediation efforts at ST012. In particular, special thanks to the beta model testers for their time providing feedback and suggestions. We also wish to thank ESTCP for their financial support, Dr. Andrea Leeson, the Environmental Restoration Program Manager at ESTCP for her guidance, and Cara Patton of Noblis for keeping the project management running smoothly.

Other individuals who contributed to the demonstration project and the generation of the Final Report include Andres Prieto Estrada who performed the numerical modeling for Site 11 and the uncertainty analyses in Section 8, Mary Scarpetti of Praxis who created and maintained the project website and provided valuable review of reports, and Yiding Zhang of Geosyntec who performed the python programming for the SCARPE calculation tools.

ABSTRACT

INTRODUCTION AND OBJECTIVES

Remediation of nonaqueous phase liquid (NAPL)-impacted sites is difficult and costly. Even with enhancements (e.g., thermal, chemical), mass transfer constraints of NAPL dissolution govern control of sources and the attainment of cleanup goals. To better manage expenditures, the Department of Defense needs a scientifically-based, process-centric method to evaluate source control provided by past NAPL remediation and the potential benefit of future treatment. Current approaches to predict the impact of remediation include (1) screening models, which are simplistic, and (2) numerical transport models, which are complex and costly. The objective of this project was to establish a practical and cost-effective method to assess source control at NAPL sites using site- and technology-specific NAPL dissolution rates in a volume-averaged source zone.

TECHNOLOGY DESCRIPTION

This project implemented a volume-averaged source zone model based on upscaling of complex NAPL dissolution processes to characteristic dimensions of multiple NAPL accumulations. The volume-averaged model allows for incremental complexity, e.g., NAPL source architecture, to be easily incorporated as additional characterization data become available. Remediation of a NAPL-contaminated source zone involves numerous interrelated, complex processes. Mathematical description of these processes was combined into a system of coupled, nonlinear, first order differential equations through volume-averaging. The output is an order-of-magnitude estimate for source zone discharge masses and concentrations over time subject to varied remedial processes, applicable to both design and performance evaluation. This effort resulted in beta versions of practical tools for multi- and single-component NAPL. The calculation tools estimate site-specific remedial impact given a modest amount of site characterization data.

PERFORMANCE AND COST ASSESSMENT

This approach was validated and demonstrated through comparisons with data, including numerical, laboratory and field-scale. The technology was applied to two demonstration sites, with various NAPL architectures exposed to multiple remedial processes. The outputs were compared to observed data and results from calibrated numerical transport models for validation. The technology was also used to evaluate past and future remedial strategies. Qualitative performance objectives for the project were ease of use and utility for supporting remedial decisions. The objectives were met based on feedback from remedial project managers, regulators, consultants and other stakeholders. The utility of the results for remedial decisions was confirmed by remedial project managers. Based on the cost assessment, implementation of the volume-averaged model is a valuable tool to support remedial decision-making for a cost significantly lower than numerical models and comparable to qualitative screening models.

IMPLEMENTATION ISSUES

During beta version testing, users cited the main implementation and utility issue as development of the conceptual source zone model and identification of input parameters. Based on this feedback, additional guidance was developed on estimating input parameters for the modeling.

PUBLICATIONS

Stewart, L.D., J.C. Chambon, M.A. Widdowson, M.C. Kavanaugh. 2022. Upscaled modeling of complex DNAPL dissolution. Journal of Contaminant Hydrology 244, 103920.

EXECUTIVE SUMMARY

INTRODUCTION

Remediation of nonaqueous phase liquid (NAPL)-impacted sites is difficult and costly. Even with enhancements (e.g., thermal, chemical), mass transfer constraints of NAPL dissolution govern control of sources and the attainment of cleanup goals. To better manage expenditures, the Department of Defense (DoD) needs a scientifically-based, process-centric method to evaluate the extent of control provided by past NAPL remediation and the potential benefit of additional treatment. Current approaches to predict the impact of NAPL remediation include (1) screening models, which lack a physical basis and are simplistic, and (2) numerical transport models, which are complex and costly. The objective of this project was to establish a practical and cost-effective method to assess source control at NAPL sites by applying a volume-averaged model with a physical basis using site- and technology-specific NAPL dissolution rates.

OBJECTIVES

Performance objectives for this project included quantitative tasks to validate the source control modeling with experimental and controlled field study data, to evaluate past remedial performance at a Navy base through cleanup, and to provide support for upcoming remedial decisions at a former Air Force base. Qualitative performance objectives were ease of use and utility for supporting remedial decisions. To achieve these objectives, published mass transfer coefficients describing NAPL dissolution specific to remedial technologies and post-remediation source depletion were compiled and incorporated within a volume-averaged model that includes coupled processes. The overall technology is referred to as Source Control and Remedial Performance Evaluation (SCARPÉ). The approach minimizes spatial specificity, limits the required site-specific inputs, and reduces the burden of parameter estimation and calibration. The method is based on mass balance principles with a physical basis and is adaptable to available data and varied processes. This approach was validated experimental data and numerical transport modeling and demonstrated at two sites with various NAPL architectures exposed to multiple remedial processes. The effort resulted in beta versions of two practical tools (SCARPÉm and SCARPÉs for multi- and single-component NAPL, respectively). The calculation tools were provided to remedial project managers, regulators, consultants and other stakeholders for feedback on the ease of use and utility of the output for remedial decisions.

TECHNOLOGY DESCRIPTION

A straightforward, upscaled NAPL mass dissolution model was developed with relatively simple input consisting of characteristic dimensions and saturations of a NAPL accumulation. Multiple accumulations are aggregated into a single source zone volume. An example source zone conceptualization is illustrated in Figure ES-1. Physically, the dissolution process is a combination of flow through the mass (advective component) and flow around the mass (dispersive component). The contribution of each component is based on initial characteristic length scales and saturations. Changes over time with the depletion of mass are captured with a changing relative permeability and a power law relationship for the fraction of initial mass remaining. Including the contributions from local dispersion in the dissolution model is a significant and useful departure from convention. The model output provides a temporal history of the mass discharge rate and the average discharge concentration. The input parameters are minimal and are found in typical NAPL source zone characterization data or can be interpreted indirectly through evaluation of the downgradient plume.

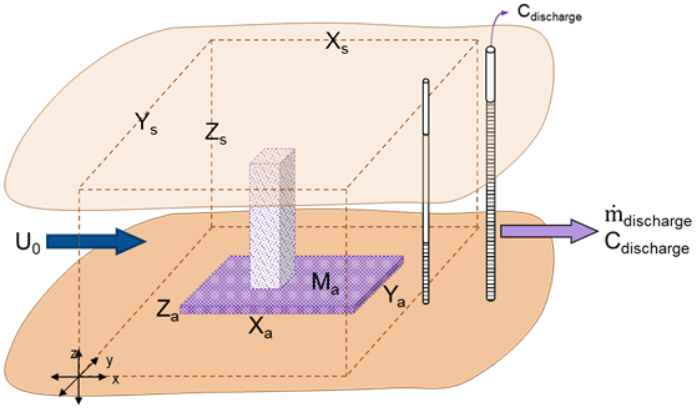

Figure ES.1. Conceptualization of a Model Source Zone and NAPL Architecture

The larger source zone volume, V_s, encompasses multiple ganglia-, pool-, or mixed-type NAPL accumulations encompassing all the NAPL masses. Multiple NAPL accumulations of relatively uniform saturation make up the NAPL architecture, each with characteristic dimensions, which can represent ganglia-, pool- or mixed-type NAPL accumulations. With dimensional variables defined in Fig. (ES.1), the governing equations for NAPL mass, M, with solubility C^* and resulting discharge concentration, C, are,

$$\frac{\mathbf{1}}{\boldsymbol{V_s}}\frac{\boldsymbol{dM_n}}{\boldsymbol{dt}} = -\boldsymbol{K_n}(\boldsymbol{C^*} - \boldsymbol{C}) = -\sum_{\boldsymbol{a=1}}^{\boldsymbol{A}} \boldsymbol{K_a}\left(\boldsymbol{C^*} - \boldsymbol{C_{a,0}}\right) \qquad \textbf{(E-1)}$$

$$R\frac{dC}{dt} = -\frac{U_0}{\phi X_s}\mathrm{C} - \frac{1}{\phi V_s}\frac{dM_n}{dt} - r(t) \qquad \text{(E-2)}$$

The NAPL mass transfer coefficient based on engineering process models (Stewart et al. 2022) is,

$$\boldsymbol{K_{a,0}(m_a)} = \frac{\boldsymbol{U_0}}{\boldsymbol{V_s}}\left[\boldsymbol{A_{a,yz}}\,\boldsymbol{k_r(m_a)} + \boldsymbol{A_{a,xy}}\sqrt{\frac{\boldsymbol{4\alpha_T}}{\boldsymbol{\pi X_{a,0}}}}\right]\left(\frac{\boldsymbol{m_a}}{\boldsymbol{m_{a,0}}}\right)^{\boldsymbol{\gamma}} \qquad \textbf{(E-3)}$$

This expression for $K_{a,0}$ is solely a function of the mass within the dense nonaqueous phase liquid (DNAPL) sub-volume given the upscaled velocity (U_0), characteristic projected area to flow (A_{yz}), a relative permeability function (k_r), tangential area for dispersion (A_{xy}) with dispersivity α_T, and a single exponent γ. The exponent value is expected to a range from 0.5 to 0.67 based on theoretical evaluations of pool and ganglia architecture, respectively. Simple approximate solutions were derived by assuming an average, constant relative permeability which in turn provides reasonable estimates for the time required for NAPL depletion.

Estimates for remediation are captured through a transient reactive term, r, which can be linked to other mass balances for remedy amendments. In addition, theoretical and empirical correlations are available from the literature to estimate remedy-specific dissolution enhancements,

$$K_n = K_{n,0} E_r E_f \,, \quad U = U_0 E_f \,, \quad E_r = f(r) \,, \quad C^* = C_0^* E_s \qquad \text{(E-4)}$$

The factor E_f represents changes in the characteristic velocity through the NAPL soil volume, e.g., pump-and-treat. E_r is a reactive enhancement on mass dissolution resulting from the addition of amendments, e.g., chemical oxidants, and is a function of these reactions. E_s is an estimated multiplier for the effective solubility in presence of a solubilizing agent, e.g., cosolvents. Theoretical and empirical approaches to estimate these enhancements are available in the literature and were demonstrated in this work.

PERFORMANCE ASSESSMENT

The first quantitative performance objective entailed validating and demonstrating the set of governing equations for the dissolution of distributed NAPL masses and the resulting discharge concentration and mass discharge rates from the NAPL-impacted soil volume. This was achieved by matching experimental data. Examples of the results are depicted below for a dissolution experiment with mixed DNAPL architecture and partial destruction of a DNAPL pool in an experiment with ISCO. The matching was successful.

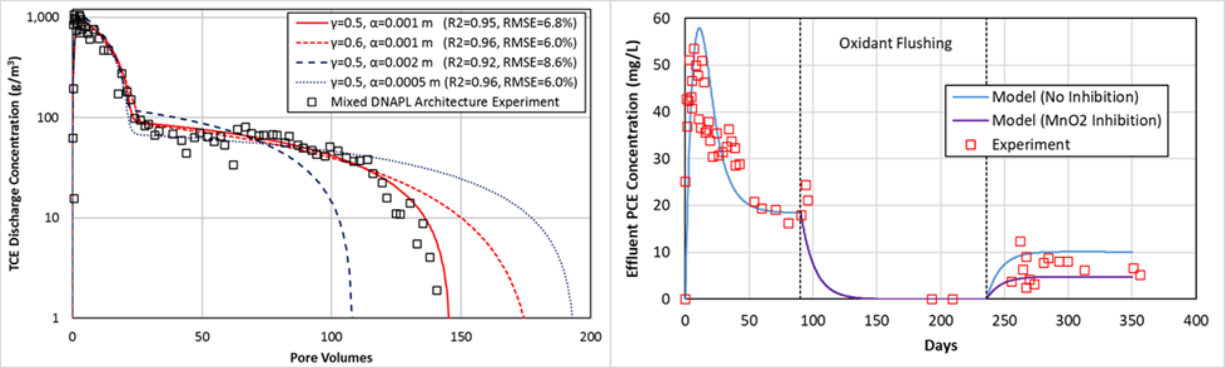

Figure ES.2. Model Applications to Dissolution and Remediation Experiments

In a second quantitative performance objective, the modeling approach was demonstrated at a well-documented DNAPL site in a moderately complex setting. At Site 11 Naval Submarine Base (NSB) Kings Bay, the model successfully provided a robust interpretation for the full life cycle of a DNAPL source zone as depicted in Figure ES.3. The interpretation was based on matching trends observed during and after site activities including natural dissolution, groundwater extraction, mass destruction through ISCO, and a long tailing associated with back diffusion. The evaluation of remedial alternatives confirmed that monitored natural attenuation (MNA) alone was unacceptable, multiple intensive applications of in situ chemical oxidation (ISCO) were highly successful, and pump-and-treat may have provided a cost competitive approach for attaining drinking water standards.

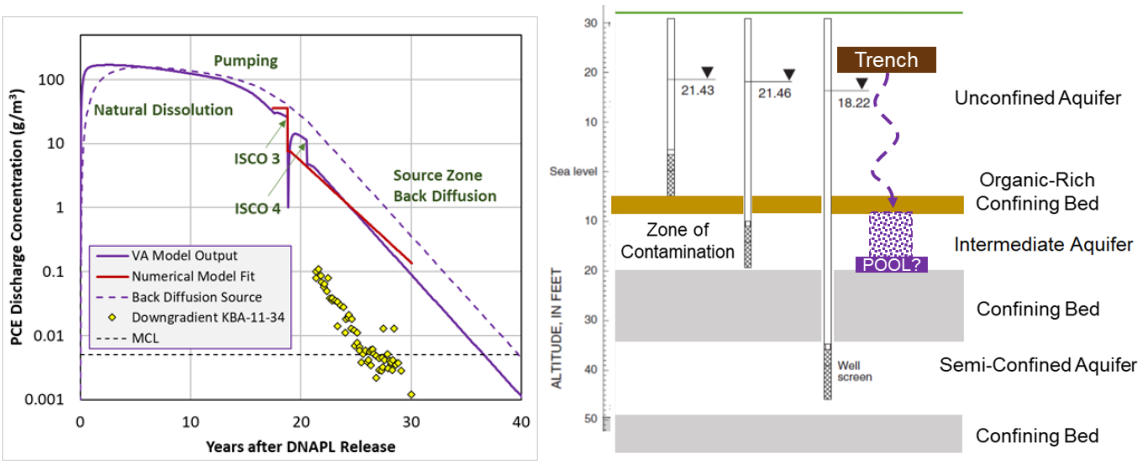

Figure ES.3. Volume-Averaged Model Interpretation of a DNAPL Source Zone Life Cycle

The third quantitative performance objective evaluated the model for supporting remedial decisions at a very complex site, ST012 at the Former Williams Air Force Base, which was contaminated by millions of gallons of kerosene-type jet fuel spread over about 10 acres. This complex site includes multiple, NAPL-impacted water-bearing units and a water table rise of 90 feet over the past 30 years. Remedial history includes limited pump-and-treat, MNA studies, thermal treatment, and on-going enhanced bioremediation.

A recent full-scale application of steam enhanced extraction (SEE) removed roughly 400,000 equivalent gallons of NAPL and fuel components from the site leaving approximately 200,000 gallons of untreated NAPL in surrounding areas. Detailed geologic logs with field NAPL test kits were collected from over 40 soil borings and present a NAPL architecture of discrete pools vertically dispersed under fine-grained material. The ST012 evaluation of remedial alternatives considered MNA, enhanced bioremediation, pump-and-treat, and ISCO with technology-specific dissolution enhancements. Example output for one target treatment zone alongside the geologic and NAPL detection data used for characterization are illustrated in Figure ES.4.

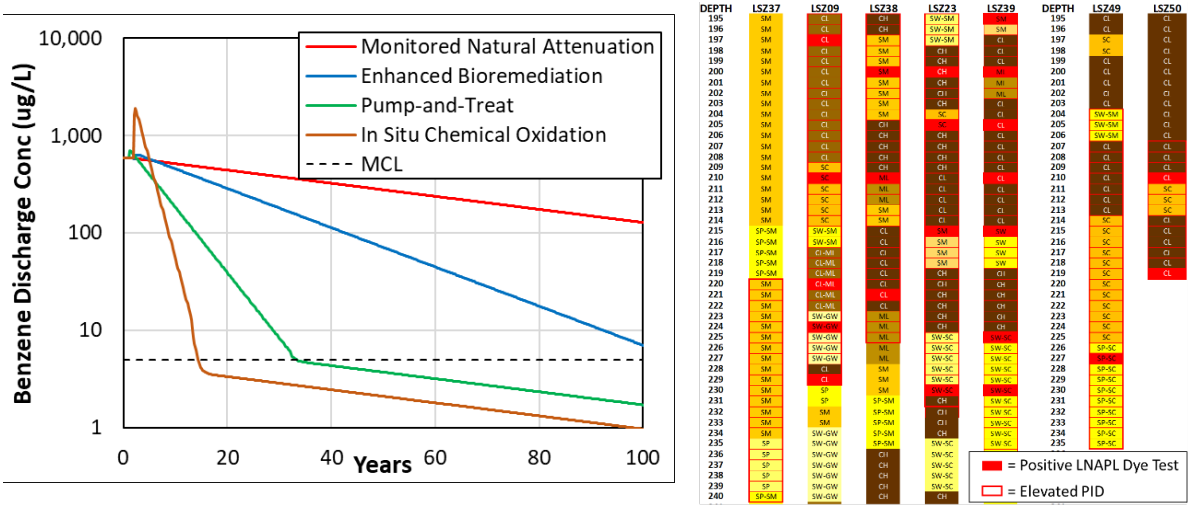

Figure ES.4. Model Comparison of Remedial Alternatives at a Complex Site

Qualitative performance objectives for the project were ease of use and utility for supporting remedial decisions. The objectives were met based on feedback obtained through direct contact with remedial project managers, regulators, consultants and other stakeholders. Users were provided with beta version tools and all were able to run these simple tools for template scenarios and assess the outputs without extensive training. The utility of the model results for remedial decisions was confirmed by remedial project managers; however, users cited the main implementation and utility issue as development of the conceptual source model and identification of input parameters (i.e., how to get the information).

IMPLEMENTATION ISSUES

Based on user feedback, additional guidance was provided on estimating input parameters for the modeling. Site investigations and associated investigation reports at NAPL sites would typically include data needed to develop the conceptual source zone model as illustrated in Figure ES-5. Therefore, access to historical investigation and remediation information and involvement of practitioners familiar with the site and its history would facilitate application of the technology. The demonstrations included extensive descriptions of methodologies for interpreting downgradient plume histories and high-resolution measurements to characterize the source zone. Sites with existing transport models can leverage the transport model for data interpretation.

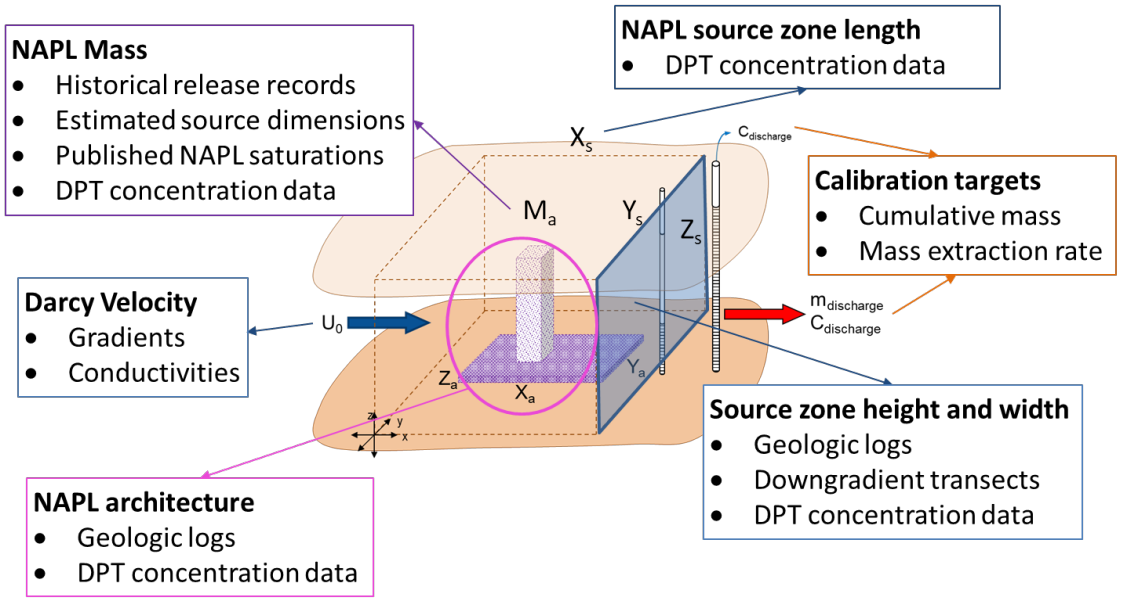

Figure ES.5. Example Sources of Data and Interpretation for Estimating Input Parameters

More complex implementations of the modeling approach can readily be implemented and solved using available coding platforms such as Matlab or FORTAN, however, it does require coding and specialty users. As part of this work, two practical ready-to-use tools, which do not require any specific training, or software and can be run on a personal laptop. When limited information is available to develop a conceptual source model, sensitivity and uncertainty analysis methods can be readily coupled with the model framework to identify controlling parameters and prioritize data collection to refine the conceptual source model.

COST ASSESSMENT

Implementation of the SCARPÉ tools relies on three cost elements; (1) data compilation and assimilation, (2) volume-averaged modeling (using a computer), and (3) analysis and reporting of results. The SCARPÉ mathematical framework and the two practical tools are provided free of charge. In addition, the data necessary to develop the conceptual source zone model and determine the input parameters are expected to be available at sites undergoing investigations and remediation. Therefore, the main cost driver for implementation of the NAPL dissolution tool is the labor cost (i.e., time). The cost to implement two SCARPÉ tools is estimated to be on the order of $23,000. This cost is a fraction of the cost to develop and use complex numerical models for NAPL dissolution, and is consistent with the costs for application of screening-level models. However, in contrast to screening-level models, the volume-averaged approach is physically-based, and provides better prediction and scientifically defensible comparisons between remedial alternatives. Application of the volume-averaged approach is also expected to provide cost-savings at DoD sites, by supporting the selection of the most efficacious remedy to achieve cleanup goals.

1.0 INTRODUCTION

1.1 BACKGROUND

Remediation of non-aqueous phase liquid (NAPL)-impacted sites is difficult and costly. Hundreds of complex sites contaminated by residual NAPL where the time to reach response complete extends to decades (National Research Council [NRC], 2013). Given the complexities of the processes associated with NAPL dissolution and remediation, practical methodologies are needed to support strategic evaluation, planning, and implementation of cost-effective remedial approaches. The mass transfer constraints of NAPL dissolution govern the rate of source depletion and the attainment of cleanup goals. Even with aggressive treatment, a fraction of the NAPL is left as a residual, long-term source of contamination (e.g., Liu et al., 2014, NRC, 2004). To better manage expenditures expecting over the next few decades of up to $30 billion (Defense Environmental Restoration Program, Fiscal Year 202 Status Tables, https://denix.osd.mil/derp/fy2020-status-tables/), the Department of Defense (DoD) needs a scientifically-based, process-centric method to evaluate: (a) the extent of control provided by past NAPL source zone remediation, (b) optimization and/or diminishing returns of ongoing remediation, (c) the potential benefit of additional treatment, (d) remedial technology selection for additional treatment, and (e) preliminary remedial design. The objective of this project is to establish a practical and cost-effective method to assess source control at NAPL sites by applying a volume-averaged model with site- and technology-specific NAPL dissolution rates coupled with technology-specific reaction models.

A common management scenario at NAPL sites is an acceptable risk to human health confirmed by data-based assessments of plume stability and vapor intrusion potential; however, regulatory-driven concerns regarding source control and lifespan remain impediments to divestment. DoD site managers and contractors are thus challenged to provide a technically-defensible assessment of source control at virtually every NAPL site, resulting in uncertain impacts on near- and long-term expenditures at DoD facilities. Current approaches to assess the impact of NAPL remediation include (1) screening models, which lack a clear physical basis and are overly simplistic, (2) numerical transport models, which are immensely complex and costly to implement, and (3) subjective experience of interested parties. Unfortunately, these approaches have significant limitations. The purpose of this project is to resolve these limitations through validation of a novel and practical approach to assess proposed or ongoing source control measures and to make this methodology accessible to DoD site managers and contractors through effective technology transition.

There is an abundance of research results on mass transfer from NAPL available from Strategic Environmental Research and Development Program (SERDP) and Environmental Security Technology Certification Program (ESTCP) projects and in other published literature. Numerous SERDP and ESTCP projects have studied NAPL dissolution and provide data from columns, test cells, and large tanks in heterogeneous systems with complex NAPL architecture. Research includes studies of natural dissolution before and after remediation (Wood et al., 2009 [ER-1295]; Brusseau, 2013 [ER-1614]; Annable et al., 2017 [(ER-1613]). Foundational research was performed in SERDP ER-1294 (Illangasekare et al., 2006) including studies of bio-treatment, surfactant-enhanced dissolution, in situ chemical oxidation (ISCO), and thermal treatment. The research generated upscaled mass transfer coefficients for various remedial processes and numerous insightful conclusions for specific processes. Additional upscalable data are available from SERDP ER-1293 (Abriola et al., 2008) applicable to surfactant flushing and reductive dechlorination.

More recently, SERDP Projects ER-1611 (Parker et al., 2011) and ER-2310 (Parker et al., 2017) studied NAPL dissolution in combination with cost data and tractable remediation models for biological degradation and ISCO. The dense non-aqueous phase liquid (DNAPL) Technology Evaluation Screening Tool (DNAPL TEST) was developed in ER-200424 (Lebrón et al., 2012) using data from published literature and modeling simulations for technology selection. Yet, the utility of these research results for quantitative remedial design and performance evaluation at NAPL sites lacks adaptability to specific site conditions and technologies. Such design and evaluation tasks are limited primarily to large, complex numerical simulators that are rarely employed in field practice. In addition, documented studies linking NAPL mass transfer with specific remedial processes are sparse outside of laboratory experiments.

This project bridges the gap between research findings on NAPL dissolution and remedial processes and their availability and accessibility to practitioners and DoD remedial project managers (RPMs) making remedial decisions. The proposed technology provides a balance between complex numerical simulators, overly simple and optimistic screening models, and sparse site-specific datasets by applying physically-based mass transfer coefficients to remedial processes as suggested by Illangasekare et al. (2006) and Parker and Park (2004). The volume-averaged approach (1) is grounded in science that incorporates mass balances on remedy components and core mass transfer processes that screening models fail to capture, (2) avoids the numerical tedium of simulators and intensive input parameter requirements, and (3) bypasses the requirement of a calibrated numerical groundwater flow model. The approach, though, is highly complementary to numerical fate and transport models. Output from the volume-averaged source zone provides a site- and technology- specific generation output for direct use in evaluating plume response to source remediation.

1.2 OBJECTIVE OF THE DEMONSTRATION

The overall objective of this project is to demonstrate a practical, cost-effective methodology for assessing cleanup and control of NAPL-impacted sites at a level of detail accessible to field practitioners and useful in supporting remedial decisions. Specific technical objectives include:

1. Compile and characterize previous research results for NAPL mass transfer coefficients specific to remedial technologies and specific to NAPL architectures in a consistent format.
2. Incorporate various mass transfer processes, remedial technologies, and multiple NAPL components into a standardized mathematical framework comprised of a volume-averaged model with upscaling, and set up the framework into Excel-based practical tools.
3. Validate the approach in three steps by calibration and comparison with:
    a. data from laboratory tests, controlled field experiments, and numerical modeling of synthetically generated sites with various NAPL architectures and implementation of various remedial processes.
    b. data from one or more moderately complex sites with well documented remediation efforts and numerical modeling results.
    c. data from a complex site undergoing remediation with pending remedial decisions.

4. Obtain peer review of beta versions of practical tools throughout the demonstration; incorporate comments from RPMs, regulators, and practitioners; and modify for maximum accessibility and future use by DoD entities.
5. Engage practitioners, DoD RPMs, and other stakeholders through technology transition efforts and disseminate the results throughout the remediation community.

The goal is to provide more realistic evaluations and predictions of NAPL sites to improve managerial decisions and planning.

1.3 REGULATORY DRIVERS

Aqueous solubilities of common chemicals of concern such as chlorinated solvents and petroleum hydrocarbons found at DoD facilities greatly exceed drinking water standards including Federal maximum contaminant limits (MCLs). Table 1.3.1 lists Federal MCLs for selected chlorinated ethenes derived from the discharge of solvents, often in the form of DNAPLs, and aromatic hydrocarbons, usually dissolved from fuel-based NAPLs trapped in the subsurface. Mass dissolution of components from NAPL can result in concentrations at locations near the source zone persistently above the MCLs for hundreds of years if left untreated.

Table 1.3.1. Federal Maximum Contaminant Levels (MCLs) for Selected NAPL Constituents

Contaminant	Federal MCL (µg/L)
Chlorinated Ethenes	
Trichloroethylene (TCE)	5
Tetrachloroethylene (PCE)	5
cis-1,2-Dichloroethylene (DCE)	70
Aromatic Hydrocarbons	
Benzene	5

Source: http://www.epa.gov/safewater/contaminants/index.html#organic
µg/L = micrograms per liter

In addition to attaining MCLs, DoD is faced with a multitude of ongoing remedial decisions regarding technology selection and the definition of cleanup (e.g., location and scale of attaining MCLs). During the life of a Superfund site, remedial decisions appear in Feasibility Studies, Records of Decision (RODs), Remedial Actions, Focused Feasibility Studies, Explanations of Significant Difference, and Technical Impracticability Assessments. The bases for these decisions often rely on empirical observations of technology performance that may not be applicable to NAPL sites that have been subjected to source control, e.g., downgradient containment pumping, and have failed to meet restoration criteria for groundwater. A need exists for a methodology that provides a site-specific assessment of technologies and anticipated outcomes that can be replicated by regulatory authorities to hasten agreement on final site cleanup definitions and acceptable timeframes for achieving remedy complete.

As a specific example, the US Air Force awarded contracts in 2020 for continued, optimized cleanups in a program known as Base Realignment and Closure (BRAC) Environmental Construction and Optimization Services (BECOS). The execution of these contracts is performance based on the maximum extent practicable. Selected contractors are responsible for designing/implementing remedies and operating systems in accordance with regulatory standards. There are significant benefits of a site-specific methodology for the US Air Force to: (1) evaluate previous efforts, (2) determine realistic, attainable site objectives for differing technologies, and (3) then assess site cleanup progress in a format that can be communicated to the regulatory community.

2.0 TECHNOLOGY

2.1 TECHNOLOGY DESCRIPTION

The technology described herein and developed as part of this work is the combination of an approach, a model, tools and a methodology, as follows:

- Approach: NAPL dissolution processes are represented based on a volume-averaged approach, resulting in mathematical equations;
- Model: the approach results in the development of a model that is solved to generate outputs;
- Tools: excel-based implementation of the model that can be used directly to apply the SCARPÉ model to a site; and
- Methodology: the results of the model are evaluated to support decision at various periods during the life cycle of a site.

The technology is referred to as Source Control and Remedial Performance Evaluation (SCARPÉ). The technology addresses a need for realistic mass discharge predictions from dissipating NAPL sources without requiring small-scale specification of source zone architecture and dissolution processes and is based on the work published in Stewart et al. (2022). An existing screening level model implements a power law relationship between the total NAPL mass and the average discharge concentration emanating across a given cross-sectional area (Rao et al. 2001, Falta et al. 2005). This power law relationship has a simplistic connection to NAPL architecture and does not capture multi-rate and multi-component mass transfer. Numerical modeling of NAPL dissolution and remediation requires a high level of expertise, generally beyond the capability of all but university researchers. This work presents the development of a volume-averaged source zone model based on upscaling of complex NAPL dissolution processes to characteristic dimensions of multiple NAPL accumulations. This upscaled approach is similar to the characterization approach presented in Luciano et al. (2012) and the process-based model presented in Kokkinaki et al. (2014); however, contributing processes are considered more explicitly in this work. The volume-averaged model allows for incremental complexity, e.g., NAPL source architecture, to be easily incorporated as additional characterization data become available. The model is validated using data from numerical modeling and well-characterized laboratory experiments and applied to a controlled field study illustrating the range and suitability of applications in Section 5.

The approach is further developed to represent more complex conditions in the source zone occurring during active remediation. In addition to supporting risk assessment and decision-making, the source zone model can provide direct inputs for numerical transport models or aid in interpreting measured source discharge histories. Used inversely, the model can estimate NAPL source characteristics at sites with detailed contaminant mass discharge data, e.g., pump-and-treat mass recovery; this information can be used to guide additional investigations and/or support remedial design. Remediation of a NAPL-contaminated source zone involves numerous interrelated, complex processes. Mathematical description of these processes was combined into a system of coupled, nonlinear, first order differential equations as described in the following sections through volume-averaging. The approach assumes flow through the averaged volume is relatively rapid compared to the processes governing the overall system, e.g., NAPL dissolution.

In most instances, the approach treats the source zone as a single or several, large independent modeling blocks to circumvent the complexities of a numerical groundwater flow model while maintaining the complexities of other processes taking place. The approach captures heterogeneities in flow through the use of engineering mass transfer concepts. The framework represents a middle ground between numerical models attempting to include mass transfer complexities in a very fine grid and the ease of implementation of qualitative screening models that lack a physical basis.

The output from the model is an order-of-magnitude estimate for source zone discharge masses and flow averaged discharge concentrations over time subject to varied remedial processes, applicable to both design and performance evaluation. Output options enable managers and practitioners to compare several proposed source control measures based on identical conceptual source models in support of decision-making. These order-of-magnitude estimates for discharge concentration are similar to the approaches for monitored natural attenuation in NAPL source zones described by Johnson et al. (2006) and Chapelle et al. (2003). This work extends those approaches to include other, more complex and targeted remedial processes.

The upscaled NAPL dissolution model outlined in this work provides a straightforward system of nonlinear, first-order differential equations. The simple model inputs are related to physical parameters found in typical NAPL source zone characterization data. Input and model solution are readily implementable in a spreadsheet. NAPL source zones often present complex architectures that are difficult to investigate and characterize in detail in the field. The volume-averaged model can be used without detailed information on the exact location and small-scale specification of source zone architecture of NAPL accumulations.

A comparison of the volume-averaged model, also known as the Source Control and Remedial Performance Evaluation (SCARPÉ) Tool, with other existing models with similar purposes is provided in Table 2.1.1. As illustrated in Table 2.1.1, SCARPÉ is the only tool that include NAPL dissolution without relying on expensive numerical simulations or oversimplification using the empirical power-law relationship. SCARPÉ does not include fractured media, but the mathematical framework could be expanded in the future to include this process (Section 8). Similarly, while SCARPÉ does not provide information at the plume scale (i.e., downgradient of the NAPL source zone), its outputs can be use as inputs for numerical models or semi-analytical solutions (e.g., Perina, 2022) to evaluate impact of NAPL source zone remediation on downgradient plumes.

Table 2.1.1. Overview of Capabilities of SCARPÉ and Other Models

	Processes						Scale		Inputs/Outputs				
	NAPL Dissolution	Remedial Alternatives	Fractured Media	Natural Attenuation	Mass Discharge	Matrix Diffusion	Source Scale	Plume Scale	Data Inputs	Data Outputs	Pros	Cons	References
SCARPÉ	Yes	Yes	No	Yes	Yes	Yes	Yes	No	- Source geometry - NAPL architecture (ganglia/pool), NAPL composition - Hydraulic conductivity, hydraulic gradient - Remediation information - NAPL mass transfer parameters	- Mass discharge over time - Mass in source zone over time - Concentration at downgradient location over time	- Excel-based - Represent both source and plume processes - Include NAPL dissolution - Can be calibrated with available monitoring data - Can be refined with additional data - Complexity can be increased with additional information - Represents a wide range of remedial alternatives - Can be used to compare remedial alternatives	- Requires estimate of NAPL architecture/volume/mass	Stewart et al., 2022 This report
3-D Numerical Solute Transport Models (MODFLOW/MT3D, MT3DMS, SEAM3D, MODFLOW-MD)	Yes	Yes	No	Yes	Yes	Yes (MODFLOW-MD, or very high-resolution grids)	Yes	Yes	- Hydrostratigraphy - Hydraulic properties - Boundary conditions - Initial concentrations - Transport properties	- Concentration over time at any location in the domain - Mass discharge at select transect - Time to reach target contaminant mass, mass discharge or concentration	- Can take advantage of already existing 3-D models for the site - Can account for complex geology heterogeneity - Can account for complex processes, such as matrix diffusion, NAPL dissolution, complex degradation pathways	- Requires large amount of data - Can require significant effort (time and money) - Requires technical capabilities, specialized software	USGS, 2022 Waddill and Widdowson, 2000 ER19-5028
Natural Attenuation Software (NAS)	Yes	Effect of pumping Source mass removal	No	Yes	No	No	Yes	Yes	- Hydraulic conductivity/gradient - Total/effective porosity - Sorption parameters - Source concentration, source width/length - Redox indicators - NAPL properties	- Distance of plume stabilization - Time of stabilization - Time of NAPL dissolution	- Accounts for both source and plume zones - Available advanced features such as redox zonation and alternate degradation pathways - Can account for the effect of pumping - Can simulate NAPL dissolution in source area	- Numerical simulations required for NAPL dissolution - Significant run times might be required for numerical simulations	https://www.nas.cee.vt.edu/index.php
Matrix Diffusion ToolKit	No	Source mass removal	No	Yes	Yes	Yes	Yes	Yes	- Loading period, source concentration, time source removal - Diffusion coefficient, tortuosity factor, porosity and sorption parameters in the low-permeability zone - Darcy velocity, hydraulic conductivity and gradient and degradation rate in the transmissive zone	- Mass discharge over time - Concentration in transmissive zone over time - Mass in transmissive zone over time - Aqueous, sorbed and total concentrations in low-permeability zone over time (Dandy-Sale Model only)	- Excel-based - Takes into account matrix diffusion - Provides mass estimates in both transmissive and low-permeability zones - Includes degradation in the transmissive zone - Includes evaluation of uncertainty, with possibility to run Monte-Carlo analysis - Can be calibrated with available monitoring data - Includes consideration of NAPL removal in the source zone	- Estimates relies significantly on the loading period and concentration during loading periods, which are difficult to estimate - Does not include degradation in the low-permeability zone, which can be an importance attenuation process - Cannot be used to estimate remedial timeframe for partial source mass removal	https://www.serdp-estcp.org/Tools-and-Training/Environmental-Restoration/Groundwater-Plume-Treatment/Matrix-Diffusion-Tool-Kit
RemChlor-MD	No	Source mass removal	Yes	Yes	Yes	Yes	No	Yes	- Hydraulic conductivity, gradient - Tortuosity, effective/total porosity - Geological setup (aquitard/aquifer layering, distance between parallel fractures, low-permeability material within aquifers) - Dispersivity parameters - Sorption parameters - Source geometry, concentration, decay rate - Source removal fraction and time - Plume biotransformation rates	- Concentration over time in plume - Mass discharge over time in plume - Mass in high and low permeability zones over time	- Excel-based - Includes decaying source - Include partial/complete source removal - Includes biotransformation (including sequential decay for chlorinated solvents) - Possible to define three reaction zones and three reaction periods for the plume - Account for matrix diffusion - Can be calibrated with available monitoring data	- Assumes uniform, one directional flow field - Cannot directly account for pumping - Relies on empirical exponent for power-function relationship - Cannot account processes in source (NAPL dissolution, remedial actions)	https://serdp-estcp.org/Program-Areas/Environmental-Restoration/Contaminated-Groundwater/Persistent-Contamination/ER-201426

2.2 TECHNOLOGY DEVELOPMENT

This section describes the development of the volume-averaged approach for modeling dissolution and remediation in NAPL source zones. The material is a summary of the derivations of dissolution modeling found in Stewart et al. (2022) and the development of equations to model specific remedial technologies provided in Appendix B.

2.2.1 Volume-Averaged Model of NAPL Source Zone Remediation

Consider the three-dimensional, transient transport of a contaminant dissolving from an immobile, single component NAPL dispersed in an aquifer subject to instantaneous sorption and rate-limited reactions, *r*; in the dissolved phase. The governing equations including generic aqueous phase reactions and rate limited dissolution are (Yang et al., 2018),

$$\boldsymbol{\phi}\frac{\boldsymbol{\partial}}{\boldsymbol{\partial t}}\left[\left(\boldsymbol{S_w}+\frac{\boldsymbol{\rho_b K_d}}{\boldsymbol{\phi}}\right)\boldsymbol{C'}\right]=\frac{\boldsymbol{\partial}}{\boldsymbol{\partial x_j}}\left[\boldsymbol{\phi S_w D_{jk}}\frac{\boldsymbol{\partial C'}}{\boldsymbol{\partial x_k}}\right]-\frac{\boldsymbol{\partial}}{\boldsymbol{\partial x_j}}\left[\boldsymbol{\phi S_w u_j C'}\right]-\boldsymbol{\phi\rho_n}\frac{\boldsymbol{\partial S_n}}{\boldsymbol{\partial t}}-\boldsymbol{\phi S_w r} \qquad \textbf{(2-1a)}$$

$$\boldsymbol{\phi\rho_n}\frac{\boldsymbol{\partial S_n}}{\boldsymbol{\partial t}}=-\boldsymbol{K_n'}(\boldsymbol{C^*}-\boldsymbol{C'}) \qquad \textbf{(2-1b)}$$

These equations represent the dissolution of NAPL (S_n = NAPL saturation, ρ_n = NAPL density) into adjacent groundwater (C' = dissolved concentration in water, S_w = aqueous phase saturation), partitioning between the soil solids and groundwater, and movement with groundwater through the aquifer by advection (u = groundwater pore velocity) and dispersion (D = dispersivity tensor). Aquifer properties include porosity (ϕ), bulk density (ρ_b) and contaminant distribution coefficient (K_d). The dissolution of mass from the NAPL phase is represented as a first order process governed by a bulk rate constant (K_n) scaled to the problem of interest. The NAPL mass transfer is linearly proportional to the compound aqueous solubility, C^*, and a representative dissolved concentration. Solutions to this problem for natural dissolution in a field setting generally utilize very complex numerical models. The inclusion of aquifer heterogeneity and complex remedial reactions within the aqueous phase make the problem effectively intractable for available numerical models, or prohibitively time consuming to execute for engineering purposes (Falta, 2003).

To circumvent the use of complex numerical solutions predicated on a complex groundwater flow model, integration over a contaminated soil volume (V_s) with dimensions *LxHxW* leads to a spatially-averaged dissolved phase concentration (Marble et al., 2008; Johnson et al., 2006), with sources integrated into the domain without exact specification of location within the volume. Consider,

$$\overline{\boldsymbol{C}}=\frac{\boldsymbol{1}}{\boldsymbol{HWL}}\iiint \boldsymbol{C'(x',y',z')dx'dy'dz'}=\frac{\boldsymbol{1}}{\boldsymbol{V_s}}\iiint \boldsymbol{C'(x',y',z')dx'dy'dz'} \qquad \textbf{(2-2)}$$

Carrying out the integration on the transport equations (2-1) eliminates the dispersion term under the assumption of zero concentration gradients on the boundaries and reduces the convective term to a function of the direction-independent volumetric flow, Q, (natural or induced) through the source zone projected area ($Q = u\,\phi\ H\ W = U_0\ H\ W$). The volumetric flow Q is based on the average unidirectional Darcy velocity, U_0, through the source zone.

Inherent in this integration is the assumption of a relatively well-mixed aqueous concentration. However, this restriction can be relaxed as discussed below. Including the NAPL mass balance yields a set of two first order equations with a bulk mass transfer coefficient upscaled to the source geometry,

$$\left(1-\bar{S}_n+\frac{\rho_b K_d}{\phi}\right)\frac{d\bar{C}}{dt}=-\left[(1-\bar{S}_n)\frac{Q}{V_s}\right]\bar{C}-\rho_n\frac{d\bar{S}_n}{dt}-(1-\bar{S}_n)\bar{r} \qquad \textbf{(2-3a)}$$

$$\phi\rho_n\frac{\partial\bar{S}_n}{\partial t}=-K_n(C^*-\bar{C}) \qquad \textbf{(2-3b)}$$

This pair of equations represents the essence of the modeling approach and provides a platform for including more complex phenomena, resulting in additional first order equations in the system related to the mass transfer coefficient, NAPL mass, and the aqueous phase reactions. These relationships are discussed in the following subsections.

2.2.2 Conceptual Model of Complex NAPL Architecture

In a field setting, the NAPL architecture and dissolution are much more complex than can be satisfactorily captured by a single lumped mass transfer coefficient and an average NAPL saturation (Saba and Illangasekare, 2000; Saenton and Illangasekare, 2007). An appropriate strategy is to address heterogeneity of NAPL architecture and dissolution using multiple, coincident NAPL sources rather than a ganglia-to-pool ratio. In addition, most sites lack the data to specify a detailed configuration of NAPL sufficient to justify numerical modeling. Yet, much effort has gone into attempts to upscale column and test bed data on dissolution. Spatial averaging provides an approach that can utilize such data in a practical format by defining sources zones based on characteristic dimensions of NAPL accumulations of relatively uniform saturation. Figure 2.2.1 provides an example conceptualization including columns of disconnected ganglia and lateral pools.

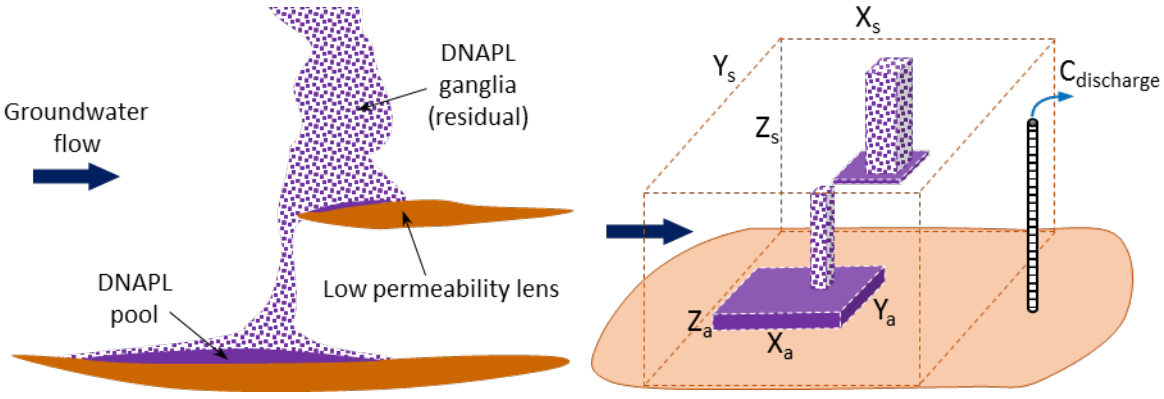

a. Field Concept b. Model Concept

Figure 2.2.1. Conceptualization of Field Conditions for Upscaled DNAPL Dissolution Modeling

In dividing a NAPL source zone into separate masses numbering A (e.g., A=4 in Figure 2.2.1b), the total NAPL mass m_n in the source zone volume is,

$$\boldsymbol{m_n = \sum_{a=1}^{A} m_a} \tag{2-4}$$

Each distinct DNAPL zone has an individual mass m_a (M) and an average DNAPL saturation S_a (dimensionless) within a characteristic soil volume $V_a = X_a * Y_a * Z_a$ (L^3),

$$\boldsymbol{S_a = \frac{m_a}{V_a \phi \rho_n}}$$

The larger source zone volume containing all the masses is then considered with dimensions characteristic of discharge measurements. Multiple NAPL accumulations of relatively uniform saturation make up the NAPL architecture. Equations (2-3) are now re-written with slightly different parameters and for multiple NAPL accumulations,

$$\boldsymbol{R \frac{d\bar{C}}{dt} = -\frac{Q}{\phi V_s}\bar{C} - \frac{1}{\phi V_s}\frac{dm_n}{dt} - (1 - \bar{S}_n)\,\bar{r}} \tag{2-5a}$$

$$\boldsymbol{\frac{1}{V_s}\frac{dm_n}{dt} = -K_n(C^* - \bar{C}) = -\sum_{a=1}^{A} K_a\left(C^* - C_{a,0}\right)} \tag{2-5b}$$

The retardation coefficient R is defined for linear, instantaneous sorption and assumes the presence of NAPL in the source zone reduces the available sorption sites:

$$\boldsymbol{R = 1 - S_n + \frac{\rho_b K_d}{\phi}} \tag{2-6}$$

The volume-averaged, bulk mass transfer coefficient K_n is referenced to V_s and represents the aggregate mass dissolution from multiple NAPL accumulations of differing architectural type (e.g., ganglia and pool). In this formulation, each individual bulk mass transfer coefficient K_a is also referenced to the larger source zone volume rather than the sub-volume defining the average saturation for the mass. This formulation is in contrast to convention wherein the bulk mass transfer coefficient is referenced to the NAPL sub-volume. The volume-averaged integration also yields a well-mixed aqueous concentration in the source zone for the concentration gradient driving dissolution. However, traditional engineering correlations for mass transfer use an entry concentration $C_{a,0}$ flowing into the NAPL sub-volume V_a to define the gradient as indicated in Eq. (2-5b). If no upgradient source exists, this concentration is zero. In such cases, each NAPL accumulation can be modeled independently. If not zero, auxiliary relationships are required to model the interaction of separate NAPL accumulations based on the flow field.

The difference in reference volumes illustrates the complexities of upscaling mass transfer relationships for numerical simulation where both the average NAPL saturation and average aqueous concentration may be arbitrarily based upon the scale of discretization. The assumption of a well-mixed aqueous concentration within a field-scale reference volume introduces more or less dilution with the scale. Figure 2.2.1 depicts a scale representative of field conditions, but finer discretization to smaller scales and smaller representative volumes may not alleviate these scale dependencies. Finer discretization is also accompanied by increased computational effort and an increased uncertainty or an increased burden on site characterization. The assumption of a well-mixed source zone volume implies the characteristic source dimensions should be commensurate with the dimensions of field measurements (e.g., well screen intervals) as illustrated in Figure 2.2.1.

2.2.3 Practical Models for DNAPL Mass Transfer Coefficients

Following previous conceptualizations, characterized accumulations in a source zone can be designated as ganglia-dominated (low saturation, $Z_g > X_g$) or pool-dominated (high saturation, $Z_p << X_p$) as illustrated in Figures 2.2.2a and 2.2.2b, respectively. Ganglia zones are characterized by dissolution dominated by flow through the volume. Pool zones are characterized by dispersion from outer boundaries and limited flow through the volume. During the life of an accumulation, both characteristics may be exhibited. Practical, a priori mass transfer models for ganglia, pool and mixed configurations are developed in this section based on previous analytical models.

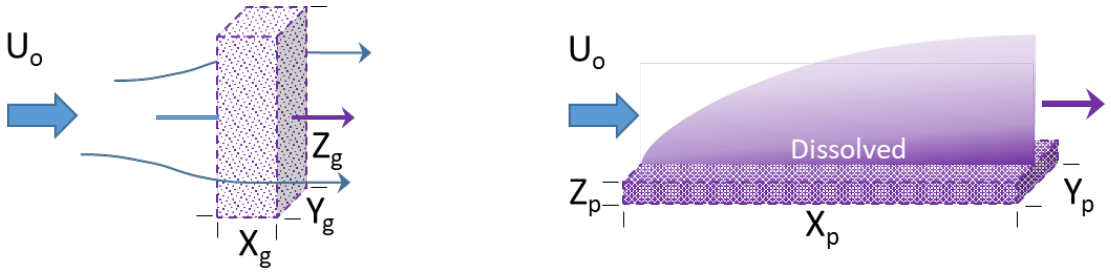

a. Ganglia Configuration b. Pool Configuration

Figure 2.2.2. DNAPL Architectural Concepts

2.2.3.1 Ganglia Zone

In a homogeneous porous medium, mass transfer from a ganglion zone is expected to be proportional to (1) the velocity of flow through a zone of uniformly distributed, residual DNAPL and (2) the interfacial area between the DNAPL and aqueous phase per unit volume (Powers et al. 1991, Luciano et al. 2012, Kokkinaki et al. 2014). Both of these parameters are functions of the DNAPL saturation and 1D column studies generally lump the saturation dependence into a single fit parameter. Effluent emerges from this zone at near equilibrium levels (Miller et al., 1990) until a narrow zone of eroding ganglia reaches the trailing edge and completes the dissolution of the DNAPL (Geller and Hunt 1993).

In a field setting, inherent heterogeneity of soils results in ganglia that are not uniformly distributed and a reduced relative permeability decreases the flow through the zone (Geller and Hunt 1993). 1D columns force all flow through the DNAPL zone and do not assess the changing flow velocity experienced in a multi-dimensional system (Saba and Illangasekare 2000). The nonuniform distribution also yields a nonuniform flow through the zone. These phenomena were illustrated in experiments of Powers et al. (1998) and DiFilippo et al. (2010). Flow bypass decreases over time as saturation decreases and the relative permeability increases as illustrated in Figure 2.2.3.

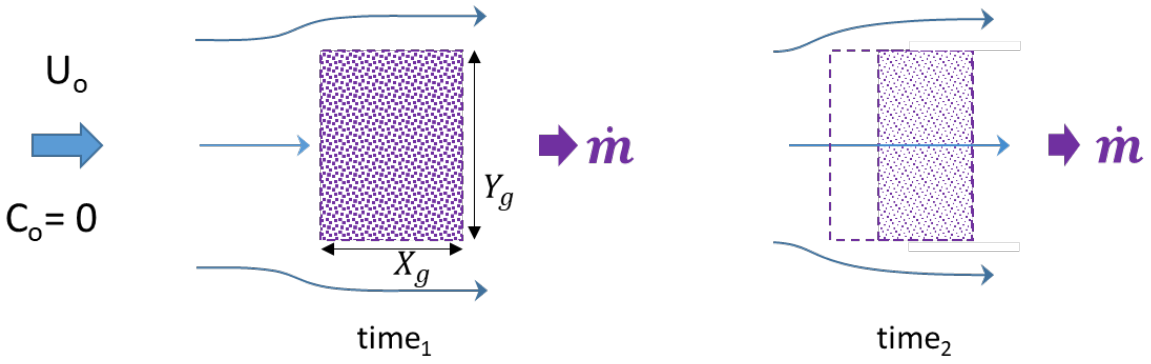

Figure 2.2.3. Ganglia Dissolution Concept

For early times and sufficiently large average saturation, the mass discharge from a ganglia-impacted zone equals the flow through the projected area ($A_{g,yz,0} = Y_{g,0}*Z_{g,0}$) multiplied by the equilibrium concentration, less any concentration entering the zone,

$$\frac{dm_g}{dt} = -U_g A_{g,yz,0}\left(C^* - C_{g,0}\right) \tag{2-7}$$

As the ganglia are dissolved, the NAPL volume and interfacial area for dissolution are reduced. The reduced NAPL volume increases the permeability to water flow thereby increasing the velocity and mass dissolution rate. Conversely, the reduced interfacial area decreases the mass transfer rate. These competing phenomena are captured by a changing relative permeability k_r (dimensionless) to water flow and a ratio of the average saturation (mass) to the initial average saturation (initial mass) raised to a dimensionless exponent, γ, (Geller and Hunt 1993),

$$\frac{dm_g}{dt} = -U_0\, k_r\, A_{g,yz,0}\left(\frac{m_g}{m_{g,0}}\right)^{\gamma}\left(C^* - C_{g,0}\right) \tag{2-8}$$

In this work, the relative permeability is defined by the widely used Wyllie correlation (Wyllie 1962),

$$k_r(m_g) = \left(\frac{1 - S_g - S_{irr}}{1 - S_{irr}}\right)^3 = \left[\left(1 - \frac{m_g}{V_g \phi \rho_n} - S_{irr}\right)/(1 - S_{irr})\right]^3 \tag{2-9}$$

Defining the bulk mass transfer rate coefficient for the NAPL-impacted zone as in Eqn. (2-5b), a field-scale relation for the bulk mass transfer coefficient referenced to the source zone volume is,

$$K_g(m_g) = \frac{U_0\, k_r\, A_{g,yz,0}}{V_s}\left(\frac{m_g}{m_{g,0}}\right)^{\gamma} \qquad \textbf{(2-10)}$$

The irreducible water saturation S_{irr} (dimensionless) typically varies from 0.05 to 0.15 depending upon the soil type (Wilson et al. 1990). The DNAPL saturation S_g (dimensionless) is based on the ganglia mass estimate and DNAPL sub-volume as defined previously. The bulk mass transfer rate coefficient (K_g) is solely a function of the transient, remaining ganglia mass given the upscaled velocity, characteristic initial dimensions for the source and DNAPL zones, a single fit exponent, and the relative permeability dependence on the mass. Eqn. (2-8) is a highly nonlinear, first order differential equation (ODE) for the ganglia mass remaining as a function of time and is straightforward to solve.

In Eqn. (2-9), the impact of mass reduction (i.e., saturation reduction) on local velocity is captured by the relative permeability and is separated from the reduction in area. The mass ratio and its exponent are a lumped representation of the reduction in interfacial area between DNAPL and water phases as well as the field-scale reduction in projected area of the DNAPL sub-volume to the flow direction. Considering dissolving spheres, the ratio of projected area reduction to volume reduction yields a theoretical exponent of γ=2/3 as does the DNAPL/water interfacial area (Powers et al. 1994). A fundamental assumption in Eqn. (2-8) is that the initial DNAPL saturation is sufficient to discharge an equilibrium concentration from the sub-volume. If not, a threshold saturation should be specified below which the initial K_g should be reduced by some constant. This scenario is described in Geller and Hunt (1993) wherein a variable mass transfer zone exceeds the length of the bulk DNAPL volume, i.e., the residence time of water in the DNAPL zone is insufficient to achieve equilibrium. However, this length is expected to be relatively small in a field setting unless the initial saturation is very low (Miller et al. 1990).

2.2.3.2 Pool Zone

Mass transfer from a pool zone is dominated by the dispersive component. Advective flow through the pool is minimized by a high DNAPL saturation. The mass dissolution rate from a single, linear pool with tangential dispersion is illustrated in Figure 2.2.4.

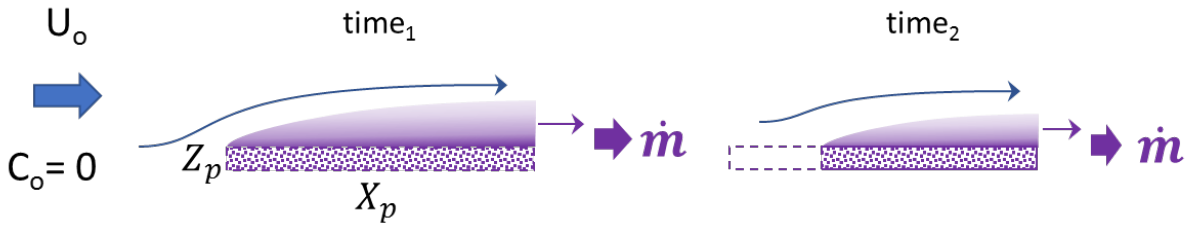

Figure 2.2.4. Pool Dissolution Concept

On the bulk scale, analytical expressions for the total mass dissolution rate, assuming vertical dispersion is the sole mechanism, are derived by Hunt et al. (1988) and Johnson and Pankow (1992) for steady state conditions, i.e., constant pool length,

$$\frac{dm_p}{dt} = -U_0 A_{p,xy}\left(C^* - C_{p,0}\right)\sqrt{\frac{4\alpha_T}{\pi X_p}} = -U_0 Y_p\left(C^* - C_{p,0}\right)\sqrt{\frac{4\alpha_T X_p}{\pi}} \qquad \textbf{(2-11)}$$

X_p is the pool length, Y_p is the pool width, α_T is the vertical dispersivity, and $A_{p,xy}$ ($= X_p * Y_p$) is the pool area for dissolution, neglecting the lateral edges for a small pool height. Over time, the pool erodes primarily at the leading edge. Assuming all dissolved mass is removed from the leading edge (Figure 2.2.4) yields a linear relationship between the length and total mass in the pool,

$$X_p \cong X_{p,0}\left(\frac{m_p}{m_{p,0}}\right) \qquad \textbf{(2-12)}$$

$X_{p,0}$ is the initial pool length. Under this assumption, a field-scale, bulk mass transfer rate coefficient for a pool zone can be defined as a function of mass by substituting Eqn. (2-12) into Eqn. (2-11), equating the result to Eqn. (2-5b), and re-introducing the initial pool dissolution area,

$$K_p(m_p) = \frac{U_0}{V_s} A_{p,xy,0}\sqrt{\frac{4\alpha_T}{\pi X_{p,0}}}\left(\frac{m_p}{m_{p,0}}\right)^{0.5} \cong \frac{U_0}{V_s} A_{p,xy,0}\sqrt{\frac{4\alpha_T}{\pi X_{p,0}}}\left(\frac{m_p}{m_{p,0}}\right)^{\delta} \qquad \textbf{(2-13)}$$

A dimensionless exponent, δ, is theoretically equal to 0.5; however, a generalized exponent is retained to allow for deviations from the pool model assumptions.

2.2.3.3 Generalized Field-Scale DNAPL Mass Transfer Coefficient

In more complex configurations the DNAPL dissolution may include commensurate or transitioning contributions from flow through the zone compared to dispersion from tangential boundaries. Simply combining Eqn. (2-10) and Eqn. (2-13) yields,

$$K_a = \frac{U_0}{V_s}\left[A_{g,yz,0}\, k_r\left(\frac{m_g}{m_{g,0}}\right)^{\gamma} + A_{p,xy,0}\sqrt{\frac{4\alpha_T}{\pi X_{p,0}}}\left(\frac{m_p}{m_{p,0}}\right)^{\delta}\right] \qquad \textbf{(2-14)}$$

The ganglia or pool bulk mass transfer rate coefficient is returned for α_T or k_r set to zero, respectively. The exponent values are expected to be close in value, on the order of 0.5 to 0.67 as described in the pool and ganglia sections, respectively. Deviations from the model assumptions and soil heterogeneity suggest considering a single value for field applications,

$$K_{a,0}(m_a) = \frac{U_0}{V_s}\left[A_{a,yz,0}\, k_r(m_a) + A_{a,xy,0}\sqrt{\frac{4\alpha_T}{\pi X_{a,0}}}\right]\left(\frac{m_a}{m_{a,0}}\right)^{\gamma} \quad \textbf{(2-15)}$$

This expression for $K_{a,0}$ is solely a function of the mass within the DNAPL sub-volume given the upscaled velocity, characteristic initial dimensions for the source and DNAPL zone, a single exponent, and a relative permeability function [Eqn. (2-9)]. Compared to previous power law models with constant coefficients, this formulation includes a transient coefficient based on mass (i.e., relative permeability k_r), in addition to the power law ratio. The remaining mass within the NAPL sub-volume over time is calculated based on the initial mass and cumulative mass discharge. The combination of Eqn. (2-15) with Eqns. (2-5) provides a complete specification of discharge from the source zone over time as a function of remaining mass. The coupled Eqns. (2-5) are highly nonlinear but constitute a generally well-behaved system of first order ODEs for the discharge concentration and the masses remaining in the DNAPL accumulations considered. Eqn. (2-15) is similar to the process-based model of Kokkinaki et al. (2014) with two significant differences. The projected area to flow in Eqn. (2-15) is constant at the initial value and changes are captured in the mass ratio. Secondly, the coefficient includes a constant term for transverse dispersion that is absent in their model. Lateral dispersion in the y-direction could also be incorporated. Advanced numerical models include a transient relative permeability in the flow calculation separate from the mass transfer coefficient. As such, the development of mass transfer correlations from statistical realizations are implicitly dependent upon the relative permeability function utilized (Saenton and Illangasekare 2007, Christ et al. 2010, Guo et al. 2020).

2.2.3.4 Multiple Interacting NAPL Zones

Characterization of NAPL architecture should also include relative locations with respect to the primary direction of groundwater flow. If no mass is found directly upgradient of any other mass, the respective mass dissolutions are all independent. If a NAPL mass is upgradient, the average aqueous concentration, $C_{a,0}$, entering the downgradient NAPL sub-volume is not zero and an auxiliary relationship is required. This condition results from discretizing the NAPL accumulations based on saturation and eliminating the volume-averaged source zone concentration as the driver for NAPL dissolution as indicated in Eq. (2-5b).

For a NAPL mass, m_d, downgradient from an upgradient mass, m_u, the entering aqueous concentration, $C_{d,0}$, is approximately equal to the discharge concentration from the upgradient mass. Assuming the masses are directly in line with flow and neglecting intervening reactions and dispersion, the discharge concentration from the upgradient NAPL is proportional to the mass remaining and solubility,

$$C_{d,0} \propto C_u \sim f(m_u)$$

Based on this proportionality, we can write a dimensionless inhibition function, I_d, for dissolution from the downgradient mass based on the remaining upgradient mass,

$$\frac{1}{V_s}\frac{dm_d}{dt} = -K_d(C^* - a_u C_u) = -K_d C^* \left[1 - a_d \left(\frac{m_u}{m_{u,0}}\right)^{\varepsilon}\right] = -K_d C^*(1 - I_d) \quad \textbf{(2-16a)}$$

$$I_d(m_u) = a_d \left(\frac{m_u}{m_{u,0}}\right)^{\varepsilon} \quad \textbf{(2-16b)}$$

The exponent on the upgradient mass ratio is assumed equal to the exponent for dissolution of the upgradient mass. The dimensionless coefficient a_d is a shape factor accounting for any difference in the overlap of projected areas between the two masses. In practice, this level of detail in NAPL characterization is not expected and this work assumes masses are either independent ($a_d = 0$) or are directly in line with each other ($a_d = 1$). For example, a thin pool located upgradient of a ganglia zone of relatively large depth interval would have little impact on ganglia dissolution ($a_d = 0$) whereas an upgradient ganglia zone would strongly inhibit downgradient pool dissolution ($a_d = 1$) until the ganglia are substantially depleted. For two nearly identical pools in series, the effect of inhibition is roughly equivalent to modeling a single pool with twice the length. If a series of sources are in line with the direction of flow, this function captures the cumulative impact. Changes in flow direction resulting from groundwater pumping or injection can be captured with changes in the shape factor, assuming the relative spatial locations of distinct masses are available.

2.2.3.5 Estimate for Time of NAPL Depletion

A simple expression is available to estimate the time of NAPL depletion if the relative permeability appearing in Eqn. (2-15) is averaged,

$$\overline{k_r} = \frac{k_r(m_{a,0}) + 1}{2}$$

The model for NAPL mass discharge becomes,

$$\frac{dm_a}{dt} = -\overline{K}_{a,0} \left(\frac{m_a}{m_{a,0}}\right)^{\gamma_a} \quad \textbf{(2-17)}$$

$$\overline{K}_{a,0} = C^* U_0 Y_a Z_a \left(\overline{k}_{r,a} + \sqrt{\frac{4\alpha_T X_a}{\pi Z_a^2}}\right) \quad \textbf{(2-18)}$$

Equation (2-17) can be solved to find,

$$\frac{m_a}{m_{a,0}} = \left[1 - \frac{\overline{K}_{a,0}(1-\gamma_a)}{m_{a,0}} t\right]^{\frac{1}{1-\gamma_a}} \quad \textbf{(2-19)}$$

The estimated time of NAPL depletion is found by setting the mass equal to zero in (2-19) and solving for t,

$$t_{deplete,a} = \frac{m_{a,0}}{\overline{K}_{a,0}(1-\gamma_a)} \quad \textbf{(2-20a)}$$

The estimated time for complete depletion of mass m_{a+1} inhibited by an upgradient mass m_a is,

$$t_{deplete,a+1} = \frac{m_{a+1,0}}{\overline{K}_{a+1,0}(1-\gamma_{a+1})} + (1-\gamma_a) t_{deplete,a} \quad \textbf{(2-20b)}$$

2.2.4 Modeling of Back Diffusion from Low Permeability Features

In addition to complex NAPL architecture, soil heterogeneity on a geologic scale, i.e., the scale of vertical changes in lithology, results in back diffusion in the source zone. This phenomenon is very difficult to model numerically because of the small scale of aqueous diffusion and the fine gridding required. Traditionally applied on the pore scale to represent stagnant water (Griffioen et al., 1998), a dual domain model is also applicable on the field scale (Haggerty and Gorelick 1995). The diffusion limited sources are treated analogously to NAPL accumulations where a fraction of the source zone volume consists of mobile water (f_m) and a fraction as immobile (f_{im}, diffusion dominated) (Feehley et al., 2000). The NAPL is also assumed to reside solely in the mobile zone. Under these assumptions, the diffusion-limited transport out of the immobile zone and into the advectively dominated mobile zone is modeled as a first-order process,

$$f_{im}\phi_{im}R_{im}\frac{d\overline{C}_{im}}{dt} = -\overline{K}_i(\overline{C}_{im} - \overline{C}_m) - f_{im}\phi_{im}r_{im} \quad \textbf{(2-21)}$$

The subscript im designates a property of the immobile zone and m designates a property of the mobile zone. C_{im} is the average aqueous concentration in the immobile fraction of the source zone. This nomenclature allows the specification of a different total porosity in each domain as soil types differ,

$$f_m + f_{im} = 1$$

$$\phi\ (\textbf{Total Absolute Porosity}) = (\phi_m f_m + \phi_{im} f_{im})$$

The expression utilizes a rate-limiting bulk mass transfer coefficient, K_{im}, generally assumed constant. However, this phenomenon has been the subject of much recent research to assess its transient behavior. More complex one-dimensional diffusion models are available (Falta and Wang 2017) and could be implemented in the proposed framework to provide more robust models of back diffusion. A separate reaction term is also maintained in this domain to allow differing processes from the mobile domain. The governing equations for the averaged source zone mobile (discharge) concentration and multiple dissolving NAPL masses are,

$$R_m \frac{d\bar{C}_m}{dt} = -\frac{Q}{f_m \phi_m V_s}\bar{C}_m - \frac{1}{f_m \phi_m V_s}\sum_{a=1}^{A}\frac{dm_a}{dt} + \left(\frac{K_i}{f_{im}\phi_m}\right)(\bar{C}_{im} - \bar{C}_m) - (1-\bar{S}_n)\bar{r}_m \quad \textbf{(2-22a)}$$

$$\frac{1}{f_m V_s}\frac{dm_n}{dt} = -\sum_{a=1}^{A} K_a\left(C^* - C_{a,0}\right) \quad \textbf{(2-22b)}$$

The bulk mass transfer coefficient between the mobile and immobile zones (K_{im}) is scaled to the full volume of the source zone considered. The NAPL saturation and bulk NAPL mass transfer coefficient are both scaled to the volume of the mobile zone to maintain consistency with the definition of the mobile zone aqueous concentration. The extension to multiple sources for back diffusion (e.g., multiple fine-grained strata) is identical to the NAPL architecture formulation and dependent upon the availability of site data (e.g., high resolution site characterization efforts).

2.2.5 Multi-Component NAPL

Extension of the approach to a multi-component NAPL of *N* components is straightforward. The number of first order equations to solve increases by a multiplier equal to *N* for the basic NAPL dissolution problem. The inclusion of a multi-component NAPL requires the additional auxiliary calculation of NAPL mole fractions at each time step to evaluate the updated component equilibrium partitioning concentration according to Raoult's law, assuming ideality (Banerjee, 1984). The NAPL mass in a source volume represented by multiple NAPL masses with multiple components, assumed to be uniformly mixed within its sub-volume, is defined by,

$$m_n = \sum_{a=1}^{A} m_a = \sum_{a=1}^{A}\sum_{i=1}^{N} m_{a,i} \quad \textbf{(2-23)}$$

The NAPL saturation, number of component moles (n_i), and component mole fractions (y_i) within each sub-volume are defined by,

$$\bar{S}_a = \frac{m_a}{\rho_n \phi V_a} = \frac{1}{\rho_n \phi V_a}\sum_{i=1}^{N} m_{a,i} = \frac{1}{\rho_n \phi V_a}\sum_{i=1}^{N} M_i n_{a,i} \quad \textbf{(2-24a)}$$

$$y_{a,i} = \frac{n_{a,i}}{n_a} = \frac{n_{a,i}}{\sum_{j=1}^{N} n_{a,j}} = \frac{1}{M_i}\frac{m_{a,i}}{\sum_{j=1}^{N}\frac{m_{a,j}}{M_j}} \quad \textbf{(2-24b)}$$

M_i is the molecular weight of each component i. Assuming no reactions take place within the NAPL phase and no concentration gradients exist within the NAPL itself over its sub-volume, the mass balance for each NAPL mass component is,

$$\frac{1}{V_s}\frac{dm_{a,i}}{dt} = -K_{a,i}\left(y_{a,i}C_i^* - \overline{C}_{a,0,i}\right) \tag{2-25}$$

Considering a multi-component NAPL within equations (2-3) results in the following system of equations written for each component making of the NAPL in the source zone,

$$\phi R_i \frac{d\overline{C}_i}{dt} = -\frac{Q}{V_s}\overline{C}_i - \frac{1}{V_s}\sum_{a=1}^{A}\frac{dm_{a,i}}{dt} - \phi(1-\overline{S}_n)\overline{r}_i \tag{2-26a}$$

$$\frac{1}{V_s}\sum_{a=1}^{A}\frac{dm_{a,i}}{dt} = -\sum_{a=1}^{A}K_{a,i}\left(y_{a,i}C_i^* - \overline{C}_i\right) \tag{2-26b}$$

Hence, the number of coupled equations to solve is *AxN+N*. To determine the change in average saturation and mole fraction within each NAPL sub-volume, the NAPL mass balance is calculated for each architectural compartment by,

$$\frac{1}{V_s}\frac{dm_a}{dt} = \frac{1}{V_s}\sum_{i}^{N}\frac{dm_{a,i}}{dt} = -\sum_{i}^{N}K_{a,i}\left(y_{a,i}C_i^* - \overline{C}_{m,i}\right) \tag{2-27}$$

This representation is a multi-source extension of the multi-component NAPL dissolution model presented in Carroll and Brusseau (2009). The bulk mass transfer coefficient for each subzone source NAPL mass differs for each component of the NAPL according to its transport properties. After determining the baseline coefficient for a reference compound in the NAPL, the component mass transfer coefficients can be scaled using a parametric relationship based on Sherwood correlations for mass transfer (Clement et al., 2004; Carroll and Brusseau, 2009),

$$K_{a,i} = K_{a,0}\left(\frac{D_i}{D_0}\right) \tag{2-28}$$

D_i is the component aqueous diffusion coefficient and D_0 is the reference diffusion coefficient. The bulk mass transfer coefficient for the NAPL captures changes in the NAPL mass.

2.2.5.1 Multiple Interacting Multi-Component NAPL Zones

For dependence on an upgradient NAPL mass, the inhibition is then compound specific,

$$\frac{dm_{d,i}}{dt} = -V_s K_{d,i}\left(y_{d,i} C_i^* - \overline{C}_{u,0,i}\right) \tag{2-29a}$$

$$\overline{C}_{u,0,i} = C_i^* \left(\frac{y_{u,i} m_u}{y_{u,i,0} m_{u,0}}\right)^{\varepsilon} \tag{2-29b}$$

2.2.5.2 Approximate Model for Multi-Component NAPL Dominated by an Insoluble Component

Dissolution of soluble components found at low mass fractions in a multi-component NAPL can be modeled approximately by assuming the majority of the NAPL mass is inert or insoluble. This condition allows the following assumptions: total NAPL mass is constant and soluble components dissolve independently. The governing equation for the mole fraction of each soluble component *i* remaining in the NAPL is approximately,

$$\frac{1}{V_{ref}} \frac{dm_{n,i}}{dt} = -K_n C_i^* y_{n,i} \tag{2-30a}$$

$$\frac{dy_{n,i}}{dt} = -K_{n,i} C^* \left(\frac{V_{ref}\, \overline{MW}_n}{m_{n,total} MW_i}\right) y_{n,i} \tag{2-30b}$$

V_{ref} is the reference soil volume for the bulk mass transfer coefficient. The bulk NAPL mass transfer coefficient, referenced to a soil volume containing the NAPL mass, is approximately constant since the total NAPL mass does not change significantly,

$$\overline{K}_{n,0} = \frac{U_0}{V_{ref}} \left[A_{n,yz}\, \overline{k}_r + A_{n,xy} \sqrt{\frac{4\alpha_T}{\pi X_{n,0}}} \right] \tag{2-31}$$

The mole fraction equation is readily solved assuming a constant mass transfer coefficient and subject to a given initial mole fraction,

$$y_{n,i} = y_{n,i,0}\, e^{-K' t}, \qquad K' = \frac{K_{n,0} C^* V_{ref} \overline{MW_n}}{m_{n,total} MW_i} \tag{2-32}$$

Under steady dissolution conditions, the time required to deplete the soluble component *i* from the NAPL to an MCL-equivalent, equilibrium groundwater concentration is,

$$t_{i,deplete\ to\ MCL} = -\left(\frac{1}{K'}\right) ln\left(\frac{y_{n,i,MCL}}{y_{n,i,0}}\right) \quad \textbf{(2-33)}$$

The discharge concentration from the reference soil volume is governed by,

$$R_i \frac{dC_i}{dt} = -\frac{Q_0}{\phi V_{ref}} C_i - \frac{1}{\phi V_{ref}} \frac{dm_{n,i}}{dt} - (1 - S_n)\lambda_i C_i \quad \textbf{(2-34)}$$

This expression includes a first order degradation process occurring within the volume prior to discharge. Substituting the mole fraction solution yields,

$$\frac{dC_i}{dt} + Q' C_i = K^* e^{-K't} \quad \textbf{(2-35a)}$$

$$Q' = \frac{1}{R_i}\left[\frac{Q_0}{\phi V_{ref}} + (1 - S_n)\lambda_i\right] \quad \textbf{(2-35b)}$$

$$K^* = \frac{K_n C_i^* y_{n,i,0}}{\phi R_i} \quad \textbf{(2-35c)}$$

Given an initial condition for the groundwater concentration, the solution for the discharge concentration is,

$$C_i = C_{i,0} e^{-Q't} + \left(\frac{K^*}{Q' - K'}\right)\left(e^{-K't} - e^{-Q't}\right) \quad \textbf{(2-36)}$$

If the mass dissolution rate is much slower than the pore volume exchange rate ($K' << Q'$), as is typical, Eqn. (2-36) can be simplified:

$$C_i \cong \left(\frac{K^*}{Q' - K'}\right) e^{-K't} \quad \textbf{(2-37a)}$$

Setting the discharge concentration equal to MCL and rearranging yields the approximate time to a discharge concentration at the MCL under natural conditions:

$$t_{i,MCL\ discharge} \cong \frac{1}{K'} ln\left[\frac{K^*}{C_{i,MCL\ discharge}(Q' - K')}\right] \quad \textbf{(2-37b)}$$

To estimate the impact of remediation on a largely insoluble, multi-component NAPL, the solution can be re-started at specified times using the current mole fraction and discharge concentration as initial conditions and applying changes to the dissolution model and degradation rate,

$$\overline{K}_n = \overline{K}_{n,0} E_r E_f \ , \qquad Q = Q_0 E_f \ , \qquad \lambda_{i,r} = E_\lambda \lambda_i \ , \qquad E_r = f(\lambda_{i,r}) \quad \textbf{(2-38)}$$

The factor E_f is an enhancement factor representing changes in the characteristic velocity through the NAPL soil volume, e.g., pump-and-treat. E_r is an estimated multiplier on the first order reaction rate resulting from the addition of amendments, e.g., electron acceptors/donors, chemical oxidants. The factor E_r represents changes in the dissolution rate attributable to changes in the first order degradation, $\lambda_{i,r}$. The change is associated with the driving concentration gradient for dissolution. The relationship between E_r and $\lambda_{i,r}$ is complex but research exists for making theoretical estimates as described in the next section.

2.2.6 Modeling of Remedial Processes

Using the framework of spatial averaging combined with architecture-specific mass transfer correlations and reactions provides a methodology to assess remedial performance commensurate with high resolution, complex, and intensive numerical modeling. A significant body of research exists describing the impact of specific remedial processes related to NAPL dissolution but very little work has been performed in evaluating these results for assessment of field implementation. The primary impediment to such an evaluation is the difficulty of executing site-specific numerical models. The proposed framework provides a more practical method to perform these assessments of remediation technologies on long-term source control.

Foundational research on mass dissolution from residual NAPL during remediation and upscaled mass transfer coefficients was developed in ESTCP Project ER-1294 (Illangasekare et al., 2006) and elsewhere. Mathematical models have been developed to simulate a range of remedial technologies, and experimental and field studies are available to support their incorporation into the framework. This work leverages the previous work and transforms the results into the volume-averaged framework as remedial enhancements to residual NAPL dissolution.

The enhancement is defined as the ratio of the NAPL mass dissolution rate under remedial conditions to the rate under natural conditions. The magnitude of the enhancement is related to technology- and site-specific implementation. In general, the enhancements can be grouped into three categories: increases in flow (E_f), reactive increases in driving concentration gradients (E_r), and increases in effective solubility (E_s). Flow enhancements can be modeled as a simple ratio of the characteristic remedial velocity to the natural groundwater velocity. Theoretical enhancement factors are available in the literature for first order reactions proximate to ganglia (Christ and Abriola 2007) and pools (Seagren et al. 1994) and for general second order reactions (Cussler 1997). These various relationships are described below. The reactive enhancements are functions of the reaction rate, first order for slow to moderate rates and second order for fast rates, and the flow rate.

Increased flow increases the dissolution rate but reduces the residence time and therefore decreases an associated reactive enhancement. Increased effective solubility is a function of the concentration of a solubilizing agent. The introduction of thermal energy can increase reaction rates and generally increases solubility (Imhoff et al. 1997, Johnson et al. 2010).

2.2.6.1 Flow Enhancements to Dissolution

The first category is the simplest to model in the volume-averaged framework as the only parameter involved is an increased water velocity through the source zone. This increase can be induced by pumping from an extraction well within the source zone or downgradient from the source zone. The increase can be included in the previous mass balance equations by a simple flow enhancement factor, E_f, which is referenced to the natural velocity of groundwater through the source zone ($E_f = U_{remedy}/U_0$). Without any appreciable in situ reactions, the volume-averaged model equations in this scenario are,

$$R\frac{d\overline{C}}{dt} = -E_f\frac{Q}{\phi V_s}\overline{C} - \frac{1}{\phi V_s}\frac{dm_n}{dt} \tag{2-39a}$$

$$\frac{1}{V_s}\frac{dm_n}{dt} = -E_f K_n(C^* - \overline{C}) = -E_f\sum_{a=1}^{A} K_{a,0}\left(C^* - C_{a,0}\right) \tag{2-39b}$$

$$K_{a,0}(m_a) = \frac{U_0}{V_s}\left[A_{a,yz,0}\, k_r(m_a) + A_{a,xy,0}\sqrt{\frac{4\alpha_T}{\pi X_{a,0}}}\right]\left(\frac{m_a}{m_{a,0}}\right)^{\gamma} \tag{2-39c}$$

As derived earlier, the mass transfer coefficient is assumed to be a linear function of the velocity. This assumption may not be strictly valid with large velocity changes but the approximation is useful. In practical terms, the increase is limited by site conditions and extraction well construction. Placement of extraction within the source zone also changes the direction of flow and may require a re-interpretation of the characteristic dimensions. For example, a well placed in the middle of a pool zone with effectively cut the pool length in half with a high characteristic velocity as compared to downgradient pumping. Changes in pumping rate or location are modeled with changes in the flow enhancement factor. As described in Section 5, an existing numerical flow model is an ideal tool for evaluating changes in flow through the source zone induced by pumping wells.

2.2.6.2 Reactive Enhancements to Dissolution

The introduction of a reactant such as an oxidant or an amendment to promote biological degradation can lower the aqueous phase concentration in the source zone as modeled by a reaction term. The decreased concentration impacts the NAPL dissolution rate by increasing the effective driving concentration gradient between the NAPL interface (assumed to be at the solubility limit) and the bulk water flowing past the NAPL. The dissolution enhancement resulting from this reaction-induced gradient, E_r, is difficult to predict; however, theory and experimental data are

available in the published literature for guidance (e.g., Cussler 1992, Chu et al. 2007, Heiderscheidt et al. 2008, Seagren and Becker 2015, Phelan et al. 2015). The enhancement is not a simple linear function of the reaction rate but also depends strongly on the advection rate, U_0, the length of the NAPL zone, X_n., i.e., the source zone residence time, the concentration of reactants, and the reaction rate. Biological reactions are generally slow and considered first order reactions whereas oxidant reactions are often sufficiently fast to be considered second order.

The discharge concentration of a soluble component *i* from the reference soil volume under generic reactive conditions is represented by,

$$R_i \frac{dC_i}{dt} = -\frac{Q_0}{\phi V_{ref}} C_i - \frac{1}{\phi V_{ref}} \frac{dm_{n,i}}{dt} - \left(1 - S_{n,ref}\right) r_i \tag{2-40}$$

r_i is the reaction sink for the contaminant. Reactions are generally described as a first order process when the reactant is provided in excess, the aqueous contaminant is limited, and rates are slow to moderate. The reaction can be characterized as second order between the reactant and aqueous contaminant when reaction rates are fast. The reaction term in (2-40) for each case is defined by,

$$\textbf{1st Order: } \boldsymbol{r_{i,1} = \lambda_i C_i} \qquad \textbf{2nd Order: } \boldsymbol{r_{i,2} = \kappa_{i,react} C_{react} C_i} \tag{2-41}$$

λ_i is a first order decay constant, C_{react} represents the concentration of introduced reactant, and $\kappa_{i,react}$ is the specific reaction rate coefficient. The most common condition for modeling reactions associated with NAPL dissolution is first order because most studies address biological enhancements which are relatively slow. However, fast reactions observed during in situ chemical oxidation can yield a second order process.

Dimensionless Parameters for Characterizing Reactive Enhancements

Theoretical enhancement factors under first order reactive conditions have been derived by Seagren et al. (1994) and Christ and Abriola (2007) for idealized NAPL pool and ganglia architectures, respectively. The relationships are written in terms of dimensionless parameters describing the relative rates of differing processes associated with the flow and NAPL architecture. The ratio of the characteristic reaction rate to the advection rate of water through the NAPL-impacted soil volume is known as the reaction-based Damköhler Number, *Da*. The Stanton Number, *St*, is the ratio of the mass dissolution rate to the advection rate. The Peclet number, *Pe*, is the ratio of the advection rate to the longitudinal dispersion rate; however, on the scale of typical NAPL source zones in the field, the Peclet number is expected to be large. *Da*, *St* and *Pe* are defined as follows, assuming a first order reaction,

$$Da = \frac{\lambda_r X_n \phi}{U_0} \qquad St = \frac{K_n X_n}{\phi U_0} \qquad Pe = \frac{U_0 X_n}{D_x \phi} = \frac{X_n}{\alpha_L}$$

α_L is the longitudinal hydrodynamic dispersivity. Substituting the upscaled mass transfer coefficient (Eqn 2-15) into the Stanton number yields an upscaled Stanton number,

$$St = \frac{1}{\phi}\left[\bar{k}_r + \frac{2}{Z_n}\sqrt{\frac{X_n \alpha_T}{\pi}} \right]$$

Inspection of the upscaled Stanton number with field-scale parameters indicates *St* is on the order of the inverse porosity or smaller. For ganglia, the relative permeability approaches one and the dispersivity term is small. For pools, with high saturations, the relative permeability may approach zero while the dispersivity term is expected to be <1 on the field scale. The longitudinal, hydrodynamic dispersivity is generally on the order of 0.1-1 m (Molz 2015) and therefore the field-scale Peclet number is expected to be greater than one.

Theoretical Dissolution Enhancements with First Order Reactions

Seagren et al. (1994) derived a theoretical expression for the reaction enhancement to NAPL dissolution during flow over a NAPL pool with a first order reaction in the aqueous phase under pseudo-steady conditions. The model neglects any flow through the NAPL zone and is solely a function of the Damköhler number,

$$\boldsymbol{E_{r,p} = \frac{1}{2}\sqrt{\frac{\pi}{Da}}\left[\left(Da + \frac{1}{2}\right) erf\left(\sqrt{Da}\right) + \sqrt{\frac{Da}{\pi}}\, exp(-Da)\right]} \qquad \textbf{(2-42)}$$

To induce an enhancement factor of 2 or larger, *Da* must be 4 or larger. Christ and Abriola (2007) derived an expression for first order reaction enhancement to NAPL dissolution during flow through ganglia, also under pseudo-steady conditions. In this architecture, the reaction enhancement is also a function of the Stanton and Peclet numbers,

$$\boldsymbol{E_{r,g} = \frac{St - \left(\frac{St}{St+Da}\right)^2 \left(St + Da - \left\{1 - exp\left[\frac{Pe}{2}\left(1 - \sqrt{1 + \frac{4(St+Da)}{Pe}}\right)\right]\right\}\right)}{1 - exp\left[\frac{Pe}{2}\left(1 - \sqrt{1 + \frac{4St}{Pe}}\right)\right]}} \qquad \textbf{(2-43)}$$

The enhancement for ganglia increases with increasing *St*, decreasing *Pe*, and increasing *Da*. For a maximum *St* of 3, i.e., inverse porosity, and a minimum Pe of 1, a minimum *Da* value of 2 or larger is required to induce an enhancement factor of 2 or more. However, for the vast majority of field applications, *Pe* for NAPL dissolution will be large and first order reactive enhancements will only be appreciable if *St* is large, i.e., >10. NAPL dissolution is relatively long process compared to a relatively short residence time; therefore, *St* is usually small. Hence, typical first order reactions are not expected to enhance ganglia dissolution where the interfacial area between water and NAPL is large as compared to the pool architecture.

Noting the theoretical enhancement factors were derived for two idealized architectures, the appropriate application of first order reaction enhancements in the upscaled dissolution model (Eqn 2-15) takes the form,

$$E_{r,1}K_{n,0} = \frac{U_0}{V_n}\left[E_{r,g}A_{n,yz}\,\bar{k}_r + E_{r,p}A_{n,xy}\sqrt{\frac{4\alpha_T}{\pi X_n}}\right] \quad \textbf{(2-44)}$$

More complex relationships specific to biological degradation assuming Monod kinetics can be found in Phelan et al. (2015).

Theoretical Dissolution Enhancements with Second Order Reactions

Second order reactions can be characterized by fast reaction rates, as opposed to limited reactant availability, paired with relatively slow mass dissolution rates even with excess reactant. The fast rate results in a deficit of both the reactant and contaminant at a reaction front distant but close to the NAPL-water interface. The result is a steep increase in the driving concentration gradient for mass dissolution. First order reactions described above assume the reaction rate is slow enough for the excess reactant and contaminant to co-exist and mingle for some time. Cussler (1992) derived a theoretical expression for these second order conditions based primarily on the ratio of bulk concentration of reactant to the cumulative effective solubilities of the NAPL components. Cussler's pure-component enhancement factor is modified for a multi-component NAPL as,

$$E_{r,2} = 1 + \frac{1}{Y_{react}}\left(\frac{C_{react}}{\sum y_i C_i^*}\right)\left(\frac{D_i}{D_{react}}\right) \quad \textbf{(2-45)}$$

Y_{react} is the stoichiometric molar mass ratio for the reaction of reactant with soluble NAPL components. The assumptions underlying this expression include a steady re-supply of the reactant to maintain a constant bulk concentration, reactions of multiple soluble components occur independently, and dissolved contaminants are completely destroyed at a reaction interface. The ratio of aqueous phase diffusion coefficients provides a small correction. The modification for a multi-component NAPL includes the complexity of a transient, depleting mole fraction. In this work, a constant enhancement is conservatively assumed based on the initial mole fraction because, as the mole fraction approaches zero, the enhancement unrealistically approaches infinity.

Transient Reactive Dissolution Enhancements

For reactive technologies utilizing chemical oxidants or other amendments, the depletion of the oxidant and/or the method of introduction to the NAPL zone can result in a transient bulk concentration and thereby a transient enhancement factor. A model for the kinetics with permanganate is described in ESTCP project ER-0626 and can be generalized for similar oxidants, such as persulfate, and incorporated into a volume averaging framework wherein contaminant oxidation is calculated assuming a second order reaction (Huang et al. 1999, Siegrist et al. 2001),

$$\bar{r} = k^{oxi}\,\bar{C}\,\bar{C}_{oxi} \tag{2-46}$$

k^{oxi} is the 2nd-order reaction coefficient for destruction of the contaminant by the oxidant at concentration, $\bar{C}_{oxi}$. If the mass of oxidant is limited, e.g., a one-time injection event, the mass balance on the oxidant in the source zone can also be added to the system solution, as described in Appendix B,

$$\frac{d\bar{C}_{oxi}}{dt} = -\frac{Q}{\phi V_s}\bar{C}_{oxi} - Y^{oxi}\,\bar{r} - \rho_b k_{NOD}^{oxi} X_{NOD}\bar{C}_{oxi} \tag{2-47}$$

Y^{oxi} is the stoichiometric molar mass ratio of oxidant to the contaminant. This expression includes a sink term for reactions with the natural oxidant demand (NOD) posed by organic carbon material in the soil solids, expressed as the mass of NOD material per mass of bulk soil, X_{NOD}. The NOD material is stationary and the mass balance for its transformation is,

$$\frac{dX_{NOD}}{dt} = -k_{NOD}^{oxi} X_{NOD}\bar{C}_{oxi} \tag{2-48}$$

After transformation of the NOD material, all oxidant is available for contaminant oxidation. Including a mass balance on the concentration of reaction products, $\bar{C}_{product}$, can also be useful if the product is used to monitor the process,

$$\frac{d\bar{C}_{product}}{dt} = -\frac{Q}{V_s\phi(1-\bar{S}_n)}\bar{C}_{product} + Y^{product}\,\bar{r} \tag{2-49}$$

$Y^{product}$ is the stoichiometric molar mass ratio of reaction product to the contaminant. Examples of monitoring include the production of chloride which provides a surrogate compound for assessing the destructed mass of a chlorinated compound or, in the case of persulfate, the production of sulfate to indicate the location and reactivity of oxidation.

The second order oxidation reaction [Eqn. (2-46)] appears in the mass balance equation for the contaminant aqueous concentration [Eqn. (2-40)] and reduces the discharge mass rate and concentration. The oxidant is not expected to act directly on the NAPL phase but a rapid reaction rate is expected to increase the driving concentration gradient between the NAPL interface and the bulk water as described by Eqn. (2-45).

The set of nonlinear, first order equations for modeling the introduction of an oxidant with a second order reaction is,

$$R\frac{d\bar{C}}{dt} = -\frac{Q}{\phi V_s}\bar{C} - \frac{1}{\phi V_s}\frac{dm_n}{dt} - (1-\bar{S}_n)k^{oxi}\,\bar{C}\,\bar{C}_{oxi} \tag{2-50a}$$

$$\frac{1}{V_s}\frac{dm_n}{dt} = -E_{r,2}(\overline{C}_{oxi})\, K_{n,0}(C^* - C_0) \quad \textbf{(2-50b)}$$

$$\frac{d\overline{C}_{oxi}}{dt} = -\frac{Q}{\phi V_s}\overline{C}_{oxi} - Y^{oxi}\,\bar{r} - \rho_b k_{NOD}^{oxi} X_{NOD}\overline{C}_{oxi} \quad \textbf{(2-47)}$$

The additional sink of NOD material is included with Eqn. (2-48) and any products of the reaction can be calculated with Eqn. (2-49). These equations are applied to laboratory experiments in Section 5 to validate the approach and demonstrate the utility in the volume-averaged modeling framework.

Measures of the reaction rate coefficient k^{oxi} are available in published studies for the most common oxidants. Experimental data are available for permanganate in ER-1290 (Siegrist et al., 2006) and ER-200623 (Siegrist et al., 2011). Mathematical details and experimental data of ISCO with persulfate are described in Waldemer et al. (2007). Other information and data for a variety of oxidants are compiled in Siegrist et al. (2011).

2.2.6.3 Chemical Enhancements to NAPL Solubility

A model quantifying the dissolution rate during surfactant flushing of entrapped DNAPL has been developed using laboratory and modeling procedures similar to those for natural dissolution (Saba et al., 2002). Correlations for surfactant-enhanced mass transfer coefficients are reported in ER-1294 (Illangasekare et al., 2006), ER-1293 (Abriola et al., 2008) and elsewhere (Ji and Brusseau 1998, Saenton and Illangasekare 2013, Demiray et al 2021) and include a term accounting for diminishing DNAPL saturation yielding diminishing returns. Correlations for the enhanced solubility of NAPL in the presence of a co-solvent are found in Wang and Brusseau (1993). Enhanced solubilization with cyclodextrin has been studied in McCray et al. (2000), Carroll and Brusseau (2009), and Demiray et al. (2021). These models and data can be incorporated into the volume-averaged framework by simply specifying an enhancement factor, E_s, on the NAPL component solubility as follows,

$$\frac{1}{V_s}\frac{dm_n}{dt} = -K_{n,0}(E_s C^* - C_0) \quad \textbf{(2-51)}$$

2.2.6.4 Thermal Enhancements to Dissolution

Modeling of moderate thermal additions such as circulation of hot water or electrical resistance heating to enhance dissolution and degradation can be implemented using a parametric approach (Clement et al., 2004) by assessing the impact of increasing temperature on system properties and correlations. In this approach, an energy balance on the system temperature (T) as a function of injected energy (E_{inject}) is included as follows,

$$\frac{dT}{dt} = -\frac{Q}{\phi V_s}T + \frac{\dot{E}_{inject}}{(\rho c)_{soil} V_s} \quad \textbf{(2-52)}$$

$(\rho c)_{soil}$ is the specific heat content of saturated soil. More specific results are available for demonstration of moderate heating to increase dissolution of DNAPL and destruction rates by both biotic and abiotic processes from ER-200719 (Macbeth et al., 2012). The enhancement to the volume-averaged equations (2-5) provided by heating can be evaluated by estimating the change in NAPL solubility and any increase in reaction rates. Published experimental work for the thermal effects on NAPL dissolution includes Imhoff et al. (1997), Johnson et al. 2010 and Popp et al. (2016).

2.2.7 SCARPÉ Framework and Practical Tools

The mathematical SCARPÉ framework based on volume-averaged modeling described in Sections 2.2.3 through 2.2.6 provides ODEs that can be coded and solved using different platforms, such as Matlab or FORTAN. The SCARPÉ framework includes multiple complex processes that can be combined (e.g., multi-component NAPL, matrix diffusion, multiple remedial processes) to represent a wide variety of sites and NAPL source zone.

In addition to the general mathematical framework, two practical tools have been developed as part of this work for two conceptual source models widely encountered at DoD sites:

- Single NAPL component assuming constant average relative permeability (Section 2.2.3.4):
  - The mathematical equations were programmed in Python and a program executable (SCARPÉs) can be ran to calculate the model outputs.
  - The model inputs are entered into an Excel spreadsheet.
  - SCARPÉs can simulate NAPL accumulations within the source zone.
- Multi-components NAPL source in which NAPL mass remains constant (Section 2.2.5.2):
  - The mathematical equations were populated in Excel and an Excel spreadsheet (SCARPÉm) can be used to calculate model outputs.
  - SCARPÉm can be used to simulate individual NAPLs within a NAPL source NAPL dominated by an insoluble component.
  - SCARPÉm is setup to provide direct comparison of mass discharge between natural attenuation (i.e., no remedial activities) and remedial alternatives.

Beta versions of the two practical tools are available for download at www.SCARPÉmodel.com, including user manual. The user manual is included as Appendix C.

2.3 SCARPÉ FRAMEWORK INPUTS

The information needed to develop a conceptual source model and apply the SCARPÉ framework includes information on the NAPL mass, NAPL source zone area, the groundwater flow field, and remedial processes under consideration.

2.3.1 Conceptual Source Model Parameters

The inputs to the conceptual source model are illustrated in Figure 2.3.1 and further described in Table 2.3.1.

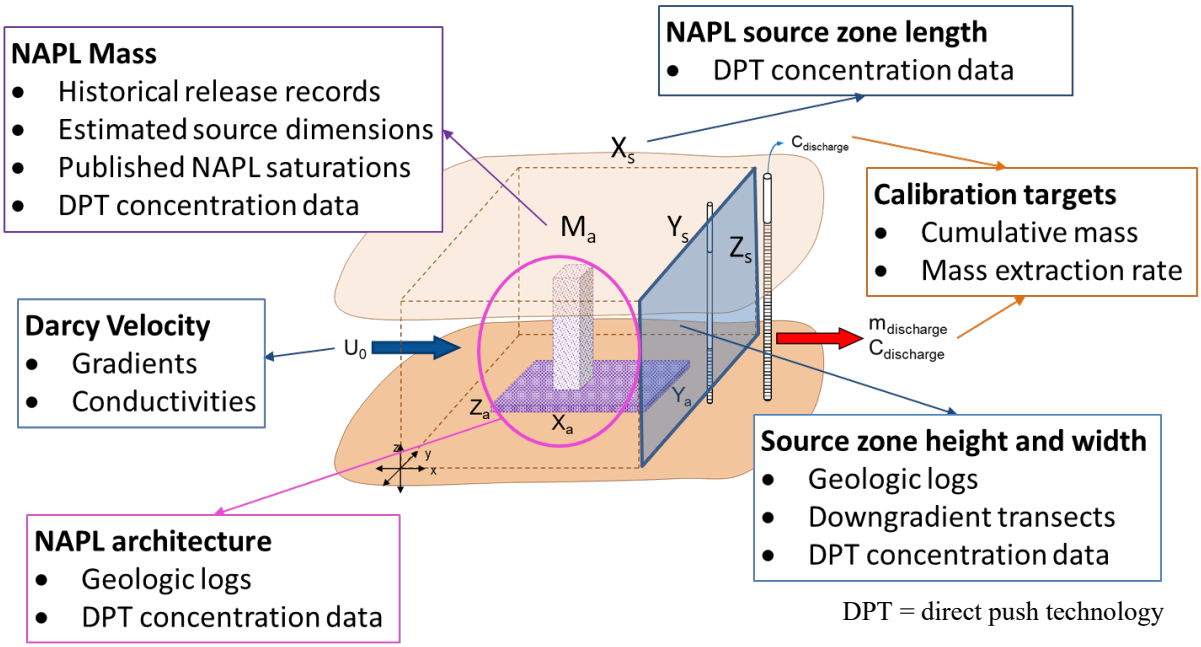

Figure 2.3.1. Illustration of Data Input for SCARPÉ Framework

The needed information for each NAPL accumulation includes estimates for the extent (i.e., characteristic dimensions), mass, and position relative to other accumulations (i.e., up or downgradient). NAPL extent can be estimated based on investigation data, such as groundwater or soil concentrations, visual observations of NAPL in soil cores, monitoring wells, and advanced characterization methods. NAPL mass can be estimated based on monitoring data, such as soil concentrations, residual saturation in various types of soil, and/or historical information on NAPL releases. Traditional designations of architecture type (ganglia vs. pool) are not required. Advective and dispersive contributions to dissolution are both included and relative contributions are determined by the specified dimensions and mass. In addition, the model requires definition of parameters characterizing the groundwater flow within and downgradient of the NAPL source, including Darcy velocity and porosity. Porosity can be measured or estimated based on lithology, and Darcy velocity can be estimated based on estimate of hydraulic conductivity (either with aquifer testing or based on typical values for lithology) and groundwater elevations, which are typically available from monitoring wells at NAPL sites. Model input also includes the dispersivity which is a correlation parameter for dispersion that varies with soil type, scale and heterogeneity. Dispersivity has been exhaustively studied for decades. In the dissolution model context, dispersion refers to hydrodynamic dispersion; equivalent to diffusion enhanced by irreversible mixing (Molz 2015) as compared to large scale plume dispersivity associated with soil heterogeneity. In interpretive mode, the volume-averaged model output can be compared with measured mass discharge from the NAPL sources and adjustments made to the NAPL source parameters (i.e., dimensions, saturation) and/or other coefficients (i.e., exponent, irreducible water saturation) to match the observed data and identify controlling processes.

Table 2.3.1. Data and Methods for Developing Conceptual Source Model for SCARPÉ Framework Field Applications

Model Parameter	Field Data for Interpretation	Method of Interpretation / Data Source
NAPL source zone height and width, i.e., projected area to flow	• Geologic logs • Downgradient transect groundwater concentrations • Direct push technology (DPT) concentration data	• Thicknesses of sand intervals in geologic logs • Transect width for contaminant detection • Numerical transport modeling including dispersion • Thickness and width of elevated contaminant detections
NAPL source zone length in flow direction	• DPT concentration data	• Length of elevated contaminant detections
Darcy velocity	• Groundwater gradients • Hydraulic conductivities	• Values in site investigation reports
Porosity	• Laboratory measures of soil samples	• Values in site investigation reports
Mobile (Permeable) fraction of the source zone	• Geologic logs	• Thicknesses of sand, silt and clay intervals in geologic logs of the source zone
Retardation coefficients	• Porosity, soil organic carbon content, bulk density, and contaminant octanol-water partitioning coefficients	• Values in site investigation reports • Standard literature values for chemical properties
Dispersivity (tangential)	• Soil type, scale and heterogeneity	• Default value of 0.001 meter
Gamma exponent	• Estimated NAPL saturation • Estimated NAPL architecture	• Values expected to fall between theoretical values of 0.5 (pool) and 0.67 (ganglia) • Can be used as a fitting parameter with discharge concentration measurements
Initial DNAPL mass	• Historical release records • Estimated NAPL source zone dimensions • Literature values for NAPL saturation in differing soil types • DPT concentration data	• Estimates of total NAPL release provided in site investigation reports • Range of calculated initial mass based on source zone dimensions, porosity, and literature saturations • Professional judgement based on DPT concentrations and refinement using initial model output
Initial DNAPL architecture	• Geologic logs • Downgradient transect groundwater concentrations • DPT concentration data	Professional judgement based on • DPT concentrations • Potential for pooling based on geologic logs • Refinement using initial model output encompassing the full life cycle of the source zone and remediation efforts

For various example conditions and scales, the power law exponent γ of the general dissolution model Eq. (2-15), which represents the diminishing surface area for ganglia and pool dissolution associated with mass reduction, is relatively constant. Theoretically, an exponent of 0.67 relates to changes in the projected flow area through dissolving spheres (ganglia) while an exponent of 0.5 relates to a diminishing tangential area for pool dissolution (pool length is decreasing) (Stewart et al., 2022).

Ganglia zones are expected to deplete more rapidly than pool zones, therefore, with limited data, a default selection of 0.5 for the exponent would be recommended. As described above, the life of a NAPL source is generally governed by the coefficient in Eq. (2-15). The exponent has a secondary effect on this life through a strong influence on the shape of the tail, decreasing or increasing the overall life. The coefficient in Eq. (2-15) includes variability with diminishing mass through the relative permeability and this variability was shown to be integral to modeling multi-component and multi-rate mass transfer.

2.3.2 Enhancement Factors for Remedial Processes

In general, remedial processes are intended to reduce the mass of contaminant in a source zone and thereby reduce the concentration of contaminant in groundwater and decrease the rate of mass discharge from source zone. Processes to enhance dissolution and accelerate mass removal fall into four broad categories as described in Section 2.2.6,

- Increases in flow through the source zone with capture and/or destruction of the contaminant, e.g., pump-and-treat;
- Introduction of reactants to destroy or degrade aqueous phase contaminants, e.g., enhanced biological degradation,ISCO;
- Introduction of chemicals to increase the effective NAPL solubility, e.g., co-solvents; and
- Introduction of energy to increase the temperature of the source zone and promote increases in a number of transport processes.

Specific remedial technologies involve some combination of these categories with increases in flow during injection of an amendment or energy or the sequential application of these processes. The most common remedial technologies are listed in Table 2.3.2 along with general estimates and references from Section 2.2.6.

For biological processes, native conditions are not expected to yield a significant increase in NAPL dissolution rates. Biological degradation is based upon the existence of a microbial community to mediate transformation of dissolved contaminants. Chlorinated and aromatic hydrocarbons of environmental interest, such as trichloroethylene and benzene, respectively, have aqueous solubilities that yield relatively high concentrations in the proximity of NAPL. These concentrations inhibit microbiological activity, i.e., the concentrations are often toxic to naturally occurring microorganisms. Instead, microbial degradation of these more soluble compounds is expected to occur primarily at a distance where concentrations are flow attenuated and do not impact the concentration gradient for dissolution. Biological enhancement to dissolution has been observed in the laboratory with specialized microorganisms (Yang and McCarty, 2002) but conditions promoting this degradation must be monitored and maintained over time. The observed enhancement under ideal conditions was on the order of two to three. A theoretical estimate for the enhancement was only 1.3 (Seagren and Becker, 2015). These results and others suggest the primary benefit of promoting biological degradation in the source zone is to reduce the mass of contaminant discharged into the aquifer. To the authors knowledge, no field studies exist documenting an enhancement to NAPL dissolution attributable to increased biological degradation rates in the aqueous phase. For conditions where aqueous diffusion of components away from the NAPL is the primary mechanism of mass depletion, a biological enhancement is more likely.

Such conditions occur where the NAPL resides in low permeability material or aquifers with very low velocities.

Table 2.3.2. Guidance for Estimating Enhancement Factors for Remedial Processes for SCARPÉ Framework Field Applications

Remedial Process	Enhancement Factor	Guidance for Estimates
Groundwater Extraction Upgradient Injection (flushing)	Flow enhancement factor, E_f, which is referenced to the natural velocity of groundwater through the source zone (Section 2.2.6.1 and Eqns. 2-39)	• Calculated based on extraction (or injection) flow rates • Numerical flow modeling to estimate velocity increase in source zone with extraction (or injection)
Enhanced Bioremediation	Dissolution enhancement factor from reaction-induced gradient, E_r (Section 2.2.6.2)	• 2 to 3 (Yang and McCarty, 2002) • 1.3 (Seagren and Becker, 2015)
ISCO	Dissolution enhancement factor from reaction-induced gradient, E_r, (Section 2.2.6.2 and Eqn. 2-44)	• ~10 to 50 Cussler (1992) and Siegrist et al. (2011) • MacKinnon & Thomsen (2002) • Schnarr et al. (1998)
Enhanced Solubilization	Solubility enhancement factor, E_s (Section 2.2.6.3 and Eqn. 2-46)	• 10 to 500 • Saenton and Illangasekare (2013) • Wang and Brusseau (1993) • McCray et al. (2000), Carroll and Brusseau (2009), and Demiray et al. (2021) for cyclodextrin
Thermal	Thermal dissolution enhancement	• ER-200719 (Macbeth et al., 2012) • Imhoff et al. (1997), Johnson et al. (2010) and Popp et al. (2016)

For ISCO, enhancement factors on the order of 10 to 50 can be derived for permanganate from Eqn. (2-45) and the data from Heiderscheidt et al. (2011) and MacKinnon and Thomsen (2002). Similarly, a reactive enhancement on the order of 10 can be derived for persulfate from the data of Schnarr et al. (1998). However, reaction products can also inhibit dissolution as described in the model demonstration of Section 5.4.3. Enhanced solubilization factors vary widely with the agent and methodology (e.g., surfactant, co-solvent, complexing agent) and range over orders of magnitude. Thermal enhancements in the aqueous phase are expected to be modest as described in Section 2.2.6.4.

2.4 ADVANTAGES AND LIMITATIONS OF THE TECHNOLOGY

Numerous DoD sites have endured a source reduction effort implementing a number of remedial technologies. The residual source is now a focus for follow-on evaluation and efforts to craft a path forward. A critical piece of knowledge is the residual NAPL architecture and accessibility, and determination of the impact additional remedial efforts may have on source control, reducing the timeframe, and/or the length of the dissolved plume. The spatially-averaged modeling methodology facilitates this evaluation and planning in a scientifically defensible and cost-effective approach.

2.4.1 Advantages Compared to Other Existing Technologies

Existing screening models consider a NAPL source zone as a single homogenized block with a focus on the downgradient dissolved plume and changes in the plume if the source term were reduced by an unspecified technology. Models, such as SCOToolkit developed under SERDP projects ER-1611 (Parker et al., 2011) and ER-2310 (Parker et al., 2017), generally employ a single parameter empirical power law model (PLM) (Rao et al., 2001; Falta et al., 2005) to describe field-scale NAPL dissolution and mass depletion. However, this screening level approach is overly simplified resulting in overly optimistic cleanup expectations. While conceptually appealing, it lacks conformance to field results and is rarely utilized for decisions regarding the final outcome for remediation of a NAPL impacted site especially with multi-component NAPL mixtures. The PLM with its single depletion exponent empirically relates aqueous discharge concentrations or mass flux to the mass remaining in the source zone relative to an assumed initial mass. The model lacks a meaningful physical interpretation and therefore lacks a pathway for further development. Studies have endeavored to demonstrate a linkage (Parker and Park, 2004; Christ et al., 2006; Marble et al., 2008; Christ et al., 2010; Abriola et al., 2013; Wood et al., 2009) to field parameters using numerical simulations, laboratory testing, and field test methods; however, the focus was on determining the pre- and post-remediation status of the downgradient solute plume rather than remediation of the NAPL. Similarly, Project ER-1614 (Brusseau et al., 2013) performed laboratory testing with mixed NAPL architecture and heterogeneous soils and attempted to mitigate discrepancies in the PLM by developing a correlation for the PLM empirical parameter based on a varying ganglia-to-pool ratio. Project ER-1613 (Annable et al., 2017) reviewed site data to link source mass discharge to NAPL mass depletion using both the PLM and the equilibrium streamtube models, before and after remediation, with limited applicability to remedial decisions.

Another alternative is the use of comprehensive numerical models for the simulation of solute transport or multiphase flow for predicting long-term effects of source treatment. This second option requires a well-calibrated site model of groundwater flow and solute transport, and a challenging number of site-specific parameters and assumptions. As a research tool, these simulators are used to discern the contributions of various coupled mass transfer processes (Yang et al., 2018) in a system of complex NAPL architecture and for upscaling empirical mass transfer correlations from bench-scale tests to the discretization scale of numerical models (Saenton and Illangasekare, 2013). First-order mass transfer between residual NAPL and groundwater is an option available in a number of MODFLOW-based transport models (e.g., RT3D, SEAM3D) and multiphase flow simulators (e.g., TOUGH family, UTCHEM, DNAPL3D-RX). However, modelers rarely employ these complex options for designing or evaluating aggressive remedial processes, and mass transfer coefficients are empirical and dependent upon the scale. If numerical modeling is performed, practitioners commonly assume equilibrium in grid blocks that contain NAPL yielding excessively optimistic predictions. To mitigate the equilibrium assumption, numerical modelers can implement ultra-fine grids, but the number of required nodes can reach millions (Falta, 2003) making input requirements intractable and solution methods unstable.

In contrast, the volume-averaged model is shown to provide accurate mass discharge predictions from DNAPL sources with limited information as well as provide interpretation of complex, multi-stage source zone discharge data without detailed numerical transport modeling (Sections 5 and 6).

Importantly, the volume-averaged model can rapidly generate reasonable estimates for NAPL source lifespans to support risk assessment and remedial decision-making. In addition, the volume-averaged model can easily be used to assess the sensitivity of the mass discharge and/or NAPL source lifespans to a range of parameters and support identification of the controlling processes. This information can be used to guide additional site investigations to help reduce modeling uncertainty or optimize remedial efforts. The demonstrated adaptability of the modeling approach to varying dimensional scales and increased characterization of smaller scale heterogeneities suggests the approach is also amenable to implementation within more complex numerical transport models.

2.4.2 Overview of Advantages

Advantages to the approach include site-specific applicability to:

- Rapid assessment of multiple technologies given a modest level of site-specific characterization data and desired endpoints,
- Multi-component NAPL including sites with multiples sources,
- Assessment of the benefit of targeted remediation of discrete NAPL accumulations, i.e., are all accumulations equal?
- Assessment of remediation of contaminant source zones in complex geological environments that cause persistent groundwater plumes and are prohibitive to collecting data sufficient for detailed numerical modeling,
- Assessment of combining existing or new technologies to address complex contaminated sites and make informed decisions on transitions from active remediation to passive technologies,
- Evaluation of sites where detailed numerical models exist; the volume-averaged model provides a management (or regulatory) level validation of output as well as facilitating a transparent discussion on assumptions regarding field conditions and technology performance, and
- Reframing and simplifying complex mathematical models to provide a practical, systematic progression of first order calculations accessible to the average engineer for evaluating remedial performance from selection and design through transition to a final remedy.

Advantages to DoD RPMs and other site managers include:

- Promoting a common understanding among team members of relationships between site characteristics and realistic assessment of remedial outcomes,
- Defining technically sound remedial performance objectives and timeframes,
- Ability to evaluate changed site conditions on a project management level by defining dominant site characteristics for remediation, and
- Ability to continually assess remedial progress and divergences with a practical, adaptive modeling approach.

2.4.3 Overview of Limitations

While the volume-averaged model can provide accurate mass discharge predictions from NAPL sources, it is based on several simplifying assumptions resulting in limitations to some field applications, including:

- The model assumes NAPL is immobile and potential for partial re-mobilization of the NAPL mass during dissolution cannot be accounted for.
- Soil heterogeneity within the source zone volume used for averaging is expected to degrade the model applicability, although modifications to the dissolution model can provide approximations.
- The volume-averaged model is not intended to model initial breakthrough curves precisely because of volume-averaging in the source zone. The averaging in the volume-averaged model is expected to yield a lesser peak concentration and to lag the time of the actual breakthrough peak.
- The results do not provide spatial specificity, such as simulating concentration history at a specific well location or compliance point, which may require additional calculations/estimates to use such data as calibration data and/or to estimate concentrations at specific well location under different remedial alternatives.

Finally, as with all models, limitations in available data for characterizing the source zone directly limit the representativeness of the results; however, the SCARPÉ framework is designed to be adaptable for accepting an increased resolution of input data, e.g., an increased number of defined mass accumulations and characterization of fine-grained lenses.

3.0 PERFORMANCE OBJECTIVES

The primary performance objective is to demonstrate the ability of volume-averaged modeling to produce effective site-specific output for making remedial decisions. The output is expected to be comparable to detailed numerical simulations but at a fraction of the effort and with the inclusion of complex remediation models. The assessment of this objective included a comparison of output with other analytical models and numerical simulations, validation using field data, and feedback from stakeholders on the utility of the model for decision-making. Table 3.1 summarizes the performance objectives, data requirements, criteria for success, and results during this demonstration.

Table 3.2.4.1. Performance Objectives

Performance Objective	Data Requirements	Success Criteria	Results
Quantitative Performance Objectives			
Validate with Published Studies	Volume-averaged model input (Section 2.3.1) Simulation or experimental results of volatile organic compound (VOC) source discharge concentration, mass flux, or total mass	Ability to simulate output or measured data quantified by a relatively low root mean square error (RMSE). Maximum relative RMSE values for success are: • Idealized numerical model < 0.2 • Laboratory experiments < 0.4 • Controlled field studies < 0.6 • Remedy implementation < 0.9 Semi-quantitative match of temporal trends/changes in concentrations or fluxes are successful if: • Inflection points match • Slopes of contaminant trends match	RMSE << objectives (See Section 6.1.1): • Idealized numerical model: 0.037 – 0.085 • Laboratory experiments: 0.052 – 0.091 • Controlled field studies: 0.12 – 0.23 • Remedy implementation < 0.86 Successful comparison of concentration discharge curves (slopes and inflection points)
Validate at Modestly Complex Site	Site characterization data to assemble volume-averaged model input (Section 2.3.1) Remedy-specific data Observed pre- and post-treatment VOC source discharge concentration (or mass flux estimates)	Error associated with volume-averaged model results are: • less than or equal to one order of magnitude of observed data, and • within the order of the error associated with the numerical modeling and observed data.	RMSE << objectives (See Section 6.1.2): • Comparison with observed data: 0.12 • Comparison of decay rate with numerical modeling: 0.09
Validate at Complex Site	Same as Modestly Complex Site.	Same as Modestly Complex Site.	Statistical comparisons not performed (See Section 6.1.3)
Qualitative Performance Objectives			
Implementation and Ease of Use	Feedback from stakeholders on applicability, ease of use, and data requirements	Respondents can successfully complete source control assessments.	Feedback was solicited from practitioners and their feedback indicated that they were able to use the practical tools for the template scenarios
Efficacy for Supporting Managerial Decisions	Feedback from stakeholders on the utility, reliability and anticipated acceptance of model results	Respondents consider the model results to be useful in achieving overall life cycle goals.	DoD RPMs, regulators and stakeholders feedback following applications to the two demonstration sites indicated that the SCARPÉ results enabled them to better understand NAPL dissolution and impacts of potential remedial strategies

For the three quantitative performance objectives listed in Table 3.1, the site-specific and remediation-specific data requirements are very similar for the approach being demonstrated. The basic data input for the modeling are illustrated in Figure 2.3.1 in Section 2.3.1 and are typically known, estimated or site-calibrated quantities, as described in Table 2.3.1. Remediation technology input is process-centric on reactions as outlined in Section 2.2.6 and the NAPL mass transfer coefficients are specific to the technology and scale of field implementation.

3.1 PERFORMANCE OBJECTIVE: VALIDATE WITH PUBLISHED STUDIES

This quantitative performance objective was used to validate the volume-averaged approach to evaluating NAPL source zone mass discharge during and after application of various remedial processes. The model estimates of mass discharge and mass remaining were compared to published studies, including synthetic numerical modeling results, laboratory experiments, and controlled field experiments. This assessment demonstrated that the volume-averaged modeling, with a limited amount of computational effort and site data, can adequately replicate complex numerical modeling results for NAPL remediation decisions.

The validation also included evaluation of the suitability of existing models of NAPL remediation for inclusion in the volume-averaged framework. Remedial processes implemented in the model (Section 2.2.6) were compared to controlled studies of source zone mass reduction.

3.1.1 Data Requirements

Data from four published studies were used to validate the volume-averaged model. Data included simulated (for synthetic numerical modeling study) and measured discharge concentration-time curves downgradient of the source zones. Data also included numerical or experiment setup information (e.g., NAPL volume releases, flow velocity).

3.1.2 Success Criteria

For each of the results in the published studies, a plot was generated to compare the volume-averaged modeling concentrations and the measured (or modeled numerically) source discharge concentrations. Quantitative success criteria specific to this performance objective were: (1) ability to simulate output or measured data quantified by a low relative RMSE that varies with the complexity of the problem as delineated in Table 3.1; and (2) achieving a semi-quantitative match of temporal trends/changes in concentrations (Table 3.1).

3.2 PERFORMANCE OBJECTIVE: VALIDATE AT MODESTLY COMPLEX SITE

The application of the volume-averaged model was demonstrated at a well-documented field site, Site 11 Naval Submarine Base (NSB) Kings Bay, described as a modestly complex site. Remedial history at this site includes pump-and-treat for containment and then source reduction, followed by ISCO and enhanced bioremediation applied in the NAPL source zone, followed by monitored natural attenuation (MNA) documented by the US Geological Survey (USGS).

Statistical analyses and parameter sensitivities were performed to assess the comparability of quantitative results for differing levels of detail in the volume-averaged approach.

3.2.1 Data Requirements

The demonstration was performed by compiling site data, including remedy-specific data, from available published reports to generate a conceptual source model that was translated into modeling input for the volume-averaged model.

3.2.2 Success Criteria

A plot was generated to compare the volume-averaged modeling concentrations and the measured source discharge concentrations, including periods with multiple remedial activities. Quantitative success criteria specific to this performance objective were: (1) ability to simulate measured source discharge concentrations within one order of magnitude; and (2) ability to provide results of similar accuracy (similar error) as numerical model outputs.

Additional success criteria specific to this performance objective were to achieve a semi-quantitative match of temporal trends/changes in concentrations and discharge mass rates to observed inflection points and decay slopes.

3.3 PERFORMANCE OBJECTIVE: VALIDATE AT COMPLEX SITE

The application of the volume-averaged model was demonstrated at a well-documented field site, Site ST012 at the Former Williams Air Force Base (AFB), described as a complex site. Remedial history at this site includes pump-and-treat, followed by MNA combined with natural source depletion, thermal treatment, and on-going enhanced bioremediation in the source zone.

A calibrated numerical model of NAPL dissolution and solute transport was developed and applied before and after a pilot test of steam enhanced extraction (SEE) in the source zone under ESTCP Project ER-200833 (Kavanaugh et al., 2011). A recent full-scale application of SEE provided new site data for assessing NAPL source depletion during SEE and post-remediation source depletion and discharge.

3.3.1 Data Requirements

See Section 3.2.1.

3.3.2 Success Criteria

See Section 3.2.2.

3.4 PERFORMANCE OBJECTIVE: EASE OF IMPLEMENTATION

This qualitative performance objective is the first of two to address Technical Objective 4. After establishing the technical validity of the modeling approach as an alternative to more complex numerical modeling, its use for supporting remedial decisions was assessed. A first step was determining the ease of implementation, required minimum background data and knowledge, and any training or support needs.

3.4.1 Data Requirements

To evaluate this objective, beta versions of the two practical tools developed for this project (Section 2.2.7) were provided to a select group of testers. The testers included a mix of remedial project managers, regulators, practitioners, and remedial subject matter experts. The testers were provided template scenarios (laboratory experiment [Section 5.4.1] and Site 11 [Section 5.5.1]) to implement and explore and asked to perform modeling at sites of their interest. A workshop was also conducted in September 2022 with practitioners and remedial subject matter experts to present the SCARPÉ framework and demonstrate the implementation of the practical tools. Feedback from testers were obtained through a questionnaire with multiple-choice questions regarding implementation of the modeling and direct feedback during the workshop.

3.4.2 Success Criteria

The objective was considered met as members of the test group could successfully implement the model for the template scenarios without extensive additional training or background information. Success was also assessed based on receiving positive feedback regarding individual, site-specific implementations including recommendations for model improvements and identification of difficulties during implementation.

3.5 PERFORMANCE OBJECTIVE: EFFICACY FOR SUPPORTING MANAGERIAL DECISIONS

This qualitative performance objective also addresses Technical Objective 4. After assessing the ease of implementation, this objective considers the utility and acceptance of the model output for managerial decisions. Assessment questions included: is the approach capable of utilizing the same NAPL architecture, hydrogeology, and other conceptual site model data as input for differing remedial processes? Does the method adequately evaluate combined or sequential remedial technologies? Are remedial timeframe projections sufficiently accurate and distinct for different remedial scenarios? Will the regulatory community provide significant weight to the model results in supporting remedial decisions? Would the inclusion of probabilistic analyses improve the utility of output? Overall, does the model serve as an improved tool to support remedial decision-making at sites, including transition to a passive management-based approach?

3.5.1 Data Requirements

To evaluate this objective, the SCARPÉ framework was applied to the two demonstration sites, and used to evaluate potential remedial technologies for additional treatment. The results were presented to the RPMs, regulators, and stakeholders and feedback was obtained through direct communication, questions, and contact.

3.5.2 Success Criteria

The objective was considered met as feedback indicated that the results of the SCARPÉ framework could support remedial decision and were useful in achieving overall life cycle goals.

4.0 SITE DESCRIPTION

4.1 SITE SELECTION

The second and third quantitative Technical Objectives involve model validation and demonstration at well-documented field sites described as "modestly complex" and "complex" in the Site Selection Memorandum (SSM). The term "complex" is relative and refers to site characteristics (hydrogeology, source zone, etc.) in relation to other contaminated sites. The two selected sites in the SSM were 1) Site 11 at the NSB Kings Bay, Georgia; and 2) Site ST012 at the former Williams AFB, Arizona, respectively. Site 11 at the NSB Kings Bay is a modestly complex site for validating the second quantitative Technical Objective. Site ST012 at the former Williams AFB is a complex site for validating the third quantitative Technical Objective.

Each site used in this demonstration has the following characteristics:

- Sufficient documentation is available to confirm or modify previously developed conceptual site models (CSM).
- Historical data sets of observed discharge mass and concentration-time curves downgradient of source zones are available for evaluating the performance objectives.
- Site remedial history includes a variety of remedial processes such as pump-and-treat, ISCO, or a combined remedy.
- The historical data sets include condition prior to, during, and after application of various source zone remedial technologies.

Table 4.1.1 lists the site selection criteria and the characteristics of the two sites for demonstrating and validating the second and third quantitative Technical Objectives of the project. These sites have complexities encompassing a wide range of heterogeneities in hydrogeology and NAPL architecture. The two sites meet the criteria of primary importance regarding the extent of available site information:

- Application of multiple full-scale remedial technologies in the source zone;
- Availability of a site-specific, calibrated numerical model for groundwater flow and solute transport; and
- Access to sufficient remedial and compliance data to complete technology evaluation vis-à-vis the project performance objectives.

The two sites also meet the criteria of secondary importance:

- Robust and potential high resolution site characterization data to adequately describe site hydrogeology;
- Sufficient data including site reports to evaluate natural attenuation preceding source reduction; and
- Reports that provide well-documented historical remedy selection.

Table 4.1.1. Site Selection Criteria

Parameter	Preferred Value(s)	Relative Importance (1-5, with 1 being highest)	Site 11, Naval Submarine Base, Kings Bay, GA	Site ST012 Former Williams AFB, AZ
NAPL presence and delineation of NAPL mass and architecture	Sufficient data to delineate initial NAPL architecture as ganglia or pool and to estimate the total initial NAPL masses and saturations	1	High PCE concentrations indicative of NAPL	Visual observations of NAPL
Extensive set of high quality geologic logs	Sufficient data to assess fraction of source zone soil volume as mobile zone (e.g., sand) or immobile zone (e.g., silt, clay); Advective fraction (f_m) > 0.2	2	Primary unit is a single layer comprised of permeable sand, therefore less complex	Multiple boring logs in source zone at each depth interval; Sand dominated permeable layers
Comprehensive hydrogeologic data	Hydraulic conductivities from pumping tests Average ambient pore groundwater velocity > 100 feet/year	2	Detailed reports available; Range of pore velocities (25 - 95) confirmed by tracer	Detailed test reports available; Range of pore velocities (130 - 300) determined by calculation
Existing site-specific, calibrated numerical model availability	Includes estimates of average source discharge concentration and source longevity.	1	Yes; See Chapelle et al. (2007)	Yes; ER-200833; however, site conditions have changed
Evaluation of natural attenuation preceding source reduction	Includes estimates of biological degradation with complexity exceeding first order degradation constants.	2	Yes; Chapelle and Bradley (1999)	Yes; BEM Systems (2000)
Full-scale application of multiple source reduction technologies	Should include time series of mass removal and remedial conditions and post-removal assessment of source discharge concentration	1	Pump-and-treat; ISCO; enhanced bioremediation (Chappelle et al., 2005)	Pump-and-treat; thermal; enhanced bioremediation (Williams AFB Admin Record)
Access to current site data	Site management and regulators agree to cooperate	1	Yes	Yes
Documented remedial decisions and pending site remedial decisions	Documentation of two previous decisions and pending decision within the next 18 months	3	Site is currently in long-term monitoring, active remediation complete, documentation available	Records of decision and explanation of significant differences; New site contractor and new remedial approach started Winter 2020

4.2 SITE LOCATION AND HISTORY

The two sites identified for validating the second and third Quantitative Performance Objectives (Table 3.1) are described in greater detail below.

4.2.1 Site 11, NSB Kings Bay, GA

NSB Kings Bay occupies 16,168 acres in Camden County, Georgia in the southeastern corner of Georgia, approximately 8 miles north of the Georgia-Florida state line (Figure 4.2.1). Currently, the base supports submarines, crew training, weapons handling and storage, submarine maintenance, and associated personnel. Site 11, part of the Old Camden County Landfill, is located along the northwestern boundary of the base and is approximately 1,400 feet long, 600 feet wide at the southern end, and 800 feet wide at the northern end. The landfill was operated by Camden County as a municipal solid waste landfill from 1974 to 1981. Municipal waste was disposed into excavated trenches. The landfill ceased operations in October 1981 and was covered with 2 feet of fill (Chapelle et al., 2005). The site is currently vegetated with grass, weeds, and pine saplings.

At least two PCE disposal events occurred during landfill operations, resulting in groundwater contamination by two DNAPL source zones (Chapelle and Bradley, 1999). The initial remedial strategy was a pump-and-treat system that operated from 1994 through 1999 to prevent off-site plume migration. ISCO was then implemented at the site using Fenton's reagent (solution of hydrogen peroxide and ferrous iron) in four remedial events between 1998 and 2001 (Chapelle et al., 2005). Following ISCO treatment, emulsified vegetable oil (soybean oil and potassium hydroxide) was injected into the aquifer between 2001 and 2002 to promote enhanced bioremediation (Chapelle et al., 2005). Given the natural bio-geochemical conditions of the aquifer at Site 11, natural attenuation was found sustainable and a long-term groundwater monitoring program was implemented (Chapelle et al., 2007).

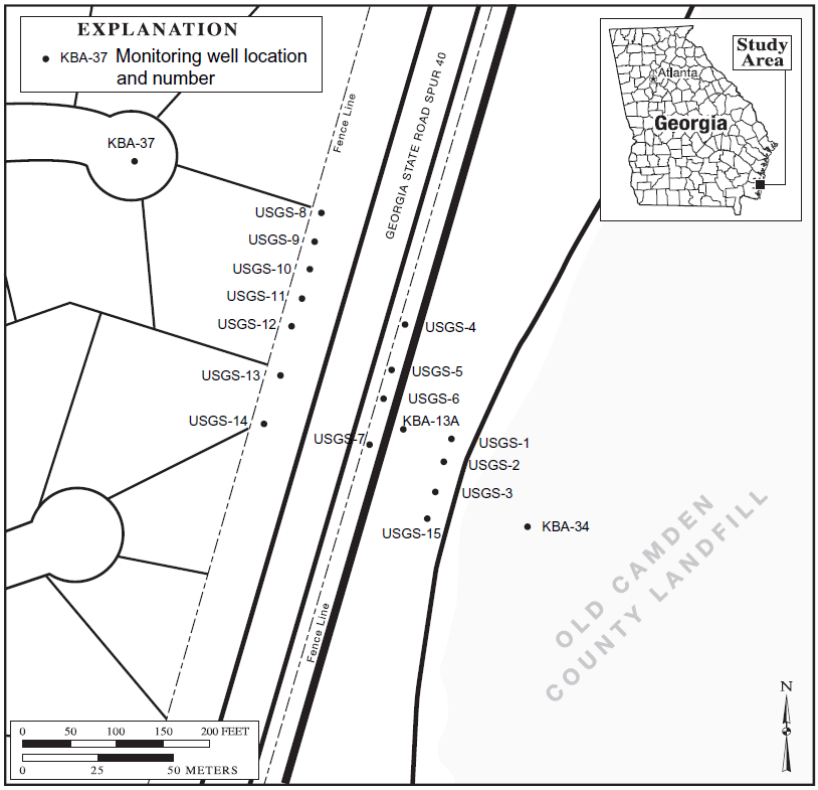

Figure 4.2.1. Map of Site 11 at NSB Kings Bay, GA (Chapelle et al., 2005).

4.2.2 Site ST012, Former Williams AFB, AZ

Originally occupying 4,042 acres, the former Williams AFB (WAFB) was constructed in Mesa, Arizona in 1941 as a flight training school. Throughout its history, pilot training was the primary mission of WAFB. A wide variety and large number of aircraft were utilized, including prop-driven and jet aircraft. Surrounding land-uses include the General Motors Desert Proving Ground, irrigated agricultural land, and commercial and residential developments. WAFB was placed on the National Priorities List in 1989 and officially closed in September 1993. The WAFB Disposal and Reuse Final Environmental Impact Statement was filed with the United States Environmental Protection Agency (EPA) in June 1994.

Site ST012 is the location of the former liquid fuel storage area, which encompasses approximately 13 acres within WAFB (Figure 4.2.2). Fueling operations were conducted at the base from 1941 until 1991. A substantial portion of the remaining cleanup at WAFB involves fuel releases at ST012. A map of Site ST012 and the footprint of the former fueling infrastructure (storage tanks, piping, pump stations, etc.) are shown in Figure 4.2.3. Soil and groundwater at ST012 have been affected by releases of jet propulsion fuel formulation 4 (JP-4). JP-4 is similar to kerosene in its makeup and is less volatile than a fuel such as automotive-grade gasoline. The primary chemical of concern in JP-4 is benzene. These releases are attributable to multiple documented fuel releases between 1977 and 1989 and other undocumented releases during base operations over a 50-year period. Estimates for the total volume released range from two to five million gallons based on historical fuel operation records and field data. All underground storage tanks (USTs) and associated fuel distribution lines were removed from ST012 in early 1991.

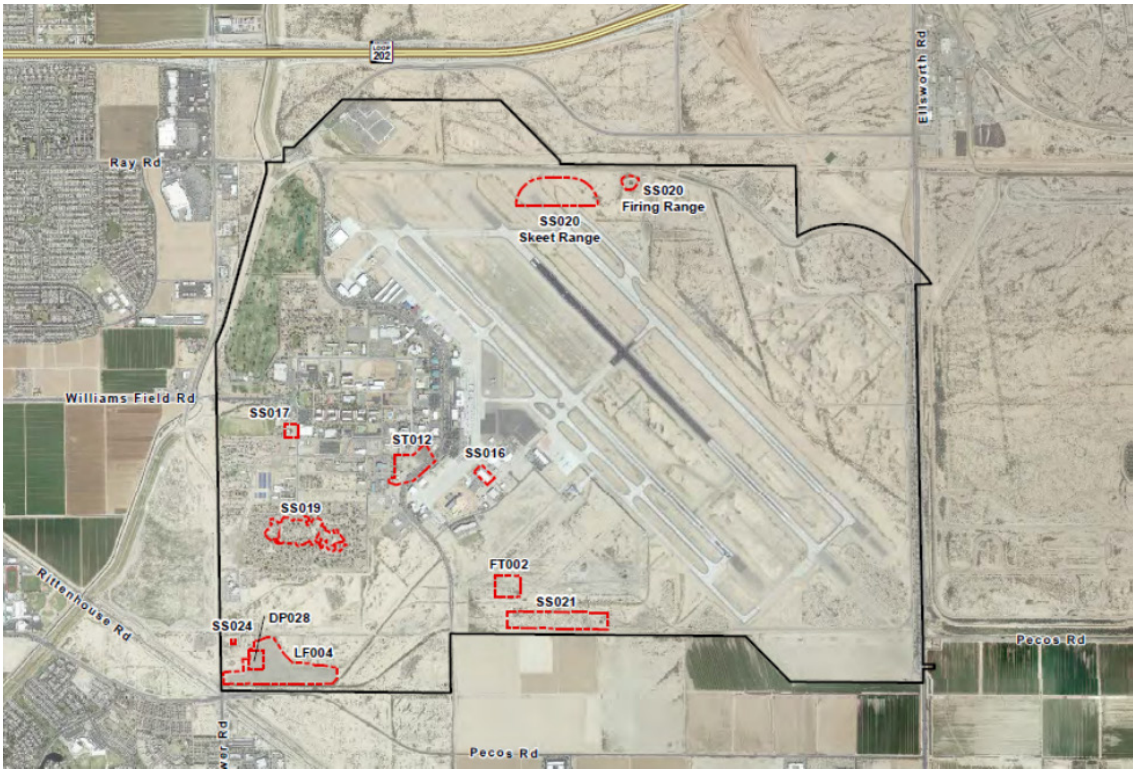

Figure 4.2.2. Location of the Former Williams AFB and Site ST012

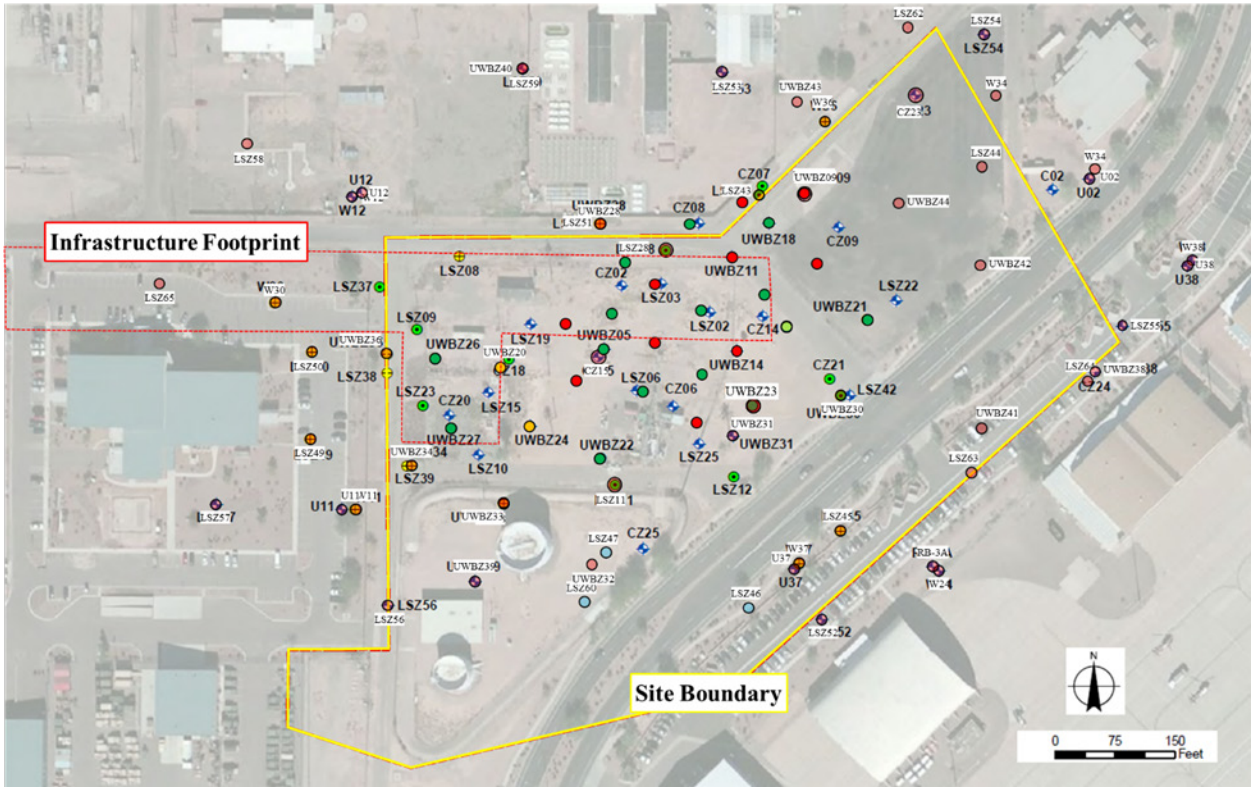

Figure 4.2.3. Map of Site ST012 and the Footprint of Former Fueling Infrastructure

A number of investigations and remediation activities have been conducted at ST012 over the past three decades (BEM Systems, 2007). Investigations have revealed fuel contamination, including NAPL, in the vadose and saturated zones. In the vadose zone, soil vapor extraction (SVE) was initiated in 1994, expanded in 2005, and continues to operate. Through November 2021, SVE has removed hydrocarbon mass equivalent to approximately 750,000 gallons of JP-4 and promoted in situ degradation with a continual draw of atmospheric air into the vadose zone.

A corrective action remedy for groundwater at ST012 was specified in a ROD dated December 1992. The remedy involved the installation of two horizontal wells for incorporation into a system that was to include groundwater extraction, air stripping, and injection or reuse of the treated water. The horizontal wells were installed during July 1992 and May 1994. Subsequent testing of the wells showed that they were not effective for extracting significant quantities of groundwater or NAPL. MNA was evaluated in multiple field and modeling efforts. The Air Force and regulatory agencies concurred that the selected remedy of pump and treat using the constructed horizontal wells would not be effective for achieving a reasonable remedial action objection in the saturated zone in 2002 but did not agree that MNA was a sufficient final remedy. The anticipated duration of the NAPL persistence was unacceptable to regulatory parties and long-term liabilities were unpredictable. Therefore, all parties agreed to a full-scale, pilot test of thermal enhanced extraction (TEE) using steam injection to promote both NAPL recovery and in situ degradation.

The TEE pilot test was performed from 2008 to 2010 and ESTCP Project ER-200833 (Kavanaugh et al., 2011) studied the change in mass transfer resulting from incomplete NAPL removal and NAPL component depletion. As a result of the pilot test, full-scale SEE was implemented from 2014 to 2016 in the saturated zone after a ROD amendment in 2012. SEE removed an estimated 2.5 million pounds of petroleum compounds (equivalent to 400,000 gallons of JP-4) with approximately 212,000 gallons recovered as NAPL. Site investigations following SEE indicate approximately 400,000 gallons of residual NAPL remained in the saturated zone (Amec Foster Wheeler, 2018).

A full-scale pilot test of sulfate injection to promote anaerobic biological degradation of benzene via sulfate reduction was initiated in 2018 and continues to be evaluated. This pilot test exemplifies the complexity of the site as the evaluation is complicated by the residual heat from SEE and its dissipation, remaining areas of treated and untreated NAPL as evidenced by the appearance/disappearance of NAPL from monitoring wells both within and outside the SEE treatment zone, orders-of-magnitude changes in benzene concentration over relatively short distances, spatially sparse data collection, and inconsistent application of groundwater pumping for containment and distribution of injected sulfate.

4.3 SITE GEOLOGY/HYDROGEOLOGY

The geology and hydrogeology of the two sites for validating the second and third Quantitative Technical Objectives (Table 3.1) are described below.

4.3.1 Site 11, NSB Kings Bay, GA

The aquifer system at Site 11 is comprised by marginal marine sediments (Figure 4.3.1). Figure 4.3.1 depicts the uppermost water bearing unit, referred to as the water table zone (Leeth 1999), which is approximately 75 to 90 feet thick and is underlain by a confining layer. These surficial sediments in the unconfined aquifer section consist of fine-to-medium sized sands of aeolian origin ranging from 7 to 10 feet in thickness, where the water table typically resides varying from 3 to 6 feet below ground surface. Below these sandy sediments is a layer of organic-matter-rich sands and clays of back-bay lagoon origin. This organic-rich layer is typically 10 feet thick and is characterized by a lower hydraulic conductivity than the surficial sands. As recharge water moves downward through the organic-rich layer during and after rainfall events, dissolved oxygen is removed producing uniformly anoxic conditions in the underlying more permeable zone (Chapelle et al., 2005). The underlying semi-confined layer also consists of fine-to-medium sized sand of aeolian origin, ranging from 10 to 15 feet in thickness at depths of 30 and 40 feet below ground surface (bgs). As noted in Figure 4.3.1, this intermediate zone serves as a conduit for a chlorinated solvent plume beneath Site 11. Because this sandy aquifer unit has a higher hydraulic conductivity than the overlying semi-confining layer, groundwater flow changes from being predominantly vertical to horizontal. Thus, the semiconfined aquifer acts as a regional “drain” moving recharge water from topographic highs near the landfill to discharge areas to the west (Chapelle et al., 2007). Groundwater flow is to the west-northwest with an approximate gradient of 0.003, and estimated Darcy velocities range from 3 to 28 feet per year (Bechtel, 1999; Chapelle et al., 2007).

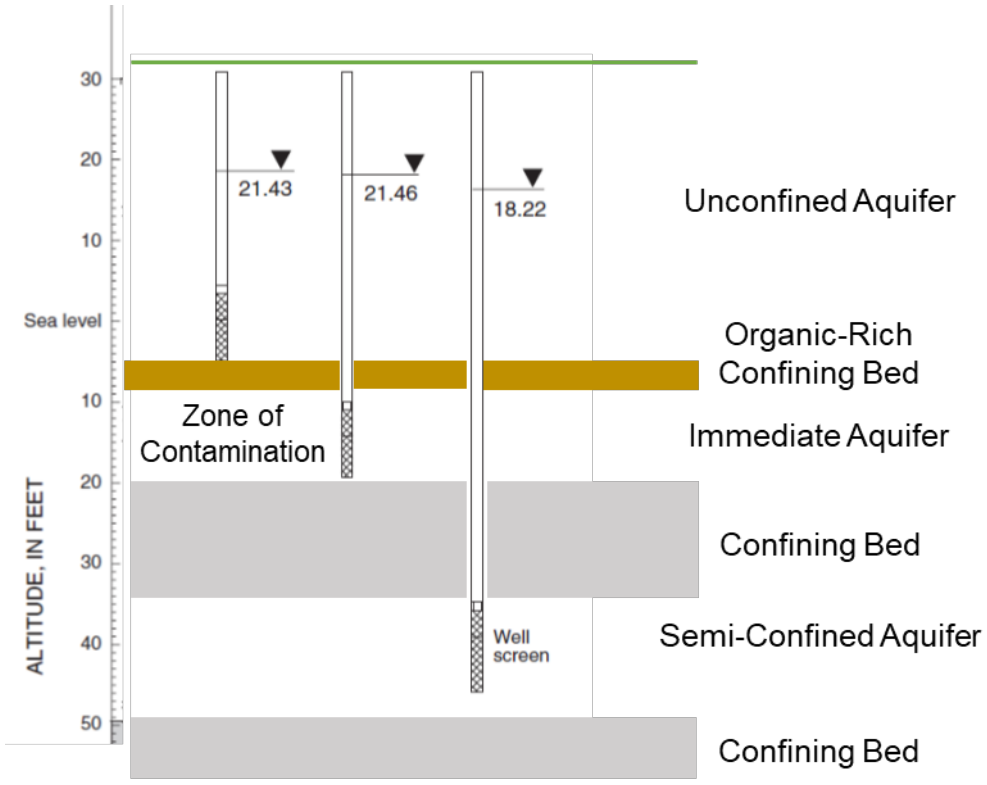

Figure 4.3.1. Hydrogeologic Cross-Section of the Kings Bay Site

4.3.2 Site ST012, Former Williams AFB, AZ

A thorough CSM describing the subsurface physical conditions of ST012 was developed by the Air Force and is available as Appendix A in the ST012 TEE Pilot Test Work Plan (BEM Systems 2007). This Work Plan provides a compilation of data from previous site investigations and describes a rise in groundwater of about 60 feet from 1990 to 2007 creating an extensive smear zone of NAPL contamination in the saturated zone. From 2007 through 2018, the water table rose more slowly and came up an additional 25 feet to approximately 140 feet bgs yielding a total NAPL smear zone thickness of about 90 feet in the upper saturated zone. This rise in the water table has created three hydrostratigraphic zones as illustrated in the conceptual cross-section provided in Figure 4.3.2. The deepest permeable interval is separated from the upper zones by a continuous low permeability clay interval. Additional data and information about the site are provided in Appendix E of this report.

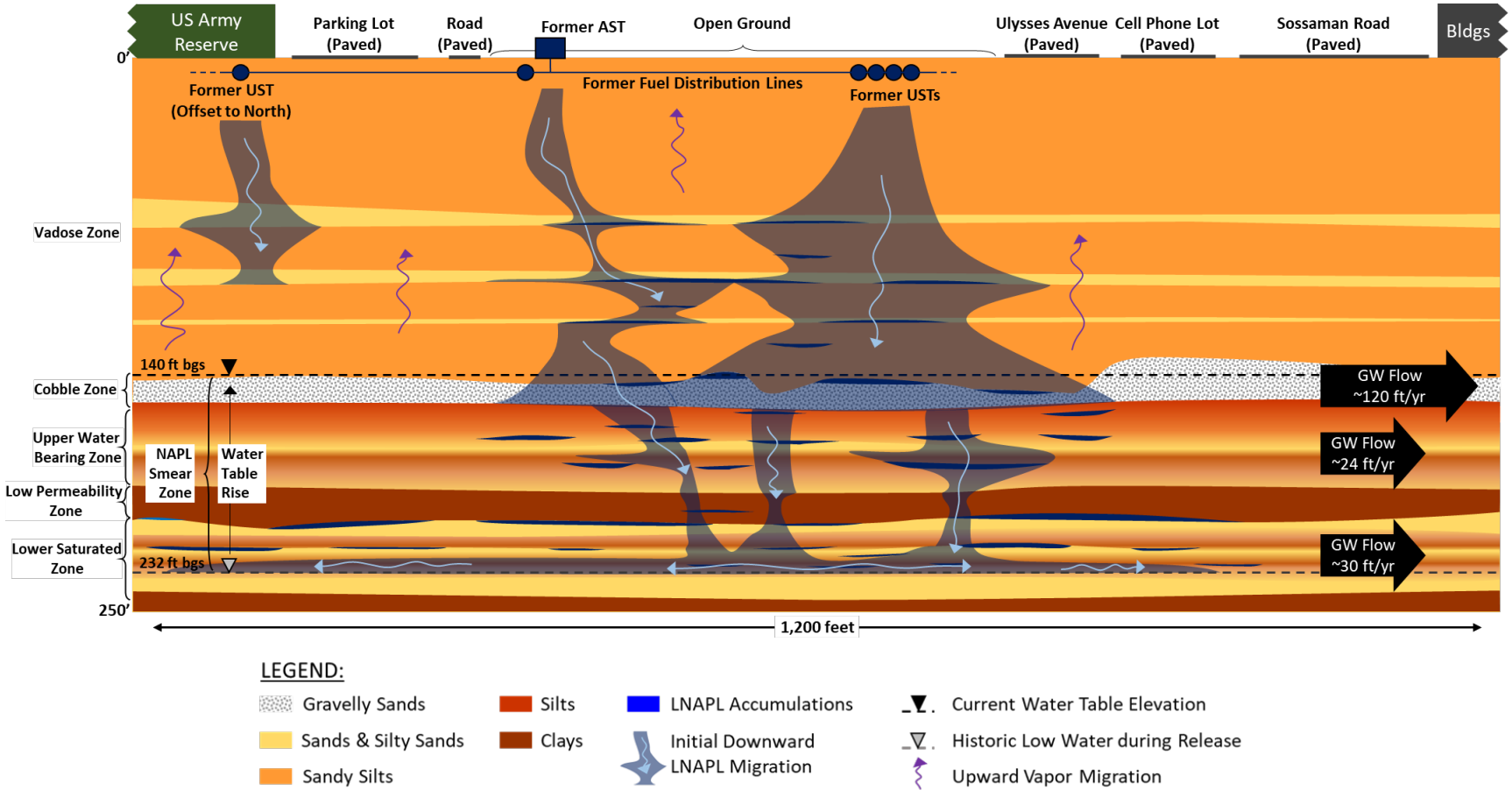

Figure 4.3.2. Summary Conceptual Model of Site ST012 Depicting the Interaction of NAPL and Geology

The vertical geologic profile (0 – 245 feet bgs) is a heterogeneous mix of alternating fine-grained and coarse-grained units. Coarse-grained units range from less than one foot to more than 20 feet thick and a few of the larger units appear to be continuous across the site. A continuous clay interval across the site is encountered at a depth of approximately 195 feet bgs and ranges in thickness from 5 to 20 feet. The geologic materials in the saturated zone have been subdivided into five main hydrostratigraphic units:

- The Cobble Zone (CZ), extending vertically from the water table (currently at approximately 140 feet bgs) to 160 feet bgs
- The Upper Water Bearing Zone (UWBZ), extending vertically from approximately 160 ft to 195 feet bgs;
- The Low Permeability Zone (LPZ), extending from approximately 195 to 210 feet bgs;
- The Lower Saturated Zone (LSZ) extending from approximately 210 to 240 feet bgs; and
- The Aquitard, occurring at approximately 240 feet bgs.

The water table has only recently entered the CZ where SVE operated from 2005 until the interval became saturated. It is expected SVE significantly depleted volatile components from NAPL in the CZ before submergence. The CZ is underlain by the UWBZ which is a heterogeneous mix of fine-grained and coarse-grained intervals with little continuity. The continuous clay interval making up the LPZ effectively separates the deeper LSZ from the shallower UWBZ. Pumping tests have shown the two zones act independently on the timescale of remediation. As a result of this independence, the mass transfer testing of Kavanaugh et al. (2011) was applied in each zone and differing remedial conditions were quantified. For modeling, the hydrogeology of the site is conceptualized as depicted in Figure 4.3.3.

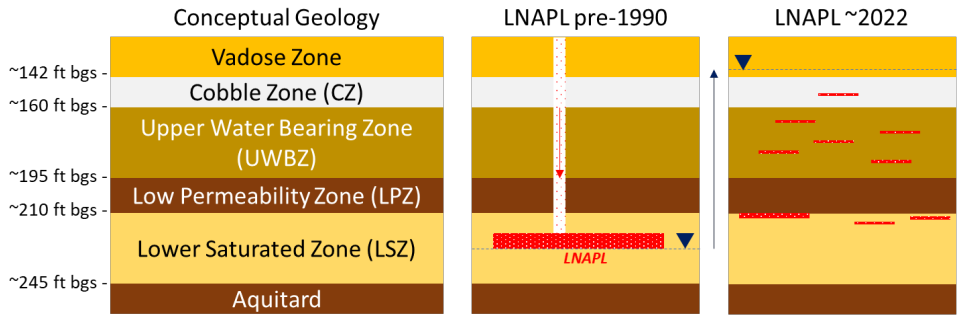

Figure 4.3.3. Conceptual Model of Site ST012 Hydrogeology

Historically, groundwater velocities at the site are very slow and consequently slow the rate of applicable natural attenuation processes. Groundwater flow direction is easterly at an average gradient of about 0.005. The LSZ groundwater flow direction before 1993 was in the southeasterly direction and therefore a gradient existed in that direction for floating NAPL to follow. The gradient gradually transitioned to a 2022 estimated northeasterly direction. Previous estimates for Darcy velocity in the CZ, UWBZ and LSZ were 125, 24 and 73 feet per year (BEM Systems, 2000). These estimates were based on hydraulic conductivity values of 70, 12.7 and 40 feet per day for the CZ, UWBZ, and LSZ, respectively, and gradients ranging from about 0.005 to 0.006.

Current average groundwater velocity and direction for each of the hydrostratgraphic units are difficult to assess because gradients across the site are relatively small, the water table is rising, and monitoring events without groundwater pumping disturbances are few.

4.4 CONTAMINANT DISTRIBUTION

The contaminant distribution at each of the two selected sites is explained below.

4.4.1 Site 11, NSB Kings Bay, GA

The disposal of PCE in the Old Camden County Landfill trenches in approximately 1980 produced two DNAPL contaminant source zones (Chapelle and Bradley, 1999). The contaminant moved downward through the organic-matter-rich confining bed and the semiconfined aquifer, forming a pool on the underlying confining bed. Horizontally flowing ground water dissolved the PCE, carrying it downgradient in the direction of a nearby housing subdivision (Chapelle et al., 2005). Because of the ambient anoxic conditions present in the semiconfined aquifer, PCE was subject to reductive dechlorination, sequentially transforming it to TCE, DCE, and vinyl chloride (VC). Each of these contaminants was subject to natural attenuation processes including advection, dispersion, sorption, and biodegradation (Chapelle et al., 2007). Concentrations of dissolved chlorinated ethenes along the axis of the plume showed that PCE and TCE predominated near the source area, and they were transformed to DCE and VC along the flowpath resulting in an extensive VC plume. Anoxic mineralization of VC was also determined as a possible natural attenuation mechanism through mass balance and modeling analyses (Chapelle et al. 2007). The estimated VC plume size circa 1992 is indicated in Figure 4.4.1 along with the approximate extent of the suspected source zone. Detailed delineations of the suspected DNAPL source zone did not occur until active remediation was underway. Multiple deployments of DPT occurred at the site and provided contaminant data in vertically discrete depths at various times between four phases of ISCO. These DPT deployments and the data collected are described in the next section with the discussion of the ISCO phases.

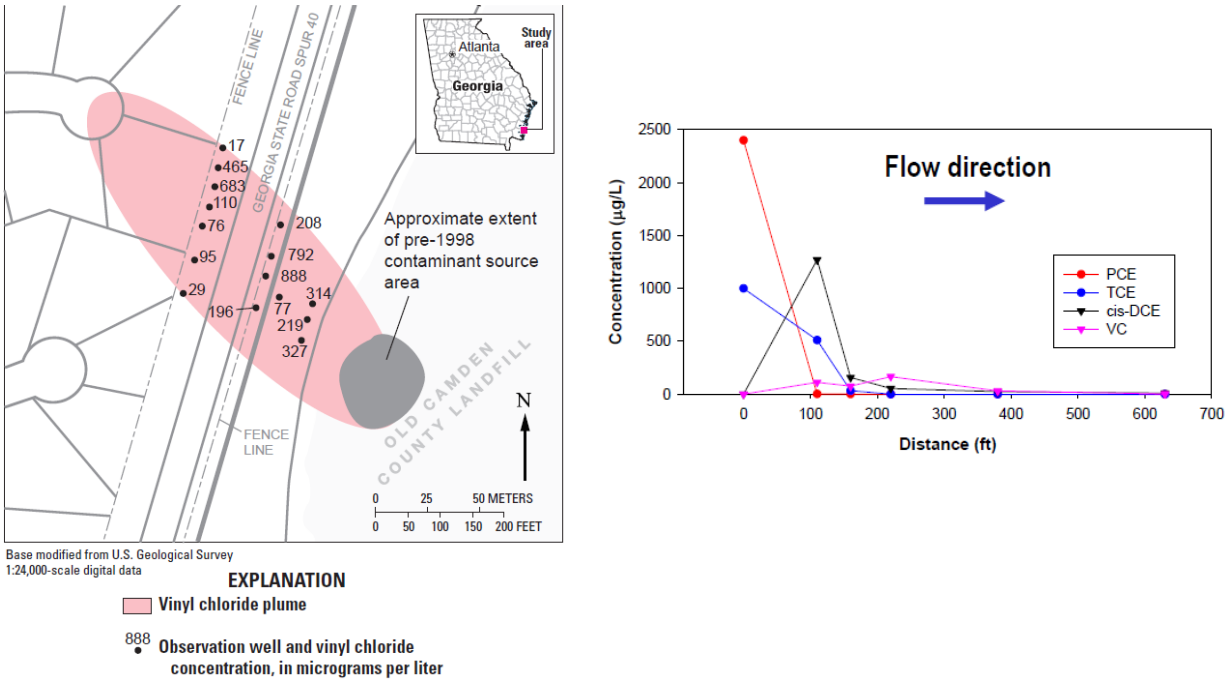

Figure 4.4.1. Extent of Downgradient Groundwater Plume circa 1992 (Chapelle et al., 200)

The implementation of active remediation technologies, including pump-and-treat, ISCO, and enhanced bioremediation, were completed in 2002 and significantly reduced groundwater impacts in the source zone and the downgradient plume. The USGS made a special study of the effects of source treatment in the landfill on the natural attenuation of the chlorinated alkenes down gradient of the landfill including a number of new wells. The wells that were installed for the USGS study (well prefix USGS) are found in three transects downgradient of the suspected source area as illustrated in Figure 4.4.2. Figure 4.4.2 also indicates the location of monitoring wells (well prefix KBA) that predated active remediation. Upon cessation of active remediation, natural attenuation has effectively reduced contaminant concentrations to target levels, as confirmed by long-term groundwater monitoring performed by the USGS and various consultants (Resolution Consultants, 2017). Concentration isocontours of PCE were developed in ESTCP Project ER-201129 (Lebrón et al., 2015) and these are shown on Figure 4.4.2 to illustrate the persistence of PCE through 2009. Concentration isocontours for TCE, DCE and VC are available in the Final Report for ER-201129 (Lebrón et al., 2015) and illustrate the sequential decay occurring at the site. The concentration histories in the USGS wells, combined with groundwater velocities yield estimates for the mass fluxes from the source zone over time following the remediation as described in Section 5.5.1.

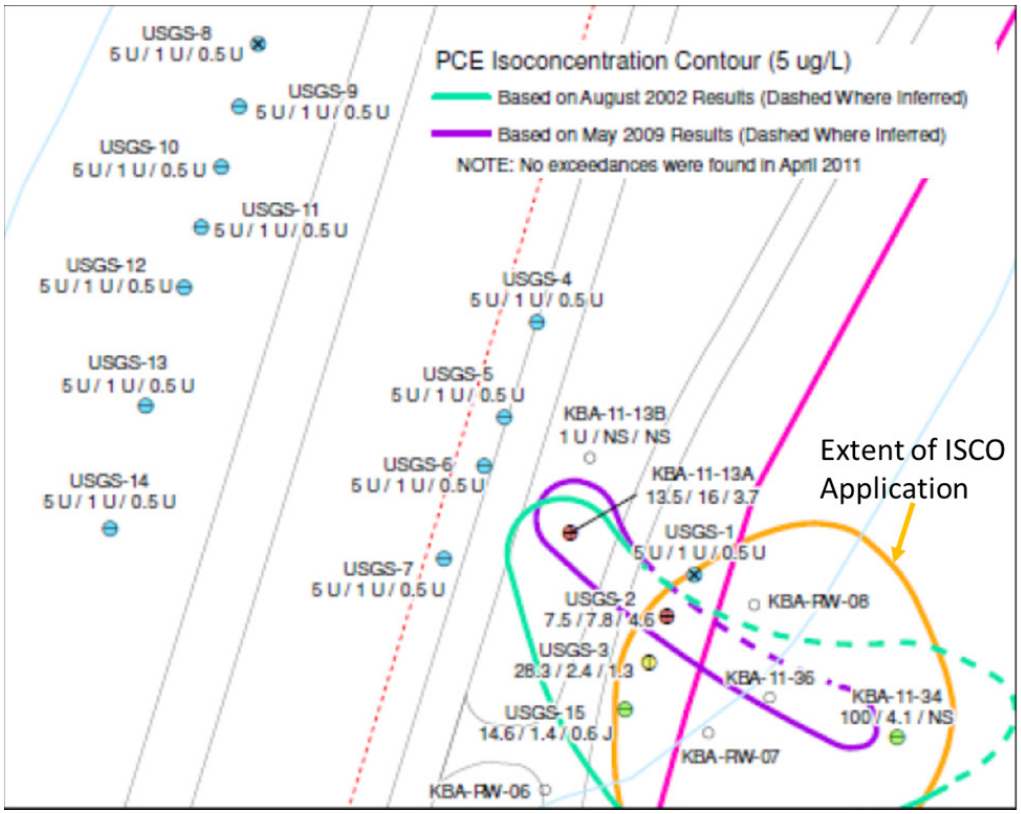

Figure 4.4.2. PCE Concentration Isocontours following Active Remediation

(2002, 2009, 2011) (Lebrón et al., 2015)

4.4.2 Site ST012, Former Williams AFB, AZ

JP-4 present in the saturated zone, as both mobile and immobile NAPL, has been a continuing source for dissolved-phase groundwater contamination for decades with benzene as the primary contaminant of concern. The total initial mass and distribution of NAPL in the saturated zone was not known, however, field evidence suggests NAPL is smeared across all but the lower 10 to 15 feet of the LSZ. Historically, the water table has not been deeper than about 235 feet bgs in the LSZ, about 15 feet above the underlying aquitard at 250 feet bgs as depicted in Figure 4.3.3. During the period of major fuel releases, the water table was at about 232 feet bgs and the LSZ was unconfined. NAPL was found in multiple studies to be floating as a large pool atop the water table in the LSZ with thicknesses on the order of several feet (IT, 1999). The approximate extent of this pool in 1990 covered an area exceeding 10 acres as illustrated in Figure 4.4.3 (orange dashed line). The rising water table fully saturated the LSZ by 1993 and the LSZ groundwater is now under semi-confined conditions. Prior to becoming saturated, the rising water table carried the NAPL upward and smeared the fuel across the overlying interval; presumably leaving smaller, immobile ganglia and pools of NAPL trapped under fine-grained lenses as depicted conceptually in Figure 4.3.2. As the water table continued to rise and enter the UWBZ, the extent of mobile NAPL in the LSZ decreased and NAPL smeared on the outer boundaries attaining a residual, or immobile, state. This observation is supported by the 1997 estimated extent of NAPL in the LSZ depicted in Figure 4.4.3 (blue dashed line) which is much smaller than the 1990 estimate. The 1997 estimate is based on observed NAPL in wells and covers about 4 acres within the approximately 10 acres delineated in 1990.

The previously detected NAPL did not disappear or coalesce toward the center; therefore, it is surmised a large volume of NAPL became smeared and immobile, i.e., did not collect in monitoring wells.

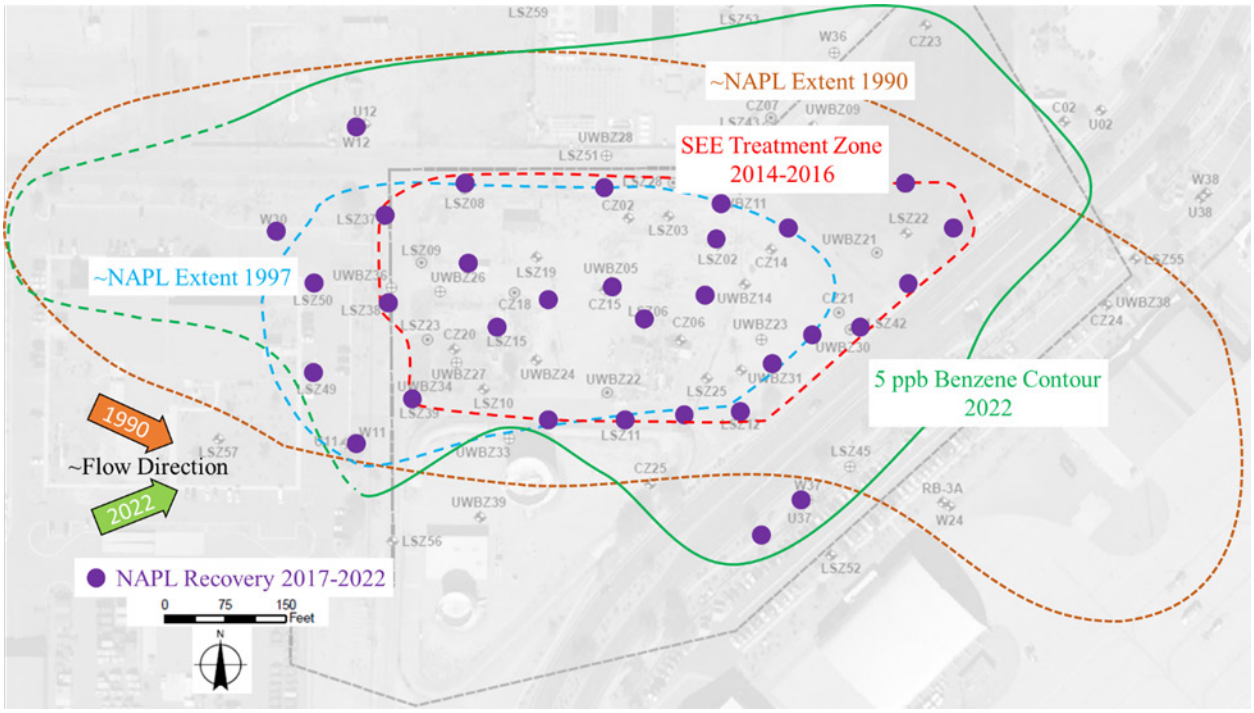

Figure 4.4.3. . Estimates of NAPL Lateral Extent in the LSZ in 1990 and 1997 and Wells with Recoverable NAPL after SEE

The concept of vertical smearing and widespread residual NAPL across the 1990 NAPL footprint is supported by the 2022 estimated isoconcentration contour of benzene in the LSZ groundwater at 5 parts per billion (micrograms per liter). As illustrated in Figure 4.4.3, the benzene contour aligns closely with the historical extent of NAPL detected in 1990 except in the southeast area. The LSZ groundwater flow direction before 1993 was in the southeasterly direction and therefore a gradient existed in that direction for floating NAPL to follow. The gradient gradually transitioned to the 2022 estimated northeasterly direction and may have resulted in the deviation in benzene contour from the 1990 NAPL footprint. Similar smearing and mobilization occurred in the overlying UWBZ and CZ as the water table rose further but this report focuses solely on the LSZ.

The implementation of SEE in the CZ, UWBZ and LSZ substantially reduced the mass of NAPL in targeted volumes of each zone. The target volume for the LSZ is indicated by the dashed red line in Figure 4.4.3. The estimate for the NAPL recovered from the three zones is equivalent to about 400,000 gallons of JP-4. Of this volume, about half was recovered in the volatile and dissolved phases and about half as pumped NAPL. Based on this recovered volume and current estimates of the remaining mass, SEE removed roughly 50% of the NAPL mass in place at the start of SEE. Figure 4.4.3 also indicates the locations and recovery of NAPL in the LSZ after SEE was terminated. Most of the recovery occurred in 2017 from wells on the interior of the SEE treatment zone as the depressed water table rebounded and NAPL disappeared from these interior wells.

These observations indicate residual NAPL remains within the treated volume. NAPL recovery continues on the periphery of the SEE treatment zone. From the end of a pumping period following SEE to the end of August 2002, nearly 3,000 gallons of NAPL were recovered in monthly, mobile pumping and bailing events.

Benzene concentrations in the LSZ groundwater measured during 2022 sampling events are presented in Figure 4.4.4. These concentrations were used to draw the isoconcentration contour in Figure 4.4.3. Within the SEE treatment zone and along its northern and eastern boundaries, benzene concentrations were reduced by one to two orders of magnitude from pretreatment values and indicate the flowing steam of SEE was effective at depleting the benzene content in residual NAPL. However, a number of the sampled internal wells yielded benzene concentrations nearly two orders of magnitude above the cleanup goal of 5 µg/L.

On the western and southern boundaries of the SEE treatment zone, the benzene concentrations remain near pre-treatment values. In addition, recoverable NAPL continues to appear in the southeast corner (well LSZ36). Beyond the SEE treatment zone, recoverable NAPL is persistent to the west and to the southeast. These areas have not undergone any remediation; although, a pilot test to enhance anaerobic degradation of dissolved benzene is underway. As described in Section 2, biological enhancements with slow degradation rates are not expected to impact the dissolution of benzene from the NAPL and therefore are not expected to reduce the timeframe for attaining and then maintaining cleanup goals across the LSZ.

The concept of partially treated NAPL, i.e., substantial depletion of benzene content, within the steam treatment zone surrounded by areas of untreated NAPL is illustrated in Figure 4.4.5. The immobile NAPL is also assumed to exist as numerous, small, disconnected pools trapped under fine-grained lenses as depicted. This conceptual model forms the basis for developing a conceptual source model for modeling future remediation as described in Section 5.5.2. Additional data and information characterizing the extent of contamination in the LSZ are provided in Appendix E of this report. The broad areal depictions of benzene contamination illustrated in Figure 4.4.4 are supplemented by dozens of geologic boring logs that include dye test results to confirm or negate the presence of NAPL in discrete soil samples collected along the boring depth. These vertically higher resolution data are presented in Appendix E and are utilized in the model input parameter development discussed in Section 5.5.2.

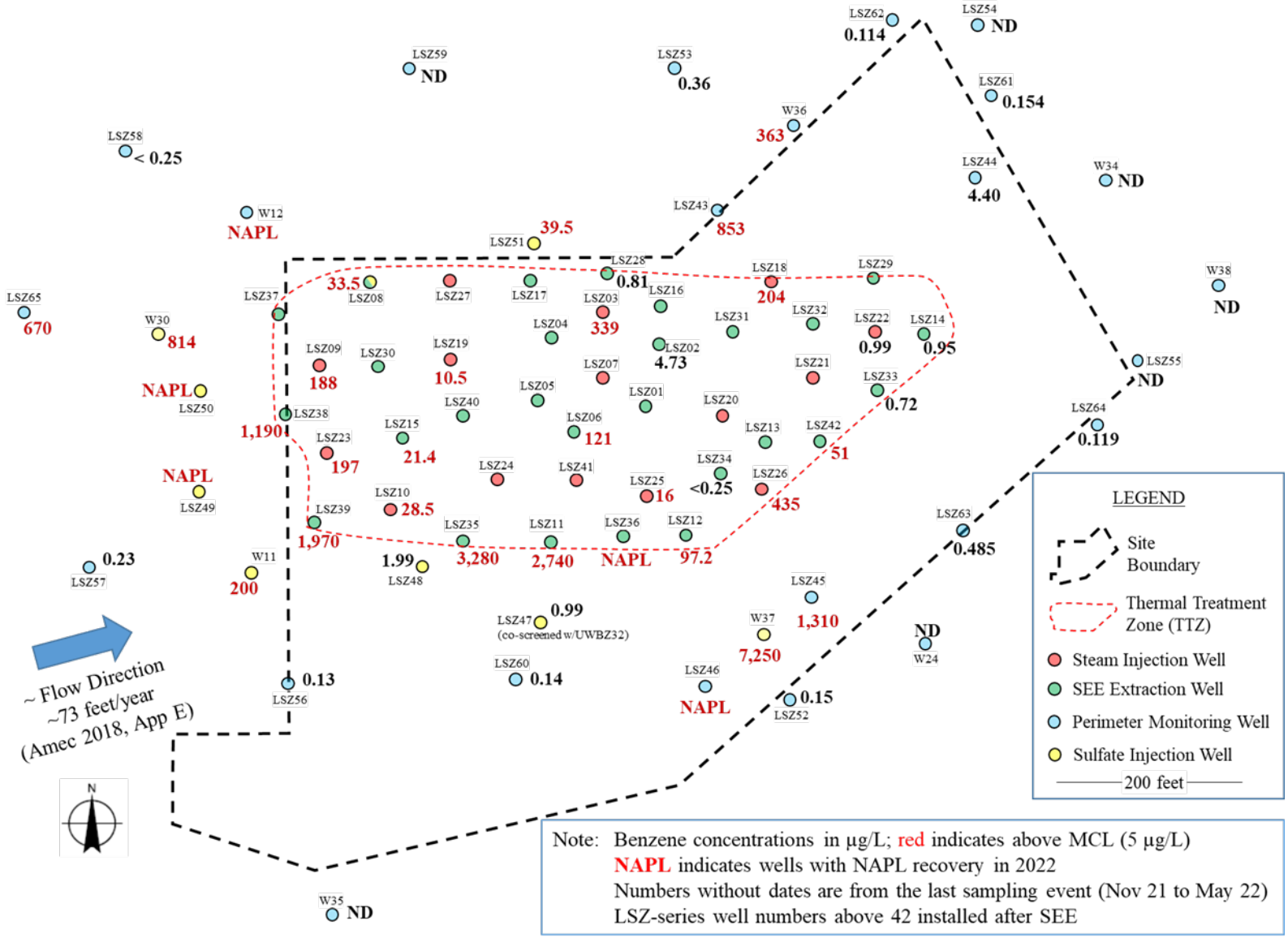

Figure 4.4.4. 2022 Benzene Groundwater Concentrations and Recoverable NAPL in Monitoring Wells in LSZ

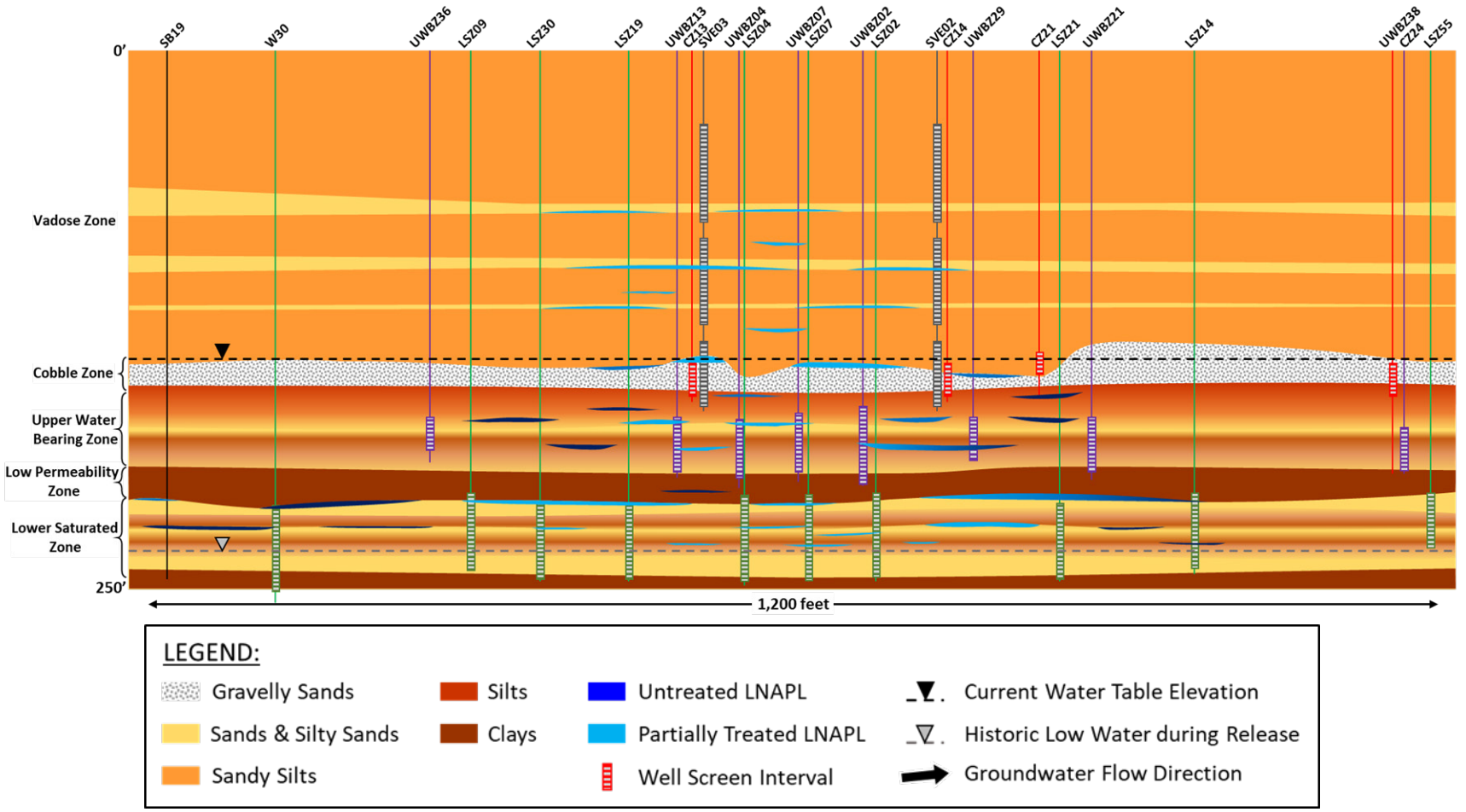

Figure 4.4.5. NAPL Vertical Extent along the Groundwater Flow Direction at Site ST012 (based on 2018 data)

5.0 TEST DESIGN

5.1 CONCEPTUAL EXPERIMENTAL DESIGN

Evaluation of technology performance was achieved by constructing source zone models using the volume-averaged approach to simulate time-dependent synthetic and measured concentration data at locations within and immediately downgradient of source zones during and after the implementation of various remedial processes. The models were capable of matching measured and interpreted trends in contaminant source depletion while explicitly addressing uncertainty of predictions. For Performance Objective 1 the volume-averaged model was applied for comparison with synthetic and measured mass discharge data generated before, during and after remediation in a) a comprehensive numerical model of a depleting NAPL source zone, b) applications of the volume-averaged model to multiple laboratory-scale experiments of NAPL dissolution and c) a controlled field-scale study of dissolution of a multi-component NAPL. The fundamental results for Performance Objective 1 were published in Stewart et al. (2022). The dissolution model in the article is described in Section 2.2 and was utilized in all subsequent remediation modeling. Real-world applications of the volume-averaged modeling framework for Performance Objectives 2 and 3 utilized historical monitoring data from a modestly complex DoD site, Site 11 at NSB Kings Bay, and a complex DoD site, Site ST012 at the former WAFB. Furthermore, the application at Site 11 illustrated the use of the model for evaluating remedial performance. The application at Site ST012 illustrated the model's utility for evaluating potential remedial performance of multiple technologies from the same conceptual site model in a complex setting.

Performance Objectives 4 and 5 are qualitative and involved engaging a sampling of the intended target audience with the implementation of the modeling approach. As described in Section 3, the demonstration included hands-on use of the model by more than 20 beta testers through both an executable with user manual for a single component NAPL and a spreadsheet implementation of the approximate solution in Section 2.2.5.2 for multi-component NAPL. Both models were accompanied by example templates and datasets for independent implementation. The testers provided feedback on the ease of implementation through the completion of a questionnaire and emails with general comments. To assess the efficacy of the approach for supporting managerial decisions, the modeling results for the demonstration at Site ST012 were presented to the regulatory community at the ST012 site in two separate webinars and the audience was polled on the scientific acceptability and the applicability of the results to support remedy selection.

5.2 DESIGN AND LAYOUT OF TECHNOLOGY COMPONENTS

This project does not involve the design and layout of technology components for a field demonstration; however, the components for application of the SCARPÉ framework are laid out in Figure 5.2.1 and described below.

The design of the technology is focused on easing the burden to assess remediation of NAPL source zones while maintaining complex controlling processes in a sound, scientific manner. The SCARPÉ framework provides a platform to input the quantitative and qualitative factors included in the conceptual source model (e.g., site physical properties, initial NAPL mass and architecture), compare with observed source discharge concentration data (if available), refine the conceptual source model based on comparison with measured data and/or availability of additional data, and

assess and compare various remedial approaches. To this end, the components of the technology generally include: (1) data review and assimilation, (2) conceptual source model development and input parameters, (3) application of the systems of ODEs and generation of outputs (mass discharge, source discharge concentration, mass depletion); using the SCARPÉ mathematical framework or directly using the two excel-based practical tools (Section 2.2.7) (4) comparison with measured discharge concentrations and iterative refinement of the conceptual source model (i.e., calibration), (5) selection of remedial processes considered separately or in combination, (6) selection and input of parameters associated with the specific form (e.g., first or second order) of the remedial models selected, (7) application of the system of ODEs and generation of outputs. The results are used to compare remedial technologies and support site remedial decision.

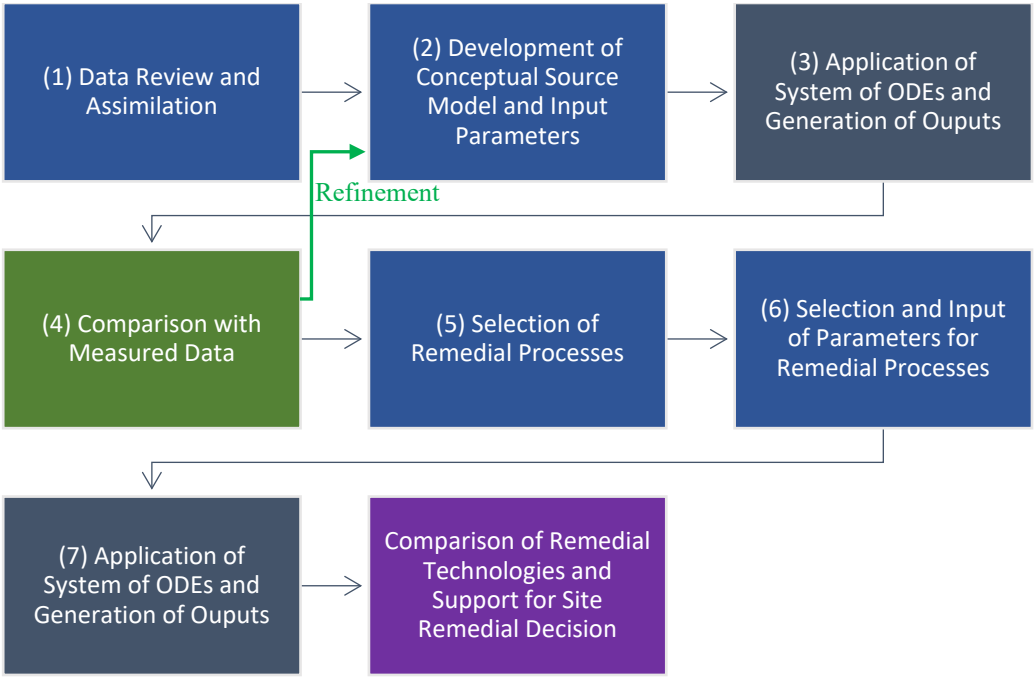

Figure 5.2.1. Layout of SCARPÉ Framework Application Components

5.3 BASELINE CHARACTERIZATION ACTIVITIES

The initial application of the volume-averaged model considered the numerical modeling results from Falta (2003). This numerical modeling effort was selected because the pool dissolution rate in the numerical model utilized identical approaches for calculating flow through the pools and dispersion from the pools as represented by Eqn. (2.13). Falta simulated mass dissolution from five identical pools in the two-dimensional domain illustrated in Figure 5.3.1. The simulation employed an integral finite difference numerical solution. The numerical discretization that most accurately represented the mass flux from the DNAPL pools used a tightly spaced grid around each of the five masses that had a total of 21,000 grid points in the x-z plane. Output from the simulation included the total mass rate of chemical and the average discharge concentration across the exit plane of the domain over time.

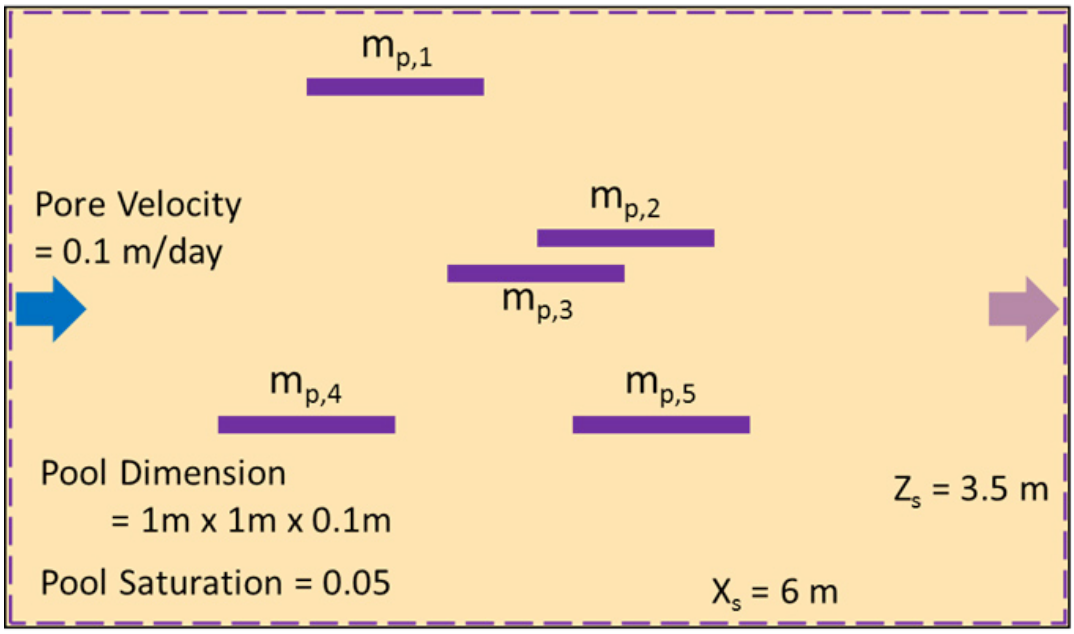

Figure 5.3.1. Representation of the Domain, DNAPL Pools (Purple Rectangles) and Source Area (Dashed Line) for the Modeling

The generalized volume-averaged model of Eqns. (2-5) and (2-15) was used to calculate dissolution from the five DNAPL pools with the inhibition relationship of Eqn. (2-16). The input parameters are summarized in Table 5.3.1. All five pools have the same dimensions, four pools are independent ($a_d = 0$), and one pool ($m_{p,5}$) is directly downgradient from another pool ($m_{p,4}$, $a_d = 1$), therefore the total mass dissolution rate is,

$$\frac{dm_{total}}{dt} = \sum_{a=1}^{5} \frac{dm_a}{dt} = -V_s K_n [4(C^* - 0) + C^*(1 - I_5)] \qquad \textbf{(5-1a)}$$

$$I_5(m_4) = \left(\frac{m_4}{m_{4,0}}\right)^{\varepsilon} \qquad \textbf{(5-1b)}$$

Table 5.3.1. Input for Volume-Averaged Model of Multiple Pools

Parameter	Value	Unit	Source
Source Zone Dimensions and Properties			
Length, X_s	6	m	Falta 2003
Width, Y_s	1	m	
Height, Z_s	3.5	m	
Volume, V_s	21	m^3	
Pore Velocity, U_0/φ	0.1	m/day	
Porosity, φ	0.35	-	
Background Conc, C_0	0	g/m^3	
DNAPL Dimensions and Properties			
Number	5	-	Falta 2003
Length, X_n	1.0	m	
Width, Y_n	1.0	m	
Height, Z_n	0.1	m	
Volume, V_n	0.1	m^3	
Initial Saturation, $S_{n,0}$	0.05	-	
Mass, $m_{n,0}$	2585	g/pool	
Solubility, C^*	110	g/m^3	
Upscaled Mass Transfer Model Parameters			
γ	0.5	-	Theoretical parameters
ε	0.5	-	
Transverse Dispersivity, [a]	0.001	m	Falta 2003
$K_{n,0}$	0.000285	1/day	Eq. (2-15) [b]

[a] Dispersion occurs on the top and bottom boundaries for consistency with Falta (2003).

[b] Relative permeability equals one for consistency with Falta (2003).

The calculated source discharge concentrations for various model parameters are compared to the numerical simulation output in Figure 5.3.2. Fitting metrics of R^2 and the normalized RMSE are also indicated in the figure for reference. Assuming a relative permeability of one and using theoretical parameters for pools (i.e., γ exponent of 0.5 and ε inhibition of 0.5) yielded a source lifespan about 25% longer than the numerical simulation. Including reduced flow through the pool with reduced relative permeability in both models may improve the match for the theoretical values. Neglecting inhibition underpredicted the life by about 16% compared to the numerical results and assumed each identical pool contributed independently and equally to the total mass discharge. Accounting for inhibition, the life of pool 5 ($m_{p,5}$) was extended beyond 17 years because the mass discharge from upgradient pool 4 (Figure 5.3.1) suppressed its dissolution as dictated by Eqn. (2-16). Nearly equivalent results for a second stage of discharge can be obtained by combining pools 4 and 5 into a single pool of 2-m length. Assuming a relative permeability of one and lowering the fit exponent γ to 0.34 yielded an excellent, best-fit reproduction of the discharge concentration history from the 21,000-gridblock numerical model. This example indicates the exponent on the mass ratio primarily governs the shape of the discharge tail and fine tunes the source lifespan while the overall magnitude of the source lifespan is governed largely by the coefficient to the ratio in Eqn. (2-15).

Additional fitting metrics and discussion are provided in Section 6.1.1.1. The results illustrate the utility of the volume-averaged model using theoretical parameters to forecast the source discharge concentration and lifespan with field scale data, as well as the ability of the volume-averaged model to reproduce complex numerical simulation results with limited adjustments of model exponents.

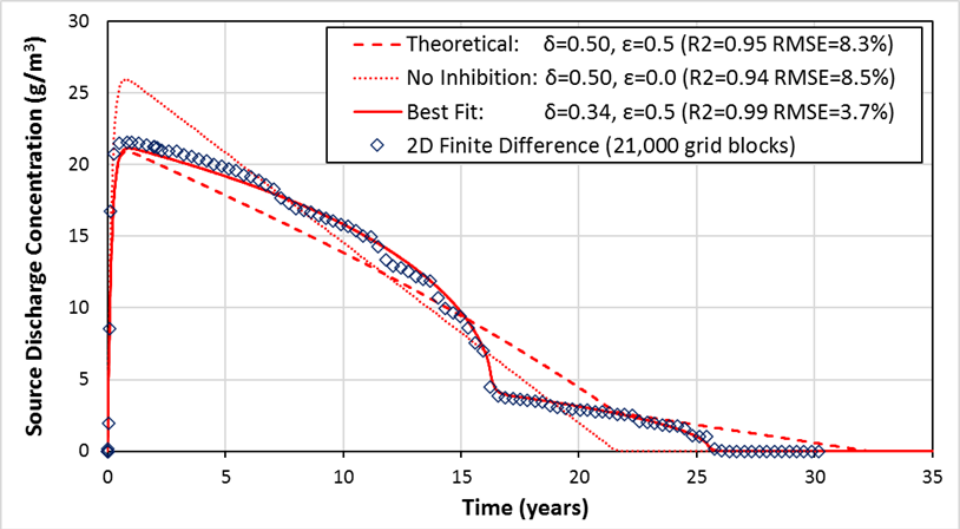

Figure 5.3.2. Comparison of Source Discharge Concentrations Simulated with the 21,000 Grid-Block Numerical Model and the Volume-Averaged Model

5.4 LABORATORY AND CONTROLLED FIELD STUDY RESULTS

5.4.1 Experimental Dissolution of Complex DNAPL Architecture

Laboratory 2D test cell experiments of DNAPL dissolution reported in DiFilippo et al. (2010) and analyzed in Guo et al. (2020) considered two scenarios: mixed DNAPL architecture in a relatively uniform soil and multiple DNAPL accumulations in heterogeneous soils.

5.4.1.1 Mixed DNAPL Architecture

The mixed DNAPL source zone experiment performed by DiFilippo et al. (2010) had a uniform pack of sand with a 2-cm-thick fine sand bottom, represented by the gray zone in Figure 5.4.1. A release of ~12 milliliters (mL) of TCE at the top of the test cell generated a vertical ganglia zone underlain by a pool as illustrated in Figure 5.4.1. The generalized model for dissolution Eqn. (2-15) was applied to the sub-volumes indicated in Figure 5.4.1 assuming a single value for γ and with no inhibition. The experimental conditions are listed in Table 5.4.1.

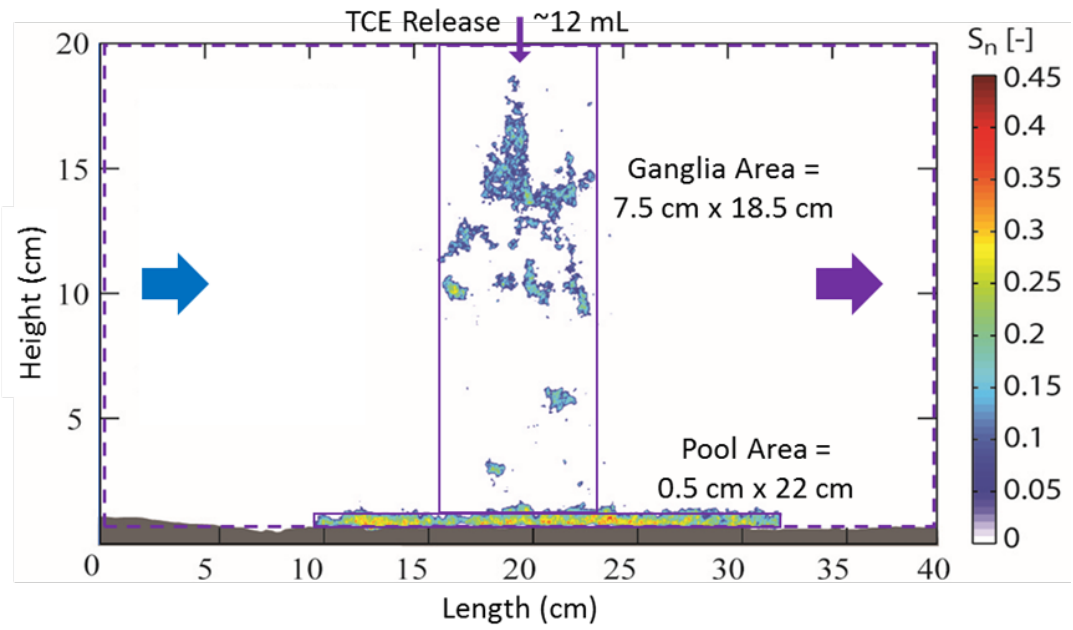

Figure 5.4.1. Representation of the Experimental Test Cell for Mixed DNAPL: Two Sub-Volumes (Purple Rectangles) and Source Area (Purple Dashed Line), Adapted from DiFilippo et al. (2010)

The initial DNAPL architecture in Table 5.4.1 was estimated from the volume released, characteristic dimensions, and the observed mass recovery. The height of the ganglia zone extended over the full sand interval as ganglia were dispersed throughout. This dimension resulted in an artificially low average initial saturation, but the measured saturations were also low with mild impact on velocity. Varying the characteristic height slightly modifies the first stage of discharge up to 25 pore volumes (PV) when mass in the ganglia zone was depleted. The remainder of the released mass was assumed to be in the pool sub-volume yielding a broad ganglia-to-pool (GTP) ratio of 1.36. DiFilippo et al. (2010) characterized the distribution of organic liquid using a light reflection visualization (LRV) method to generate the DNAPL saturation distribution reproduced in Figure 5.4.1. Based upon the LRV method, the initial GTP ratio was 1.7; however, this determination was based upon a threshold saturation of 0.2 applied to discrete measures (resolution of 0.02 mm^2) of saturation without regard to location in contrast to the upscaled approach.

Table 5.4.1. Input for Volume-Averaged Model of Mixed DNAPL Architecture

Parameter	Value		Unit	Source
Source Zone Properties				
Length	40		cm	DiFilippo et al. 2010
Width	2.6		cm	
Height	19		cm	
Volume	19.3		L	Calculated
Q	4.7		L/day	DiFilippo et al. 2010
Darcy Velocity	0.98		m/day	Calculated
Pore Velocity	2.17		m/day	Calculated
Porosity	0.45		-	Calculated
Inlet Conc, C_0	0		g/m^3	DiFilippo et al. 2010
DNAPL (TCE) Source Properties				
Volume Released	0.0118		L	DiFilippo et al. 2010
DNAPL Density	1,460		g/L	DiFilippo et al. 2010
Total DNAPL Mass	17.2		g	Calculated
Retardation	1.0		-	Guo et al. 2020
Solubility, C*	1,100		g/m^3	DiFilippo et al. 2010
DNAPL Architecture				
	Ganglia	**Pool**		
Z	18.5	0.5	cm	Est. characteristic dimensions illustrated in Figure 5.4.1
W	2.54	2.6	cm	
L	7.5	22	cm	
V_a	0.35	0.028	L	Calculated
V_{NAPL}	0.0068	0.005	L	Estimated
$S_{n,0}$	4.3	40	%	Calculated
$k_{r,0}$	0.86	0.15	-	Calculated
δ	0.5	0.5	-	Theoretical parameters
α_T	0.001	0.001	-	
$K_{n,0}$	2.16	0.225	1/day	Eqn. (2-15)

Comparisons of the discharge concentrations measured during the experiment with applications of the volume-averaged model are provided in Figure 5.4.2. The solid red line represents volume-averaged modeling with a general exponent γ=0.5 indicative of pool dissolution and a default value of 0.001 m for the tangential dispersivity. These values yield a realistic representation of the discharge concentration history using the volume-averaged model and generally match the lifespan of the source. Limited parameter sensitivity is illustrated in Figure 5.4.2 along with associated fitting metrics for data collected after the first pore volume flush.

The volume-averaged model is not intended to capture details of the breakthrough curve because of volume-averaging over the length of the source zone. A general exponent γ=0.6, closer to the theoretical value of 2/3 derived for ganglia dissolution, had a small impact on the early-stage ganglia dissolution and slightly improved the fitting metrics. However, the source lifespan was overpredicted by 25%. Doubling the default dispersivity (α_T = 0.002 m) underpredicted the lifespan by 23% and degraded the fitting metrics. Halving the dispersivity (α_T = 0.0005 m) increased the life by 36% compared to the default value. The model was unable to capture a small, temporary increase in discharge concentration after 60 PV, assumed to result from an increased relative permeability for water flow through the pool zone. Additional fitting metrics and discussion are provided in Section 6.1.1.2. The results validate the volume-averaged model and theoretical parameters demonstrating reasonably accurately a forecast of the source discharge concentration and lifespan of a complex DNAPL architecture given limited characterization data.

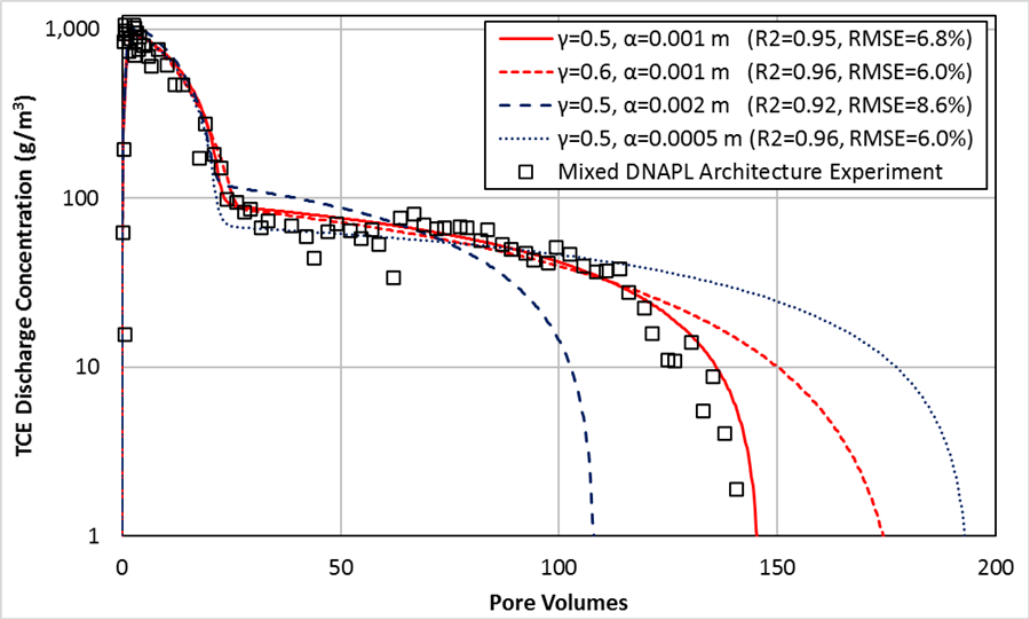

Figure 5.4.2. Comparison of Mixed DNAPL Experiment and Volume-averaged Model Discharge Concentrations

5.4.1.2 Complex DNAPL Architecture in Heterogeneous Materials

The volume-averaged model was applied to interpret dissolution data from a heterogenous soil experiment performed by DiFilippo et al. (2010). The experiment had lenticular zones of finer and coarser sand, represented by gray and black-outlined lenses, respectively, embedded in an otherwise uniform sand shown in Figure 5.4.3. Approximately 14 mL of TCE were released from two ports in the top of the test cell. The release generated three distinct mass accumulations with saturation distributions based on the LRV method. The most upgradient release of ~9 mL resulted in an accumulation above a fine-grained lens. The central release of ~5 mL yielded two distinct accumulations: one above a fine-grained lens and one within a coarse-grained lens. The coarse lens had an intrinsic permeability approximately 3.5 times higher than the surrounding bulk sands (DiFilippo et al., 2010). Hence, the velocity through this material was higher than in the surrounding material. Experimental conditions are listed in Table 5.4.2.

The saturation distributions of Masses 1 and 3 exhibit mixed characteristics of both ganglia and pools. Mass 1 also has a large extent of ganglia with a core zone of higher saturation. In the interpretation to follow, Mass 1 was further discretized into the two sub-volumes (1a and 1b) shown in Fig. 5.4.1.3 and compared to the single sub-volume result. The architecture provided in Table 5.4.2 includes the model for Mass 1 (3-Mass Model) and the subdivided Masses 1a and 1b (4-Mass Model). Masses 2 and 3 are identical for both models. Sequential inhibition was assumed for the two downgradient masses. A comparison of the discharge concentrations measured during the experiment with volume-averaged model interpretations using Eqn. (2-15) and the parameters in Table 5.4.2 is provided in Figure 5.4.4 along with the fitting metrics for concentrations measured after the first pore volume flush.

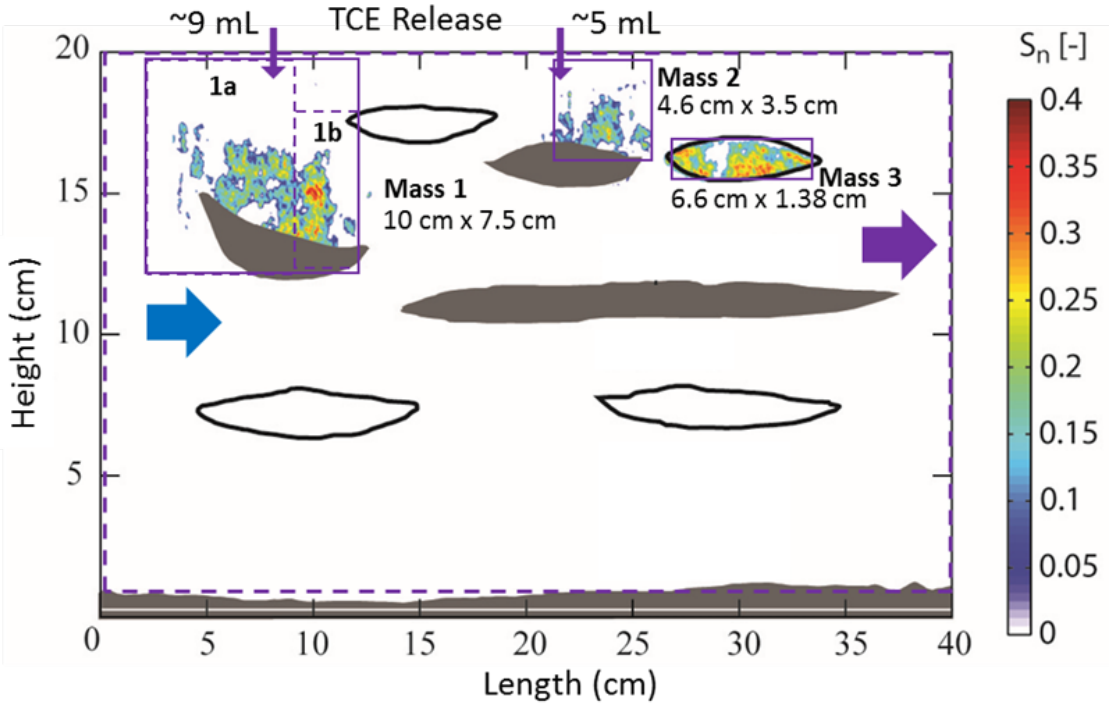

Figure 5.4.3. Conceptualization of the Experimental Test Cell for Heterogeneous Soils with Multiple DNAPL Sub-volumes Within an Upscaled Source Zone

Adapted from DiFilippo et al. (2010)

Table 5.4.2a. Input for Volume-averaged Model of Heterogeneous Soil

Parameter	Value	Unit	Source
Source Zone Properties			
Length	40	cm	DiFilippo et al. 2010
Width	2.6	cm	
Height	19	cm	
Volume	19.3	L	Calculated
Q	4.8	L/day	DiFilippo et al. 2010
Darcy Velocity	0.99	m/day	Calculated
Pore Velocity	2.48	m/day	Calculated
Porosity	0.40	-	Calculated
Inlet Conc, C_0	0	g/m^3	DiFilippo et al. 2010
DNAPL (TCE) Source Properties			
Volume Released	0.014	L	DiFilippo et al. 2010
DNAPL Density	1,460	g/L	DiFilippo et al. 2010
Total DNAPL Mass	20.4	g	Calculated
Retardation	1.0	-	Guo et al. 2020
Solubility, C*	1,100	g/m^3	DiFilippo et al. 2010

Table 5.4.2b. DNAPL Architecture for Volume-averaged Model of Heterogeneous Soil

Parameter	Unit	Mass 1	Mass 1a	Mass 1b	Mass 2	Mass 3	Source
Z	cm	7.5	7.5	5.5	3.5	1.38	Est. characteristic dimensions (Fig. 9)
W	cm	2.54	2.54	2.54	2.54	2.54	
L	cm	10.0	7.0	3.0	4.6	6.6	
V_a	L	0.191	0.133	0.042	0.041	0.023	Calculated
V_{NAPL}	L	0.0082	0.0036	0.0053	0.0012	0.0039	Estimated [a]
$S_{n,0}$	%	11.7	6.75	31.6	7.33	42.1%	Calculated
$k_{r,0}$	-	0.64	0.78	0.25	0.76	0.13	Calculated
γ	-	0.60	0.55	0.55	0.55	0.55	Theoretical
	m	0.001	0.001	0.001	0.001	0 [b]	Theoretical
ε	-	-	-	-	0.55	0.55	Theoretical
a_d	-	-	-	0	1	1	Assumed
$K_{N,0}$	1/day	0.777	0.889	0.259	0.449	0.080 [c]	Eqn. (2-15)

[a] Approximately two-thirds of the total released volume (14 mL) was occurred at the upgradient port with the balance released in the middle (DiFilippo et al. 2010).

[b] Dispersive dissolution from Mass 3 into the surrounding, lesser permeable material is neglected.

[c] Velocity through Mass 3 is multiplied by 3.47 to reflect the higher intrinsic permeability of the coarse material in the lens compared to the surrounding material (15.02 / 4.33 = 3.47, DiFilippo et al. 2010 Supporting Information).

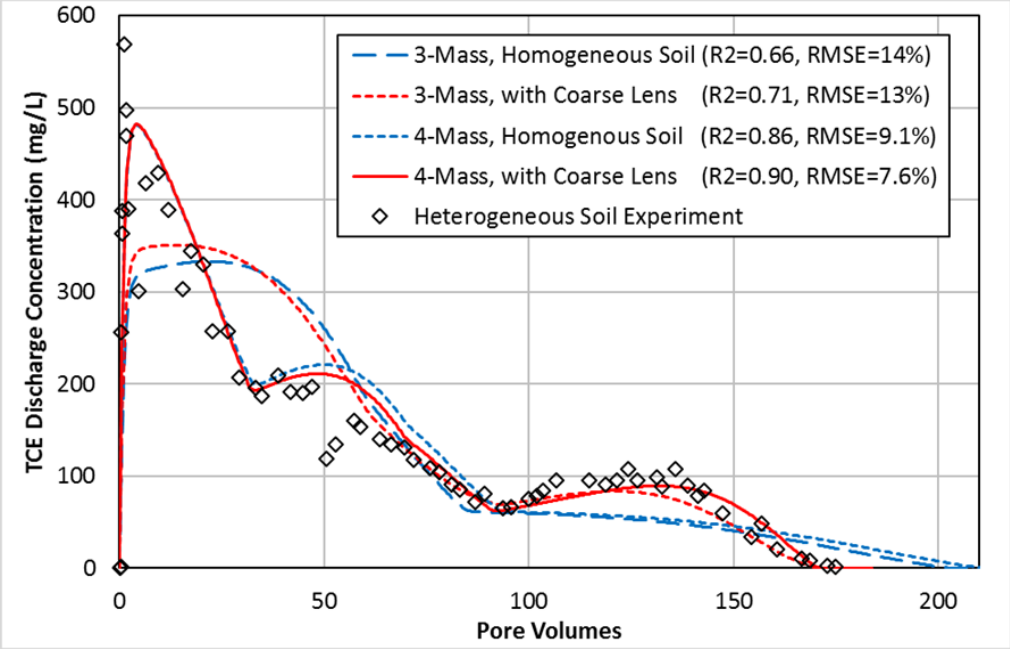

Figure 5.4.4. Interpretation of Measured Discharge Concentration Using Volume-averaged Models for Heterogeneous Soil and Multiple DNAPL Zones

The peak experimental discharge concentration coincided with the first pore volume flush and included emplacement contributions from Masses 2 and 3 that quickly dissipated to values below 500 milligrams per liter (mg/L). A single sub-volume model for Mass 1 (3-Mass Model) yielded a low peak concentration of 350 mg/L and did not capture the early observed trends. Inspection of the trends and the initial saturation distribution suggested two model sub-volumes Masses 1a and 1b (4-Mass Model). This concept replicated the observed trends through 50 PV and yielded a peak discharge concentration of 480 mg/L along with improved fitting metrics. This peak represents a concentration of about 44% of the TCE solubility limit. Assuming an initial sub-zone discharge concentration at this limit, a simple mass balance indicates a projected vertical flow interval of roughly 8 cm (i.e., 44% of the test cell height) was experienced by the DNAPL zone discharge. For this reason, the characteristic vertical dimensions of Masses 1 and 2 extended from the top of the apparatus to the upper fine-grained lenticular lenses. This observation also suggests residual DNAPL existed initially at the top of the cell below the DNAPL saturation detection limit of the LRV method.

Measured discharge concentrations after 35 PV were increased until 50 PV and, as interpreted by the model, resulted from an increasing flow through Mass 1b as the relative permeability increased. A similar increase in concentration was observed between a PV of roughly 90 and 130 and is interpreted to coincide with an increasing relative permeability through Mass 3 as mass was depleted. These increases are also a function of the power law exponents. As indicated in Table 5.4.2b, an intermediate value between 0.5 and 0.6 (0.55) was used for the model exponents (γ for all DNAPL zones and ε for Masses 2 and 3 located downgradient of Mass 1). A value of 0.6 flattened the curves while a value of 0.5 sharpened the increases. Other exponents yielded improved fitting metrics; however, the timing of trends and complete depletion were off target. Results for variations in the exponents and tangential dispersivity are presented in Section 5.7.

The exponent values, as with other such models, are also directly linked to the particular relative permeability function employed. Changing the exponent in the Wyllie correlation Eq. (2-9) for relative permeability significantly altered the discharge curve as does the irreducible water saturation, although to a lesser extent.

Including the increased velocity through Mass 3 (with Coarse Lens) and neglecting dispersion (α_T = 0 m) for Mass 3 yielded the excellent trend replication for the 4-Mass Model illustrated in Figure 5.4.4. Including both the increased velocity and dispersion shortened the total life of the DNAPL to less than 100 PV and did not replicate observed trends. Hence, this model interpretation indicates dispersion within the coarse lens did not translate into a significant interaction with the smaller-grained surrounding material and the coarse lens acted as a one-dimensional channel for flow and DNAPL dissolution. Neglecting an increased velocity through the coarse lens containing Mass 3 (Homogeneous Soil) while retaining a dispersivity of 0.001 m yielded a reasonable fit with extended lifespans. The added dissolution partially compensated for the lesser advective contribution. This example demonstrates the utility of Eqn. (2-15) for straightforward interpretation of observed discharge data in a field setting without resorting to more complex numerical modeling.

5.4.2 Controlled Field Study of Multicomponent DNAPL Dissolution

Broholm et al. (1999) present the results of a controlled 3D field test performed in a cell constructed by the installation of four interlocking sheet pile walls and lines of injection and extraction wells on each end to mimic natural gradient flow. The plan view of infrastructure and a conceptual cross-section are illustrated in Figure 5.4.5. The test consisted of a 3-component DNAPL release into the aquifer followed by 225 days of steady flushing through the cell. At Day 225, a constant rate methanol-water pulse was introduced that lasted for 5.5 days followed by continuous water flushing until Day 300.

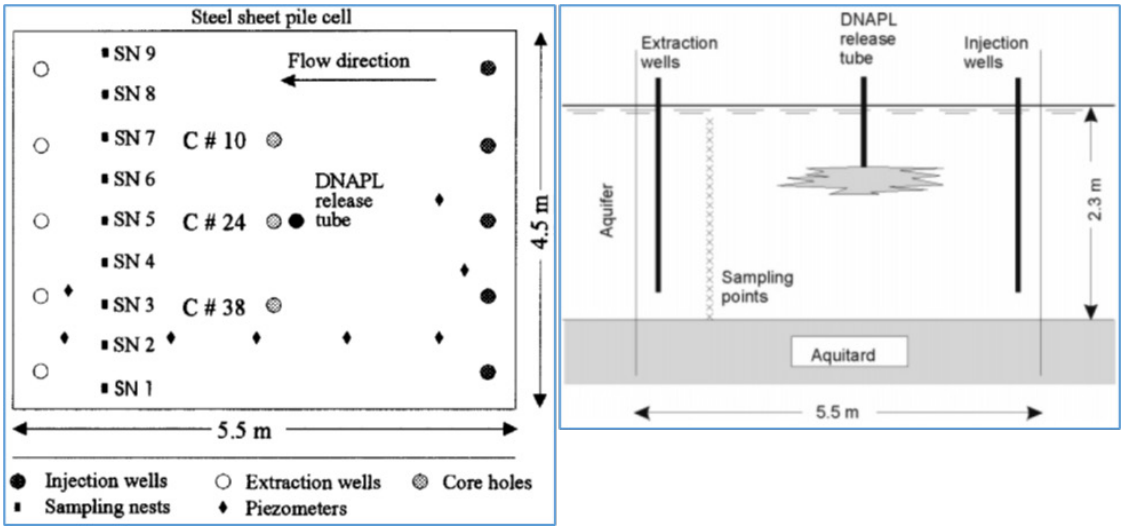

Figure 5.4.5. Plan View and Cross-Section of Field Test Cell

Adapted from Brohom et al., 1999

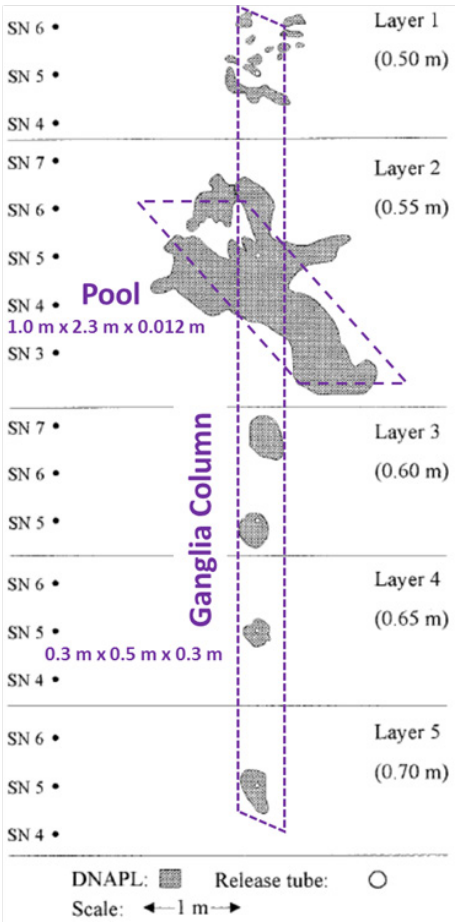

Figure 5.4.6. Initial DNAPL Distribution in the Controlled Field Test

Adapted from Broholm et al. (1999)

The volume-averaged model assumed the DNAPL release formed a dual-architecture source consisting of a single pool (4.0 liters) and one vertical column of ganglia (1.0 liter). This architecture was based on the conceptual layering and characterization provided in Broholm et al. (1999) and reproduced in Fig. 5.4.2.2. The DNAPL consisted of three components: trichloromethane (TCM), TCE, and PCE at initial DNAPL volumetric contents of 10%, 40% and 50%, respectively.

The volume-averaged model of Eqn. (2-26) was implemented with the generalized mass transfer coefficient Eqn. (2-15) to calculate the source discharge concentration of each component. The mathematical problem consisted of nine coupled, first order equations in time supplemented with auxiliary relationships for changing mole fractions and DNAPL saturations. The mathematical system was solved with an implicit Runge Kunta routine (Hairer and Wanner 1999). The estimated characteristic dimensions of each DNAPL mass are indicated on Figure 5.4.6. Table 5.4.3 summarizes the input data for the volume-averaged model.

Volume-averaged model output for the mass discharge concentrations of each DNAPL component was compared with the measured field data and the results of a detailed numerical model simulation (Mobile et al., 2012). The numerical simulation was calibrated to groundwater concentrations measured at transects of multi-level samplers and the mass discharge rates through Day 206.

The calibration included estimates for constant mass transfer coefficients from DNAPL using the NAPL package in SEAM3D (Waddill and Widdowson, 2000). Comparisons of each component concentration are provided in Fig. 5.4.2.3 along with fitting metrics for data through Day 206. The volume-averaged model was applied through the end of the test period including the 5-day methanol injection (Day 225.5 to Day 231) and post-injection flushing. The modeling assumed a steady flow through the source zone. Discharge from the source was translated in time downgradient to extraction wells (~1.5 m) proportional to the average velocity and retardation coefficients. Of note, the water table fluctuated significantly during the experiment due to the clogging and re-development of wells (Broholm et al., 1999). Re-development around Day 135 resulted in a rapid, one-meter rise in the water table that produced significant scatter in the observed data, in particular for TCE.

Table 5.4.3. Input for Volume-averaged model of Controlled DNAPL Dissolution Field Test

Parameter	Value			Unit	Source
Source Zone Properties					
Length	2.5			m	Estimated, Broholm et al. (1999)
Width	4.5			m	
Height	1.82			m	
Volume	20.5			m^3	Calculated
Q	360			L/day	Broholm et al. (1999)
Darcy Velocity	0.044			m/day	Calculated
Pore Velocity	0.13			m/day	Broholm et al. (1999)
Porosity	0.33			-	Broholm et al. (1999)
Inlet Conc, C_0	0			g/m^3	Broholm et al. (1999)
DNAPL Source Properties					
Total DNAPL Volume	5.0			L	Broholm et al. (1999)
Component	**TCM**	**TCE**	**PCE**		
Volumetric Fraction	0.10	0.40	0.50	-	Broholm et al. (1999)
Density	1.48	1.46	1.62	kg/L	
Initial Mass	0.74	2.92	4.05	kg	Calculated
Retardation Coeff, R	1.0	1.1	1.6	-	Rivett et al. (1994)
Solubility, C^*	8,700	1,400	240	g/m^3	Broholm & Feenstra (1995)
DNAPL Architecture & Upscaled Mass Transfer Model Parameters					
	Mass 1 (Ganglia)	**Mass 2 (Pool)**			
Length, X_n	0.3	1.0		m	Est. characteristic dimensions illustrated in Fig. 12
Width, Y_n	0.5	2.3		m	
Height, Z_n	0.3	0.012		m	
V_a	45.0	27.6		L	Calculated
V_{NAPL}	1.0	4.0		L	Estimated (GTP = 0.25)
Initial Sat., S_n	6.7%	44%		-	Calculated
Init. Rel Perm, k_r	0.78	0.11		-	Calculated, Wyllie (1962)
γ	0.6	0.5		-	Theoretical
Dispersivity,	0.001	0.001		m	Theoretical

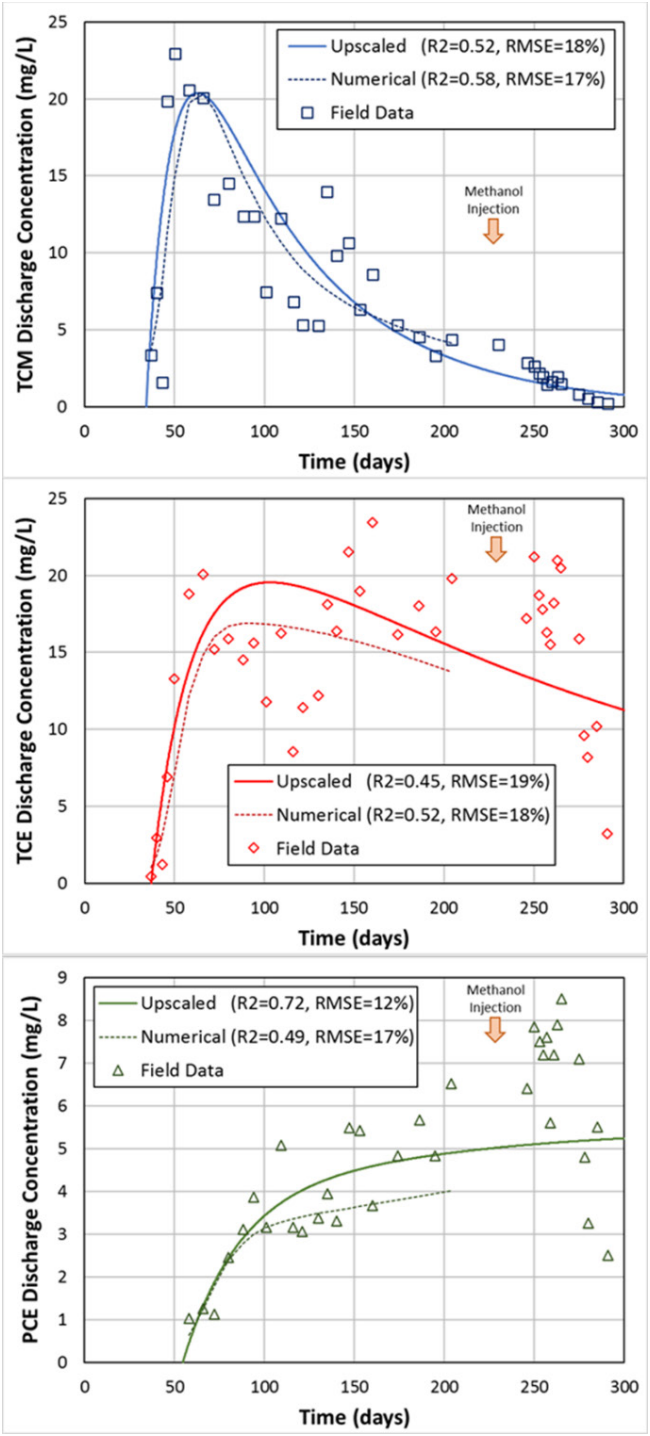

Figure 5.4.7. Comparison of Volume-averaged Model Calculations with Measured Effluent Concentrations in the Field Test and Output from a Calibrated Numerical Simulation

(Mobile et al., 2012)

The volume-averaged model outputs using theoretical model parameters compare well with both the field data and the calibrated numerical simulation. The match included the timing of conversion from increasing to decreasing discharge concentrations for TCM and TCE around Days 60 and 100, respectively, and the timing for a change in increasing PCE discharge concentration slopes around Day 125. Additional discussion of the fitting metrics is provided in the Supplementary Material. The volume-averaged model underpredicts the observed concentrations between Days 225.5 and 270. The higher observed concentrations are likely due to enhanced dissolution following the 5-day methanol injection from Day 225.5 to Day 231, which is not represented in the model. The difference in values provides a crude estimate for the methanol enhancement on DNAPL dissolution. The calculated lifespans using the volume-averaged model with steady flow, not accounting for enhanced dissolution with methanol injection, are 1.5, 6 and 11 years, for TCM, TCE and PCE, respectively, and illustrate consistency with the approximate, extrapolated lifespans at the termination of the experiment.

This application demonstrates the ability of the volume-averaged model with theoretical parameters to reproduce DNAPL dissolution in a field test data. In addition, the volume-averaged model generated results commensurate with output from a computationally intensive numerical simulation. These results support use of the volume-averaged model to forecast DNAPL source lifespan and quantify enhanced DNAPL dissolution with remedial actions, such as solvent injection. Additional statistical metrics for the fit between field data and model output are presented and discussed in Section 6.1.1.3.

5.4.3 Experimental Dissolution with In Situ Chemical Oxidation

MacKinnon and Thomsen (2002) performed a laboratory investigation using a physical model designed to assess the effectiveness of using permanganate (MnO_4^-) as an oxidant to reduce the mass of a PCE pool. The physical model was 2.5 m long and 0.45 m high and was filled with silica sand overlying a silica flour base, simulating a two-dimensional saturated sand zone overlying a capillary barrier. A mass of 690 grams of PCE resided in the model on top of the silica flour base, forming a dense NAPL pool at the start of the experiment. The experimental apparatus is illustrated in Figure 5.4.8. The pool was allowed to equilibrate for 35 days in the quiescent water and covered the full length of the capillary barrier.

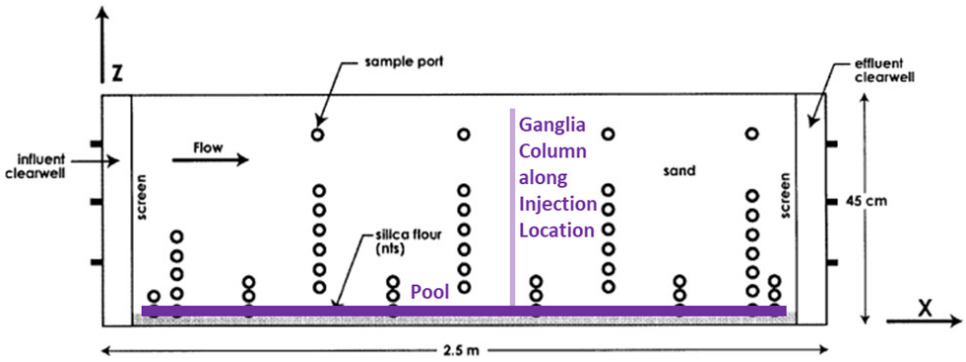

Figure 5.4.8. Schematic of Model Aquifer Comprised of Sand Over Silica Flour with a Dense NAPL Pool at the Sand/Silt Interface

After the equilibration period, the experimental steps were followed, all at a constant flow rate (pore velocity of 0.21 m/day),

- 90 days of water flushing
- 146 days of oxidant flushing at 10,000 mg/L MnO_4^-
- 142 days of post-oxidation water flushing

During the initial water flushing, the effluent aqueous phase PCE concentration reached a maximum of 54 mg/L after 7 days and then decreased to a relatively steady concentration of ~20 mg/L equivalent to mass load of 0.12 g/day (flow x concentration) as shown in Figure 5.4.9. The total mass of PCE removed from the physical model during this initial 90-day water flush was estimated to be 8.1 g.

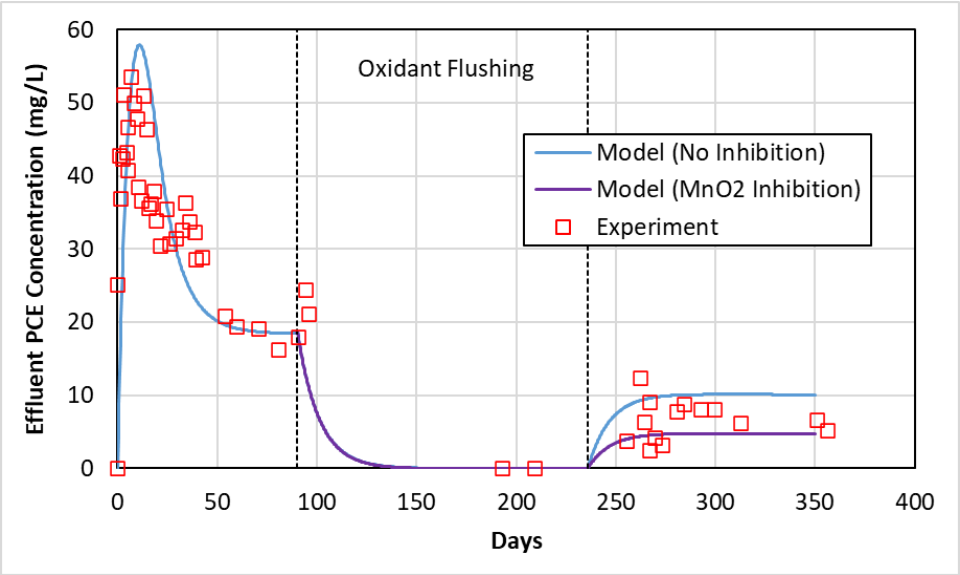

Figure 5.4.9. Effluent PCE Concentration in the Pool Oxidation Experiment

During the first two weeks of the oxidant flush, monitoring included daily measurements of chloride, permanganate and pH from the influent, effluent, and spatial sample ports. Subsequently, effluent samples were obtained twice a week and 26 spatial sampling rounds were conducted. Chloride, the conservative reaction product, was measured to assess the mass and extent of pool oxidation. The effluent chloride concentration gradually rose from near zero to 450 mg/L during the first 40 days of oxidation flooding as shown in Figure 5.4.10. The concentration decreased from this maximum to 180 mg/L over the next 106 days. Based on stoichiometric considerations, 180 mg/L of chloride corresponds roughly to the aqueous solubility limit of PCE. This equivalent concentration of PCE was an order of magnitude higher than the quasi-steady pre-oxidation concentration of ~20 mg/L showing that the presence of the oxidant had increased the overall mass transfer rate from the pool by an order a magnitude. The introduction of permanganate was terminated after partial pool mass reduction to assess the change in dissolution rate and while the chloride concentration was continuing to decay. The oxidation reaction was also expected to produce hydrous manganese dioxide (MnO_2), a solid precipitate, which poses a potential interference with the dissolution process.

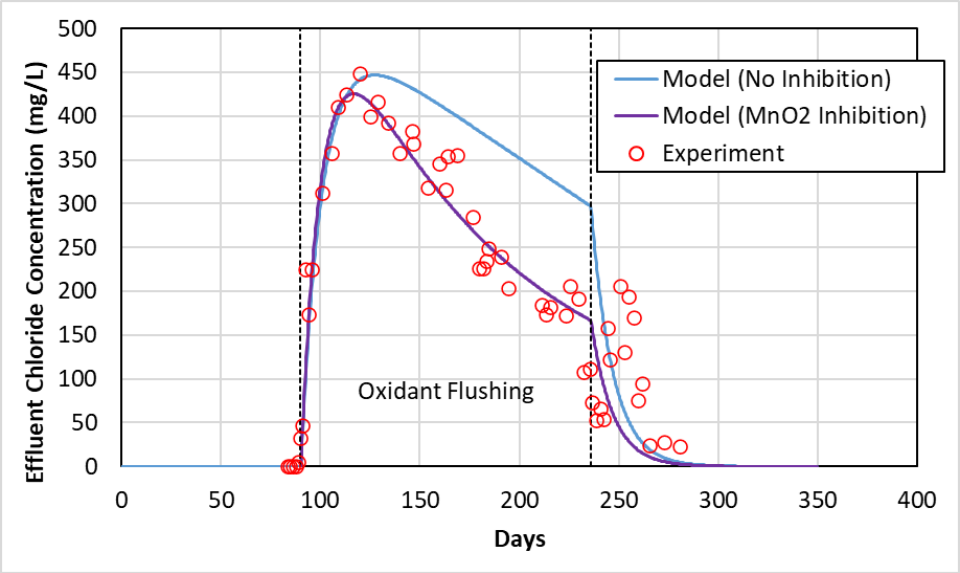

Figure 5.4.10. Effluent Chloride Concentration in Pool Oxidation Experiment

The water flushing that followed oxidation swept remaining permanganate and chloride out of the system. The aqueous effluent PCE concentration rebounded to a pseudo-steady state value of ~8 mg/L over the first 40 days following oxidation as illustrated in Figure 5.4.9. The rebound in PCE suggests the oxidant flushing reduced the pool mass dissolution rate by approximately 50% from the initial ~20 mg/L. An overall mass balance for the PCE based on flows and effluent concentrations is provided in Table 5.4.4. As indicated, the pre-oxidation flush removed a small mass in the dissolved phase while the introduction of the oxidant enhanced dissolution and depleted approximately 45% of the initial PCE mass (initial mass was 690 grams).

Table 5.4.4. Mass Balance for PCE during the Controlled DNAPL Dissolution Field Test

DNAPL Mass Depleted (mg)	Experiment	Model - Uninhibited	Model - Inhibited
Pre-Oxidation Water Flush	10	15	15
Oxidation Flush	310	460	350
Post-Oxidation Water Flush	4	6	3
Total	324	481	368

After the termination of the post-oxidation water flushing, nine soil cores were extracted from the apparatus and analyzed to quantify the mass of PCE remaining in the system and the presence of residual MnO_2 deposits. Spatial measurements of chloride during the oxidant flush and of PCE in the soil cores suggested that the oxidation reaction occurred primarily at the upgradient edge of the PCE pool as assumed in the derivation of Eqn. (2-15). For a pool DNAPL, the mass dissolution rate is expected to be roughly proportional to the interfacial area with the water. If the oxidation occurred primarily at the upgradient edge of the eroding pool then the decrease in dissolution rate would be inversely proportional to the cumulative mass depleted from the pool.

The excavation of the porous medium provided an opportunity to visually observe the distribution of MnO_2 deposits. Two important observations were drawn from the distribution. First, high quantities of MnO_2 deposits appeared over the bottom 8 cm of the sand near the location of the original pool with increasing thickness of this MnO_2 layer towards the effluent end. A sharp contrast was observed in all of the soil cores between the highly concentrated MnO_2 deposits and the overlying sand. Hence, the oxidation occurred in close proximity to the pool and the increasing thickness suggests possible amorphous transport of the MnO_2 through the aquifer. Secondly, one exception was observed in the distribution of deposits near the pool. A tall, narrow column of MnO_2 deposits was identified near the location of the PCE injection. These deposits indicate some of the injected PCE migrated vertically along the inserted injection point, or had smeared during withdrawal of the injection point. The vertical smearing of PCE during injection appeared to yield a column of ganglia over the full height of the experiment near the middle of the aquifer length. As ganglia, this PCE mass would oxidize efficiently during the initial sweep of permanganate.

Two objectives for this experimental study were to assess the enhancement to dissolution provided by the oxidant and to assess the impact of MnO_2 deposits on this enhancement. MnO_2 deposits within the model aquifer potentially decrease the velocity of water directly above a pool and/or reduce the accessible interfacial area between the NAPL and bulk water and thereby decrease the overall mass transfer from the remaining PCE pool. The volume-averaged model was applied to these experimental conditions and compared to the results to provide a quantitative assessment of the mass dissolution rate and the enhancement provided by the oxidant.

As derived in Section 2, the reaction between permanganate and aqueous PCE is considered second order,

$$\bar{r} = k^{oxi}\,\overline{C}_{PCE}\,\overline{C}_{oxi} \tag{2-40}$$

With this reaction, the mass balance equations (based on Eqn. 2-45) for dissolved PCE and the mass of PCE as dense NAPL are, respectively,

$$R\frac{d\overline{C}_{PCE}}{dt} = -\frac{Q}{\phi V_s}\overline{C}_{PCE} - \frac{1}{\phi V_s}\frac{dm_n}{dt} - (1-\bar{S}_n)\bar{r} \tag{5-2a}$$

$$\frac{1}{V_s}\frac{dm_n}{dt} = -E_r(\overline{C}_{oxi})\sum_{a=1}^{2} K_a\left(C^* - C_{a,0}\right) = -E_r(\overline{C}_{oxi})\sum_{a=1}^{2} K_a C^* \tag{5-2b}$$

The NAPL is assumed to exist as two, independent architectural structures: ganglia in a column near the middle of the simulated aquifer and a pool occupying nearly the full length of the simulated aquifer as illustrated in Figure 5.4.8. This architecture is consistent with the observed elevated PCE concentration in the initial water flushing effluent (Figure 5.4.9) and the excavation of the simulated aquifer. The mass transfer coefficients are calculated with Eqn. (2-15). The enhancement to the dissolution rate is assumed to be a function of the bulk oxidant concentration in the simulated aquifer and is estimated using the second order approximation described by Eqn. (2-44),

$$E_r(\overline{C}_{oxi}) = 1 + \frac{1}{Y^{oxi}}\left(\frac{\overline{C}_{oxi}}{C^*}\right)\left(\frac{\mathcal{D}_{contaminant}}{\mathcal{D}_{oxi}}\right) \qquad \textbf{(2-44)}$$

In the experiment, NOD material in the sand is negligible and the mass balance equation for the oxidant expressed by Eqn. (2-41) becomes,

$$\frac{d\overline{C}_{oxi}}{dt} = -\frac{Q}{\phi V_s}\overline{C}_{oxi} - Y^{oxi}\,\overline{r} \qquad \textbf{(5-3)}$$

Mass balances on the reaction products are expressed by Eqn. (2-43). Applied to chloride produced by mineralizing PCE and manganese dioxide produced by transform permanganate, the two mass balances are, respectively,

$$\frac{d\overline{C}_{Cl}}{dt} = -\frac{Q}{V_s\phi(1-\overline{S}_n)}\overline{C}_{Cl} + Y^{Cl}\,\overline{r} \qquad \textbf{(5-4a)}$$

$$\frac{d\overline{C}_{MnO_2}}{dt} = Y^{MnO_2}\,\overline{r} \qquad \textbf{(5-4b)}$$

The MnO_2 is assumed to precipitate and reside in the location of the reaction as suggested by its observed general distribution in the excavated aquifer.

The six governing equations listed above were solved with the properties and characteristic dimensions and masses delineated in Table 5.4.5 for the source zone (i.e., simulated aquifer), ganglia column, and pool. The parameters for modeling the oxidation process with permanganate are listed in Table 5.4.6.

Table 5.4.5. Input for Volume-Averaged Model of Pool Oxidation Experiment

Parameter	Value		Unit	Source
Source Zone Properties				
Length	230		cm	MacKinnon & Thomson 2002
Width	15		cm	
Height	43		cm	
Volume	148		L	Calculated
Q	5.69		L/day	Calculated
Darcy Velocity	0.0882		m/day	Calculated
Pore Velocity	0.21		m/day	MacKinnon & Thomson 2002
Porosity	0.42		-	MacKinnon & Thomson 2002
Inlet Conc, C_0	0		g/m^3	MacKinnon & Thomson 2002
DNAPL (PCE) Source Properties				
Volume Released	0.432		L	Calculated
DNAPL Density	1,620		g/L	MacKinnon & Thomson 2002
Total DNAPL Mass	690		g	MacKinnon & Thomson 2002
Retardation	1.0		-	MacKinnon & Thomson 2002
Diffusivity,	0.5184		cm^2/day	MacKinnon & Thomson 2002
Solubility, C*	200		g/m^3	MacKinnon & Thomson 2002
DNAPL Architecture				
	Ganglia	**Pool**		
L	4	220	cm	Est. characteristic dimensions illustrated in Figure 5.4.8
W	15	15	cm	
Z	25	1.0	cm	
V_a	1.5	3.3	L	Calculated
m_{NAPL}	6	684	g	Estimated (Total = 690 g)
V_{NAPL}	0.0037	0.413	L	Calculated
$S_{n,0}$	0.59	29.1	%	Calculated
$k_{r,0}$	0.98	0.29	-	Calculated
γ	0.67	0.5	-	Theoretical parameters
α_T	0.0004	0.0004	-	
$K_{n,0}$	0.0223	0.00367	1/day	Eq. (2-15)

Table 5.4.6. Oxidation Parameters for Volume-Averaged Model of Pool Oxidation Experiment

Parameter	Unit	MnO_4^-	MnO_2 (s)	Cl^-	Source
Molecular Weight	g/mol	118.92	86.93	35.45	Calculated
Density	g/L		5,000		Estimated
Diffusivity	cm^2/day	0.7			Estimated
Y	-	0.956	0.855	0.699	Stoichiometry
Injection Conc	mg/L	10,000	0	0	MacKinnon & Thomson 2002
k^{oxi}	L/mg/day	0.03			Hood, 2000
Time start	day	90			MacKinnon & Thomson 2002
Time end	day	236			MacKinnon & Thomson 2002
E_r (max)	-	40			Calculated Eqn. (2-44)

The output from the volume-averaged model for the PCE effluent concentration is plotted in Figure 5.4.9 with the experimental measurements. The blue line with no inhibition represents the model output without any correction for the precipitation of manganese dioxide. The small mass of PCE in the central ganglia column yielded an early peak exceeding 50 mg/L, roughly 25% of the PCE solubility limit. This mass was depleted after about 50 days of flushing and the PCE concentration approached a pseudo-steady value of about 18 mg/L when the oxidant flushing was initiated. The PCE rapidly disappeared from the effluent and was fully destroyed by permanganate before reaching the extraction well. After ceasing the oxidant flushing and continuing a water flush, the PCE reappeared in the effluent at a reduced concentration that was captured by the volume-averaged approach with the dissolution model of Eqn. (2-15) although the model results were higher than the observed PCE concentrations. The uninhibited dissolution model calculated a reduction in discharge rate after oxidation that was slightly less than 50%.

The destruction of PCE during the oxidant flushing was tracked with the chloride concentration measured in the effluent as presented in Figure 5.4.10. The dissolution model and enhancement factor of Eqn. (2-44) captured the initial peak of chloride, the subsequent decay as the pool mass and surface area decreased, and the disappearance when the oxidant flushing was terminated. However, the model overpredicted the rate of PCE destruction beyond the initial peak and, as a result, overpredicted the cumulative mass of PCE depleted from the pool. As indicated in Table 5.4.4, the experimentally estimated cumulative PCE mass destruction was 310 grams. The model estimate without accounting for MnO_2 inhibition was 460 grams. As a result, an inhibition function was introduced to account for the precipitation of MnO_2. The difference in slopes between the model and experimental data suggested a simple, linear function was appropriate,

$$I = 1 - \left(\frac{C_{MnO_2}}{C_{MnO_2,reference}} \right) \tag{5-4}$$

The reference concentration for the precipitate represents an estimate for the mass sufficient to cover fully the interfacial area and bring dissolution to a halt. Fitting the experimental data yielded a reference concentration of 8,000 mg/L but this is also a function of the pool length. Developing other physical interpretations and associated functions is left for future research. The results of incorporating this simple inhibition function, along with the enhancement factor, in the dissolution model are plotted in Figures 5.5.2 and 5.5.3 and yield an improved match to the effluent concentrations. Including the MnO_2 inhibition function also reduced the model estimate for the PCE mass depletion from the pool during oxidation to 350 g, closer to the experimental estimate of 310 g (Table 5.4.4).

This effort demonstrated the validity of the volume-averaged approach for modeling NAPL dissolution coupled with remediation processes. Performing a similar calculation with a numerical model such as CORT3D would require a much greater effort. The numerical models also do not have the ready adaptability to test trial functions for modeling different processes.

5.5 FIELD TESTING

No field testing was performed during the execution of this project; testing of the technology was based on existing data. The field testing occurred in two tasks corresponding with the technical performance objectives:

- Demonstrate the methodology at a modestly complex site (Site 11, NSB Kings Bay, GA)
- Demonstrate the methodology at a complex Site (Site ST012, Former Williams AFB, AZ)

5.5.1 Site 11, NSB Kings Bay, GA

5.5.1.1 Summary of Remedial Actions and Site Characterization Activities

Site 11 was regulated under the Resource Conservation and Recovery Act (RCRA) program and a pump and treat system was installed and operated from 1994 to 1999 to contain and treat the dissolved plumes. After a period of containment pumping, the estimated time of remediation for the downgradient pump and treat system to achieve remediation goals was lengthy and the results of an evaluation of natural attenuation processes to remediate the site in a reasonable time frame were positive (Chapelle and Bradley, 1999). The remediation focus shifted in 1999 from pump-and-treat to more targeted source reduction of contaminants with ISCO using catalyzed hydrogen peroxide (CHP) in four phases. The ISCO was followed by MNA to polish residual concentrations. Long term monitoring programs have been conducted at Site 11, including monitoring as required by the RCRA Permit and performed by Navy contractors since 1999 and monitoring conducted from 1999 to 2011 by the USGS in coordination with the Navy to evaluate the effectiveness of MNA (USGS, 2009). Details of the remedial actions relevant to the modeling of the source zone remediation over time are described in Appendix D. A summary timeline of site remedial activities is provided in Table 5.5.1.

Table 5.5.1. Summary of Primary Remedial Activities

Activity	Date
DNAPL Release	~1981
Containment Pumping	1994-1996
Pump-and-Treat	1996-1998
Multiple Phases of ISCO	1998-2001
MNA	1999-Present

The chronological order and type of data collected at Site 11 were driven by site priorities. Initial characterization efforts focused on defining the downgradient plume and the risk to potential receptors as indicated in Figure 4.1.1.1. This effort was followed by an interim measure to contain the plume within the site boundaries with downgradient pumping and then to reduce the risk to potential receptors by shrinking the plume. These risk-focused activities provided sparse data regarding the then-suspected upgradient DNAPL source zone. Later activities focused on locating, characterizing, and remediating this source zone. Hence, collection of direct data nearby and within the DNAPL source zone only occurred after two decades of natural dissolution, several years of pump-and-treat, and the first two phases of downgradient ISCO.

The final two phases of ISCO were implemented within the suspected DNAPL source zone with Phase 3 applied within the contaminated aquifer and Phase 4 in an underlying silt interval. The source characterization and remediation data are described in detail in Appendix D and cited in this section as needed in developing the conceptual source zone model.

5.5.1.2 Conceptual Model for the DNAPL Source Zone

The primary variables of interest for modeling the DNAPL source zone at Site 11 were estimates of the characteristic dimensions for its vertical and lateral extent, the initial DNAPL mass, the DNAPL architecture, and the total mass discharge rate of PCE from the time of release through DNAPL depletion and back diffusion. The wide array of data employed to develop these estimated parameters included:

- Geologic logs and interpretations;
- PCE and total chlorinated concentrations in downgradient monitoring wells, transects, and associated groundwater velocities;
- PCE and total chlorinated VOC mass extraction rates from pumping wells;
- Vertically discrete sampling of groundwater in the source zone with DPT; and
- Extent and oxidant mass of ISCO applications

The parameterized conceptual model for the DNAPL source zone is provided in Table 5.5.2. These parameters were estimated from the site data described in Section 4, the site characterization and remediation data provided in Appendix D, and the data interpretation methods described in this section. The values represent best-estimates within the bounds for the various parameters derived from direct and indirect measurements and the data interpretation. The dimensions of the source zone were estimated initially from the high-resolution data collected by DPT during the ISCO phases as described in Section 1.2 of Appendix D. The ISCO was implemented in four phases with intermediate groundwater sampling. The injection wells also served as monitoring wells after the oxidant had dissipated. This observational approach led to the location of the suspected DNAPL source after the second phase. Results from DPT and ISCO injection well sampling after Phase 2, i.e., pre-Phase 3, were interpreted at that time by the site contractor as depicted in the left-hand sketch of Figure 5.5.1. The engineer suspected a deeper DNAPL source at the interface of the transmissive aquifer and underlying silt. Similar sampling was performed after Phase 3 ISCO and results are shown on the right-hand sketch.

Table 5.5.2. Site 11 Volume-Averaged Model Source Zone Parameters

Parameter	Value		Unit	Source
Source Zone Parameters				
Length (X_s)	3		m	Estimated as described in Section 5.5.1
Width (Y_s)	8		m	
Height (Z_s)	3		m	Aquifer thickness
Darcy Velocity	0.024		m/day	Chapelle et al. 2007
Porosity	0.3		-	Chapelle et al. 2007
Mobile fraction, f_m	0.89			Estimated in Section 5.5.1
K_{im}	0.00025		1/day	Clay penetration depth
DNAPL (PCE) Source Properties				
Initial DNAPL Mass	600		kg	Estimated in Section 5.5.1
DNAPL Density	1,620		g/L	
Retardation	1.6		-	Chapelle et al. 2007
Solubility, C*	200		g/m^3	
DNAPL Architecture				
	Ganglia	**Pool**		
L	3.0	3.0	m	Est. characteristic dimensions illustrated in Figure 5.4.8
W	7.0	6.0	m	
Z	3.0	0.1	m	
m_{NAPL}	527	73	kg	Estimated (Total = 600 kg)
V_{NAPL}	325	45	L	Calculated
$S_{n,0}$	0.017	0.083	%	Calculated
γ	0.6	0.5	-	Theoretical parameter
α_T	0.001	0.001	-	Theoretical parameter
$K_{n,0}$	0.00673	0.00027	1/day	Eqn. (2-15)

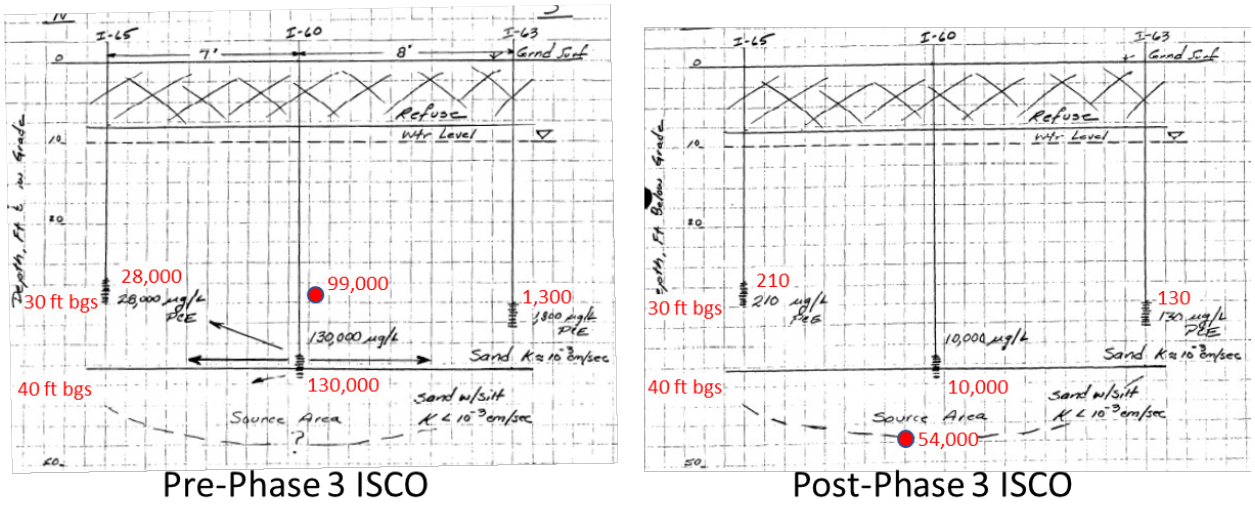

Figure 5.5.1. Discrete Groundwater Sampling Results (PCE in µg/L) in the Suspected DNAPL Source Zone

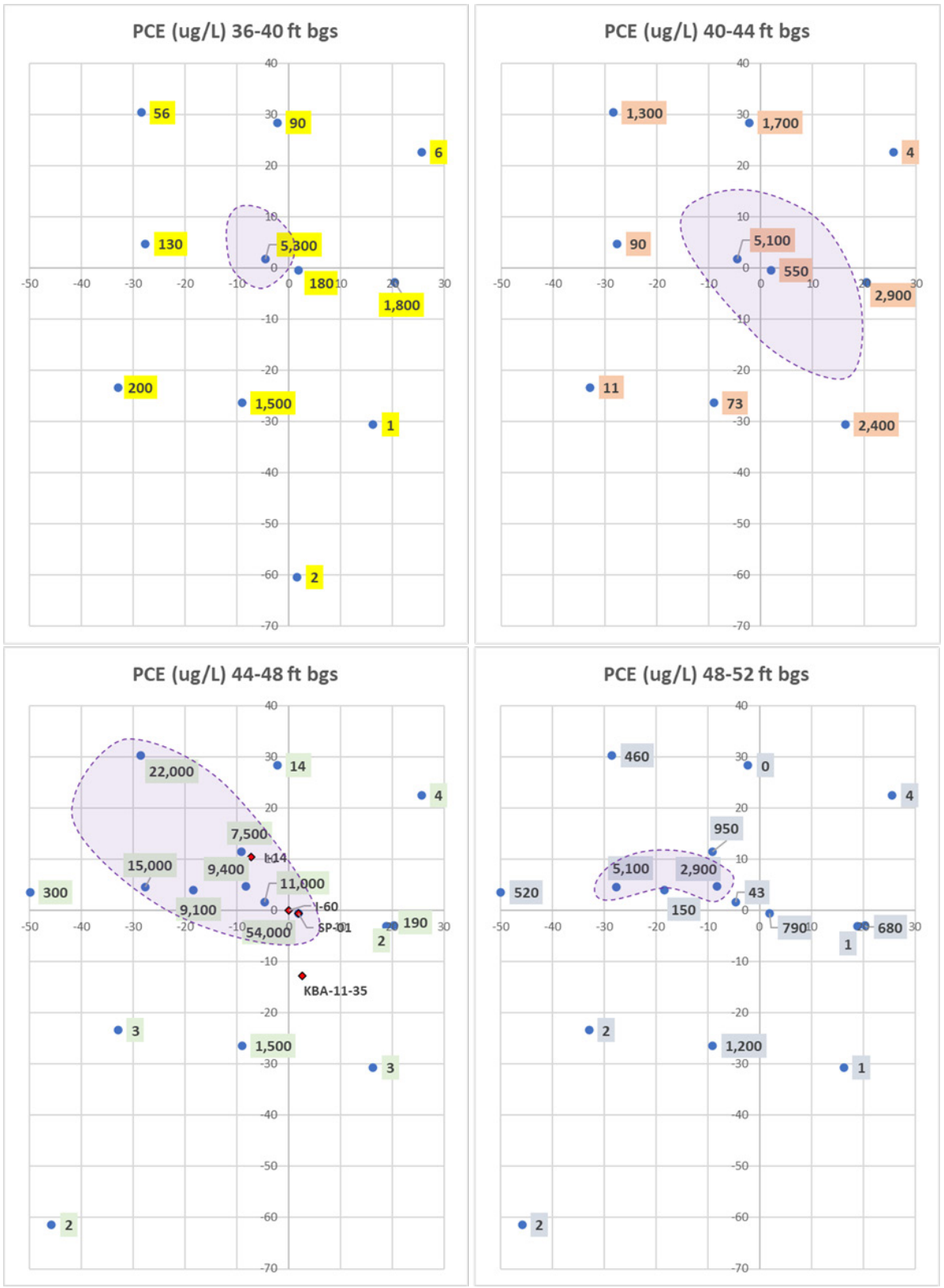

Figure 5.5.2. Lateral and Vertical Delineation of PCE Concentrations in the DNAPL Source Zone

Additional groundwater concentrations collected after Phase 3 ISCO in discrete wells and DPT points are shown at four depth horizons in Figure 5.5.2 across the bottom of the aquifer at approximately 40 feet bgs to 52 feet bgs. The detection of high PCE concentrations in the underlying silt interval led to Phase 4 of ISCO in this interval. The locations of the final CHP points installed at the site and used for the injections are indicated in Figure 5.5.3. The conceptual location of the suspected DNAPL source zone among the final phase of ISCO injection points is illustrated in Figure 5.5.3. The area indicated aligns with the characteristic source dimensions provided in Table 5.5.2 and are consistent with the sketch shown in Figure 5.5.1. The vertical height of the source zone aquifer was bounded by the geologic logs describing the thickness of this sand interval as conceptualized in Figure 4.3.1. The Darcy velocity was available from site investigation reports cited in Appendix D along with soil properties such as porosity and the retardation coefficient for PCE (Chapelle et al., 2007). Other PCE properties can be found in the literature. The assumed DNAPL architecture and mass accumulation dimensions for a ganglia zone and underlying pool were estimated were also estimated from these data and tested with the volume-averaging model. This scenario is commonly observed and assumed at DNAPL sites.

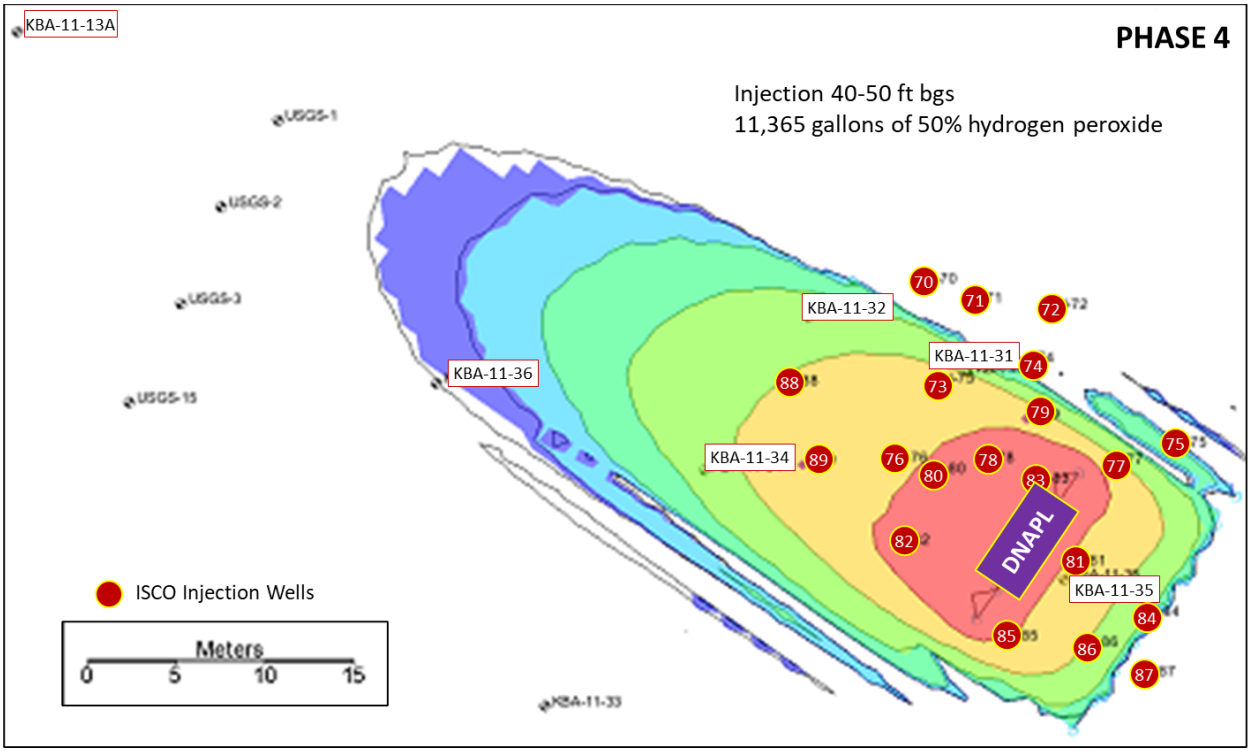

Figure 5.5.3. PCE Source Zone and ISCO Injection Locations (Phase 4)

Estimates for the initial DNAPL mass were based on,

- historical records for possible release volumes,
- the dimensions of the source zone from high resolution characterization coupled with literature-suggested DNAPL saturations for different soil types, and
- professional judgement based on DPT concentrations and refinement using initial volume-averaged model output.

In 1999, excavation in the vicinity of the source zone uncovered several 5-gallon containers and one approximate 20-gallon container. All containers were either crushed or severely deteriorated except one 5-gallon container. The uncrushed 5-gallon container appeared to contain a gray-colored, paint-looking waste. The 20-gallon container contained a black sludge looking waste. Analytical results for the black waste showed PCE at 14 milligrams per kilogram making it an indeterminant source of PCE but provided evidence for the types of waste disposal at the landfill. Therefore, the actual volume, mass and phase of the PCE release(s) were unknown and a range of estimates were used in the volume-averaged modeling of the site activities.

5.5.1.3 Calibration/Validation Targets for the Volume-Averaged Modeling and Additional Input Parameter Estimation

The primary calibration targets for the source zone model at Site 11 were the estimated total mass discharge rates of PCE throughout the life of the source zone. These included the estimated PCE mass discharge rates from the source zone during natural dissolution following DNAPL release and continuing until the groundwater extraction was initiated. The average mass discharge rate during this period was calculated initially from the estimated total mass of chlorinated compounds (cVOC) in the dissolved plume divided by the elapsed time from the DNAPL release. For this calculation, PCE was assumed to be the sole parent compound for its daughter products (TCE, DCE, VC). This estimate was further refined by employing an existing numerical fate and transport model of the site in SEAM3D used to evaluate the natural attenuation capacity of the system. The numerical modeling is described in Appendix D. For input, estimates for natural groundwater velocities were available from site investigation reports as was the extent of the dissolved plume, i.e., its leading edge and width including PCE and its daughter products. The numerical model was calibrated to the available monitoring data and other site measured properties by iterating a constant discharge mass of PCE from the source zone until the model reasonably replicated the extent of the dissolved plume. This calculation provided an estimate of 90 grams per day on average for the initial ten years of dissolution following the release. The numerical model, data and details of this calculation are described in Appendix D.

The numerically refined discharge estimate also provided a lower bound on the projected area to flow of the DNAPL source zone, i.e., its width and height. The average discharge concentration cannot exceed the solubility limit of PCE (200 mg/L). The height of the aquifer (approximately 3 m) provided an estimate for the height of the source zone. Paired with the Darcy velocity (0.024 m/day), the minimum width for the DNAPL source zone was estimated to be about 6 m,

$$Mass\ Disch\arg e\ = Velocity \times Width \times Height \times Solubility$$

$$Width = \frac{Mass\ Disch\arg e}{Velocity \times Solubility \times Height}$$

$$Minimum\ Width \approx \frac{Mass\ Disch\arg e}{Velocity \times Solubility \times Height} \approx \frac{90}{0.024 \times 200 \times 3} \approx 6\,m$$

Groundwater extraction for plume containment in downgradient wells was initiated roughly 13 years after the DNAPL release. The mass discharge rate from the source zone during groundwater pumping was estimated from the pumping rates, measures of the cVOC concentrations in the extracted water, and the complete capture zone for the pumping. The capture zone was evaluated at the time of implementation and found to extend across the full dissolved plume width. Initial cVOC mass extraction rates were not representative of the source discharge because of the plume shape. After pumping more than an equivalent plume pore volume from the aquifer, pseudo-steady concentrations were expected at the recovery wells. However, data reporting was very sparse. To perform the volume-averaged modeling, an estimate for the increased groundwater velocity through the source zone was required. This calculation required additional assumptions regarding the hydraulic conductivities of layers at the site because the recovery wells were screened over multiple, distinct soil intervals. The numerical flow model utilized the location of extraction wells and average pumping rates to find the downgradient containment pumping roughly doubled the velocity through the source zone. In addition, the flow model verified that the travel time from the source zone to the recovery wells had been exceeded.

After 2.5 years of downgradient containment pumping, a new extraction well was installed closer to the source zone and brought into the extraction configuration. Acting as a pump-and-treat well to increase the removal of mass from the DNAPL source zone, this well was prioritized and pumped at a relatively high extraction rate. Using the numerical flow model and the pumping wells and rates cited in Appendix D, the groundwater velocity through the source zone was increased to a factor of about 5 over the natural gradient. This increased velocity was maintained for almost two years before the system was shut down for the implementation of ISCO to accelerate the cleanup. Combined with the measured concentrations in the extraction wells, the average PCE mass discharge rate after about 4.5 years of pumping was an estimated 40 g/day. This rate was assumed to be representative of the mass discharge from the source zone 4.5 years after the pumping started. This estimate provides a second calibration target for the volume-average model of the source zone. The validity of the estimate was also corroborated by decreased concentrations of daughter compounds (DCE and VC) and increased concentrations of the parent (PCE) in a monitoring well between the source zone and pumping wells. The change in contaminant distribution was consistent with a reduced residence time for degradation to occur.

The average PCE mass discharge rate from the source zone after pumping ceased was estimated to be 14 g/day using the calibrated SEAM3D model and fitting to subsequent groundwater monitoring data from wells immediately downgradient of the source as described in Appendix D. The estimate is corroborated through a comparison with the final pumping estimate. The characteristic velocity through the source decreased by a factor of roughly 2.6 when the pumping ended. Dividing the pumping mass discharge estimate of 3.6 yields a natural gradient discharge rate of 15 g/day with is close to the numerically derived value from matching downgradient monitoring well concentrations. The estimates for the PCE mass discharge rate from the source zone are summarized in Table 5.5.3. The estimated mass discharge rates serve as the first set of calibration/validation targets for the application of volume-averaged modeling and the conceptualization of the Site 11 source zone from the time of release through the start of the ISCO effort. A key point in this validation is the required consistency in the source zone model that is maintained by the volume-averaged approach, i.e., the characteristic dimensions and initial masses remain unchanged and only the timescales change in transitioning from activity to another.

Conditions at the end of the pump-and-treat (high pumping rate phase) were automatically carried over as the initial conditions for the implementation of ISCO.

Table 5.5.3. Estimated PCE Mass Discharge Rates from the Site 11 Source Zone before ISCO

Time (years)	Period	Interpreted PCE Mass Discharge Rate (g/day)
0	Release	-
2.5	Natural Dissolution	90
15.6	Final Groundwater Pumping Rate	40
17.5	Pre-ISCO Natural Dissolution	14

Volume-averaged modeling of ISCO with permanganate and persulfate is practical as described in Section 2.2.6.3 and demonstrated in Section 5.4.3. However, ISCO with CHP is much more difficult because of the extremely fast reaction rates and lack of reactive persistence in the subsurface. The CHP was injected in relatively large volumes (i.e., high percentage of the target pore volume) and with a tight grid spacing in an effort to bring the CHP in close proximity to contaminants quickly. The injections were grouped into four major events to allow monitoring and assessment of progress between events. Therefore, detailed modeling of the CHP processes at Site 11 was not attempted. Instead, the CHP at Site 11 was modeled simply as an instantaneous DNAPL mass subtraction from the source zone. The DNAPL mass at the end of groundwater pumping was used as the initial mass and an iterative process was undertaken to estimate mass destroyed by the CHP. Once more, the SEAM3D model was iterated to match the observed groundwater concentrations directly downgradient in monitoring well (KBA-11-13A) in the period following CHP. As with the initial natural dissolution modeling, the PCE mass discharge was iterated until a reasonable match was achieved with data from the target monitoring well after a new equilibrium was achieved. The calibrated mass discharge from the numerical model was compared to the volume-averaged model estimate for mass discharge after iteratively subtracting mass from the volume-averaged model DNAPL source zone. The mass subtraction in the volume-averaged model yielding a match in the PCE mass discharge estimates was taken to be the DNAPL mass destroyed by CHP. Details of this calculation are provided in Appendix D.

The downgradient plume was extensively monitored after CHP with new nearby transects of monitoring wells (USGS-series) installed to supplement existing long-term monitoring wells (KBA-series) and provided projected areas of contaminant flow and mass fluxes over time. The locations of the KBA wells and the first line of USGS monitoring wells are shown on Figure 5.5.3. Data from the KBA wells downgradient and lateral to the source are plotted in Figure 5.5.4 along with an indicator of the ISCO phases. These data were used with the volume-averaged model to assess the residual DNAPL mass and discharge rate after ISCO and to assess back diffusion from the source zone over the subsequent decade.

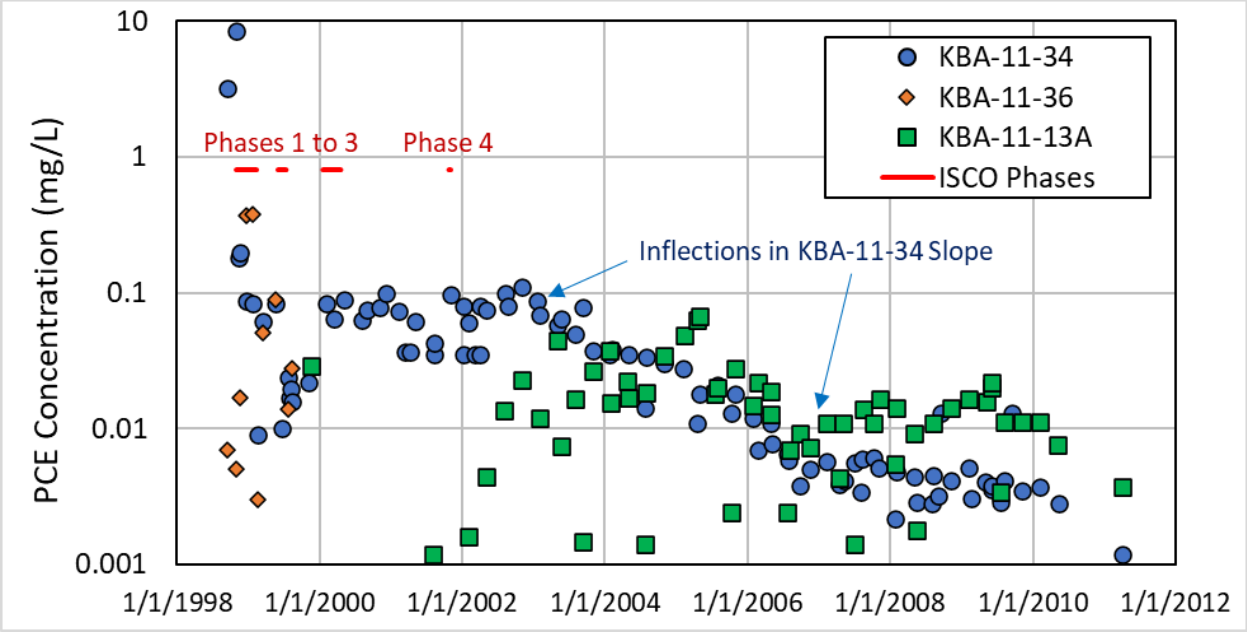

Figure 5.5.4. Long-Term Monitoring of Downgradient PCE Groundwater Concentrations

Well KBA-11-34 was located approximately 13 m downgradient from the model DNAPL source zone. The travel time from the DNAPL source zone to KBA-11-34 under the natural gradient was about 2 years. The travel time to KBA-11-13A was about 10 years. The dissolved plume across this area was treated with ISCO and likely depressed the natural degradation processes allowing PCE to serve as a direct indicator of source zone discharge. The post-ISCO concentration trend at KBA-11-34 displays two inflection points as indicated in Figure 5.5.4 and replotted in Figure 5.5.5. The first occurs roughly 3 years after Phase 3 and about 1 year after Phase 4. The PCE concentration at KBA-11-34 was relatively steady just under 0.1 mg/L after the first two phases of ISCO which included the plume area around it. Before the application of any ISCO the PCE concentration was more than an order-of-magnitude higher. The first inflection point is assumed to be associated with DNAPL mass destruction in the source zone during Phases 3 and 4. After the first inflection point, the PCE concentration decay was exponential for about four years at a rate of 0.00163 day^{-1} (0.6 yr^{-1}). This period appears to coincide with back diffusion in the source zone. The concentration then changed to a slower exponential decay. The second inflection point, roughly 5 years after Phase 4, is assumed to indicate the time of near full depletion of contaminant mass in the source zone. Accounting for a two-year travel time, this observation also suggests the residual mass after ISCO was solely in the aqueous phase within the underlying silt, i.e., complete destruction of the DNAPL mass during ISCO. This hypothesis is tested in model calculations to follow. The exponential decay in concentration following the second inflection point is surmised to be the result of back diffusion in the intervening aquifer material between the original DNAPL source zone and KBA-11-34. This conjecture is supported by noting the second inflection point also represents the time when the PCE concentration in KBA-11-34 fell persistently below the concentration in further downgradient KBA-11-13A as shown in Figure 5.5.4.

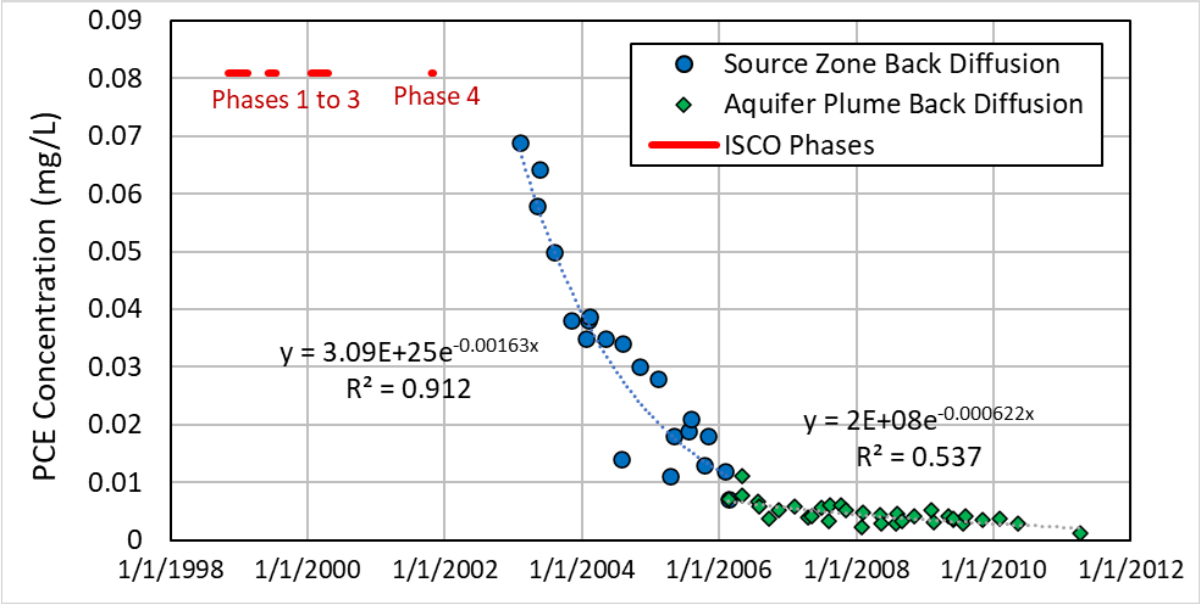

Figure 5.5.5. Trends in Long-Term, Downgradient Monitoring at KBA-11-34

Detailed modeling of back diffusion is beyond the scope of this effort and various physical interpretations for the first order decay constant can be found in Haggerty and Gorelick (1995). In this application back diffusion is modeled as uniformly distributed lenses of fine-grained material in the source zone wherein aqueous diffusion dominates the mass transfer process. Hence, lens thickness, porosity and surface sorption parameters determine this first order coefficient. Guidance and equations for estimating the back diffusion decay constant can be found in Liu and Ball (2002), Parker et al. (2008), and Yang et al. (2015). Other methods for modeling back diffusion can be found in Muskus and Falta (2018) and ESTCP project ER-201426.

5.5.1.4 Remediation Modeling

The best estimate for the model parameters spanning the full life of the DNAPL source zone at Site 11 are provided in Table 5.5.2. The development of parameter estimates was described in the previous section along with the calibration targets. The results of the volume-averaged model applied to Site 11 are illustrated in Figure 5.5.6 for the PCE mass discharge rate and in Figure 5.5.7 for the PCE discharge concentration. Figure 5.5.7 includes monitoring data from well KBA-11-34 located approximately 13 m downgradient from the model DNAPL source zone (see Figure 5.5.3). This well was installed at the end of ISCO Phase 4 and the travel time from the DNAPL source zone to KBA-11-34 under the natural gradient was about 2 years. The slope of the decaying concentration at this location is assumed to represent the decay in mass discharge following multiple applications of ISCO in the DNAPL source zone; although the magnitude of the concentration is expected to be significantly attenuated by natural processes compared to the average source discharge concentration. The numerical model result is described in Appendix D. This figure also includes an estimate for the average PCE concentration in fine-grained material within the source and its decay over time during back diffusion. The back diffusion considered a mobile-immobile (i.e., sand-clay) zone bulk mass transfer coefficient (K_{im}) of 0.00025 1/day based on a clay penetration depth of 1.0 meter and an immobile zone fraction (f_{im}) of 0.11.

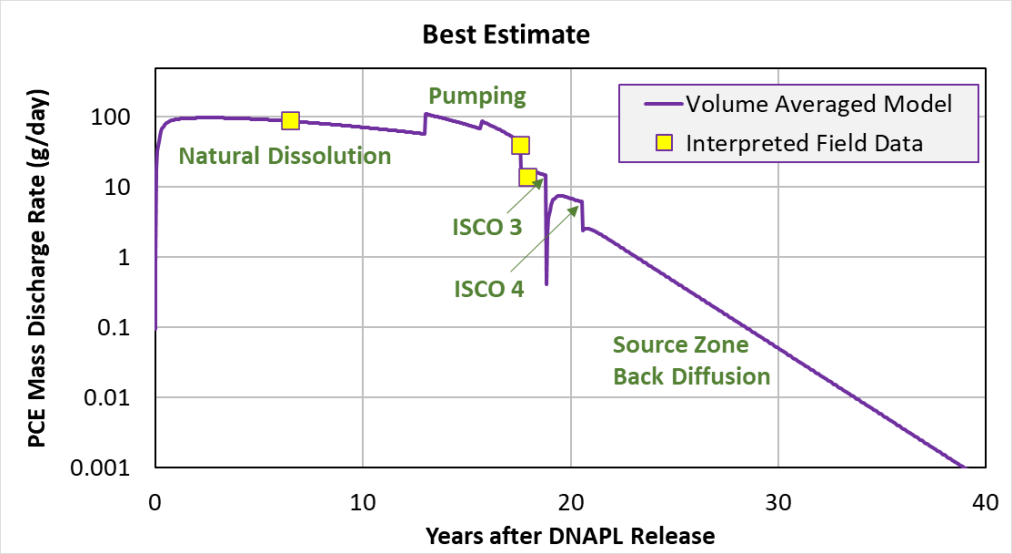

Figure 5.5.6. Model Estimates for PCE Mass Discharge Rate and Interpreted Field Data

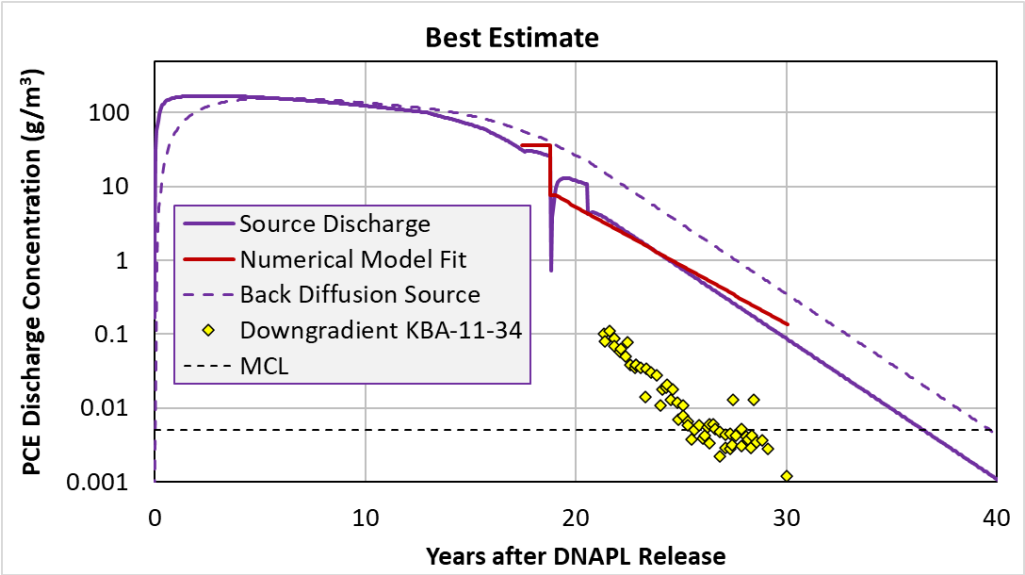

Figure 5.5.7. Model Estimates for PCE Discharge Concentration, Numerical Model Fit, and Downgradient Monitoring Data

The application of the model to the implementation of ISCO Phases 3 and 4 required the specification of destruction efficiencies for the mass destroyed in the DNAPL and the dissolved phase in the mobile and immobile zone pore volumes. These destruction efficiencies are listed in Table 5.5.4 for Phase 3 and Phase 4. As discussed in Section 5.5.1.2, Phase 3 was applied primarily to the mobile zone with ganglia DNAPL and did not impact the bottom interface with the silt. Therefore, Phase 3 destructed a portion of the ganglia DNAPL (~80%) but did not impact the pool. The ISCO application in Phase 3 was widespread and therefore assumed to destroy 90% of the dissolved mass in the mobile zone and none of the dissolved mass in the immobile zone (0%).

Phase 4 was applied at the bottom of the mobile zone and into the immobile zone, i.e., the underlying silt interval to target the DNAPL pool. The model assumes Phase 4 did not impact the ganglia DNAPL (0%) but completely destroyed the pool DNAPL (100%). Phase 4 was applied across a portion of the source zone therefore destruction of the dissolved mass in the mobile zone was assumed to be 50% while no destruction was assumed for the dissolved mass in the immobile zone.

Table 5.5.4. Estimated PCE Mass Removal at the Site 11 Following ISCO Phases 3 and 4

Treatment Zone	Phase 3 ISCO	Phase 4 ISCO
Ganglia DNAPL	80%	0%
Pool DNAPL	0%	100%
Mobile Zone Dissolved Mass	90%	50%
Immobile Zone Dissolved Mass	0%	0%

The back diffusion was simply modeled to match the observed decay rate (0.6 yr^{-1}) in KBA-11-34 and indicated in Figure 5.5.5. Referring to Eqn. (2-21), a first order rate coefficient of 0.09 yr^{-1} and an immobile zone fraction of 0.11 provide a decay rate matching the observed back diffusion decay rate.

5.5.1.5 Evaluation of Remedial Alternatives

The best estimate model assumed the pool made up 16.2% of the initial DNAPL mass with ganglia assumed for the remainder. This pool to ganglia ratio provided the best match to the estimated source mass discharge rates through the pump-and-treat efforts. The MNA timeframe for this architecture was on the order of a century to attain MCL for the source discharge concentration. If all of the mass had been assumed ganglia, the MNA timeframe was less than 50 years. The addition of a small pool, 8.1%, did not add a significant period to the MNA timeframe. However, increasing the pool percentage to 12.1% yielded an MNA timeframe over 70 years. Assuming a pool mass fraction of 24.3% increased the MNA timeframe beyond 130 years. A larger pool percentage than about 25% was clearly not consistent with the mass discharge history observed through the end of the pump-and-treat effort.

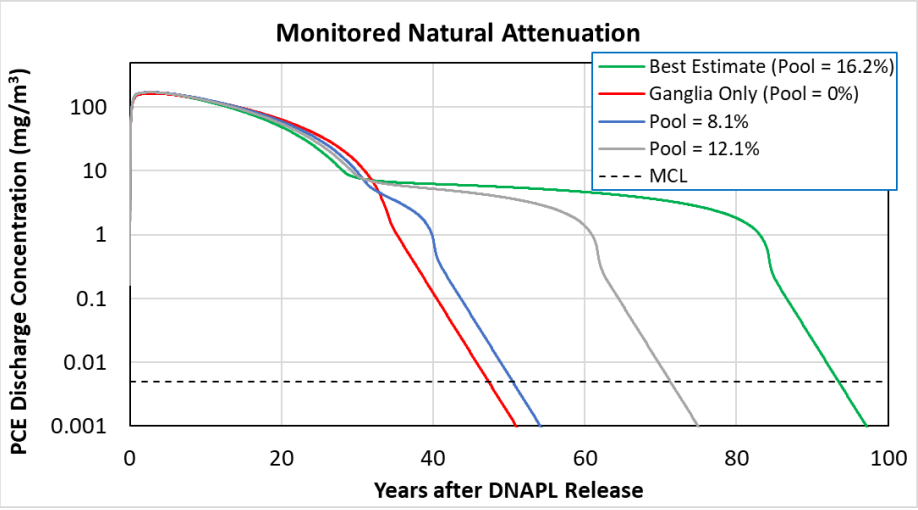

Figure 5.5.8. Model Estimates for PCE Discharge Concentration with Dissolution under Natural Gradients

Calculation results for ISCO implementations which varied from the actual operations are illustrated in Figure 5.5.9. The results for the PCE discharge concentration suggest destruction of the pool was pivotal for reaching cleanup goals. The additional time to reach cleanup without implementing Phase 3 (Phase 4 Only) was inconsequential suggesting Phase 3 was unnecessary. However, from a practical perspective, identifying the pool location within the source zone would have been very difficult without first destroying the nearby ganglia and suppressing the local cloud of elevated dissolved phase concentrations.

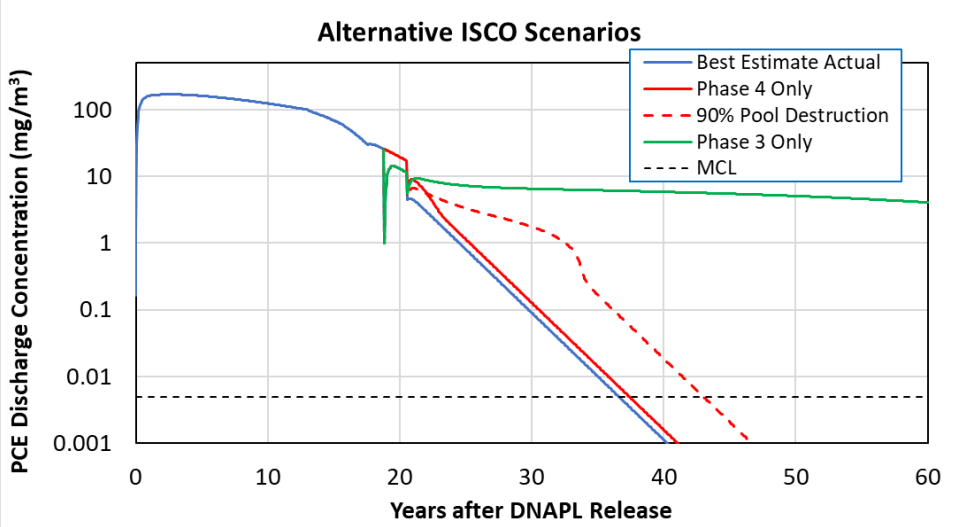

Figure 5.5.9. Model Estimates for PCE Discharge Concentration with Differing ISCO Implementations and Pool Destruction Efficiencies

A pool mass destruction efficiency of 100% was required to match observed trends in downgradient monitoring concentrations. This observation is surmised from the calculation result assuming a pool destruction efficiency of 90% (90% Pool Destruction) shown in Figure 5.5.9. Leaving this residual pool DNAPL may have required a decade of dissolution under natural gradient conditions to complete the DNAPL depletion. The associated mass discharge predicted a much slower concentration decay than was observed in the monitoring data (see Figure 5.5.7). If the DNAPL pool had not been located and ISCO had been terminated after Phase 3 (Phase 3 Only), the cleanup timeframe would have looked very similar to natural attenuation (see Figure 5.5.8).

Calculation results for continued pump-and-treat operations were also evaluated. In these scenarios, ISCO was not implemented. PCE mass discharge rates assuming pumping was continued for 20 years as actually implemented are illustrated in Figure 5.5.10 and the associated PCE discharge concentrations are shown in Figure 5.5.11. These figures also provide results assuming a new pumping well was installed in the vicinity of the DNAPL source and yielded flow velocities through the source zone that were 5 times higher than the natural gradient. The practicality of such a rate was not evaluated for well drawdown and yield.

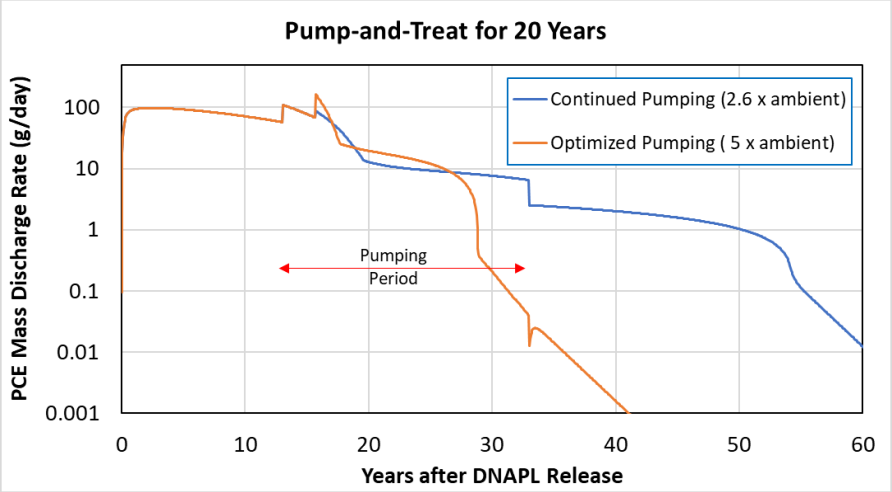

Figure 5.5.10. Model Estimates for PCE Mass Discharge Rates with Differing Pump-and-Treat Scenarios

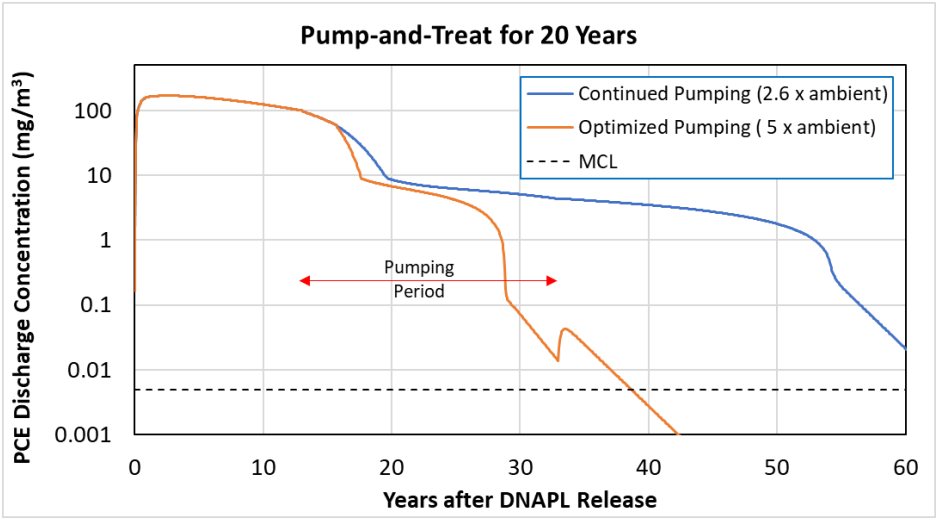

Figure 5.5.11. Model Estimates for PCE Discharge Concentration with Differing Pump-and-Treat Scenarios

Continuing to pump to induce a velocity 2.6 times the natural gradient was not likely to provide significant benefit. This conclusion is evident in the results when pumping was terminated after 20 years. The mass discharge rate remained high and the discharge concentration was little changed. However, the optimized rate indicated complete DNAPL depletion could be achieved within that time period. At the termination of the pumping, a rebound in discharge was predicted as the mobile and immobile zones re-equilibrated in response to the slower velocity. If the pump-and-treat were operated until MCL was achieved in the extraction well and extraction was terminated, rebound would bring values in the source zone back above MCL for several years. The optimized pumping cleanup timeframe was on the order of the best estimate timeframe with two phases of ISCO in the source zone. Hence, this alternative may have been given more serious consideration if these model results had been available at the time. The choice would have required estimating costs for this option, the practicality of pumping at higher rates, and other site priorities and goals.

5.5.2 Site ST012

5.5.2.1 Summary of Remedial Activities

Site ST012 is the location of the former liquid fuel storage area, which encompasses approximately 13 acres within WAFB (Figure 4.2.2.1). Operations were active from 1941 through 1991 when the site was closed. Fuel releases to the environment are suspected throughout the operation; however, major releases of JP-4 were known to occur at a fuel transfer pump station in the 1980s. JP-4 is similar to kerosene in its makeup and impacted soil and groundwater. Estimates for the total volume released range from two to five million gallons based on historical fuel operation records and field data. The primary chemical of concern is the benzene component of the JP-4. WAFB was placed on the National Priorities List in 1989, including Site ST012, and the base was officially closed in September 1993. Hence, the site is regulated under Comprehensive Environmental Response, Compensation, and Liability Act.

As described in Section 4, numerous investigations and remediation activities have been conducted at ST012 over the past three decades. Since 1990, the water table has also risen approximately 90 feet from 230 feet bgs to 140 feet bgs complicating interpretation of site characterization data as conditions are constantly changing with the NAPL smearing across four distinct intervals in the saturated zone as described in detail in Section 4. In the vadose zone, SVE was initiated in 1994, expanded in 2005, and continues to operate. Through November 2021, SVE has removed hydrocarbon mass equivalent to approximately 750,000 gallons of JP-4 indicating a significantly larger NAPL volume remained.

A corrective action remedy of pump-and-treat for groundwater at ST012 was specified in a 1992 ROD when the water table was low. Implementation of extraction through horizontal wells installed over long distances in a relatively narrow saturated interval was operationally ineffective and pump-and-treat was abandoned. Site conditions have changed substantially since that attempt. Several studies followed advocating NAPL skimming and MNA for containment and a final remedy; however, the anticipated persistence of benzene in the groundwater above cleanup goals for centuries was unacceptable under the Comprehensive Environmental Response, Compensation, and Liability Act requirements and the long-term liabilities for DoD were unpredictable. Subsequently the base closure team agreed to a full-scale, pilot test of TEE using steam injection to promote NAPL recovery, depletion of benzene from residual NAPL, and in situ degradation. The TEE pilot test recovered the equivalent of about 18,000 gallons of jet fuel, but the benzene mass removal was the equivalent to its depletion from about 100,000 gallons of weathered JP-4. The success of the TEE pilot test led to a ROD amendment in 2012 and the implementation of full-scale SEE from 2014 to 2016 in the saturated zone. SEE removed an estimated 2.5 million pounds of petroleum compounds (equivalent to 400,000 gallons of JP-4) with approximately 212,000 gallons recovered as NAPL. Site investigations following SEE indicate approximately 400,000 gallons of residual NAPL remain in the saturated zone. A pilot test of sulfate injection to promote anaerobic biological degradation of benzene via sulfate reduction was initiated in 2018 and continues. Containment pumping in select wells was performed from 2018 to 2021 to ensure the dissolved plume remained within the site boundaries. The potential for biological activity alone to provide the containment is currently being evaluated. However, as described in the calculation results to follow, MNA alone would require centuries to attain site cleanup goals. A summary timeline of site remedial activities is provided in Table 5.5.5.

Table 5.5.5. Summary of Primary Remedial Activities

Activity	Date
NAPL Release	~1980s
Pump-and-Treat	1992
TEE Pilot Test	2008-2010
Full-Scale SEE	2014-2016
Containment Pumping	2018-2021

As described above, only three remedial activities have resulted in substantial removal of NAPL mass and NAPL component masses in dissolved and vapor phases: SVE, SEE and a small mass during TEE. The total equivalent volume of jet fuel removed is estimated to be 1,170,000 gallons. An unknown mass has been biologically degraded in situ via natural source zone depletion. The cumulative degraded mass could be substantial but was not estimated. The application of SEE did not monitor the CZ, UWBZ, and LSZ individually for the volume of water extracted or the masses of NAPL and its components recovered. Rough estimates for the steam injection into each horizon were provided by the contractor. Based on these data and subsequent sampling, the majority of NAPL recovery occurred from the LSZ. The SEE treatment targeted a volume of about 200,000 cubic meters (m^3) in the LSZ and the total soil porosity is estimated to be 0.3. Assuming the cumulative total NAPL mass recovery during SEE of 400,000 gallons (1,500 m^3) of JP-4 was from the LSZ, the minimum saturation of NAPL in the LSZ before SEE was 0.025. This metric provides a first estimate for the NAPL saturation in the remaining untreated portions of the LSZ where pooled NAPL formerly resided atop the deep, water table. However, when SEE was terminated, the recovery rate of NAPL components remained undiminished and had not appreciably decayed. This observation suggests additional NAPL remained in the treatment zone and/or the recovery of NAPL on the perimeter and outside of the target treatment continued.

Site characterization data has been collected since the 1980s. The primary data collection has resulted from the installation of wells for a variety of purposes and the sampling of the wells. Conceptual site models for the hydrogeology and the contaminant distribution are described in Sections 4.3.2 and 4.4.2, respectively. Figures 4.3.2 and 4.4.3 provide a visual history for the migration, re-distribution, and detection of NAPL at the site in response to the geology, hydrogeology, and rising water table. The demonstration at Site ST012 is intended to support remedial decisions moving forward; therefore, the conceptual model of the NAPL source zone was developed based on the most recent data informed by the site history. Given the documented complexities for remediating the site and site priorities, the modeling demonstration at Site ST012 focused solely on the deepest impacted aquifer, the LSZ. Similar modeling and analyses could be performed to support remedial decisions in the UWBZ.

The primary sources of recent data in the LSZ are more than 40 wells installed for the LSZ for the SEE process (LSZ-series up to 42), older perimeter monitoring wells (W-series) outside the SEE target treatment zone, and ~20 wells installed outside the SEE treatment zone after SEE was terminated (LSZ-series above 42). The locations for the majority of these wells across the LSZ are indicated on the site map in Figure 4.4.4.

5.5.2.2 Conceptual Model for the NAPL Source Zone and Model Parameter Estimation

The expanse of the NAPL-impacted area in the LSZ is defined by the delineation of NAPL performed when the water table was located in the unconfined LSZ. The boundary for this 1990 area is illustrated in Figure 4.4.3. This map also denotes wells from which NAPL has been recovered since 2017 and includes seven well outside the SEE treatment area. Combining these observations with the recent measures of benzene concentrations in the wells shown in Figure 4.4.4 suggests remaining NAPL treatment is primarily along the full perimeter of the targeted treatment zone for SEE. Benzene concentrations within the SEE treatment zone indicate significant depletion in residual, treated NAPL. Hence, the focus of future treatment is the banded region surrounding the SEE treatment zone. The span of this NAPL-impacted region and the scale of well placement suggests breaking the region into several treatment zones with length scales commensurate with remedy implementation, e.g., well spacing for injection and extraction. These smaller treatment areas are illustrated in Figure 5.5.12. The pool designations represent higher saturation, laterally extensive lenses of NAPL within the volume while the ganglia zones represent lower saturation, more vertically dispersed accumulations as described below. Selection of the areas also considered the operation of the SEE system which emphasized treatment on the downgradient side to the east. Less steam was injected on the western, upgradient side. Pool 1 lies upgradient and along the western boundary of the SEE treatment zone. The volume-averaged modeling demonstration considered each area individually and collectively in the remedy evaluation.

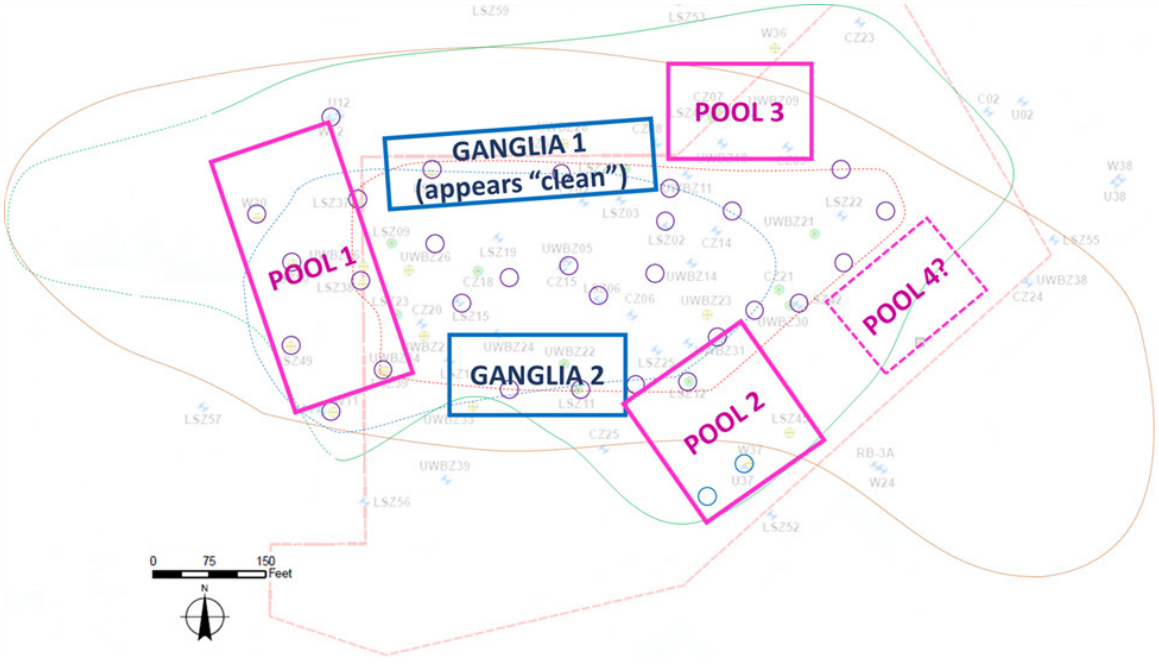

Figure 5.5.12. Target Zones for NAPL Remediation in the LSZ

The primary variables of interest for modeling the target treatment zones were estimates of the characteristic dimensions for the vertical and lateral extent, the initial NAPL mass, the NAPL architecture, and the proportion of components making up the multi-component NAPL. The lengths and widths were selected as indicated in Figure 5.5.12. The vertical interval was estimated as the span of the LSZ and the screen length of its monitoring wells, i.e., 30 feet. The data employed to develop the estimated NAPL mass and architecture in each target volume included:

- 40 geologic logs for wells installed for SEE treatment and wells installed after SEE to characterize NAPL on the boundary and outside the SEE treatment volume,
- Discrete testing for NAPL presence using dye tests at depths indicated by elevated VOC concentrations during the drilling of wells,
- Benzene and total petroleum hydrocarbon concentrations in monitoring wells,
- Detection and removal of NAPL from wells across the LSZ,
- Laboratory analyses on NAPL samples to characterize the content of benzene and other components making up the NAPL mixture,
- Design and operation of the SEE system, and
- Historical rise in the water table and consequent changes in NAPL appearance across the site since 1990 (IT, 1992; IT 1999; BEM Systems, 2011; Amec Foster Wheeler, 2018).

The conceptual model parameters defining the characteristic length scales for each target volume in the LSZ depicted in Figure 5.5.12 and the estimated flow through the volume are listed in Table 5.5.6. The flow through the volume is based on an estimated groundwater Darcy velocity of 73 ft/yr (22.3 m/yr) and the soil porosity is estimated to be 0.35 (BEM Systems, 2007). For this study, back diffusion is not considered. Biological activity is known to be active and therefore any slow discharge of dissolved contaminant from fine-grained material is assumed to be treatable through MNA.

Table 5.5.6. Characteristic Source Zone Dimensions for each Site ST012 Target Treatment Volume

Parameter	Unit	Pool 1	Pool 2	Pool 3	Pool 4	Ganglia 1	Ganglia 2	Source
Length (X_s)	m	48.8	56.4	56.4	51.5	104.9	69.1	Figure 5.5.13
Width (Y_s)	m	103.6	56.9	37.5	36.8	30.1	31.6	
Height (Z_s)	m	9.14	9.14	9.14	9.14	9.14	9.14	LSZ monitor well screen length
Soil Volume (V_s)	m^3	46,203	29,288	19,315	28,895	19,967	17,290	Calculated
Volume Flow (Q)	L/d	57,769	31,684	20,895	16,798	17,617	20,485	Calculated

Geologic logs around the perimeter of the SEE treatment zone and further outside were evaluated and collected into groups coinciding with the six treatment areas shown in Figure 5.5.12. The locations of the wells and the transects considered are shown in Figure 5.5.13. Example geologic input for developing the conceptual models is summarized in Figure 5.5.14 for Pool 1 and include positive NAPL detections and elevated handheld photoionization detector readings from soil cores. The geologic designations for soil were taken from the reported boring logs and follow USGS standards. Similar logs were collected and evaluated in developing the models of the other NAPL treatment zones. These logs and collections are provided in Appendix E.

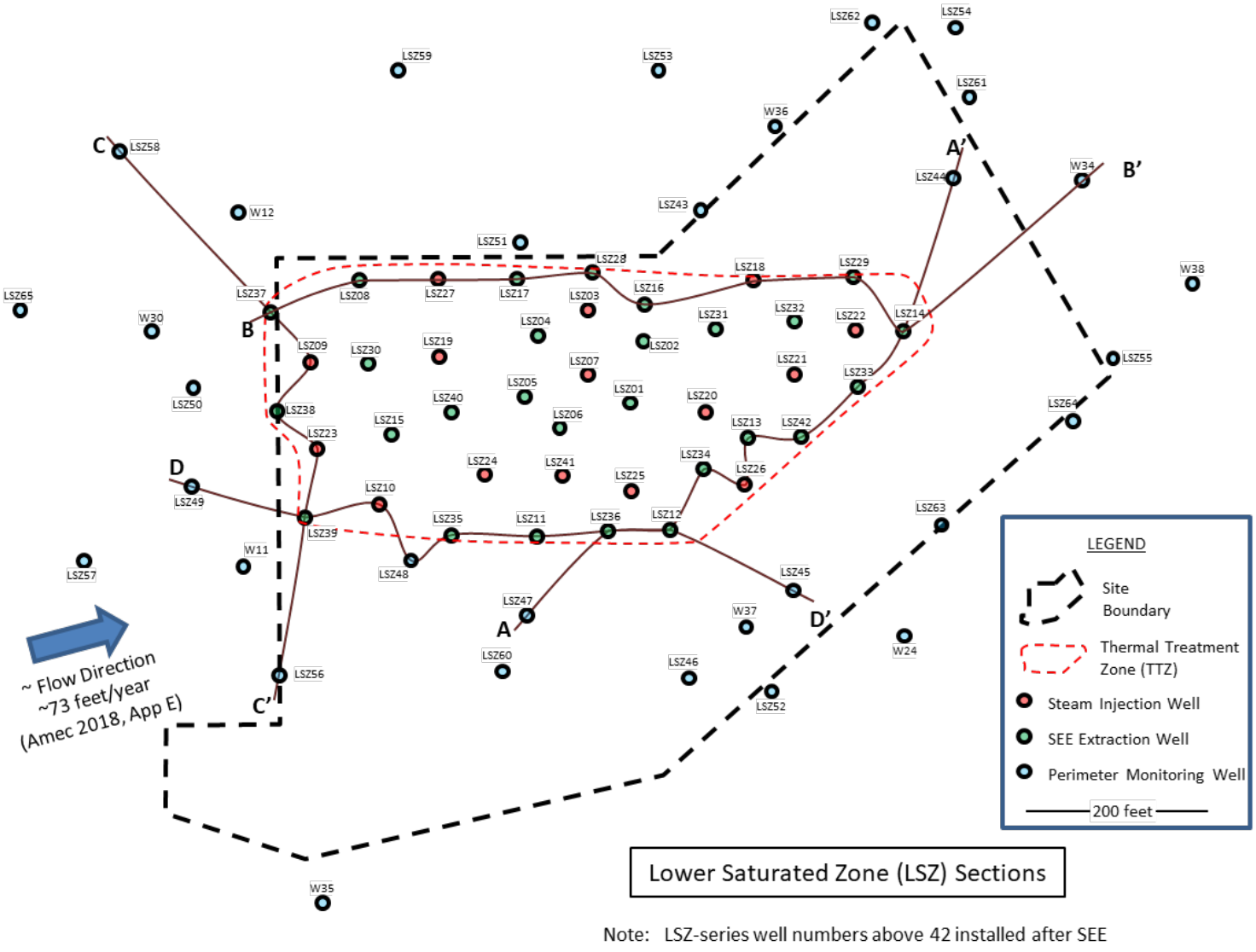

Figure 5.5.13. Location of Boring Logs and Transects

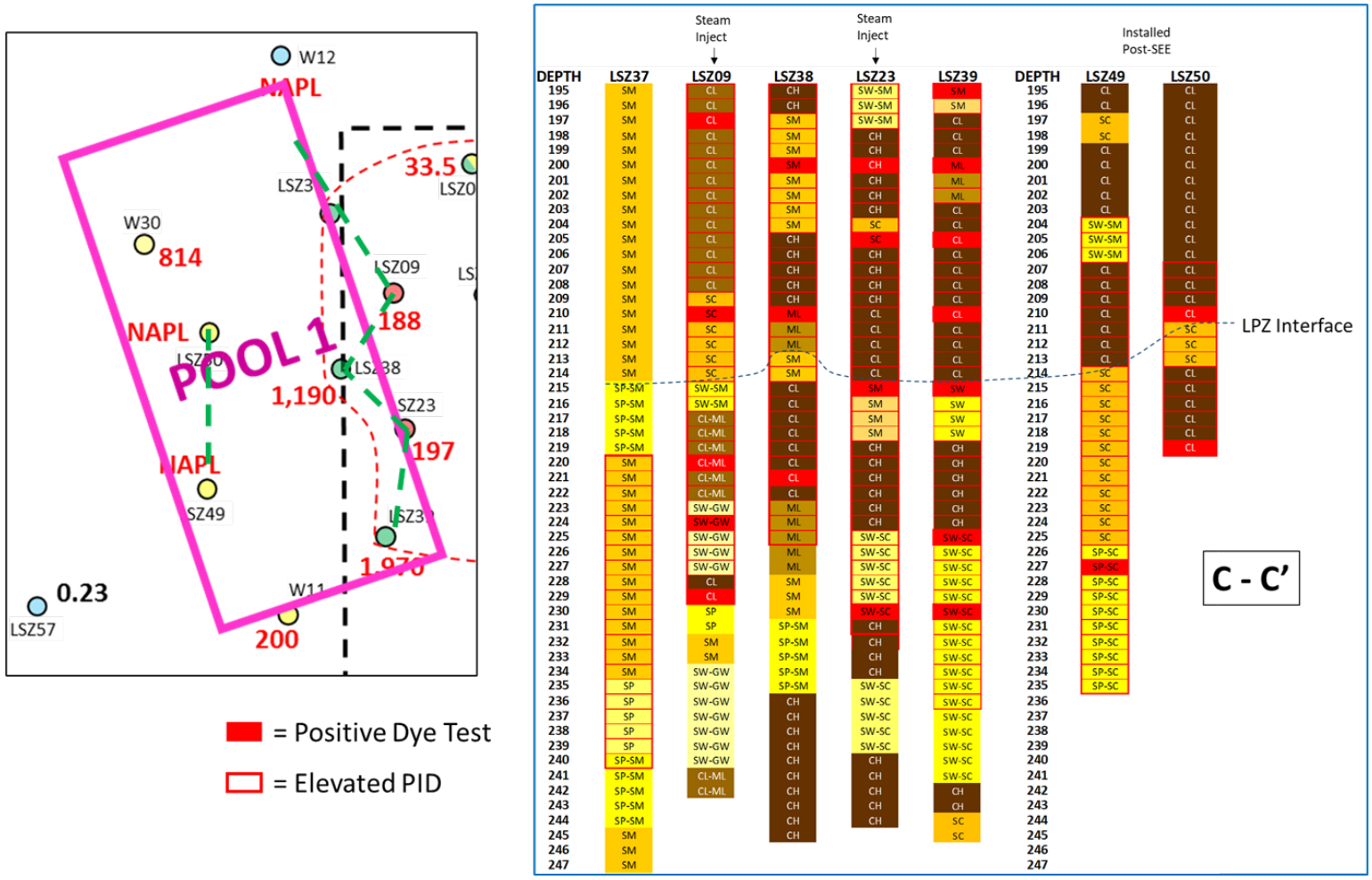

Figure 5.5.14. Boring Logs Defining the Pool 1 Volume

One consistent geologic feature of the site is the continuous existence of a LPZ, characterized as clay, providing a semi-confining layer above the LSZ. The approximate bottom of the clay is indicated in Figure 5.5.14 by a blue dashed line. The bottom of this clay interval is typically found from 205 to 215 feet bgs and is typically 5 to 15 feet thick. The red blocks in the logs indicate positive tests for the presence of NAPL and red outlines indicate elevated photoionization detector readings. The logs along the steam treatment boundary were collected before steam injection and the two logs further west were collected after treatment was terminated. As indicated in the logs, discrete detections of NAPL tended to coincide with the interface of finer grained material overlying coarser material. This phenomenon is consistent with pooled NAPL floating on the water table in 1990 at a depth of approximately 232 feet bgs and rising approximately 90 feet over the past 30 years. As the water table came up, light NAPL was trapped underneath the finer grained material in discrete pools dictated by the shape of the interface left behind as residual ganglia. In addition, as the water table rose, this trapped NAPL was increasingly "squeezed" by the increasing hydrostatic pressure resulting in more lateral movement through coarser lenses. These processes resulted in NAPL appearing and disappearing in a number of wells. Interpretation is further complicated by screen interval locations. For example, a number of wells formerly with NAPL detections have top of screens below the LPZ interface and therefore NAPL reside in the vicinity of the well but does not enter the well.

Figures 5.5.13 and 5.5.14 also indicate which wells were used for steam injection and which wells were used for extraction during the SEE implementation. The screen intervals of all the SEE wells were from 210 to 240 feet bgs. As indicated in the boring logs of Figure 5.5.14, steam injection wells LSZ09 and LSZ23 had extensive NAPL detections before SEE as did extraction wells LSZ-38 and -39. Hence, NAPL contamination extending beyond this boundary was known before SEE implementation. Extraction in wells LSZ37, -38 and -39 was intended to capture any mobilized NAPL and contain the steam zone within the defined treatment volume. Based upon energy balances from the SEE operation data, it is unlikely containment occurred and no temperature monitoring was performed on the western boundary of the SEE operations. Additionally, operation of the extraction pump in LSZ37 was problematic and reduced or shutdown during extended periods of the SEE operation during which no containment occurred in the northwest corner of the site. These observations and the detection of NAPL in the subsequent drilling, coring and monitoring of LSZ49 and LSZ50 suggest a relatively large volume of NAPL remains in the area of Pool 1. Also of note, the drilling of LSZ50 was terminated at a depth of 220 feet bgs even though NAPL was detected and the log from LSZ-49 suggested additional NAPL may reside in deeper sands. Inspection of the logs in Figure 5.5.14 suggests pools may reside on two horizons, at the LPZ interface and in the deeper sand interval around 225 feet bgs. These observations resulted in the designation of the treatment area as Pool 1 to indicate the architecture is dominated by pools. Conceptual source models for the NAPL architecture in the other accumulations were developed similarly.

The total NAPL volume and mass within each target treatment volume can be estimated by developing a range of potential estimates and refining the estimate based on literature reported saturations, the observed NAPL detections during well installation, and the appearance of NAPL in wells during monitoring. As described in the previous section, an overall NAPL mass balance from the SEE operations yielded a minimum, aggregate, average NAPL saturation of about 2.5% over the extremely large treatment volume. This value provides an initial average estimate.

A detailed evaluation of typical NAPL saturations was performed during the TEE pilot test (BEM Systems, 2007) including a literature review of field measures of residual NAPL saturation at fuel-contaminated sites. The reported range in NAPL saturation values was roughly 0.03 to 0.5; however, the works of Adamski et al. (2005) and Charbeneau (2007) were used to select representative average NAPL saturations for each hydrostratigraphic layer in the LSZ. These values are listed in Table 5.5.7 along with values for the average layer thickness, soil type, and total soil porosity. In this approach, the average NAPL saturation in the LSZ was estimated to be 0.047 which is nearly double the value estimated from the SEE mass balance. However, this approach is based on residual ganglia as the architecture.

Table 5.5.7. NAPL Saturation Assumptions for the LSZ from Literature

Hydrostratigraphic Unit	Layer Average Thickness (feet)	Soil Type	Total Soil Porosity	NAPL Saturation
LSZ + 1	9.3	Sand w/Fines (SM)	0.32	0.059
LSZ + 2	4.3	Silt/Clay (CL)	0.35	0.028
LSZ + 3	5.3	Sand w/Fines (SM)	0.32	0.059
LSZ + 4	5.3	Silt/Clay (CL)	0.35	0.028
LSZ Average NAP Saturation				0.047

Estimates for fuel saturation when pooled atop a water table are available from Interstate Technology RC (ITRC, 2018). Examples of measured saturations in homogeneous soils and heterogeneous soils like the LSZ are illustrated in Figure 5.5.15 and are reproduced from ITRC (2018). Based on these illustrations, a saturation of 0.30 provides a reasonable representation for the NAPL saturation in the LSZ.

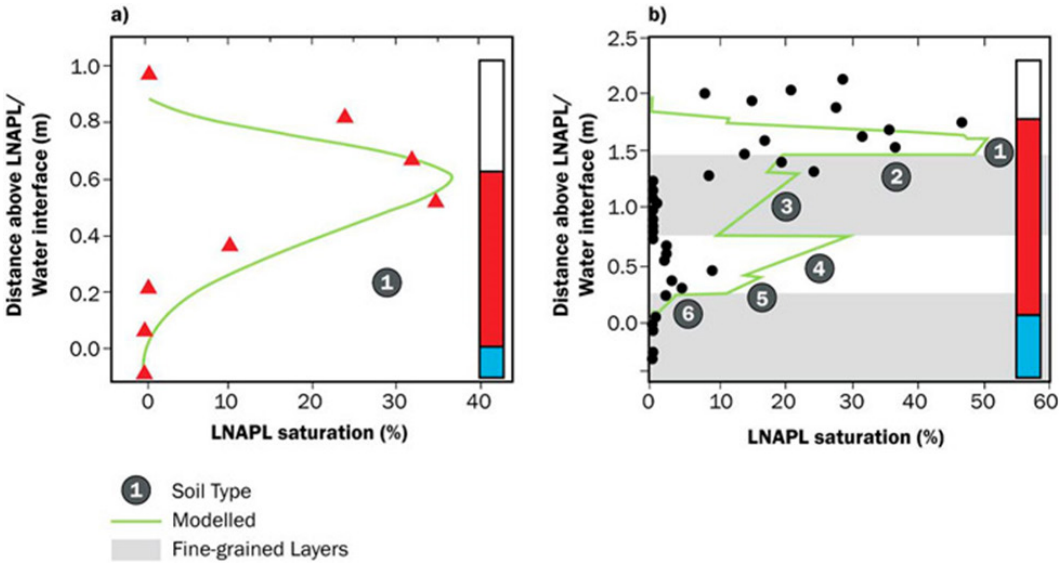

Figure 5.5.15. Measured NAPL Saturations for Fuel Floating on the Water Table in Homogeneous and Heterogeneous Soils (reproduced from ITRC, 2018)

Hence, two approaches are available for calculating the total NAPL volume in the designated treatment volumes: a uniform residual saturation throughout the volume and a pool saturation in discrete, narrow horizons. Two values calculated for a uniformly average NAPL saturation were 0.025 and 0.047, based on the SEE mass balance and literature values, respectively. A reasonable estimate within this range is assumed to be 0.03. In addition, the vertical extent for this average in the LSZ is estimated to be 20 feet (6.7 m) representing the interval from 210 to 230 feet bgs (see Figure 5.5.14). For the pool scenario, a reasonable estimate is 0.30 and the vertical extent is assumed to be 1 foot (0.3 m) based on the geologic logs and NAPL detections. The resulting calculated NAPL volumes in each treatment zone are provided in Table 5.5.8 along with the cumulative total volume in the LSZ. The pool scenario includes sums for one and two distinct pool horizons. The total NAPL volume for a uniform saturation of 0.03 was 1.24 million liters (327,000 gallons) and the total assuming one distinct pool interval was 554,000 liters (146,000 gallons). For the scenario of two distinct pool intervals as described above, the total is similar to the estimate for a uniform average saturation. The contractor estimate for the untreated NAPL residing in the outer areas of the LSZ after the implementation of SEE (Amec Foster Wheeler, 2018) was 100,000 gallons (380,000 liters). The range of calculated total NAPL volume in the LSZ exceed this estimate although the scenario of a single pool is similar.

Table 5.5.8. NAPL Volume Estimates for each Site ST012 Target Treatment Volume

Parameter	Unit	Pool 1	Pool 2	Pool 3	Pool 4	Ganglia 1	Ganglia 2
Length (X_s)	m	48.8	56.4	56.4	51.5	104.9	69.1
Width (Y_s)	m	103.6	56.9	37.5	36.8	30.1	31.6
Porosity	-	0.35	0.35	0.35	0.35	0.35	0.35
Ganglia Scenario							
NAPL Saturation	-	0.03	0.03	0.03	0.03	0.03	0.03
Ganglia Zone Height	m	6.71	6.71	6.71	6.71	6.71	6.71
NAPL Volume	L	355,761	225,517	148,725	133,130	222,491	153,746
Total NAPL Volume	L	1,239,370					
Pool Scenario							
NAPL Saturation	-	0.3	0.3	0.3	0.3	0.3	0.3
Pool Height	m	0.3	0.3	0.3	0.3	0.3	0.3
NAPL Volume	L	159,161	100,892	66,537	59,560	99,539	68,783
Total NAPL Volume	L	554,472					
Total Volume 2 Pools	L	1,108,943					
Combination Scenario							
NAPL Saturation	-	0.3	0.3	0.3	0.3	0.03	0.03
NAPL Interval Height	m	0.3	0.3	0.3	0.3	6.71	6.71
NAPL Volume	L	159,161	100,892	66,537	59,560	222,491	153,746
Total NAPL Volume	L	762,387					

The pool scenario is most likely for the LSZ at ST012; however, a scenario of combined architecture is assumed for the demonstration. This combination is denoted in Table 5.5.8 and provides a comparison of cleanup timeframes for the two architectures. The ganglia assumption yields a larger estimated mass but the mass dissolution rate from NAPL is faster; whereas, the pools have a smaller mass and also dissolve more slowly. A benefit of the volume-averaged modeling approach is the ease and rapidity with which such varied scenarios can be evaluated. The benefit of coupling the modeling with parameter estimation software is demonstrated in Section 8.2.

With the six treatment volumes specified and estimates for the NAPL volumes within each source zone, the primary remaining parameters to define the conceptual source models are the content fractions of each individual component making up the multicomponent NAPL mixture and their transport properties. The measured mass contents in NAPL samples collected from multiple wells in 2006, 2010, 2018, and 2021 are provided in Table 5.5.9.

The measured mass contents were converted to mole fractions using the molecular weights of each model compound, or family of compounds in the model NAPL listed in Appendix E. The equilibrium groundwater concentration for each compound was then estimated using Raoult's Law. Results for benzene are presented in Table 5.5.10. The results of recent groundwater sampling and analyses are also listed in the table for wells that currently exist. The reasonable correlation between the calculated and measured groundwater concentrations corroborates the calculated mole fractions of benzene. In the modeling to follow, the initial mole fractions of components of concern are assumed equal to the 2006 model mole fractions to provide conservative estimates for remediation effectiveness.

The corroboration between NAPL content and groundwater analyses also indicates that groundwater concentrations can be used to infer the proximity of NAPL to wells even when NAPL does not appear in the well. The NAPL analyses also indicate a vast majority of the benzene mass remaining at ST012 is part of the NAPL hydrocarbon mixture rather than dissolved in groundwater or sorbed to soil solids.

Table 5.5.9. Measured Mass Content of NAPL Mass

Compound	Aqueous Solubility	2006	2010				2018			2021			
		LSZ Model	W-01	MWN-3B*	W-03	RB-2C	LSZ 16*	LSZ 50	W37	W12	LSZ46	LSZ50	LSZ49
	(mg/L)		(% mass)										
Benzene	**1780**	**0.83**	**0.60**	**0.22**	**0.83**	**0.44**	**<0.02**	**0.31**	**0.19**	**<0.017**	**0.27**	**0.23**	**0.42**
Toluene	515	2.90	1.80	1.50	2.90	3.00	0.17	2.84	1.76	<0.016	1.84	0.18	0.34
Ethylbenzene	152	1.40	1.40	1.10	1.30	1.70	1.18	1.70	1.66	0.89	1.62	1.59	1.60
m&p-Xylenes	162	2.20	2.20	1.80	2.10	2.40	2.88	4.56	3.77	1.28	3.80	1.24	2.25
o-Xylene	175	0.83	0.70	0.67	0.83	1.10	1.31	1.49	1.34	0.19	1.31	0.78	1.01
Naphthalene	32	0.50	0.60	0.22	0.83	0.44	0.30	0.11	0.17	0.08	0.13	0.23	0.15

* within SEE or TEE treatment zones

Table 5.5.10. Calculated Benzene Mole Fractions, NAPL-Equilibrium Water Concentrations, and Recent (2021) Measured Groundwater Concentrations

LSZ Benzene Data		Mole Fraction	Equilibrium Concentration (µg/L)	Recent Concentration (µg/L)
2006	LSZ Model	0.01156	20,700	
2010	W-01	0.00840	15,000	-
	MWN3B*	0.00308	5,510	-
	W-03	0.01162	20,800	-
	RB-2C	0.00616	11,000	-
2018	LSZ16*	0.00028	<500	-
	LSZ50	0.00422	7,550	2,980
	W37	0.00297	5,320	7,250
2021	W12	0.00024	<430	17
	LSZ46	0.00379	6,780	1,860
	LSZ50	0.00344	6,160	2,980
	LSZ49	0.00578	10,300	5,490

* within the TEE or SEE treatment zones

Properties of components of concern of the JP4 mixture relevant to dissolution and transport are provided in Table 5.5.11. These properties are utilized as input to the dissolution and remediation model. The retardation coefficient, *R*, was calculated from the equation below and utilized the site-wide soil properties listed in Table 5.5.12.

$$R = 1 + \frac{\rho_b f_{oc} K_{oc}}{\phi}$$

Table 5.5.11. NAPL Component Properties and Initial Mole Fractions

Property	Unit	Benzene	Toluene	Naphthalene
Molecular Weight, MW	g/mol	78.114	92.141	198.394
Solubility, C^*	mg/L	1806.6	556.2	111.7
Cleanup Concentration, C_{MCL}	mg/L	0.005	1	0.027[a]
MCL Mole Fraction, y_{MCL}	-	2.768E-06	0.0017979	0.0002417
Initial Mole Fraction, y_0	-	0.011557	0.034234	0.004243
NAPL Equil Solubility, $y_0 C^*$	mg/L	20.8794	19.0410	0.4739
Octanol-Carbon Coeff, K_{oc}		56.234133	117.48976	912.01084
Retardation, R		1.0830	1.1735	2.3465

[a] Naphthalene does not have an MCL but the site ROD specifies a cleanup goal of 27 ug/L.

Table 5.5.12. Site ST012 Soil Properties

Property	Unit	Value
Total Soil Porosity,	-	0.35
Soil Bulk Density,	kg/L	1.723
Organic Carbon Fraction, f_{oc}	-	0.0003

5.5.2.3 Calibration Targets and Remediation Modeling Assumptions

SEE is the only remedial technology applied previously at the site under conditions similar to the current conditions. Modeling a multiphase process like SEE can be accomplished using the volume-averaged modeling approach by including an energy balance to evaluate the size of the steam zone and by assuming a fraction of the NAPL is recoverable, e.g., 50-60%, with the remaining fraction being residual. Mass removal rates from the residual NAPL can be estimated with flow rates of steam and NAPL component volatility to calculate the depletion of individual components. Such a model is feasible and could be compared to the previous SEE implementation but the effort is beyond the scope of this work. In addition, SEE is not considered in the remedial evaluation of remaining NAPL areas at Site ST012 because these NAPL areas were known prior to the previous implementation of SEE. The base closure team agreed that the disruption created to the existing surface infrastructure in these areas, e.g., a building and major thoroughfare, made the areas impractical for the installation and operation of SEE wells, pumps, piping, and electrical. Instead, the 2012 ROD amendment called for the application of an unspecified biological enhancement process to accelerate the treatment of NAPL in these outer areas.

Following the SEE termination, push-pull testing was performed in two perimeter wells to evaluate the addition of sulfate for promoting sulfate reduction of dissolved contaminants. The testing and cost analyses led the Air Force contractor to select this approach to promote anaerobic degradation over methods of introducing oxygen to promote aerobic degradation. The 2012 ROD amendment had set a goal of 20 years for attaining the groundwater cleanup standards and a full-scale pilot test of sulfate injection was initiated in 2018 to assess sulfate reduction against this metric. The pilot study is currently being evaluated by the Air Force.

Containment pumping was performed in the LSZ from 2018 to 2021; however, the pumping strategy was also designed to distribute injected sulfate across target areas of the LSZ. As a result, the pumping was inconsistent and no extended, quasi-steady periods of extraction are available with flows and mass removal estimates sufficient to evaluate pump-and-treat in any area of the site. Hence, no remedial activities from the site's history are available to provide calibration targets for the volume-averaged modeling. In addition, natural groundwater velocities are relatively slow and natural biological processes at the site are sufficiently effective to attenuate concentrations over relatively short distances, i.e., prior to arriving at downgradient wells. Without a groundwater plume spanning multiple monitoring wells, biological degradation is difficult to quantify other than to provide a minimum rate of degradation.

The lack of consistent groundwater pumping at ST012 precludes any interpretation of data for estimating current or historical mass discharge rates from the designated treatment areas around the LSZ. The relatively rapid degradation of dissolved contaminants precludes any interpretation of data for estimating current or historical discharge concentrations from the treatment areas.

The only available estimate for the mass discharge rate is the groundwater velocity multiplied by the projected area and component equilibrium concentrations. However, these mass discharge rates are the assumed values for the model input. Hence, the demonstration at ST012 lacks any calibration targets derived from plume transport modeling or remedy implementation. Interpreting the SEE operational data to deduce a mass discharge rate is beyond the scope of this project as described above. The site demonstration of the modeling proceeded with a focus on informing future remedial decisions based on the conceptual source models and the estimated remedial efficiencies required to achieve cleanup goals in a reasonable timeframe.

The demonstration of the model for the remaining target treatment zones of the LSZ at ST012 and delineated in Figure 5.5.12 included evaluations of the following remedial technologies:

- Monitored natural attenuation
- Enhanced biological degradation
- Pump-and-Treat
- In situ chemical oxidation

The approximate dissolution model for multicomponent NAPL described in Section 2.2.5.2 is applicable to the JP4 NAPL at ST012. Soluble aromatic compounds make up roughly 12% of the NAPL with the remainder consisting of low and very low solubility saturated hydrocarbons as described in Appendix D. The approach to modeling remediation is described in Section 2.2.6 and generally consists of estimating technology-specific enhancement factors to the NAPL dissolution rate. Generic enhancement factors are defined in Eqn (2-37) and were applied to Eqn (2-31). The enhancement included simple changes in the flow (E_f) and changes in the dissolution rate resulting from aqueous phase reactions (E_r) to increase the driving concentration gradient. Aqueous phase reactions also reduce the discharge mass rate and discharge concentration. For ST012, this reaction was modeled by the first order reaction rate term in Eqn (2-34).

The conditions for MNA include the baseline, natural gradient velocity (73 ft/yr) with no enhancement (E_f=1) and existing biological degradation. The existing degradation rate is assumed to be 0.001 day^{-1}. This degradation rate was estimated from simplified Monod kinetics and background electron acceptors moving into the site. This estimated degradation rate is slow; however, the velocity through the NAPL-impacted volume is also slow. This balance of processes is evident in the lack of a discernible downgradient plume. The ratio of the characteristic residence time of water in the NAPL-impacted soil volume to the characteristic reaction time is known as the Damkohler number, Da, and is defined by,

$$Da = (ResidenceTime)/(ReactionTime) = (X_n \lambda_r)/(U_0 \phi)$$

Seagren et al. (1994) derived a theoretical expression for the reaction enhancement to NAPL dissolution during flow over a NAPL pool with a first order reaction in the aqueous phase. The expression is solely a function of the Damkohler number,

$$E_r = \frac{1}{2}\sqrt{\frac{\pi}{Da}}\left[\left(Da + \frac{1}{2}\right) erf\left(\sqrt{Da}\right) + \sqrt{\frac{Da}{\pi}}\, exp(-Da)\right]$$

A method to estimate enhancement to NAPL dissolution with first order reactions for flow through ganglia architecture was derived by Christ et al. (2007) and reviewed by Seagren and Becker (2015). With the ganglia architecture, the reaction enhancement is also a function of the Stanton number, St, which is the ratio of the residence time to the characteristic mass transfer time,

$$St = (ResidenceTime)/(MassTransferTime) = (X_n K_n)/(U_0 \phi)$$

and the Peclet number, Pe, which is the ratio of the advection rate to the dispersion rate. However, for the vast majority of field applications, the Peclet number for NAPL dissolution will be very large and reactive enhancements will only be appreciable if the Stanton number is large, i.e., >10. NAPL dissolution is relatively long process compared to a relatively short residence time, i.e., St is small. Therefore, typical first order reactions are not expected to enhance ganglia dissolution where the interfacial area between water and NAPL is large as compared to the pool architecture. The results of applying these theoretical enhancements to MNA and enhanced biological degradation to each target treatment zone in the LSZ are provided in Table 5.5.13. Small differences in values result from differing assumed pool lengths. For MNA, the estimated background degradation rate provides a small but significant enhancement to the dissolution rate of pools. As described above, no enhancement is expected for the ganglia architecture.

Table 5.5.13. Remedy Enhancement Factors for each ST012 Target Treatment Volume

Parameter	Unit	Pool 1	Pool 2	Pool 3	Pool 4	Ganglia 1	Ganglia 2
NAPL Zone Length (X_n)	m	48.8	56.4	56.4	51.5	104.9	69.1
Monitored Natural Attenuation							
E_f	-	1	1	1	1	1	1
λ_r	1/day	0.001	0.001	0.001	0.001	0.001	0.001
Da	-	2.29	2.64	2.64	2.41	4.91	3.24
E_r	-	1.63	1.71	1.71	1.66	1	1
Enhanced Bioremediation							
E_f	-	2	2	2	2	2	2
λ_r	1/day	0.005	0.005	0.005	0.005	0.005	0.005
Da	-	11.43	13.21	13.21	12.06	24.57	16.19
E_r	-	3.13	3.34	3.34	3.20	1	1
Pump-and-Treat							
E_f	-	10	10	10	10	10	10
λ_r	1/day	0.001	0.001	0.001	0.001	0.001	0.001
E_r	-	1.63	1.71	1.71	1.66	1	1
In Situ Chemical Oxidation							
E_f	-	2	2	2	2	2	2
λ_r	1/day	0.1	0.1	0.1	0.1	0.1	0.1
E_r	-	15	15	15	15	15	15

The implementation of enhanced anaerobic degradation via the introduction of sulfate salt to promote sulfate reduction involves both flow and reactive enhancements to dissolution. The pilot study of enhanced sulfate reduction as currently operated is not expected to enhance dissolution.

Large quantities of sulfate were injected in wells and have been left to drift across the site. Given the slow groundwater velocity and the lack of mixing, the sulfate is not expected to be well dispersed. Therefore, in the modeling demonstration, a recirculation cell is assumed to be operated in each of the treatment zones. A constant, low level of flow provides a flow enhancement dissolution, estimated to be a factor of 2 over the natural gradient, while also dispersing the sulfate more uniformly across the cell and re-supplying the sulfate as it is utilized. The recirculation system is assumed to have the capability to monitor the effluent and add amendments as necessary, e.g., nutrients, to maintain the degradation rate until cleanup goals are achieved. An increase in the sustained degradation rate by a factor of five was estimated from Monod kinetics. The Damkohler number increased accordingly and the theoretical enhancement for the pool dissolution calculated with the expression above yielded an increase of approximately 3, in line with estimates from other sites (Seagren and Becker 2015), and as indicated in Table 5.5.13. If an order-of-magnitude increase in the degradation rate could be generated, the enhancement factor increased to about 4.5 for the pools, nearly tripling the MNA enhancement.

The implementation of pump-and-treat was very straightforward and only involved a flow enhancement factor linearly proportional to the increase in characteristic velocity through the target zone. The increased flow may accelerate the introduction of background electronic acceptors to promote increased degradation rates but this increase is offset by the decreased residence time of water in the volume. Hence, no reactive enhancement over natural conditions is assumed as indicated in Table 5.5.13.

ISCO provides rapid reaction rates for the dissolved contaminants when the oxidant is well dispersed and constantly supplied. Therefore, in the modeling demonstration, it is assumed a partial recirculation cell is created in each of the treatment zones. The oxidant is introduced and moves through saturated soil depleting reactive carbon from the soil solids and, when this sink is satisfied, reacts effectively with dissolved contaminants. The oxidant demand of the soil solids was not included in this modeling. The partial recirculation system provides a flow enhancement to the dissolution and mixing with the oxidant. The rapid reaction rate makes this process closer to second order than first order; therefore, the reactive enhancement factor was calculated using the second order estimate of Cussler (1992) provided in Eqn. (2-44). For the modeling demonstration, the selected oxidant is presumed to be persulfate. A byproduct of the oxidation reaction is sulfate which can then migrate downgradient and be utilized by sulfate reducing bacteria to promote aqueous degradation in other areas of the site.

5.5.2.4 Evaluation of Remedial Alternatives

The evaluations of remedial alternatives for the LSZ at ST012 were performed for each of the target treatment volumes indicated in Figure 5.5.12 with each of the following remedial alternatives:

- Monitored natural attenuation
- Enhanced biological degradation
- Pump-and-treat
- In situ chemical oxidation

The dimensions of each target zone and the flow moving through under natural gradients are provided in Table 5.5.6. The volume of NAPL and its assumed architecture for each target are described in Table 5.5.8. The initial mole fraction of each of the relevant NAPL components and their transport properties are listed in Tables 5.5.9, 5.5.11, and 5.5.12. The calculated target-specific dissolution enhancement factors and technology-specific reactive enhancements for each remedial alternative are listed in Table 5.5.13. These data comprise the model input parameters used with Eqns. (2-31), (2-34) and (2-37) to perform the temporal calculations for mass discharge rate and discharge concentration for each scenario.

Calculations for the benzene discharge concentrations from Pool 1 are illustrated in Figures 5.5.16 to 5.5.18 for each remedial alternative compared to MNA. The plots on the right-hand side of each figure are calculated mole fractions of benzene remaining in the pool. The mole fraction corresponding to an aqueous equilibrium concentration equal to the benzene MCL (MCL-equivalent) represents NAPL depletion. Attaining this level of depletion ensures meeting cleanup criteria on any measurement scale. For these figures, the remedial activity was terminated at discharge MCL rather than MCL-equivalent mole fraction. The benzene discharge concentration on the left-hand side is also function of the target zone height and width. Recall, for this site demonstration a height of 30 feet (9.14 m) was assumed for all target source zones as this height corresponds to the length of monitoring well screen intervals in the LSZ.

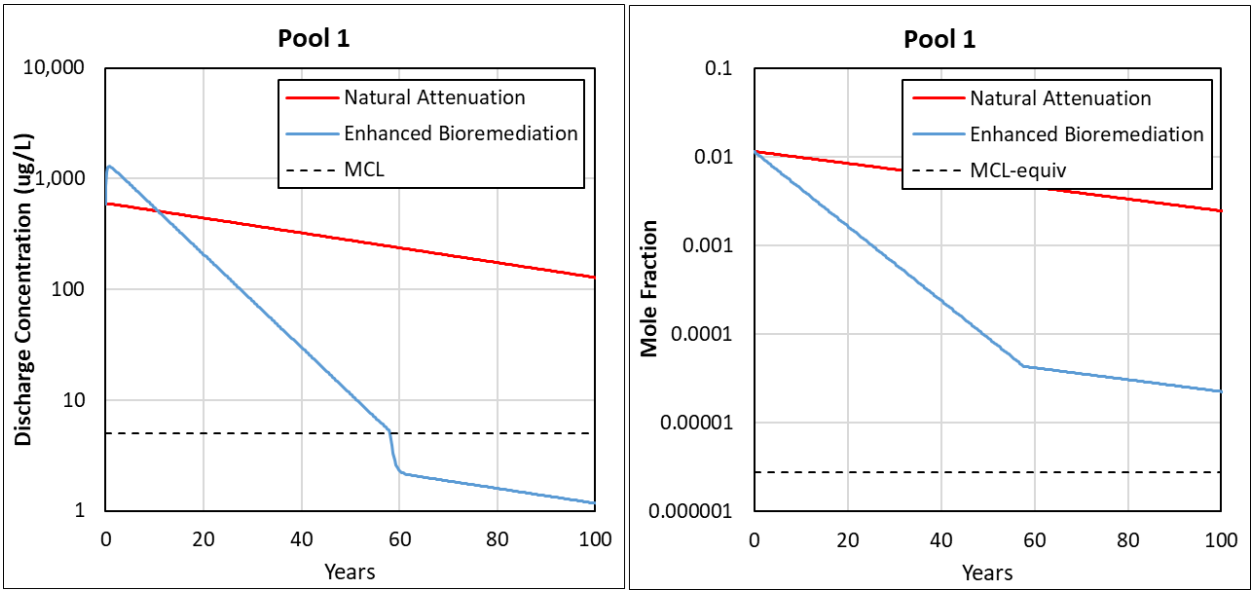

Figure 5.5.16. Model Output for Enhanced Bioremediation with Recirculation in Pool 1

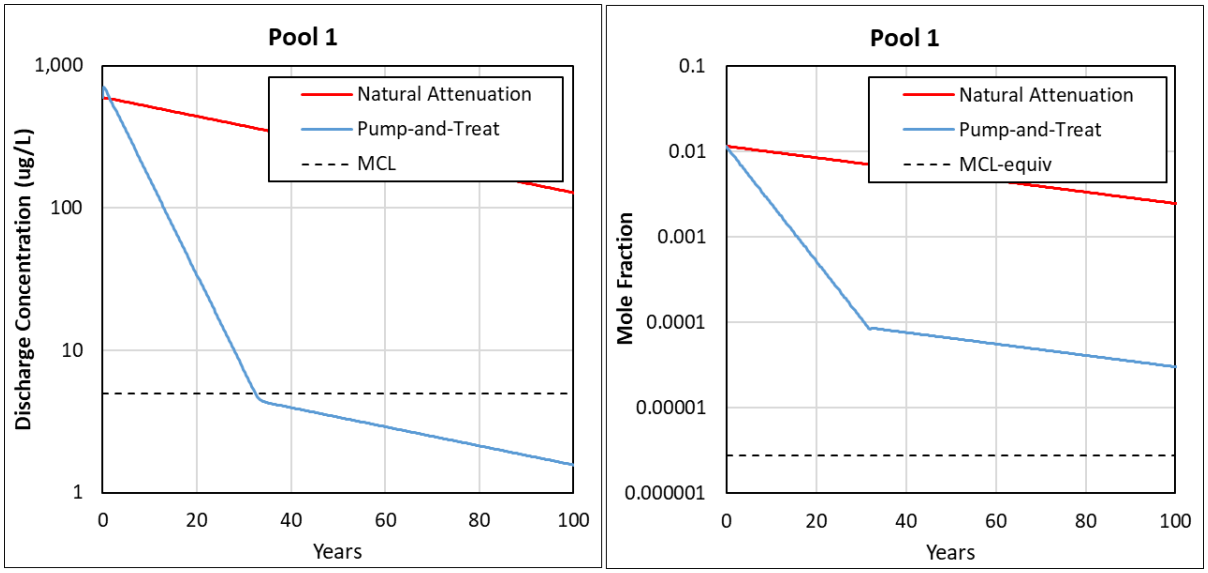

Figure 5.5.17. Model Output for Pump-and-Treat in Pool 1

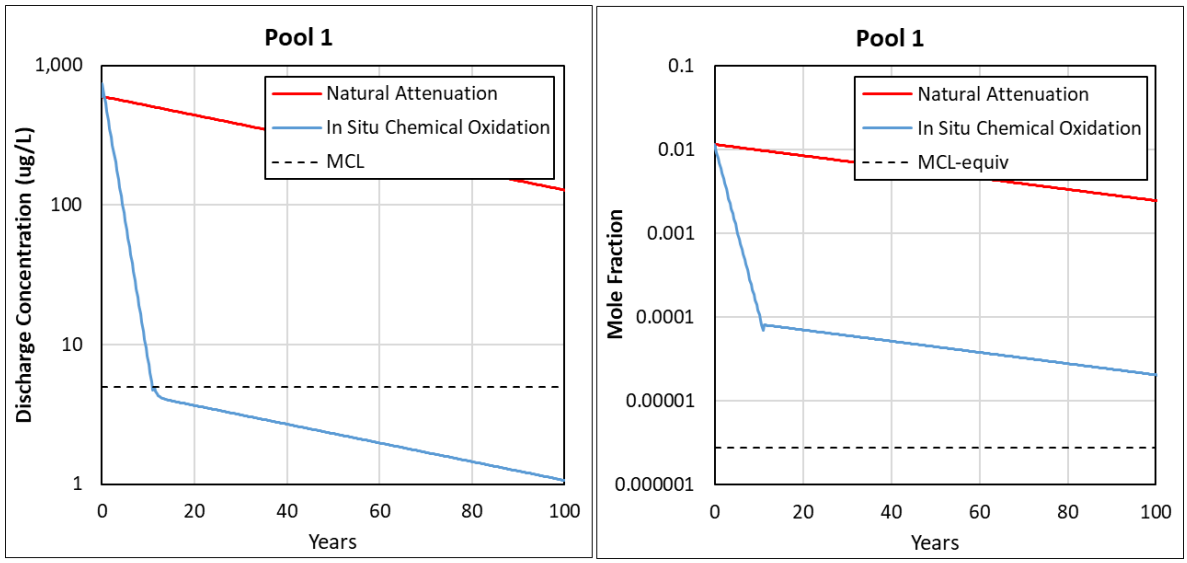

Figure 5.5.18. Model Output for ISCO with Recirculation applied to Pool 1

The calculated durations of treatment to attain MCL for benzene in each target treatment zone are listed in Table 5.5.14. The initial pool dimensions and saturations were similar for each target pool volume and therefore the calculation results are all similar. As expected, assuming ganglia architecture yielded much shorter durations as the mass transfer coefficients were significantly higher before enhancement. Smaller, more discrete pools of similar total NAPL volume would yield faster cleanup times than the assumed single pools. In evaluating such scenarios for the conceptual source model and each technology, the input can be edited and calculations performed in real-time during a roundtable discussion of stakeholders. This activity would facilitate a group discussion on the specific technical issues for the site and remedy and avoid unfounded conjecture. In other words, disagreements would manifest as differing input parameters rather than speculation.

Table 5.5.14. Summary of Operational Years for Remedy Alternatives to Attain Cleanup Goals

Parameter	Pool 1	Pool 2	Pool 3	Pool 4	Ganglia 1	Ganglia 2
Monitored Natural Attenuation						
MCL	310	351	322	325	122	82
NAPL Depletion	540	609	556	565	136	90
Enhanced Bioremediation						
MCL	58	66	60	61	21	14
NAPL Depletion	85	97	89	90	22	15
Pump-and-Treat						
MCL	32	37	34	34	13	8
NAPL Depletion	54	61	55	56	13	9
In Situ Chemical Oxidation						
MCL	11	12	11	11	4	3
NAPL Depletion	18	20	19	19	4	3

Natural attenuation for the pooled features was calculated to be over 300 years to attain MCL for benzene at the discharge plane. The pool scenarios yield timescales of 500 years to deplete benzene from the NAPL. The two ganglia scenarios attain MCL and depletion on the order of 100 years. As expected, the pool scenarios are the drivers of cleanup time.

For the assumed increased biological degradation rate and its maintenance with recirculation, the cleanup time was substantially reduced to an order of 60 years. However, an evaluation of the design and operation of such a system to meet these metrics is likely to find such a long period of active intervention is cost prohibitive. Pump-and-treat could lower the cleanup to about 30 years. The effort would require the installation and operation of a system capable of handling approximately 350 gallons per minute. The recirculation for enhanced bioremediation and ISCO requires the extraction and injection rate on the order of 80 gallons per minute. The implementation of ISCO has the potential to meet a cleanup timeframe of about a decade. However, this would require installing and operating a relatively high maintenance system for a long period. Determining the feasibility of an oxidant to meet the performance requirements for the enhancement would likely require a full-scale field pilot test.

The durations required to attain MCL for each remedial alternative are summarized in Figure 5.5.19. Calculations for toluene and naphthalene yielded much faster cleanup times as their modeled initial mole fractions are close to their MCL values.

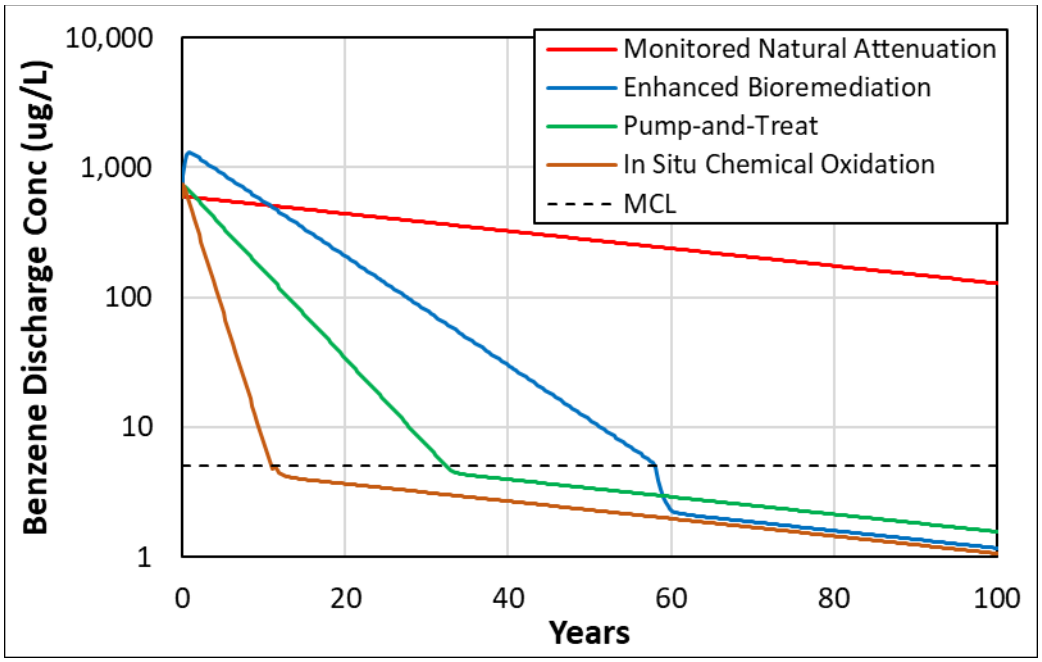

Figure 5.5.19. Volume-Averaged Model Comparison of Remedial Alternatives for Pool 1

5.6 EVALUATION METHODS FOR MODEL OUTPUT

5.6.1 Performance Objective 1

For Performance Objective 1, with the synthetic model results, the source zone properties and contaminant distribution are completely specified and known. Hence, these data provide calibration opportunities for the upscaling associated with the volume-averaged modeling approach. In addition, these data allow a demonstration of the flexibility in the volume-averaging approach to match the complexity of available site data. The numerical NAPL distribution is well-known such that different upscaled NAPL sources can be compared in the volume-averaging: a single mass (assumed in screening models), dual mass (ganglia and pool), or multiple masses. The resulting comparison of mass discharge estimates yields a range of statistical errors for evaluating the approaches and the sensitivities to input parameters. A robust quantitative match to these numerical modeling results is defined as a relative RMSE less than 0.2 as cited in Table 3.1. The RMSE is defined by the following relationships for calculated parameters of interest (e.g., average discharge concentration, source mass discharge rate),

$$Root\ Mean\ Square\ Error\ (RMSE) = \left[\frac{1}{N}\sum_{i=1}^{N}(calculated_i - observed_i)^2\right]^{1/2}$$

$$Relative\ RMSE = \frac{RMSE}{(observed)_{maximum} - (observed)_{minimum}}$$

The data analyses will also include the coefficient of determination defined by,

$$Coefficient\ of\ Determination\ (R^2) = 1 - \frac{\sum_{i=1}^{N}(calculated_i - observed_i)^2}{\sum_{i=1}^{N}\left(observed_i - observed_{average}\right)^2}$$

Semi-quantitative metrics that were used in the analysis of the volume-averaged model output include,

- Predicted/measured inflection points of contaminant concentration profiles and when these occur in time (i.e., change from equilibrium or peak to a decreasing trend with time)
- Predicted/measured slopes of contaminant concentration profiles (i.e., matching the rate of concentration depletion over time).
- Predicted/measured contaminant concentration trends for different NAPL components over time.

Laboratory experiments used to validate the volume-averaged modeling have well specified source masses and well specified porous matrices. The focus of the experiments is developing an understanding of complex physical, chemical and thermal processes related to remediation. In addition, the data are subject to experimental and analytical error. For these reasons, a robust match between the volume-averaged model and these experiments is defined as a relative RMSE less than 0.4.

A controlled field study with known masses of contaminant release was also evaluated following the approach of comparing the model calculations of mass discharge to the study results. With this controlled experiment, we have considerable information on source characterization and mass balances for contaminant, water, and methanol addition. In addition to field observations, results from a numerical model applied to the field study were also available for comparison. SCARPÉ outputs were compared to the field data and the numerical results by plotting the results and calculating the RMSE. A robust match between the volume-averaged model and this controlled field study is defined as a relative RMSE less than 0.6.

5.6.2 Performance Objectives 2 and 3

For each of the two field sites demonstrated in Performance Objectives 2 and 3, the site source data was divided into a calibration set using pre-remediation data and a validation set using data collected during and/or after aggressive remediation efforts. At both sites numerical models are available from previous evaluations of natural attenuation of the NAPL sources preceding more aggressive remedial efforts. For Site 11, King's Bay, a period of MNA preceded the application of ISCO. At Site ST012, Williams AFB, steam enhanced extraction was implemented over a majority of the source zone. For Site 11, the calibrated numerical model was updated based on the results of the remediation efforts and compared with post-remediation data. This evaluation was not performed for ST012, and the application of the volume-averaged model at that site was used to assess its ease of implementation, applicability, and acceptance as a viable tool for supporting remedial decisions.

The volume-averaging approach for the two field demonstration sites followed a four-step process of:

1. modeling MNA in predictive mode,
2. adjusting parameters to provide a best match to field data and numerical modeling results for MNA
3. modeling aggressive remedial efforts in predictive mode,
4. adjusting parameters to provide a best match to field data for aggressive remediation, and
5. modeling post-remediation data.

Comparisons with numerical modeling results for Site 11 was used to assess the comparability of the volume-averaging approach to the numerical modeling results. Success for the volume-averaging approach is defined by generating results with an error (RMSE as described in Section 5.6.1) that is:

- less than or equal to one order of magnitude of observed data, and
- within the order of the error associated with the numerical modeling and observed data.

5.6.3 Performance Objectives 4 and 5

Qualitative performance objectives 4 and 5 were evaluated based on user feedback through questionnaire, workshops, and direct contact.

6.0 PERFORMANCE ASSESSMENT

Qualitative and quantitative performance metrics were initially established and performance assessed through project execution. Performance was assessed using the performance objectives listed in Section 3 as a benchmark. The following subsections relate to the results that pertain to these metrics and goals.

6.1 QUANTITATIVE PERFORMANCE OBJECTIVES

6.1.1 Validate with Published Studies

As detailed in the sections below, this performance objective was met; RMSE for comparison of the model outputs with published studies met the success criteria, and the SCARPÉ outputs reproduced the main features of the mass discharge curves from published studies (inflection points and slopes).

6.1.1.1 Numerical Modeling Comparison (Baseline Characterization Activities)

Table 6.1.1 presents the fitting metrics for the volume-averaged model applied to the numerical simulation of five identical pools including a single pool (pool 5) directly downgradient from another pool (pool 4) as described in Section 5.3 and illustrated in Figure 5.3.2. Application of the volume-averaged model with the theoretical value for the pool mass ratio exponent, γ=0.5, yielded an RMSE of 8.3% and an R^2 of 0.95. Minimizing the RMSE by varying the exponent for two significant digits yielded a best-fit value of γ=0.34 with RMSE of 3.7% and R^2=0.99 and also matched the depletion time for the source zone mass. The theoretical values overpredicted the mass depletion time by 24%.

Table 6.1.1. Fitting Metrics for Volume-averaged Model of Multiple Pool Simulation

Model parameter inputs			
γ (all pools)	**0.34**	0.50	0.50
ε (pool 5)	**0.50**	0.50	None
Metrics for all data (N=91)			
R^2	0.99	0.95	0.94
RMSE (%)	3.7	8.3	8.5
Match of source zone depletion time			
Years to Deplete[a]	**26.1**	32.3	21.9
Error (%)	0.0	24	-16

[a] Depletion of source zone mass is defined as a discharge concentration < 0.01 mg/L.

Ignoring inhibition for dissolution of pool 5 and setting γ=0.5 did not significantly change the fit metrics from the theoretical calculation; however, the time to deplete the mass was underpredicted by 16%. In addition, this assumption failed to display the inflection in the discharge curve associated with the extended dissolution time for pool 5. Of note, all cases considered yield R^2 of 0.9 or higher.

As illustrated in Figure 5.3.2, semi-quantitative metrics were as follows:

- Predicted/measured inflection points of contaminant concentration profiles and when these occur in time (i.e., change from equilibrium or peak to a decreasing trend with time):

  - The best fit model provides accurate representation of the measured inflection points (peak time and time when a transition in the source characteristics impact the mass discharge)
  - The other two models provide reasonable fit of the peak time, but did not reproduce the observed transition time
- Predicted/measured slopes of contaminant concentration profiles (i.e., matching the rate of concentration depletion over time):
  - The three model iterations match the depletion time reasonably well and therefore provide a reasonable estimate of the observed concentration depletion over time

These two metrics are demonstrated in Figure 5.3.2. Point (A1) represents the time when the peak concentration is observed. This point of inflection is identified at the time where a consistent decline of contaminant concentration is observed. The second inflection point (A2) corresponds to the time when a transition in the source characteristics impact the mass discharge. The slope (B1) is the initial rate of decline in the concentration between points A1 and A2. The slope (B2) is the resulting change in the rate of contaminant depletion following the transition point A2.

6.1.1.2 Comparison to Laboratory Experiment

Table 6.1.2 presents the fitting metrics for the volume-averaged model applied to the mixed DNAPL architecture experiment (Section 5.4.1.1). Metrics were calculated for differing values of the mass ratio exponent, γ, for each of the two masses. The first mass has characteristics of ganglia (theoretical γ_1=0.67) and the second those of a pool (theoretical γ_2=0.5). These theoretical exponent values yielded an R^2 of 0.84 and an RMSE of 13% for the full set of concentrations (N=74) as shown in the first column of results. Yet, the volume-averaged model is not intended to capture details of the breakthrough curve because of volume-averaging over the length of the source zone. Considering only discharge data measured after a single pore volume flush yielded improved metrics: R^2 = 0.96 and RMSE = 5.7% (N=66). A third, and possibly more important metric is the time (i.e., number of pore volumes) to deplete of the source zone mass. Experimentally, the depletion was achieved in about 144 pore volumes and the theoretical values over-predicted this time by only 2.5%.

Table 6.1.2. Fitting Metrics for Volume-averaged model of Mixed DNAPL Architecture Experiment

Model parameter inputs								
γ_1 (~ganglia)	**0.67**	0.485	0.50	0.60	0.67	0.70	0.67	0.67
γ_2 (~pool)	**0.50**	0.485	0.50	0.60	0.67	0.70	0.50	0.50
α_T (m)	**0.001**	0.001	0.001	0.001	0.001	0.001	0.002	0.0005
Metrics for all data (N=74)								
R^2	0.84	0.83	0.83	0.83	0.84	0.84	0.83	0.84
RMSE (%)	13.0	13.5	13.4	13.1	13.0	13.0	13.4	13.1
Metrics for data beyond 1 PV flush (N=66)								
R^2	0.96	0.95	0.95	0.96	0.96	0.97	0.94	0.97
RMSE (%)	5.7	7.0	6.8	6.0	5.7	5.6	7.4	5.2
Match of source zone depletion time (PV=143.8)								
PVs to Deplete[a]	147.4	**143.8**	147.5	179.1	210.8	226.8	110.2	195.1
Error (%)	2.5	0.0	2.6	25	47	58	-23	36

[a] Depletion of source zone mass is defined as a discharge concentration < 0.1 mg/L.

Table 6.1.3 presents the fitting metrics for the volume-averaged model applied to the heterogeneous DNAPL experiment (Section 5.4.1.2). As described in Section 5.4.1.2, the source was modeled as 3 masses, as 4 masses, and with uniform soil properties. Metrics for each of these scenarios are provided in Table 6.1.3. For simplicity, the mass ratio exponent, γ, was held constant for all masses considered and the inhibition exponent, ε, was equal to the preceding mass γ. The exponents were varied from 0.5 to 0.8. Considering only discharge data measured after a single pore volume flush, γ=0.55 yielded: R^2 = 0.90 and RMSE = 7.6% (N=58) and matched the source depletion time of 175 PV. Theoretical values of γ=0.50 and γ=0.67 yielded similar concentration metrics; however, the depletion time was underpredicted and overpredicted, respectively. The overall metrics for matching discharge concentrations improved slightly as the exponent increased; however, the source depletion time was increasingly overpredicted with exponents larger than 0.55 for the 4-mass model and 0.60 for the 3-mass model. Although not shown, observed inflection points at PV equal to 33 and 93 were also increasingly missed and smoothed out with larger exponents.

Table 6.1.3. Fitting Metrics for Volume-averaged model of Heterogeneous Experiment

Model parameter inputs								
γ (for all masses)	0.50	0.55	0.60	0.67	0.80	0.55	0.55	0.55
ε (all masses after 1)	0.50	0.55	0.60	0.67	0.80	0.55	0.55	0.55
α_T (m) (Mass 1 & 2)	0.001	0.001	0.001	0.001	0.001	**0.002**	**0.0005**	0.001
α_T (m) (Mass 3)	0	0	0	0	0	0	0	**0.001**[b]
4-Mass Model								
Metrics for all data (N=64)								
R^2	0.80	0.81	0.82	0.82	0.82	0.81	0.80	0.78
RMSE (%)	10.6	10.4	10.3	10.2	10.2	10.6	10.6	11.2
Metrics for data beyond 1 PV flush (N=58)								
R^2	0.89	0.90	0.91	0.91	0.92	0.87	0.91	0.86
RMSE (%)	8.1	7.6	7.4	7.3	7.1	8.7	7.5	9.1
Match of source zone depletion time								
PVs to Deplete[a]	168.9	174.9	180.4	192.5	230.4	169.8	177.3	211.5
Depletion Fit (%)	-3.4	0.0	3.1	10.1	32	-2.9	1.4	20.9
3-Mass Model								
Metrics for all data (N=64)								
R^2	0.56	0.59	0.60	0.61	0.63	0.60	0.56	0.54
RMSE (%)	15.9	15.5	15.2	15.0	14.6	15.2	15.9	16.3
Metrics for data beyond 1 PV flush (N=58)								
R^2	0.68	0.71	0.73	0.75	0.78	0.71	0.70	0.65
RMSE (%)	13.9	13.2	12.7	12.2	11.6	13.2	13.5	14.5
Match of source zone depletion time								
PVs to Deplete[a]	160.2	165.3	171.9	184.5	222.6	162.4	167.5	203.0
Depletion Fit (%)	-8.4	-5.5	-1.7	5.5	27.5	-7.1	-4.2	16.1

[a] Depletion of source zone mass is defined as a discharge concentration < 0.1 mg/L.

[b] A uniform soil matrix was modeled by including dispersion for Mass 3 and eliminating the enhanced velocity through the coarse-grained lens of sub-volume 3.

6.1.1.3 Comparison to Multi-Component DNAPL Field Test

Table 6.1.4 presents the fitting metrics for the volume-averaged model applied to the controlled field experiment (Section 5.4.2) when comparing to the observed data. Separate evaluations were carried out for the flushing data through Day 225.5 and then for the full flushing data including the methanol pulse.

Table 6.1.4. Fitting Metrics for Volume-averaged model of Multi-Component DNAPL Field Test

	Flushing Dissolution (Days 0 to 225.5)				Flushing with Methanol Pulse (to Day 291)			
	Average	R2	RMSE	Relative RMSE	Average	R2	RMSE	Relative RMSE
TCM	0.00363	0.446	0.00158	0.192	0.00260	0.726	0.00130	0.157
TCE	0.00510	0.376	0.00170	0.201	0.00524	0.119	0.00194	0.230
PCE	0.00128	0.695	0.00029	0.124	0.00173	0.552	0.00056	0.184

Semi-quantitative metrics of matching inflection points and slopes were successful in this example as evidenced by the matches in peaks and the slopes preceding and following the peaks of TCM and PCE (Figure 5.4.7). The peak in TCE concentration did not match and appears to have an unexplained relationship with the rapid change in the water table, as discussed in Broholm et al. (1999). An additional semi-quantitative metric for multi-component NAPL is matching anticipated trends based on relative solubilities (or other properties) among the components. This application was successful in demonstrating an early peak for TCM, followed by a later peak in TCE, and then PCE based on the compound solubilities.

Statistical evaluations were also carried out for the numerical model fit of Mobile et al. (2012) to the observed field data and also between the volume-averaged model and the numerical modeling results. The calculated statistical parameters are provided in Table 6.1.5.

Table 6.1.5. Fitting Metrics for Volume-averaged model of Multi-Component DNAPL Field Test (Numerical Modeling)

	Numerical Model to Field (Days 0 to 206)				Volume-Averaged Model to Numerical Model			
	Average	R2	RMSE	Normalized RMSE	Average	R2	RMSE	Normalized RMSE
TCM	0.00363	0.584	0.00137	0.166	0.00360	0.631	0.00111	0.153
TCE	0.00509	0.515	0.00150	0.177	0.00494	0.703	0.00088	0.145
PCE	0.00134	0.490	0.00039	0.165	0.00112	0.705	0.00018	0.122

The relative RMSE for the volume-averaged model fit to the observed data was approximately the same as the relative RMSE for the numerical model validating the volume-averaged model approach. The relative RMSE for the volume-averaged model output compared to the calibrated numerical model was only slightly better than obtained for the observed field data.

More detailed analyses of the experiments from Section 6.1.1 are described in Section 8.2 as a step toward providing comprehensive guidance on site characterization efforts, the relation to model parameters, and the prioritization of data collection activities.

6.1.2 Validate at Modestly Complex Site (Site 11, NSB Kings Bay, GA)

The performance objectives for Site 11 were met for the statistical comparison of mass discharge rates and the features of the mass discharge inflections and slopes after the implementation of ISCO. An RMSE value of 12% was achieved between the volume-averaged model output for mass discharge rates during the initial period of natural dissolution and groundwater pumping compared to the interpretation of field data for these rates. The interpreted rates were the result of detailed analyses of field data and the output from a calibrated numerical fate and transport model (SEAM3D) as described in Section 5.5.1.3. The calculated R^2 was 0.99.

The initial DNAPL mass and the fraction of mass present as a pool are strongly related to the mass discharge rate from the source zone as discussed in Section 5.5.1. The best estimate for the initial DNAPL mass at Site 11 was 600 kg with 16.2% of the mass residing in a pool. Fitting metrics for the mass discharge rate with varying initial mass and pool fraction are presented in Table 6.1.6. In performing these calculations, the characteristic dimensions of the DNAPL source zone were held constant, i.e., the characterization data and interpretation were assumed to provide good parameter estimates. As described in Section 5.5.1 the data for estimating the characteristic dimensions included a measure of projected area at a close-in transect of monitoring points and DPT vertical profiling of contaminant distribution.

Table 6.1.6. Fitting Metrics for Volume-Averaged Model of Mass Discharge Through Groundwater Pumping Activities

	Best Est.	Initial Mass +50%	Initial Mass - 50%	Pool Fraction +50%	Pool Fraction-50%	Pool Fraction (No Pool)	Pool Fraction (All Pool)
Initial Mass (kg)	600	900	300	600	600	600	600
Pool Mass (%)	16.2	16.2	16.2	24.3	8.1	0	100
Metrics for Mass Discharge Estimates during Natural Dissolution and Pumping							
R^2	0.99	0.008	0.41	0.91	0.84	0.67	-0.51
RMSE (%)	12	3,000	923	120	174	340	4,000

Increasing and decreasing the best estimate for the total mass (600 kg) by 50% yielded 3,000% and 1,000% for the RMSE, respectively, in comparison to the interpreted mass discharge rates during dissolution and pumping. Hence, multiple measures for interpreting the mass discharge at different times or under different conditions, e.g., pumping to increase the velocity, are highly useful in reducing the uncertainty of the initial DNAPL mass if the length of the DNAPL source zone is also characterized independently, e.g., an array of DPT points. Long-term pump-and-treat with a full accounting of the mass removed and extraction rates over time (mass discharge rates) is therefore expected to provide an excellent data set if supplemented with a detailed investigation of the source zone characteristic dimensions. If a pump-and-treat system is operated long enough to observe statistically significant inflections in the discharge rate, the basic DNAPL architecture can be deduced as well as the point of DNAPL depletion. The DNAPL depletion is associated with a sharp downturn in the mass discharge rate as described in Section 5.5.1.5.

The fraction of the initial mass present as a pool was also varied. Increasing and decreasing the best estimate of 16.2% pool mass by 50% yielded RMSE of 120% and 170%, respectively. Early in the life of the source zone, the ganglia dissolution dominates and pool fraction is less influential than total mass. In general, a pool is difficult to assess from indirect, downgradient data until after the majority of the ganglia mass is depleted. This is illustrated by assuming no pool existed. For no pool, the RMSE was 340%. Conversely, assuming the mass was present solely as a pool yielded an RMSE of 4,000 and a negative correlation to the data. Hence, any reasonable estimates for the early mass discharge, even a single point, and the source zone dimensions could determine the likelihood of either bounding architecture. This observation also lends emphasis on the need to characterize source zone dimensions; a low mass discharge rate could easily be misinterpreted as a small DNAPL mass rather than a larger mass in a pool configuration with a very long lifespan.

A semi-quantitative success criterion for this performance objective was to match the decay rate in the source mass discharge rate. The interpretation of the field data to estimate the decay rate constant following the ISCO implementation yielded a value of 0.00163 day^{-1} as described in Section 5.5.1.3. The primary field data for the interpretation was measured in a downgradient monitoring wells (KBA-11-34) and the attenuation between the source zone and the well location had to be considered. The transport from the source zone to the monitoring well was modeled with the calibrated SEAM3D as described in Section 5.5.1.3 and the numerical model yielded a decay rate constant of 0.00174 day^{-1}. The volume-averaged model output utilized a value of 0.00158 day^{-1} assuming values of 0.00025 day^{-1} for the first order mass transfer coefficient (K_{im}) between the mobile and immobile zones and an immobile zone fraction (f_{im}) of 0.11. These two parameters are described in Sections 2.2.4 and 5.5.1.3. The error between the volume-averaged model and the field interpretation for the decay was –3% and the error between volume-averaged and numerical models was –9%. Hence, this semi-quantitative metric was satisfied.

The assumed percentage of the pool destroyed by the ISCO Phase 4 was varied in Section 5.5.1.4. As illustrated in Figure 5.5.9 any residual DNAPL remaining after ISCO would be expected to yield a much slower concentration decay rate than was observed in the monitoring data (see Figure 5.5.7). The mass discharge rate would have remained elevated until the DNAPL was depleted before decaying at the rate dictated by back diffusion. Hence, a semi-quantitative comparison of inflection points and slopes aided in the interpretation of the ISCO destruction efficiencies.

6.1.3 Validate at Complex Site (Site ST012, Former Williams AFB, AZ)

The application of the volume-averaged model was demonstrated at a well-documented field site with a long history, Site ST012 at the Former Williams AFB. This complex site includes three transmissive, water-bearing units impacted by NAPL and a water table rise of 90 feet over the past 30 years. Remedial history at this site includes limited pump-and-treat, followed by MNA combined with natural source depletion, thermal treatment, and on-going enhanced bioremediation in the source zone. Early implementation of remedial technologies occurred under very different site conditions than currently exist as a result of the rising water table.

A calibrated numerical model of NAPL dissolution and solute transport was developed and applied before and after a pilot test of TEE in the LSZ source zone under ESTCP Project ER-200833 (Kavanaugh et al., 2011). A recent full-scale application of SEE provided new site data for assessing initial NAPL mass and architecture as well as NAPL source depletion during and after SEE.

Attempts to apply the previous calibrated numerical model to the current site conditions following SEE were thwarted by continually changes conditions after SEE was terminated. The water table took one to two years to re-equilibrate from the deep drawdown created by SEE and the treated areas of the site remain at elevated temperatures years later. Inconsistent pumping of wells has added to these disturbances. In the outer areas where untreated NAPL remains, the placement and spacing of groundwater monitoring wells is such that the dissolved phase plume monitoring is not sufficient for meaningful modeling. The site conditions are undeniably complex.

SEE is the only remedial technology applied at the site under conditions similar to the current conditions. Modeling a multiphase process like SEE can be accomplished using the volume-averaged modeling approach by including an energy balance as described in Section 2.2.6.4 to evaluate the size of the steam zone and by assuming a fraction of NAPL with the remainder subject to dissolution governed by flowing steam and NAPL component volatility. Such a model is feasible and could be compared to the previous SEE implementation but the effort is beyond the scope of this work. In addition, SEE is not considered in the remedial evaluation of remaining NAPL areas at Site ST012 because these NAPL areas have existing surface infrastructure, e.g., a building and major thoroughfare, that make them impractical for the installation and operation of SEE wells, pumps, piping, and electrical. The 2012 ROD amendment called for the application of an unspecified biological enhancement process to accelerate the treatment of NAPL in these outer areas and a pilot study of sulfate reduction is underway. This technology was evaluated using the volume-averaged modeling approach; however, insufficient site data exist for a statistical comparison with the volume-averaged modeling.

Containment pumping was performed in the LSZ from 2018 to 2021; however, the pumping strategy also included distributing injected sulfate across target areas of the LSZ. The pumping was inconsistent and no extended, quasi-steady periods of extraction are available with flows and mass removal estimates sufficient to evaluate pump-and-treat in any area of the site. Hence, no remedial activities from the site's history are available to provide calibration targets for the volume-averaged modeling.

For these multiple reasons, statistical comparisons of the volume-averaged modeling output as described in Section 5.6 could not be performed with numerical modeling results or interpreted field data. The demonstration of the modeling at Site 11 and the development of the ST012 model input parameters described in Section 5.5.2.2 lend scientific credence to the output from the modeling demonstration at ST012. The primary objectives for the volume-averaged modeling demonstration were to evaluate its ease of implementation, applicability, and acceptance as a viable tool for supporting remedial decisions as described in the qualitative performance objectives described in the next section.

6.2 QUALITATIVE PERFORMANCE OBJECTIVES

As outlined below, the qualitative performance objectives were met.

6.2.1 Implementation and Ease of Use

Developing an easy-to-use framework for assessing NAPL dissolution to support site assessment and remedial decision was one of the main objectives of this project. This performance objective was met.

This assessment was performed through user feedback on the SCARPÉ framework and two practical tools available to the user community. Feedback was gathered through direct contact with approximately 10 RPMs and regulators and approximately 25 consultants and other stakeholders in three workshops. Beta versions of the two practical tools (SCARPÉm and SCARPÉs) were provided to the groups of testers after the project team performed multiple internal revisions of the tools and deemed these tools ready for testing by non-team members. An email explaining the purpose of the tools and providing a link to download the tools and user manual was sent to groups of colleagues including practitioners, remedial subject matter experts, and the Arizona Department of Environmental Quality (ADEQ). The recipients were also invited to attend workshops demonstrating the use of the practical tools and the SCARPÉ framework.

SCARPÉs is an executable file compiled from a python implementation of the model equations for single component NAPL described in Section 2.2.7. To expedite its use, a spreadsheet was created for parameter input and includes guidance and consistency checks. The executable file reads input directly from this spreadsheet. A screenshot of the spreadsheet input file and an example graphic output of the NAPL architecture are provided in Figure 6.2.1.

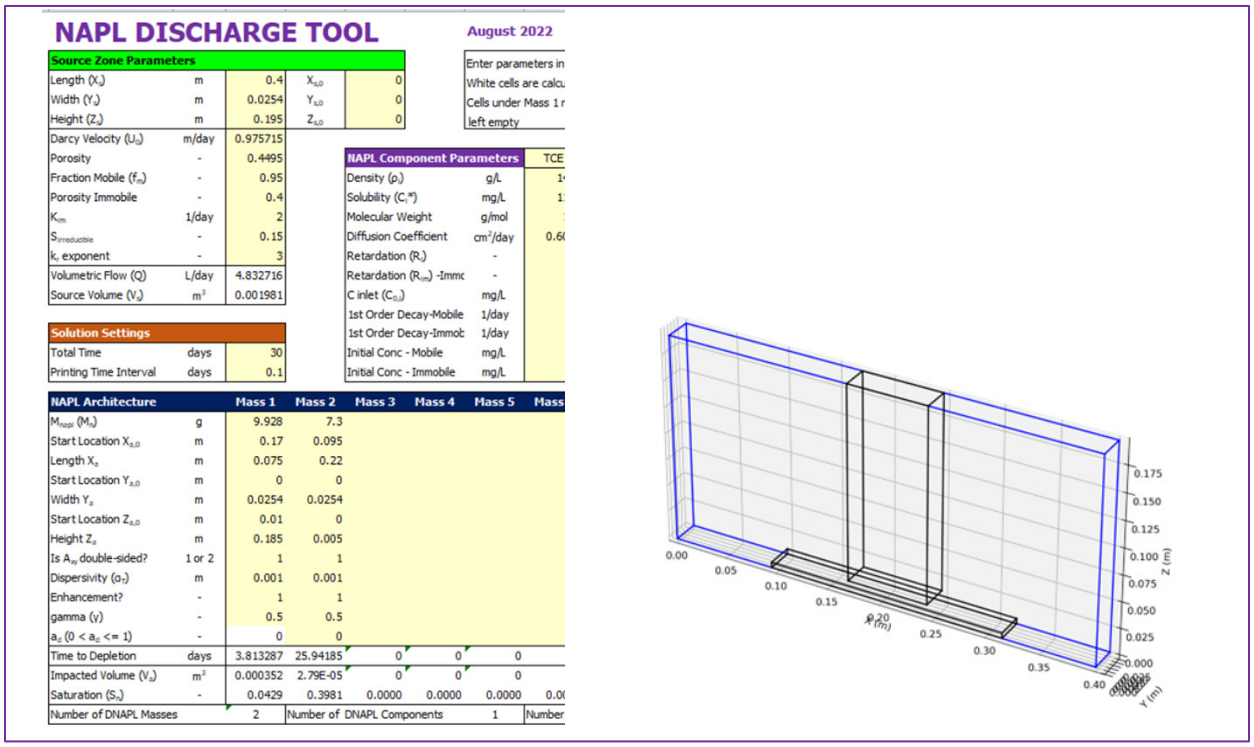

Figure 6.2.1. Screenshot of Spreadsheet Input File and Example of Graphic Output of SCARPÉs.

SCARPÉm is a spreadsheet implementation of the model equations for multicomponent NAPL as described in Section 2.2.7. A screenshot of the interface and an example plot of the temporal discharge concentration and mass rate are provided in Figure 6.2.2.

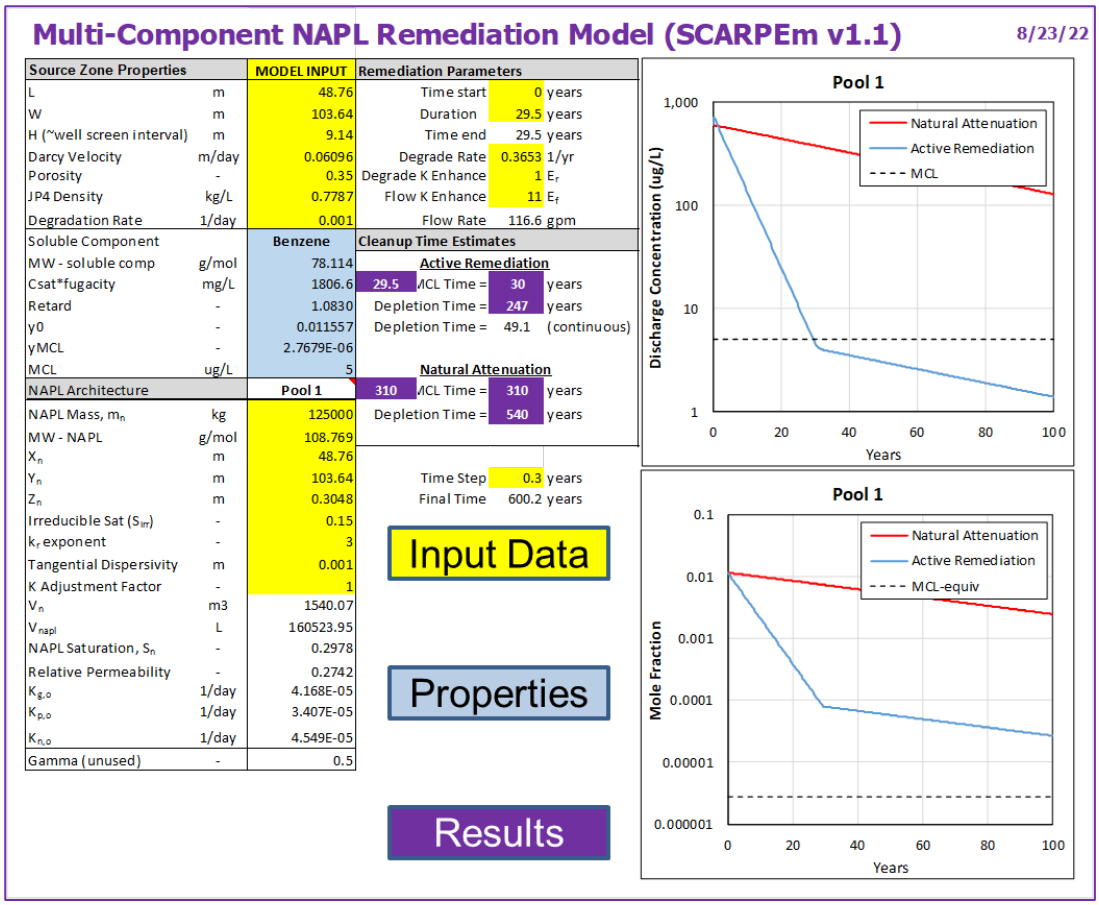

Figure 6.2.2. Screenshot of SCARPÉm spreadsheet for Multicomponent NAPL

User feedback, obtained primarily through direct contact at three workshops, was used to assess whether the performance metrics were met and identify what modifications/changes to the framework and practical tools were needed. The survey form shown in Figure 6.2.3 was provided to approximately 30 of the workshop participants. Yet, no completed forms were returned despite extensive efforts and pleadings. However, all participants except one responded with verbal confirmations that the model was downloaded, the example file was entered, and the model was executed successfully, and output could be observed and saved. The one negative response was the result of an inability to download the model because of an internal firewall. The entire user group also indicated verbally that the model inputs, illustrated in Figures 6.2.1 and 6.2.2 as well as Table 1 in Appendix C, were understood. Several users indicated that the main implementation issue was related the development of the conceptual source model and identification of input parameters (how to get the information?). Based on this feedback, additional guidance is provided in this report on inputs for the SCARPÉ framework (Section 2.3) and was added to the user manual for the practical tools. The demonstration at Site 11 provides examples for interpreting site plume data with an existing numerical fate and transport model and integrating these results with high resolution site characterization data to provide a consistent and logical set of model input parameters.

SCARPE NAPL Discharge Tool v1.0 (beta)

Feedback

Please fill out this survey and send it to jchambon@geosyntec.com. Thank you.

Model Theory

Please indicate how understandable the NAPL dissolution and remediation model are

☐ 1 ☐ 2 ☐ 3 ☐ 4 ☐ 5

Difficult/Advanced — Easily understood

Please indicate your opinion on the technical level of quantitative results from the model (be honest)

☐ 1 ☐ 2 ☐ 3 ☐ 4 ☐ 5

Screening level — Equivalent to simulators

General Tool Information

Please rate how useful and applicable you think this tool may be for your NAPL sites

☐ 1 ☐ 2 ☐ 3 ☐ 4 ☐ 5

Unclear/Unsure — Very applicable

Please indicate on how many sites you think you could apply this tool

☐ None ☐ 1-3 ☐ 4-10 ☐ > 10

Do you generally have the following information to apply the tool at NAPL sites?

NAPL mass ☐ Yes | ☐ No

NAPL architecture ☐ Yes | ☐ No

Discharge concentration ☐ Yes | ☐ No

Please rate how helpful this tool may be to better understand the CSM at a NAPL site and impact of NAPL dissolution processes

☐ 1 ☐ 2 ☐ 3 ☐ 4 ☐ 5

Not helpful/confusing — Very helpful

Please rate how helpful this tool may be to compare remedial technologies at NAPL sites

☐ 1 ☐ 2 ☐ 3 ☐ 4 ☐ 5

Not helpful/confusing — Very helpful

Please rate how helpful this tool may be to communicate challenges with NAPL sites to PRPs, regulators, stakeholders

☐ 1 ☐ 2 ☐ 3 ☐ 4 ☐ 5

Not helpful/confusing — Very helpful

Other outputs and/or formats you would like to see?

Tool Ease of Use

Were you able to create a new input file and run the tool?

☐ Yes | ☐ No

Did you find the following easy to understand?

Launch the tool ☐ Yes | ☐ No

Example input file ☐ Yes | ☐ No

What to modify for a new site ☐ Yes | ☐ No

Output graphs ☐ Yes | ☐ No

Output .csv file ☐ Yes | ☐ No

How to define/estimate inputs ☐ Yes | ☐ No

Where the results are saved ☐ Yes | ☐ No

Overall, please rate how easy you think the tool is to use

☐ 1 ☐ 2 ☐ 3 ☐ 4 ☐ 5

Very difficult — Very easy

Please rate how helpful you think the user manual is

☐ 1 ☐ 2 ☐ 3 ☐ 4 ☐ 5

Not helpful/confusing — Very helpful

Other information/materials you would recommend be included in the user manual?

Please share any additional comments or suggestions.

Figure 6.2.3. SCARPÉ Model Survey Form

6.2.2 Efficacy for Supporting Managerial Decisions

The volume-averaged model demonstration at Site 11 provided a robust interpretation for the full life cycle of the DNAPL source zone. The life cycle interpretation was based on matching trends observed during and after site activities including natural dissolution, pumping, mass destruction through ISCO and long-term back diffusion. The evaluation of remedial alternatives confirmed that MNA was unacceptable and that ISCO was highly successful. The results also indicated that a small implementation of ISCO would have been sufficient for the cleanup; however, identifying the location of this small zone would have been very difficult without the preceding implementation of ISCO over a larger area. The evaluation of optimized pump and treat indicated this approach, if operated until MCL was achieved, yielded a cleanup timeframe on the order of the best estimate timeframe with two phases of ISCO in the source zone. Hence, this alternative may have been given more serious consideration if these model results had been available at the time. The choice would have required estimating costs for this option, the practicality of pumping at higher rates, and other site priorities and goals. The model input parameters and output were sufficient for generating these estimates.

Site ST012 evaluation of remedial alternatives provided a scientifically sound comparison of the potential outcomes from the implementation of MNA, enhanced bioremediation, pump-and-treat, and ISCO. The model results, including the full duration of on-site labor activities, and development of model input parameters provided sufficient information for developing robust, credible cost estimates for implementation of each technology considered.

The ease of model use facilitates the evaluation of varied scenarios for the conceptual source model and assumptions for technology effectiveness. The input can be edited and calculations performed in real-time during a roundtable discussion of stakeholders. This feature facilitates group discussions on specific technical issues for sites and remedies and avoids unfounded conjecture. In other words, disagreements would manifest as differing input parameters rather than speculation.

Feedback from Users

Based on feedback from users, the performance objective was met. The SCARPÉ framework and the two practical tools enable users to rapidly generate reasonable estimates for NAPL source lifespans and mass discharges under a range of future conditions. This information enables RPM, practitioners, and regulators to assess and compare anticipated outcomes for multiple remedial alternatives so that rational site management decisions can be made. The evaluation of this performance objective was performed through end-user feedback on SCARPÉ framework and the two practical tools through direct contact with RPMs, regulators, and stakeholders. Following application of the SCARPÉ framework to Site ST012, meetings were conducted with RPMs, environmental consultants, regulators and stakeholders to present the approach and review the results. These meetings and direct follow-up with the participants were used to evaluate the utility and acceptance of the model output for managerial decisions. Participants indicated that the outputs provided a better understanding of the conceptual source model, provided a fair comparison between different remedial technologies, and were useful information to support site strategy decisions. Specific feedback from participants is provided below:

"*This looks to be a powerful tool to simplify a system in a meaningful way and test the known and unknown inputs efficiently and systematically. Much less of a black box than numerical methods*."

- Daniel Sola, Arizona Department of Environmental Quality (ADEQ) Principal Hydrogeologist

"*The advantage to using this approach is that modeling the source zone becomes a more manageable task, and facilitates an evaluation of remedial alternatives. … I believe the model described in the memorandum has a well-founded theoretical basis. I believe the utility of the model is in making relative comparisons as completed to compare remedial alternatives*."

- Michael C. Brooks, Ph.D., P.E., EPA Environmental Engineer, EPA Office of Research and Development National Risk Management Research Laboratory, Ground Water and Ecosystems Restoration Division

7.0 COST ASSESSMENT

This section provides sufficient cost information that a remediation professional should be able to reasonably estimate costs for implementation of the volume-averaged NAPL dissolution tools presented in this report. In addition, this section provides a discussion of the cost benefit of using the tools.

7.1 COST MODEL

This report presents a technology to assess NAPL dissolution and source zone mass discharge under multiple remedial alternatives based on site-specific data and physical processes. As described in Section 6, the site-specific outputs (NAPL dissolution timeline and mass discharge) can be used for making remedial decisions.

The mathematical framework is applicable to a wide variety of sites, contaminants, NAPL architectures, and remedial histories. In addition to the general mathematical framework for volume-averaged NAPL dissolution, two practical tools have been developed for two conceptual models widely encountered at DoD sites (Section 2.2.7):

- Program executable with an Excel input file for a single NAPL component (SCARPÉs); and
- Excel spreadsheet for a multi-component NAPL source in which NAPL mass remains constant (SCARPÉm).

This cost assessment is focusing on the application of the two practical tools developed as part of this work. With implementation of the tools, the output is expected to be comparable to detailed numerical models for source zone treatment but at a small fraction of the effort required to implement numerical models.

The complexity and effort in implementing this approach is expected to vary with the complexity of the available conceptual site model and the understanding of remedial processes considered. A baseline site characterization is assumed to be part of the standard site investigation or is accompanying a remedial effort and need not be included in assessing the costs of this innovative approach. Hence, the cost assessment for this technology demonstration will only address the incremental costs of compiling and assimilating existing data, performing the volume-averaged modeling, and evaluating and reporting the modeling results. In addition, since the tools are available to the user free of cost, only the time/duration estimated to apply these tools will be considered in the cost assessment.

Three cost components are considered: data compilation and assimilation, volume-averaged modeling (using a computer), and analysis and reporting of results. These cost elements are summarized in Table 7.1.1.

Table 7.1.1. Cost Elements for Implementing Volume-Averaged Modeling of NAPL Source Zone Remediation

Cost Element	Data Tracked during the Demonstration
Data Compilation and Assimilation	Amount of existing information about the CSM Amount of input data Labor categories and hours
Computer Modeling	Calibration objectives Number of remedial alternatives (scenarios) assessed Labor categories and hours
Analysis and Reporting of Results	Number of remedial alternatives (scenarios) assessed Number of outputs Labor categories and hours

7.1.1 Data Compilation and Assimilation

The first step of the volume-averaged modeling approach involves compiling and assimilating existing data. An advantage relative to PLM-based empirical screening models is that the volume-averaged modeling approach provides physical representation and better prediction of NAPL dissolution processes with no substantial increase to the number of model input parameters. Required input parameters are determined and selected from the existing data by qualified practitioners; the input parameters are typically known or estimated quantities. A general description of the input parameters is found in Section 2.3, including Tables 2.3.1.1 and 2.3.2.1. The proposed approach provides the user with links to references of compound-specific physical-chemical input parameters. A key step in this effort is the development of a conceptual source model (NAPL source zone dimensions, individual NAPL mass dimensions, characteristics, and saturations). Effort associated with this cost element depends on the amount of data, the existence of a conceptual source model, and the need to refine it.

The cost associated with this element is dependent on the type of personnel required to conduct the compilation, assessment, and selection (engineer, program manager, etc.) and their associated labor hours. This element is unlikely to be significantly influenced by physical scale of the site.

7.1.2 Computer Modeling

Users will input the select parameters as described under Section 7.1.1 into the Excel spreadsheet for the selected tool (either SCARPÉs or SCARPÉm), perform model calibration (if data are available, see below), run a variety of remedial scenarios, and compile the outputs. Each task is further described below:

- Enter input parameters: this task is straight-forward following the selection of the input parameters and development of the conceptual source model under Cost Element 1.
- Perform model calibration: if historical data, such as mass discharge, downgradient concentration and/or mass extraction rates, is available, input parameters such as NAPL mass, NAPL dimensions, or the gamma exponent, can be adjusted to better match observations. The effort for this task will depend on the calibration objectives, the amount of calibration data, and the complexity of the conceptual source model.

- Run remedial scenarios: the users define the remedial alternatives to be evaluated and determine the enhancement factors applicable to the remedial technology. Guidance is provided for determining enhancement factors for specific to source zone remediation technologies and post-remediation scenarios (Sections 2.2.6 and 2.3.2). The users will create an Excel spreadsheet for each of the remedial scenarios and run the model (either using the program executable for SCARPÉs or directly within Excel for SCARPÉm). A key advantage of the approach is the near direct transition from assessing one remedial process to another without the need to re-enter baseline site data such as the contaminant mass and distribution.
- Compile model outputs: this task is straightforward following performance of the model runs.

The cost associated with this element is dependent on the type of personnel required to conduct the modeling (engineer, program manager, etc.) and their associated labor hours. This element is unlikely to be significantly influenced by physical scale of the site. The tools are provided free of charge.

7.1.3 Analysis and Reporting of Results

Outputs (depletion time, NAPL mass, mass discharge and discharge concentration over time) are generated in individual Excel files for each scenario. These outputs provide order-of-magnitude estimates of these metrics with varied remedial processes, applicable to both design and performance evaluation. The users will process the outputs to compare several proposed source control measures, for example by creating graphs with outputs for multiple scenarios and/or generating tables summarizing time to achieve cleanup targets for multiple scenarios in support of decision-making remedial processes. Analysis and reporting of results are not expected to vary significantly from similar efforts using other types of models. The cost associated with this element is dependent on the type of personnel required to analyze and document the results (engineer, program manager, etc.) and their associated labor hours.

7.2 COST DRIVERS

As outlined in Section 7.1, the main cost driver for implementation of the NAPL dissolution tool is the labor cost (i.e., time) to compile and assimilate the data, run the model, and analyze and document the results. Familiarity of the users with the site and historical information will result in higher efficiency in implementation of the tool. In contrast, if the users are new to a site, additional effort is anticipated to be required for data review and development of the conceptual source model. In addition, the format of the existing data (i.e., electronic vs. pdf) and ease of access to previously compiled information (i.e., electronic files with bookmarks vs. hard copies) will impact the amount of effort required for data compilation, review, and assimilation. Additional effort is anticipated if manual data entry (for example from a pdf of boring logs or NAPL observation field notes) is required prior to data review and analysis.

7.3 COST ANALYSIS

The NAPL dissolution tools are easy-to-use packages that will require input of several key parameters and characteristics of the NAPL source zone and aquifer. It is anticipated that the required data will already be available for a site as part of the site characterization effort to support remedial decisions. A simple cost model has been developed for the technology and is provided in Table 7.3.1.

The cost to implement the NAPL dissolution tools will be on the order of $23,000. This cost includes review of existing (historical) data to refine an existing conceptual source model, setting up and running the model, including calibration using observation data and evaluation of five remedial scenarios, and analysis and documentation of the results. It is assumed that the user will have an understanding of NAPL delineation technologies and NAPL dissolution processes and be familiar with the remedial options. This cost does not include communication and meetings with the regulatory agencies that may be required as part of the remedial decision process.

Table 7.3.1. Cost Model

Cost Element	Labor Category	Labor Hours	Costs
Data Compilation and Assimilation	Project Engineer	40	
	Principal Engineer	8	$9,000
	Administrative	10	
Computer Modeling	Project Engineer	32	$7,000
	Principal Engineer	8	
Analysis and Reporting of Results	Project Engineer	32	$7,000
	Principal Engineer	8	
		Total	**$23,000**

The volume-averaged modeling approach represents a middle ground between numerical models attempting to include mass transfer complexities in a very fine grid and the ease of implementation of qualitative screening models (e.g., PLM-based screening models). Based on previous experience, it is expected that development and use of complex numerical models for NAPL dissolution would cost upward of $100,000, and each additional scenario would add significantly to the total costs. In contrast, implementation of qualitative screening models (e.g., PLM-based screening models) may require less effort on data compilation and assimilation than the volume-averaged modeling approach, but similar effort is anticipated for running the model and analysis and documenting the results. In addition, the volume-averaged approach provides physical representation and better prediction. Therefore, implementation of the volume-averaged modeling approach, which is physically-based and provides scientifically defensible comparisons between remedial alternatives, is a valuable tool to support remedial decision-making for a cost significantly lower than numerical models and comparable to qualitative screening models.

RPMs who apply the volume-averaged NAPL dissolution tools can realize substantial cost-savings for several reasons:

- The volume-averaged NAPL dissolution tools can be used in-lieu of high resolution, complex, and intensive numerical models that would be required to quantify mass discharge and evaluate different remedial alternatives. The tools provide outputs comparable to outputs from complex numerical models (see Section 6.1) but effort to set up the model and evaluate multiple remedial scenarios is minimal.
- The volume-averaged NAPL dissolution tools provide guidance regarding remediation technology selection and implementation. This means that RPMs can avoid expenditures for a technology that is inappropriate to accomplish cleanup goals at a given site.

For example, the tools will allow recognition of technologies that may provide limited benefits (either based on mass removal or mass discharge remediation targets), suggesting that alternate remedies must be considered.

- The volume-averaged NAPL dissolution tools incorporate the current scientific understanding of dissolution and remedial processes that affect the mass removal and mass discharge of NAPL source zones. The NAPL tools greatly improve the accuracy of mass discharge and NAPL source lifespans compared to PLM-based screening models, facilitate the remedial evaluation and decision process, and their application likely will increase the number of sites where the most efficacious remedy will be implemented to achieve cleanup goals. Implementation of this tool promises to avoid unnecessary capital and O&M costs while simultaneously reducing environmental impact at many sites.

In addition, use of the SCARPÉ framework at NAPL sites can support DoD RPMs with cost forecasting over the life cycle of the site, including taking into account uncertainty associated with outcomes of remedial activities.

8.0 IMPLEMENTATION ISSUES

This section provides information that will aid in the future implementation of the technology. The SCARPÉ framework provides a system of ODEs based on the volume-averaged approach to represent NAPL dissolution and calculate relevant outputs for remedial-decision making, such as mass discharge, discharge concentration, and NAPL mass remaining. This system of ODEs can be readily implemented and solved using available coding platforms, such as Matlab or FORTAN, however, it does require coding and specialty users. This is a consequence of the high flexibility and adaptability of the volume-averaged framework. As part of this work, two practical ready-to-use tools, which do not require any specific training, or software and can be run on a personal laptop, were developed for two simplified conceptual source models (Section 2.2.7). Future development of the SCARPÉ framework will include further enhancements of the practical tools so that they can be used for a wider variety of sites and remedial technologies. Including mass balances of specific remedial amendments, e.g., oxidants and co-solvents, would allow calculations of amendment concentration and transient enhancement to facilitate the model's use for remedial design and detailed performance evaluations.

As illustrated with the successful demonstrations at two sites, SCARPÉ provides RPMs with an approach to enable science-based decision-making. Detailed guidelines document the proper application of the framework and its limitations; application of the SCARPÉ framework provides model outputs only; ultimately, decisions are made by RPMs and site owners. Guidelines, documentation, and background on NAPL dissolution processes minimize the risk of improper use of the SCARPÉ framework outputs for decision.

One of the potential challenges is the acceptability of the model outputs by regulators as a basis for comparing remedial options and making site managerial decisions. Early involvement of the regulators and other stakeholders in the development of the conceptual source model for the NAPL source and selection of the remedial technologies can minimize this risk. In addition, the ability to compare model outputs with historical data (if available) can provide higher confidence in the model outputs and its use for forecasting future conditions. As described in Section 8.2, pairing the model with parameter estimation software like PEST (Doherty 2015) yields robust estimates for uncertainty and the identification of key parameter measurements to increase confidence.

As with all models, development of the conceptual source model is based on an understanding of the historical and current site conditions, historical sampling and operational data, and ongoing investigations. An understanding of NAPL release(s) and dissolution processes is a critical step in the successful application of the SCARPÉ framework. Subsequently, identification of the input parameters for the model, based on the conceptual source model was highlighted as a potential challenge by the beta testers. This is addressed further in the following two sections.

8.1 CONCEPTUAL SOURCE MODEL AND CHARACTERISTIC PARAMETERS

Guidance for identification of the input parameters and development of the conceptual source model is provided in Section 2.3. The input parameters necessary to complete the modeling are described in Table 2.3.1 and illustrated in Figures 6.2.1 and 6.2.2. Extensive guidance on the estimation of parameters, with references to other research, is provided in Table 1, Input Variable Descriptions, of Appendix C. Site investigations and associated investigation reports at NAPL sites would typically

include data needed to develop the conceptual site model, such as groundwater or soil concentrations, visual observations of NAPL in soil cores, advanced characterization methods, groundwater flow estimate, historical information, cross-sections and plume maps. Most of the NAPL sites have a long history of investigations and remediations, therefore relevant information may be spread over multiple investigation events and reported in separate reports, and may require a comprehensive analysis of the data to develop a conceptual source model and identify input parameters. Access to historical investigation and remediation information and involvement of practitioners familiar with the site and its history would facilitate application of the SCARPÉ framework.

The two site demonstrations described in Section 5.5 along with site details and data interpretation provided in Appendices D and E provide thorough and varied illustrations of model input parameter estimation. These examples included extensive descriptions of methodologies for interpreting downgradient plume histories and high-resolution measurements to characterize the source zone. Sites with existing transport models can heavily leverage the model for data interpretation to build a mass discharge history and estimate the total initial mass.

8.2 PRELIMINARY UNCERTAINTY ANALYSES AND PRIORITIZATION OF DATA COLLECTION

At sites where available data is not sufficient to develop a conceptual source model with adequate confidence, application of the SCARPÉ framework can still provide useful information, support development of a better understanding of the site and guide future data collection. Applying the model to multiple "book-end" scenarios (for example ganglia vs. pool type NAPL accumulations) can provide a range of potential outcomes and help identify controlling parameters and prioritize needed data to refine the conceptual source model. In this section statistical analyses were employed to (i) identify the relative contribution of volume-averaged mass transfer parameters to source zone dissipation uncertainties, and (ii) investigate how model parameterization influences predictive bias through monitoring data assimilation. The contribution of input parameters to predictive uncertainties was quantified with first-order second-moment (FOSM) analysis facilitated by PEST software and the linear analysis utilities GENLINPRED and PREDUNC (Doherty 2015, Watermark Numerical Computing 2018). The predictive uncertainty associated with the estimated remedial timeframes for the different remedial technologies was quantified using the prior-based Monte Carlo functionality of the iterative ensemble smoother PESTPP-iES (White 2018, White et al. 2020), with 20 randomized model realizations per adjustable parameter.

The upscaled modeling of DNAPL dissolution described in this report provides a practical approach for assimilating site characterization and monitoring data to constrain future system behavior. Difficulties in estimating NAPL dissolution rates stem from source zone heterogeneities, which may be difficult to characterize in detail, compounded by a lack of scalable methodologies connecting source zone characterization with discharge monitoring. Thus, several monitoring and site characterization technologies have been developed to support performance-based remedial efforts, which are typically uninformed by uncertainty evaluations predicated on NAPL mass transfer processes. To bridge that gap, we investigated the impact of data-driven conceptual assumptions on predictions of source zone behavior by coupling the NAPL dissolution modeling approach with uncertainty quantification methods. Simulations of the flow-cell experiments described in Section 5.4.1 demonstrate the worth of NAPL delineation for constraining source zone depletion uncertainties, estimated a priori through parameterization of NAPL distributions.

In turn, parameterizing system heterogeneities in greater detail was necessary to estimate unbiased source zone characteristics and lifespans, derived from the assimilation of complex NAPL dissolution trends observed in monitoring profiles. These preliminary results provided below demonstrate how available site data can be integrated into a decision-support modeling framework to inform data collection strategies and remedial designs. In addition, the identical statistical methods were applied to the source model for Pool 1 of Site ST012 described in Section 5.5.2.2 to assess the degree of accuracy of the modeling approach and identify the most critical parameters.

8.2.1 Sensitivity Analysis

As shown in Figures 8.2.1 and 8.2.2, the greatest model sensitivities, X, with respect to matching TCE concentrations (X_{TCE}) in the two experiments of Section 5.4.1 corresponded to the source zone area (Z_S and Y_S) orthogonal to the flow direction and groundwater velocity (U_0). The former accounts for any dilution in the monitoring scale, while the latter had a prominent impact on the time of depletion in both experiments. The role of V_S and U_0 on scaling mass transfer processes emphasized the need to constrain them by the monitoring scale to avoid model errors induced by data assimilation. Figure 8.2.1 indicated that the cross-sectional area facing flow (YZ_g) of the ganglia-dominated accumulation was responsible for peak aqueous-phase concentrations. Similarly, Figure 8.2.2 shows the cross-sectional area YZ_{1A} of the most upgradient, low-saturation accumulation 1A (see Figure 5.4.3) in a high-ranked position. These X_{TCE} results suggested that saturation parameters (V_a and *Mass*) of ganglia-dominated accumulations that are responsible for peak concentrations do not impact time of depletion, yet their estimation via history-matching may be valuable for remedial designs. Conversely, sensitivity with respect to time of depletion (X_{TOR}) was dominated by NAPL pool saturation parameters, transverse dispersivity ($\alpha_{T,p}$), and the mass depletion exponent (γ^p). The negligible X_{TCE} values of pool parameters suggested difficulty in estimating them from monitoring data alone.

In contrast to negligible X_{TCE} values by pool parameters in the mixed experiment (Figure 8.2.1), X_{TCE} rankings of saturation parameters pertaining to "accumulation 3" in the heterogeneous experiment (Figure 8.2.2) suggested that high-saturation NAPL accumulations may not exclusively reflect pool fractions of source zones. Typically, the small cross-sectional areas available for dissolution by groundwater flow through DNAPL pools reduces their relative contribution to mass flux, compared to ganglia-dominated accumulations. However, as indicated in Figure 8.2.2, the morphology of DNAPL accumulation 3, controlled by flow-field heterogeneity, influenced both X_{TCE} and X_{TOR} rankings in the heterogeneous experiment. The predictive advantage of generalizing mass transfer processes irrespective of saturation over upscaled models predicated on the ganglia-to-pool mass ratio, was further evidenced by a similar effect on X_{TCE} and X_{TOR} incurred by perturbing $\alpha_{T,3}$ (Figure 8.2.2). Conversely, the variability of other α_T parameters in both experiments only influenced sensitivity for the time of depletion, X_{TOR}.

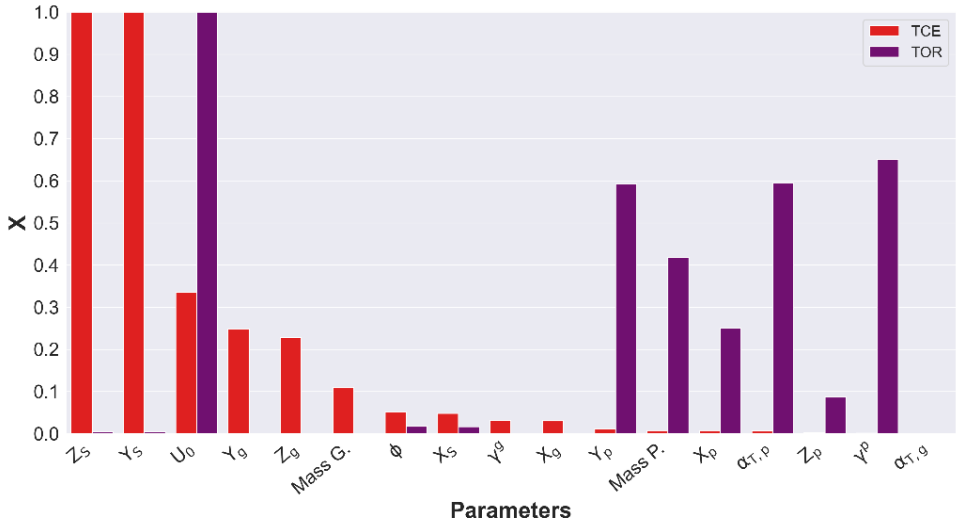

Figure 8.2.1. Bar Plot Showing the Greatest Sensitivity Coefficients with Respect to Source Discharge Concentrations Measured and Time of Depletion in the "Mixed Architecture" Experiment Described in Section 5.4.1.1.

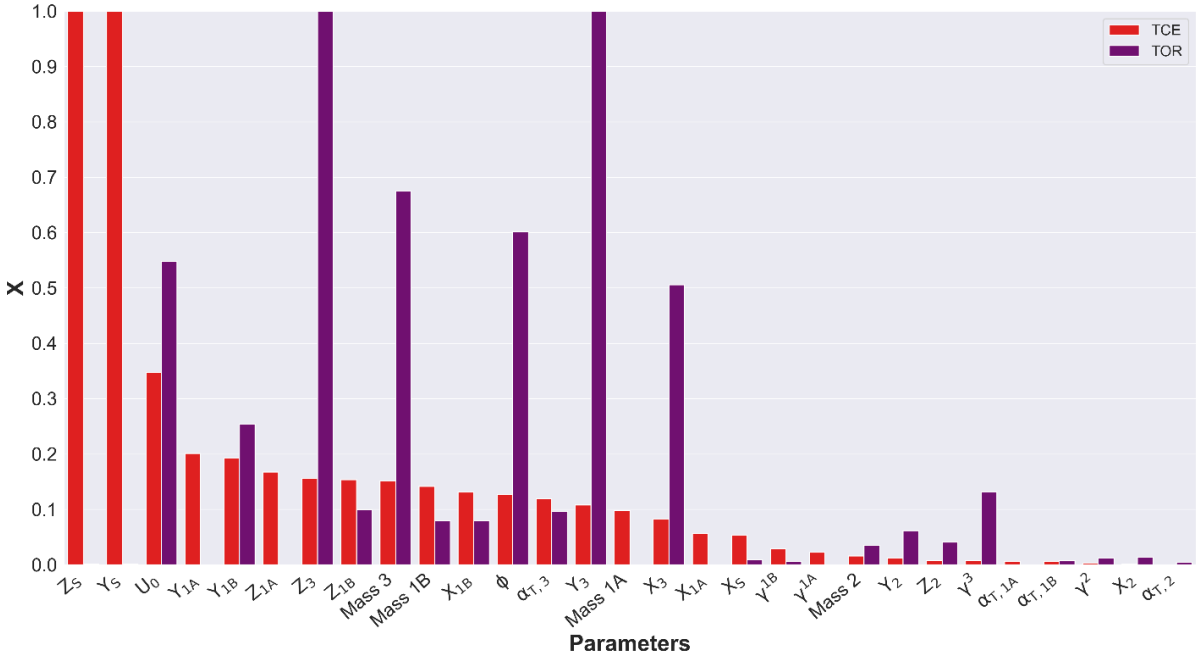

Figure 8.2.2. Bar Plot Showing the Greatest Sensitivity Coefficients with Respect to Source Discharge Concentrations Measured and Time of Depletion in the "Heterogeneous Architecture" Experiment Described in Section 5.4.1.2.

8.2.2 Linear Analysis

Prior (σ_{TOR}) and posterior (σ'_{TOR}) standard deviations of time of depletion uncertainty estimated with first-order second-moment (FOSM) analysis (Doherty, 2015) and mean (μ_{TOR}) values for both experiments are presented in Table 2. Results shown were calculated using the complete TCE monitoring profiles. As indicated, history-matching significantly constrained prior time of depletion uncertainties despite low X_{TCE} values of time-of-depletion-sensitive parameters pertaining to high saturation accumulations.

Table 8.2.1. Predictive Uncertainty of Mixed and Heterogeneous Experiments

Experiment	σ_{TOR} (days)	σ'_{TOR} (days)	μ_{TOR} (days)
Mixed	19.8	8.6	27.9
Heterogeneous	20.5	1.7	28.6

8.2.2.1 Relative Parameter Uncertainty Variance Reduction

Figures 8.2.3 and 8.2.4 show the benefit of history-matching for reducing prior parameter uncertainties. Despite negligible X_{TCE} values corresponding to the pool mass and $\alpha_{T,p}$ of the mixed experiment (Figure 8.2.1), history-matching reduced the prior uncertainty of these parameters by ~70% and ~60%, respectively (Figure 8.2.3). The low uncertainty reduction of γ^p (Figure 8.2.3), to which time of depletion was sensitive (Figure 8.2.1), demonstrated the benefit of coupling upscaled modeling with stochastic analysis tools for quantifying DNAPL longevity when mass transfer parameters remain unconstrained. In turn, sensitivity and FOSM analyses of the mixed experiment coincided in a low-ranked $\alpha_{T,g}$, suggesting that its prior (default) value of 0.001 m is reasonable for simulating dissolution of ganglia-dominated accumulations.

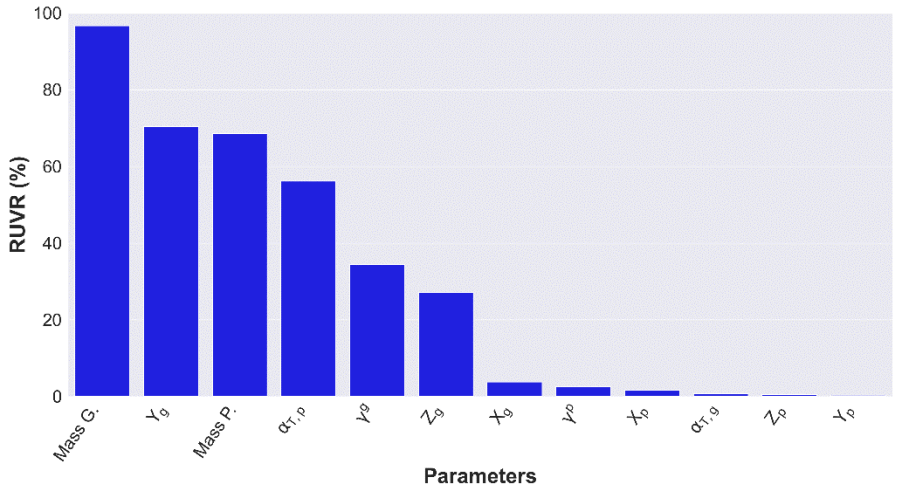

Figure 8.2.3. Relative Uncertainty Variance Reduction of VA Model Parameters of Mixed Experiment.

Difficulties in reducing prior uncertainty of the γ parameters in the heterogeneous experiment are reflected in Figure 8.2.4. Yet modest uncertainty reductions (~50%) of the dimensions and mass representing the saturation of DNAPL accumulations 1B and 3, were attained. 3.1.1.

The higher relative parameter uncertainty variance reduction (RUVR) of saturation with respect to other saturation parameters was attributed to the sequential dissolution of upgradient DNAPL masses, allowing the tailing segment of the TCE monitoring profile to constrain the remaining source architecture. These results implied that modeling efforts supporting the characterization of sites with aged, pool-dominated source zones, may benefit from history-matching of monitoring profiles. However, situations with scarce monitoring data and significant uncertainties on saturation distributions along groundwater flow paths may warrant high resolution site characterization efforts. In turn, source characterization data such as DyeLIF and Hydraulic Profiling Tool (Horst et al., 2018) can be leveraged with VA modeling, while FOSM analyses can help guide additional data collection efforts and constrain DNAPL dissolution trends.

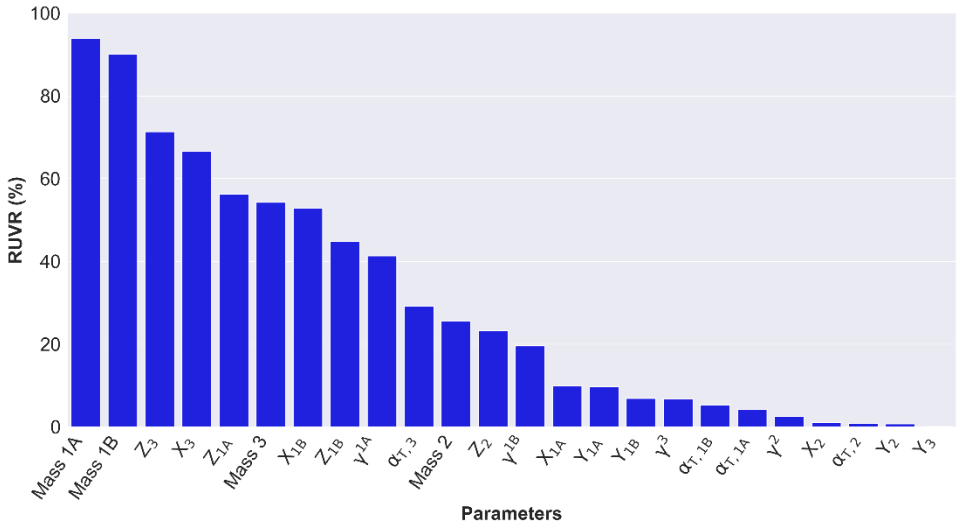

Figure 8.2.4. Relative Uncertainty Variance Reduction of VA Model Parameters of Heterogeneous Experiment.

8.2.2.2 Prior and posterior parameter contributions to predictive uncertainty

As shown in Figure 8.2.5, FOSM analyses validated negligible X_{TOR} values caused by the ganglia parameters in the mixed experiment. Although the pool dispersive area (YX_p) and γ^p influenced X_{TOR} results (Figure 8.2.1), prior and posterior time of depletion uncertainties of the mixed experiment were clearly driven by the pool mass and $\alpha_{T,p}$ (Figure 8.2.5). Likewise, Figure 8.2.6 indicated that the primary drivers of prior time of depletion uncertainty in the heterogenous experiment were saturation, $\alpha_{T,3}$, and γ^3. Repeating FOSM calculations with uncertainty bounds defined as $0 < \alpha_T < 0.01$ for all NAPL accumulations in the heterogeneous experiment did not alter the uncertainty rankings shown in Figure 8.2.6. Results of both experiments agreed on the significance of dispersive mass transfer (α_T) from high-saturation NAPL accumulations in regulating time of depletion. However, the accurate replication of the heterogenous source dissolution trend with $\alpha_{T,3} = 0$ m was attributed to the contrast in grain sizes, limiting dispersion from the coarse-grained lenticular zone into the finer surrounding sands despite high $S_{3,0}^N$ values.

Unlike the empirical mass depletion exponent γ^3, α_T may be directly measured at contaminated sites to directly constrain mass transfer uncertainties. Examples of field methods include push-pull tracer tests, borehole and HPT logging, and discrete groundwater sampling with direct push technology.

These data may be interpreted with spatial moment analysis (Rockhold et al., 2016), grain-size correlations with soil hydraulic conductivity and α_T (Carey et al., 2018), and 2D analytical modeling (Huang et al., 2010), respectively. Nonetheless, the α_T component of DNAPL dissolution should not be confused with plume-scale macrodispersion. While dispersivity at the source-zone and plume scales is driven by mechanical or hydrodynamic mixing along tortuous flow paths (Molz, 2015), coupling a VA model of DNAPL dissolution with a downgradient contaminant plume model may require two different α_T values based upon site-specific conditions. Several studies have demonstrated the relationship between soil grain size and α_T (Carey et al., 2018), concurring with its role on DNAPL mass transfer (Figures 8.2.5 and 8.2.6). This is in contrast to Gilland-Sherwood mass transfer correlations which rely upon aqueous-phase transport models for the contribution of α_T to DNAPL dissolution (Yang et al., 2019).

As indicated in Figure 8.2.6, the primary driver of posterior time of depletion uncertainty, γ^3, reflected its role in regulating source discharge concentrations over several orders of magnitude. While a lack of extensive groundwater monitoring at contaminated sites could limit γ constraining via history-matching, saturation and flow-field heterogeneities may also pose additional uncertainties on mass transfer assumptions. In this case, TCE dissolution tailing, primarily regulated by saturation, was also modulated by flow channelization in the coarse sand lens (Figure 5.4.1). Transient reductions in NAPL interfacial areas, which limit mass transfer rates through the γ parameter, were obfuscated by a local increase U_0 and k_r in the heterogeneous experiment (Stewart et al., 2022). Although the level of characterization detail available for the flow-cell experiment would not be available at field sites, VA modeling provides an efficient means to evaluate conceptual assumptions of system heterogeneities and quantify mass transfer uncertainties. The prior uncertainty rankings of saturation parameters (Figure 8.2.6) emphasized the level of effort for NAPL delineation required for adequate model parameterization.

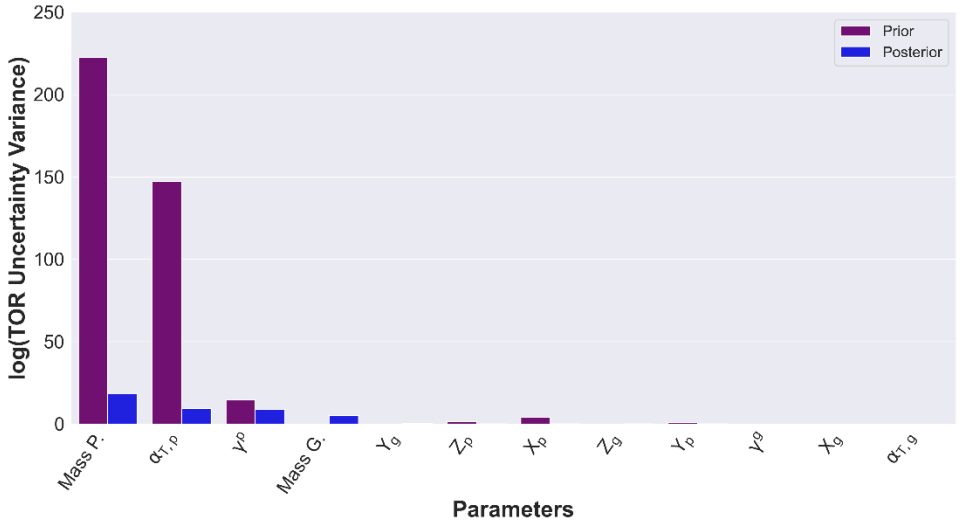

Figure 8.2.5. Prior and Posterior Parameter Contributions to TOR Uncertainty in the Mixed Experiment.

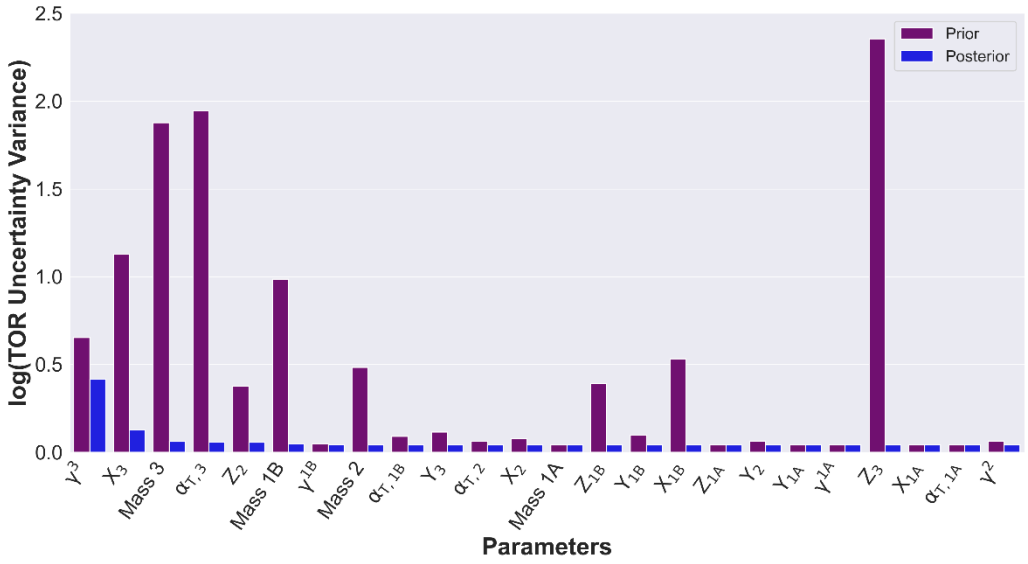

Figure 8.2.6. Prior and Posterior Parameter Contributions to TOR Uncertainty of Heterogeneous Experiment.

8.2.2.3 Data Worth Analysis

The worth of TCE monitoring profiles of the mixed and heterogeneous experiments is shown in Figures 8.2.7 and 8.2.8, respectively. Figures 8.2.7.1 and 8.2.8.1 indicate worth of individual measurements for constraining prior time of depletion uncertainty (σ_{TOR}), whereas Figures 8.2.7.2 and 8.2.8.1 depict increases in posterior (constrained) TOR uncertainty (σ'_{TOR}) caused by data removal. As shown in Figure 8.2.7, a tendency of increasing data worth in the mixed experiment started at point C, when the pool mass transfer area ($A_{p,xy}$) was sufficiently reduced to onset dissolution tailing. Similar prior and posterior data-worth trends in the mixed experiment suggested that peak concentrations emanating from ganglia-dominated accumulations do not constrain time of depletion. In turn, the RUVR of pool mass (~70%) and $\alpha_{T,p}$ (~60%) controlling time of depletion uncertainty was attributed to TCE monitoring after point C (Figure 8.2.7), highlighting the benefit of history-matching for characterizing sites with aged source zones and simple architectures. In these experiments, point C represents a rough mid-point for the DNAPL TOR despite an 80% reduction in the total DNAPL mass.

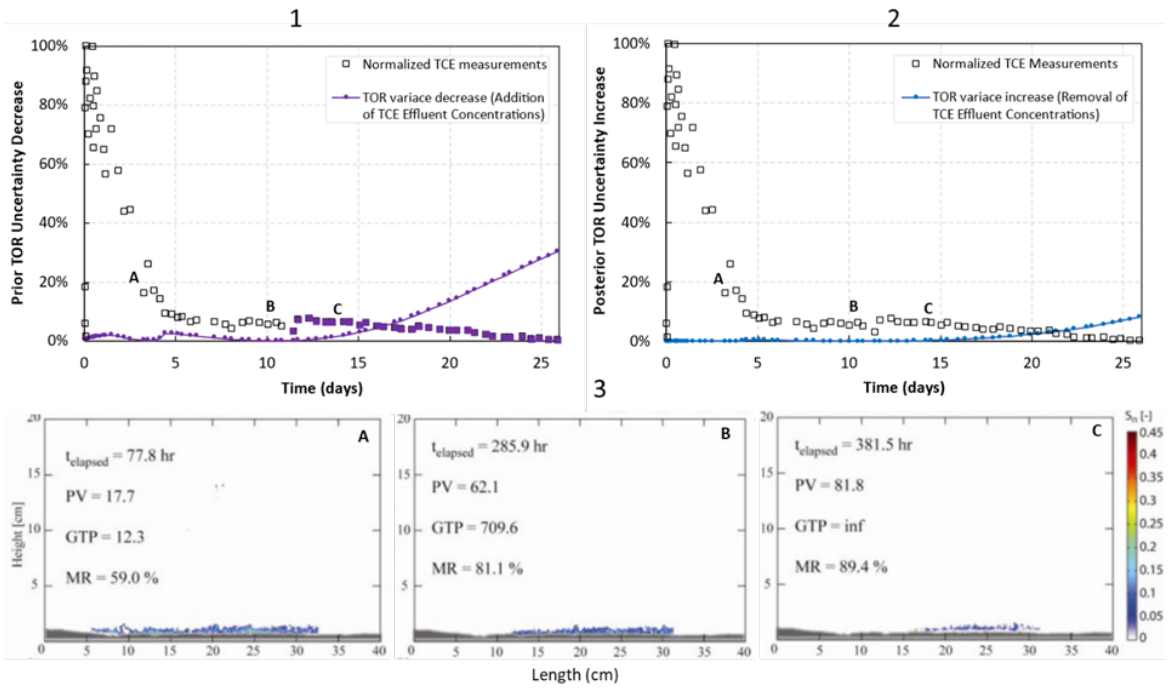

Figure 8.2.7. Monitoring Data Worth for Constraining TOR Uncertainty of the Mixed Experiment.

1) Decrease in prior uncertainty with addition of individual TCE concentrations. The filled data points highlight the greatest information content for reducing prior TOR uncertainty. 2) Increases in posterior uncertainty with data removal. 3) Points A, B, C show DNAPL depletion images measured by DiFilippo et al. (2010).

Figure 8.2.8.1 shows the worth of breakthrough inflection points along the TCE monitoring curve of the heterogeneous experiment for constraining σ_{TOR}. The first peak in the σ_{TOR} decrease curve coincided with point A, indicating the onset of rapid dissolution of NAPL accumulation 1B after 1A was completely dissolved. The second peak of σ_{TOR} reduction occurred during a slight increase in TCE concentrations, reflecting an increased k_r through mass 2, after mass 1B was dissolved. The final peaks of σ_{TOR} reduction (Figure 11.1) and σ'_{TOR} increase (Figure 11.2) coincided with the final stage of NAPL dissolution associated to mass 3. These results highlighted disadvantages of predicting future system behavior from limited monitoring profiles, corresponding to situations where remaining source architectures and heterogeneities have not been reflected in historical dissolution trends.

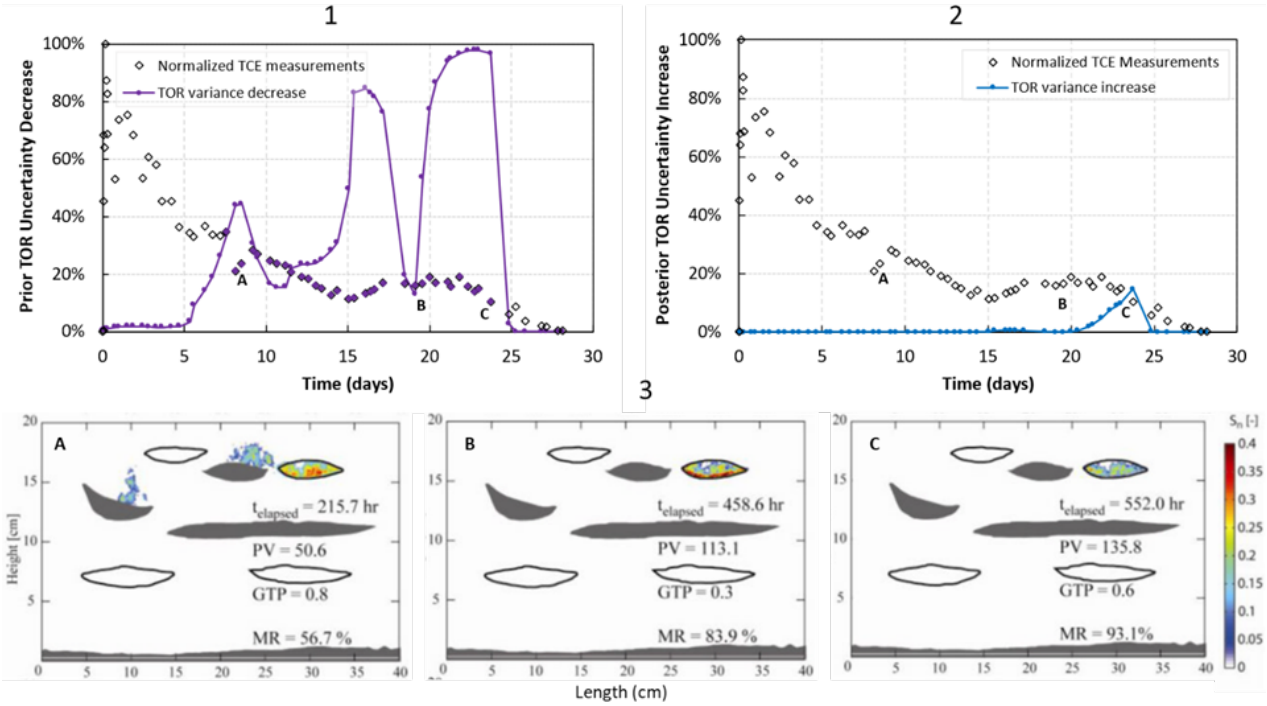

Figure 8.2.8. Worth of TCE Dissolution Measurements for Reducing TOR Uncertainty of the Heterogeneous Experiment.

1) Decrease in prior uncertainty with addition of individual history-matching constraints. The filled data points highlight the greatest information content for reducing prior TOR uncertainty. 2) Increases in posterior uncertainty with data loss. 3) Points A, B, C show the DNAPL depletion measured by DiFilippo et al. (2010).

8.2.3 Nonlinear Uncertainty Analyses

Figure 8.2.9 indicates that all prior and posterior source dissipation timeframes of the mixed experiment included the "true time of depletion" (μ_{TOR} = 27.9 days). All posterior analyses underestimated the initial NAPL mass in the mixed experiment by ~11%, yet the known value of 17.2 g was included within 95% confidence limits (results not shown). The average estimated S_g^N and S_p^N values were 4% and 40%, respectively, consistent with initial experimental conditions. Prior and posterior TOR uncertainties in Figure 8.2.9 demonstrated the utility of VA modeling for estimating unbiased depletion timeframes, by leveraging NAPL-delineation or limited monitoring data pertaining to source zones with simple architectures and flow conditions.

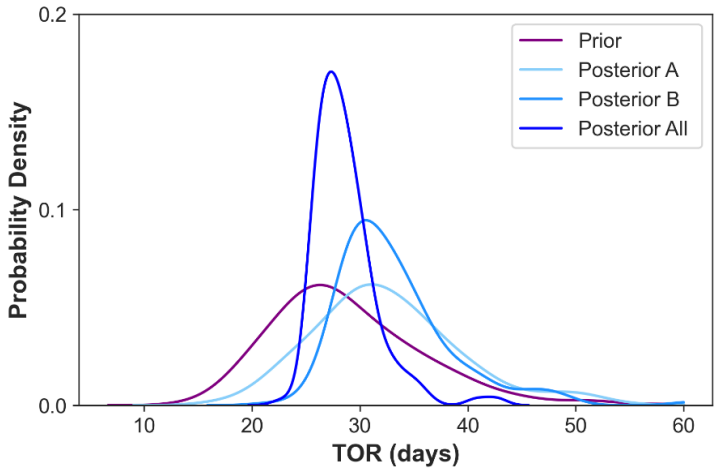

Figure 8.2.9. Prior and Posterior TOR PDFs of Mixed Experiment.

Posterior A and B were estimated by history-matching TCE concentrations through day 11.7 and 20 (Figure 8.2.7), Respectively.

The stochastic optimization of the heterogeneous experiment models underestimated initial NAPL mass by ~7%, with 95% confidence limits encompassing the injected amount of 20.4 g (results not shown). As shown in Figure 8.2.10, posterior S_a^N uncertainties reflected the averaging by model resolutions required to history-match the complete TCE dissolution profile and quantify time of depletion uncertainty (Figure 8.2.11). Figure 8.2.11 shows all posterior TOR PDFs encompassing the "true" TOR of 28.6 days, emphasizing the worth of final DNAPL dissolution stages for constraining TOR with various model resolutions. The 2M and 3M models required removing peak TCE concentrations from day 0 through day 9 (Figure 8.2.12). Not doing so did not impact the accuracy of estimated NAPL mass, but resulted in an artificially low initial S_I^N of lumped mass 1 from inadequate parameterization complexity (results not shown). Sufficient source architecture parameters are thereby necessary to assimilate complex dissolution profiles to avoid misleading injection-based remedial designs.

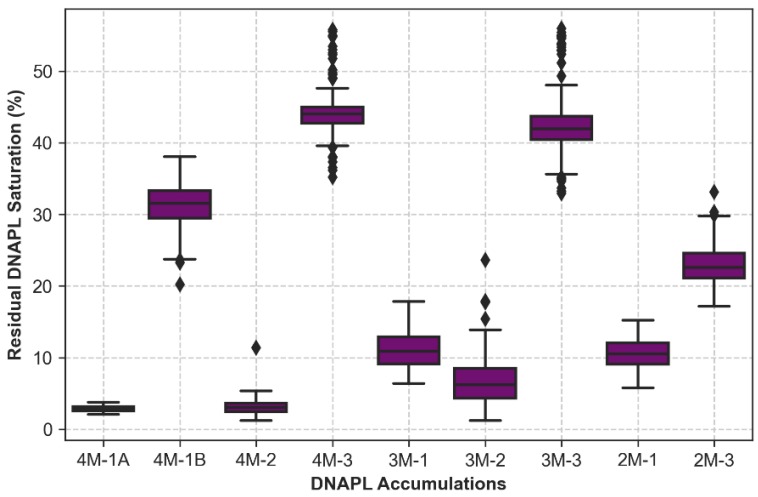

Figure 8.2.10. Posterior DNAPL Saturation Distributions of Each DNAPL Accumulation in the 4M, 3M, and 2M VA Models of the Heterogeneous Experiment.

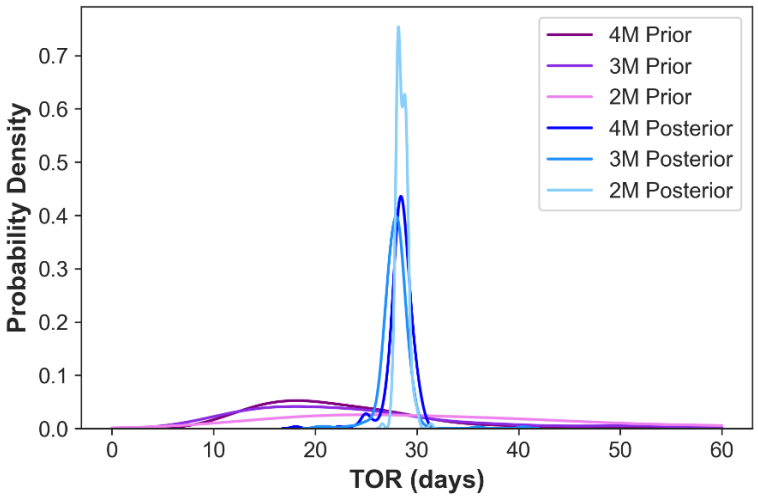

Figure 8.2.11. Prior and Posterior TOR PDFs of the Heterogeneous Experiment Conceptualized by 2, 3, and 4 NAPL Accumulations.

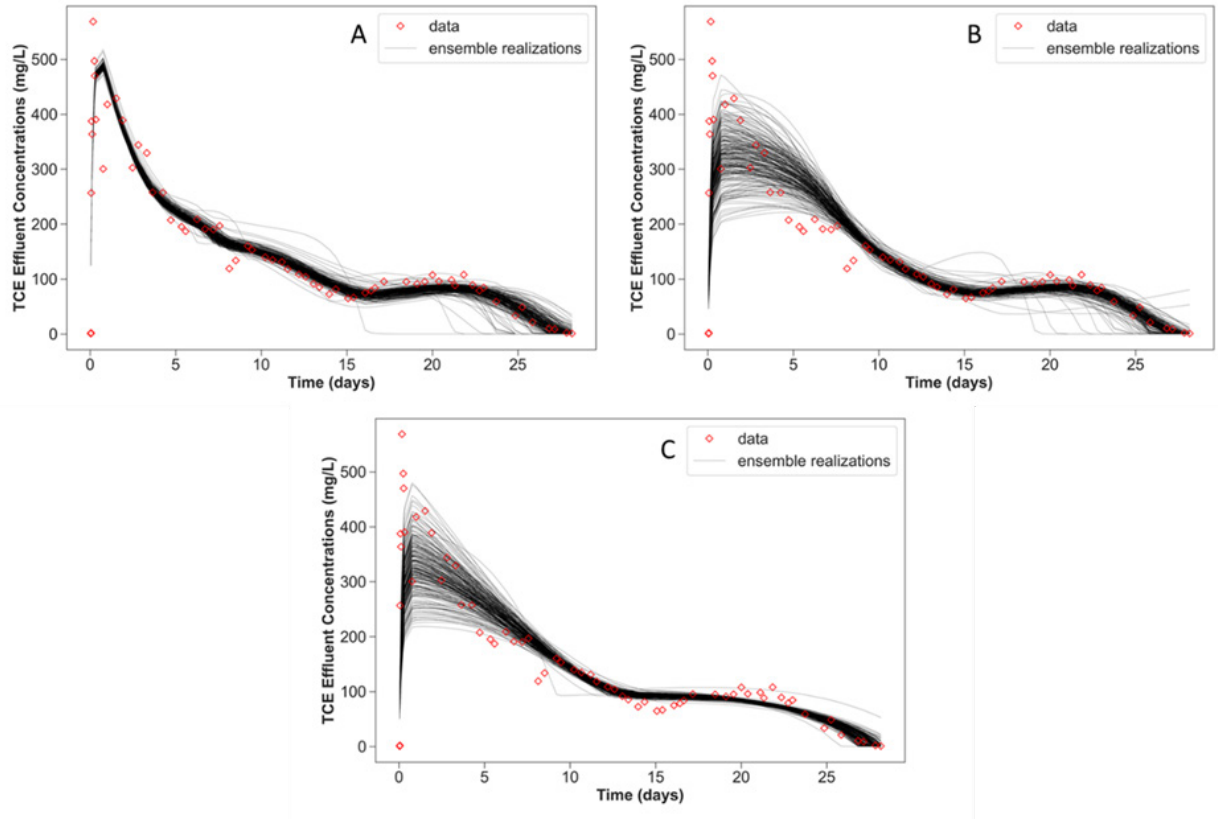

Figure 8.2.12. Posterior Model Ensembles of the Heterogeneous Experiment Corresponding to (A) 4, (B) 3, and (C) 2 NAPL Accumulations.

Figure 8.2.13 shows prior predictive PDFs approximated with S_a^N constraints ensuing 2M and 3M optimization results (Figure 8.2.9). The S_a^N prior constrains assumed availability of high resolution site characterization data to inform model parameters. Despite low probability densities, all prior PDFs encompassed the μ_{TOR} = 28.6 days, suggesting that even a low-resolution model (2M) accounting for saturation distribution along the flow path can predict unbiased source dissipation timeframes. However, Figure 8.2.13 depicts biased posterior 2M PDFs tending to exclude μ_{TOR} because of inadequate parameterization complexity. Unlike 2M, 3M included an adjustable "dissolution enhancement factor" representing increased U_0 through the coarse lens. Omitting that parameter from the 3M model (fixing it at a value of 1) did not impact σ'_{TOR} estimated from the entire TCE profile (Figures 8.2.11 and 8.2.12). However, σ_{TOR}, and σ'_{TOR} estimated from partial TCE profiles, were also overestimated (excluding μ_{TOR}) and the nonmonotonic increase in TCE concentrations from day 15 through day 20 could not be reproduced (results not shown). Hence, the unbiased Posterior A and B results of the 3M model shown in Figure 8.2.13, suggested that in addition to adequate representation of NAPL distribution along the local flow path, parameterization of flow field heterogeneity is also necessary to avoid biasing model estimates through history-matching of multistage and nonmonotonic dissolution profiles.

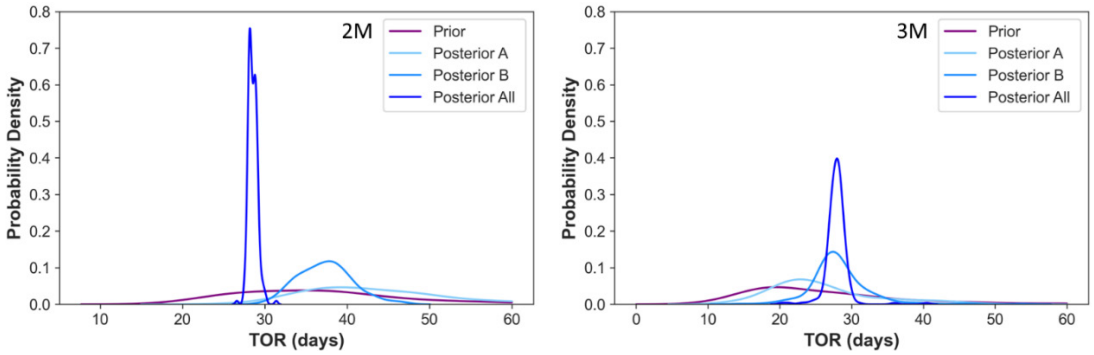

Figure 8.2.13. Probability Density Functions of TOR Approximated with 2M and 3M Models of Heterogeneous Experiment.

Posterior A and B PDFs include TCE history-matching constraints through day 14 and 20, respectively.

8.2.4 Discussion of Uncertainty Results for Site Characterization

These preliminary analyses demonstrated a practical approach for estimating NAPL dissolution timeframes coupling upscaled modeling with uncertainty analysis methods. Assimilation of monitoring data may induce model predictive bias without sufficient parameterization complexity, including sequential dissolution of NAPL accumulations distributed along the flow path. In both experiments, saturation parameters and transverse dispersion of pool-dominated NAPL accumulations controlled source zone longevity, and were constrained by tailing of final effluent concentration stages despite their negligible influence on measured effluent concentrations. Because the VA model provides TOR as a direct output, FOSM analysis can be used to guide additional high resolution site characterization efforts for reducing uncertainties. As demonstrated for the heterogeneous experiment, field mapping of aquifer hydraulics and/or estimation of source zone architecture using physically-based inversion methods can be leveraged to refine conceptual assumptions encapsulated in VA model parameters. This includes direct constraining of transverse vertical dispersivity at the source zone scale, regardless of DNAPL saturation, differentiating its contribution to DNAPL dissolution from macrodispersion at the contaminant plume scale.

Local groundwater velocity and source zone dimensions had a prominent impact on mass discharge and NAPL persistence because of their scaling role on mass transfer processes. Hence, these parameters require constraining by monitoring and site characterization scales, promoting adequate dilution and flow bypassing effects on NAPL dissolution. Conversely, saturation parameters of ganglia-dominated NAPL accumulations, which may not be directly measured at field sites, did not impact source longevity timeframes when pools were present. Yet their influence on peak discharge concentrations justifies their parameterization to avoid erroneous estimates of NAPL saturation distributions and mass recovery rates. Although accurately simulating mass discharge was possible with increased resolution of source zone architecture, exclusive designations of ganglia and pool fractions of NAPL may be inadequate for mass transfer modeling. The high-saturation NAPL accumulation embedded in the coarse sand lens of the heterogeneous experiment, controlled the source zone longevity without dispersive mass transfer. Moreover, lumping the downgradient saturations and ignoring flow field heterogeneity, biased lifespan estimates of the heterogenous source zone and degraded the replication of nonmonotonic NAPL dissolution tailing. While this level of characterization detail may not be available for contaminated sites, upscaled modeling and stochastic analyses of site conceptual assumptions can support risk-based decision making through data assimilation and hypothesis testing with a physical mass transfer basis.

8.2.5 Preliminary Uncertainty Analyses for Site ST012

To assess the degree of accuracy of the volume-averaged modeling approach demonstrated at Site ST012 (Section 5.5.2), sensitivity and uncertainty analyses identical to those described above were conducted. Input parameters and bounds were determined based on the CSM and available data and are described in detail in Appendix E. Each input parameter was selected within an estimated uncertainty bound, which reflects variability in site data and uncertainty in conceptual assumptions. The predictive uncertainty associated with the estimated remedial timeframes for the different remedial technologies was quantified using the prior-based Monte Carlo functionality of the iterative ensemble smoother PESTPP-iES (White 2018, White et al. 2020), with 20 randomized model realizations per adjustable parameter. The sensitivity and uncertainty analyses were performed on the remedial timeframe estimates for Pool 1. Parameter bounds and details of the sensitivity and uncertainty analyses are provided in Appendix E.

The NAPL saturation and dimensions contribute significantly to the predictive uncertainty of remedial timeframes for all remedial scenarios. Those parameters define the initial NAPL mass in the source zone which, along with the mass dissolution rate, control the source depletion times. These observations emphasize the need and value of high-resolution site characterization for identifying discrete DNAPL accumulations and their characteristics, as well as the need for the development of best practices to develop NAPL source conceptual models based on multiple lines of evidence (Mumford et al. 2022). For the pump-and-treat and ISCO remedies, the remedial enhancement factors are the most sensitive parameters. For enhanced bioremediation, the remedial timeframes are more sensitive to the NAPL source characteristic parameters (i.e., saturation and dimensions) than the degradation rate.

The predictive uncertainties are illustrated in Figure 8.2.14, which depicts the distribution of estimated remedial timeframes for Pool 1 with randomized model realizations. Despite the uncertainty associated with input parameters, this analysis indicates the VA model provides a range of timeframes within an order of magnitude for the different remedial technologies (i.e.,

MNA remedial timeframes are 100 to 300 years, pump-and-treat remedial timeframes are 20 to 60 years, enhanced bioremediation remedial timeframes are 50 to 150 years, and ISCO remedial timeframes are below 20 years). In addition, the relative performance of remedial technologies remains consistent across the randomized realizations, with remedial timeframe estimates increasing from ISCO, pump-and-treat, enhanced bioremediation, and MNA. While uncertainty in input parameters may affect the estimated remedial timeframes, the comparison of different technologies is robust and can be used to support decision making at complex sites.

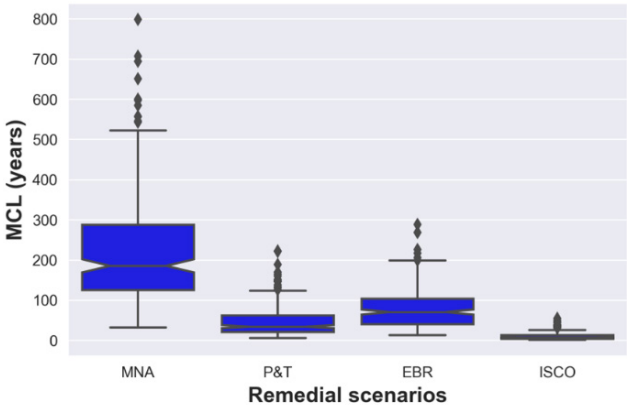

Figure 8.2.14. Boxplots of Nonlinear Uncertainty Distribution of Timeframes to Discharge MCL for Remedial Alternatives.

Notches indicate 95% confidence intervals around median values.

8.3 CONCLUSIONS AND FUTURE WORK

The results of this project were demonstrated to bridge the gap between research findings on NAPL dissolution, remedial processes and their availability and accessibility to practitioners and DoD remedial project managers (RPMs) making remedial decisions. The modeling framework provides a balance between complex numerical simulators, overly simple and optimistic screening models, and sparse site-specific datasets by applying physically-based mass transfer coefficients to remedial processes. As validated by application to multiple experimental data sets and controlled field studies, the volume-averaged approach (1) is grounded in science that incorporates mass balances on remedy components and core mass transfer processes that screening models fail to capture, (2) avoids the numerical tedium of simulators and intensive input parameter requirements, and (3) bypasses the requirement of a calibrated numerical groundwater flow model. The approach, though, is highly complementary to numerical fate and transport models. Output from the volume-averaged source zone provides a site- and technology- specific generation output for direct use in evaluating plume response to source remediation. Future work will include an effort to incorporate this source control model as a module in DoD's Groundwater Modeling System. With this module, the remediation of NAPL could be efficiently modeled and the mass discharge could be evaluated with established numerical transport models such as SEAM3D. The output, as illustrated in the two site demonstrations, will be useful to remedial project managers and decision makers for both technology selection and remedy evaluation.

The demonstrated modeling framework is also applicable to PFAS source terms. The purpose of the framework is to convert complex processes, such as those associated with PFAS retention and transport, into a readily solvable system of equations for providing transient, realistic sources for groundwater transport models.

Future work will also include the statistical analyses described in Section 8.2 in a seamless framework to promote identification of site-specific critical parameters for assessing source longevity and thereby prioritize site characterization efforts.

Finally, future work will incorporate more technology-specific remediation models as utilized in Section 5.4.3 and described in Appendix B. For example, separate, more detailed models of ISCO with permanganate and persulfate could include associated inhibitions to dissolution, transient dissolution enhancements, and mass balances on the oxidants and products for both remedy design and remedy evaluation. Appendix B also describes detailed models for enhanced bioremediation and bioaugmentation for similar purposes.

9.0 REFERENCES

Abriola, L.M., P. Goovaerts, K.D. Pennell, and F.E. Loffler. 2008. SERDP Project No. ER-1293: Development of Assessment Tools for Evaluation of the Benefits of DNAPL Source Zone Treatment. Final Report available online: https://serdp-estcp.org.

Abriola, L.M., E. Miller, K. Pennell, A. Ramsburg, and J. Christ. 2013. SERDP ER-1612: Metric Identification and Protocol Development for Characterizing DNAPL Source Zone Architecture and Associated Plume Response. Final Report available online: https://serdp-estcp.org.

Adamski, M., V. Kremesec, R. Kolhatkar, C. Pearson, and B. Rowan, 2005, "LNAPL in Fine-Grained Soils: Conceptualization of Saturation, Distribution, Recovery, and Their Modeling," Ground Water Monitoring & Remediation, Vol. 25, No. 1, pp. 100-112.

Amec Foster Wheeler Environment & Infrastructure, Inc. 2018. Final Pilot Study Work Plan for Operable Unit 2, Revised Groundwater Remedy, Site ST012, Former Williams Air Force Base, Mesa, Arizona. United States Air Force. April 2018. Available online: http://afcec.publicadmin-record.us.af.mil/

Annable, M., K. Hatfield, J. Jawitz, M. Brooks, L. Wood, and P. Rao. 2017. SERDP Project ER-1613: Predicting DNAPL Source Zone and Plume Response Using Site-Measured Characteristics. Final Report available online: https://serdp-estcp.org.

Bechtel Environmental, Inc. 1999. Semi-Annual Corrective Action Assessment Interim Measures Progress Report for Site 11 NSB Kings Bay GA. Oak Ridge, TN: Department of the Navy Southern Division Naval Facilities Engineering Command.

BEM Systems, Inc. 2000. Draft Technical Report of Contaminant Fate and Transport Modeling at Liquid Fuel Storage Area (ST-12), Williams ARB, Arizona. United States Air Force. October 2000. Available online: http://afcec.publicadmin-record.us.af.mil/

BEM Systems, Inc. 2007. Final ST012 Phase 1 Thermally Enhanced Extraction (TEE) Pilot Test Work Plan. Former Williams Air Force Base, Mesa, Arizona. United States Air Force. November 2007. Available online: http://afcec.publicadmin-record.us.af.mil/

BEM Systems, Inc. 2011. Final Phase 1 Thermal Enhanced Extraction (TEE) Pilot Test Performance Evaluation Report, prepared for Air Force Center for Engineering and the Environment, Lackland AFB, Texas, March 2011.

Banerjee S. 1984. Solubility of organic mixtures in water. Environmental Science and Technology; 18(8):587–591.

Broholm, K., S. Feenstra, and J.A. Cherry. 1999. Solvent Release into a Sandy Aquifer, 3: Overview of Source Distribution and Dissolution Behavior. Environmental Sci & Tech. 33(5):681–690.

Brusseau, M. 2013. ER-1614: Impact of DNAPL Source-Zone Architecture on Contaminant Mass Flux and Plume Evolution in Heterogeneous Porous Media, Report available online: https://serdp-estcp.org.

Carroll, K.C. and M.L. Brusseau. 2009. Dissolution, Cyclodextrin-Enhanced Solubilization, and Mass Removal of an Ideal Multicomponent Organic Liquid, Journal of Contaminant Hydrology, Vol 106, Pages 62–72.

Chapelle, F.H. and P.M. Bradley. 1999. Selecting Remediation Goals by Assessing the Natural Attenuation Capacity of Groundwater Systems. Proceedings of the Technical Meeting Charleston, South Carolina. March 8-12, 1999, Volume 3 of 3 Subsurface Contamination From Point Sources, Water-Resources Investigations Report 99-4018C. U.S. Geological Survey.

Chapelle, F.H., M. Widdowson, J. Brauner, E. Mendez, and C. Casey. 2003. Methodology for Estimating Times of Remediation Associated with Monitored Natural Attenuation. USGS Water Resources Investigation Report 03-4057. Available at http://pubs.usgs.gov/wri/wri034057/pdf/wrir03-4057.pdf.

Chapelle, F.H., P.M. Bradley, and C.C. Casey. 2005. Behavior of a chlorinated ethene plume following source-area treatment with Fenton's reagent. Ground Water Monitoring & Remediation. 25(2), 131-141.

Chapelle, F.H., J. Novak, J. Parker, B.G. Campbell, and M. Widdowson. 2007. A framework for assessing the sustainability of monitored natural attenuation. USGS Circular 1303, 35 pp.

Charbeneau, Randall, 2007. LNAPL Distribution and Recovery Model (LDRM) Volume 1: Distribution and Recovery of Petroleum Hydrocarbon Liquids in Porous Media. API Publication 4760, January.

Christ, J.A., Ramsburg, C.A., Pennell, K.D., Abriola, L.M. 2006. Estimating mass discharge from DNAPL source zones using upscaled mass transfer coefficients: An evaluation using multiphase numerical simulations. Water Resources Research, 42: W11420, doi:10.1029/2006WR004886.

Christ, J.A., and L.M. Abriola. 2007. Modeling metabolic reductive dechlorination in dense non-aqueous phase liquid source zones. *Advances in Water Resources* 30 no. 6–7: 1547–1561. http://dx.doi.org/10.1016/j.advwatres.2006.05.024

Christ, J., C.A. Ramsburg, K.D. Pennell, and L.M. Abriola. 2010. Predicting DNAPL mass discharge from pool-dominated source zones, Journal of Contaminant Hydrology. Volume 114, 18-34.

Chu, M., Kitanidis, P.K., McCarty, P.L., 2007. Dependence of lumped mass transfer coefficient on scale and reactions kinetics for biologically enhanced NAPL dissolution. Adv.Water Res. 30, 1618–1629.

Clement, T., T. Gautam, K. Lee, M. Truex, and G. Davis. 2004. Modeling of DNAPL-Dissolution, Rate-Limited Sorption and Biodegradation Reactions in Groundwater Systems. Bioremediation Journal. 8(1-2): p. 47-64.

Cussler, E.L. 1992. Diffusion: Mass Transfer in Fluid Systems. Cambridge University Press, pp. 631.

Demiray, Z., N. Akyol and N. Copty. 2021. Experimental Assessment and Modeling of Enhanced Solubilization of Pool-dominated Tetrachloroethene Source Zone in Heterogeneous Porous Media. Water Air Soil Pollut. 232:516 https://doi.org/10.1007/s11270-021-05454-z

DiFilippo, E. L., K. C. Carroll, and M. Brusseau .2010. Impact of organic-liquid distribution and flow field heterogeneity on reductions in mass flux, J. Contam. Hydrol., 115, 14–25.

Doherty, J. 2015. Calibration and Uncertainty Analysis for Complex Environmental Models. Brisbane, Australia: Watermark Numerical Computing.

Falta, R.W. 2003. Modeling sub-grid-block-scale dense nonaqueous phase liquid (DNAPL) pool dissolution using a dual-domain approach, Water Resources Research, Vol. 39, No. 12, 1360, doi:10.1029/2003WR002351.

Falta, R.W., P.S. Rao, and N. Basu. 2005. Assessing the impacts of partial mass depletion of in DNAPL source zones. 1. Analytical modeling of source strength functions and plume response. Journal of Contaminant Hydrology, 78(4): 259-280.

Falta, R.W. and W. Wang. 2017. A semi-analytical method for simulating matrix diffusion in numerical transport models. Journal of Contaminant Hydrology. Volume 197, Pages 39-49.

Feehley, C.E., Chunmiao Zheng, Fred J. Molz. 2000. A dual-domain mass transfer approach for modeling solute transport in heterogeneous aquifers: Application to the Macrodispersion Experiment (MADE) site, Water Resour. Res., 36, 2501–2515.

Geller, J. and Hunt, J. 1993. Mass Transfer from Nonaqueous Phase Organic Liquids in Water-Saturated Porous Media, Water Resources Research, 29(4): 833–845.

Guo, Z., A.E. Russo, E.L. DiFilippo, Z. Zhang, C. Zheng and M.L. Brusseau. 2020. Mathematical modeling of organic liquid dissolution in heterogeneous source zones, Journal of Contaminant Hydrology, 235, Article 103716. https://doi.org/10.1016/j.jconhyd.2020.103716

Griffioen, J.W., D.A. Barry and J.-Y. Parlange. 1998. Interpretation of two-region model parameters. Water Resources Research, 34(3), 373-384.

Haggerty, R. and S. Gorelick, 1995. Multiple-rate mass transfer for modeling diffusion and surface reactions in media with pore-scale heterogeneity, Water Resources Research, 31(10) pp 2383-2400, https://doi.org/10.1029/95WR10583

Hairer, E. and G. Wanner (1999), Stiff differential equations solved by Radau methods. Journal of Computational and Applied Mathematics, 111, 93-111.

Heiderscheidt, J. L., R. L. Siegrist, and T. H. Illangasekare (2008), Intermediate-scale 2D experimental investigation of in situ chemical oxidation using potassium permanganate for remediation of complex DNAPL source zones, J. Contam. Hydrol., 102(1–2), 3–16, doi:10.1016/j.jconhyd.2008.07.002.

Hood, E. 2000. Permanganate Flushing of DNAPL Source Zones: Experimental and Numerical Investigation. Ph.D. Dissertation, University of Waterloo, Waterloo, ON. 243 pp.

Horst, J., Welty, N., Stuetzle, R., Wenzel, R., & Germain, R. (2018). Fluorescent dyes: A new weapon for conquering DNAPL characterization. *Groundwater Monitoring & Remediation, 38*(1), 19-25. doi:10.1111/gwmr.12261

Huang, K.-C., Hoag, G.E., Chheda, P., Woody, B.A., Dobbs, G.M. 1999. Kinetic study of oxidation of trichloroethylene by potassium permanganate. Environ. Eng. Sci. 16(4), 265–274.

Huang, J., J.A. Christ and M.N. Goltz. 2010. Analytical solutions for efficient interpretation of single-well push-pull tracer tests. *Water Resources Research*. doi:10.1029/2008WR007647

Hunt J.R., Sitar N, Udell KS. 1988. Nonaqueous phase liquid transport and cleanup, 1, Analysis of mechanisms. Water Resour. Res. 24(8):1247–1258.

Illangasekare, T., Munakata Marr, J., Siegrist, R., Kenichi Soga, K. 2006. SERDP Project No. CU-1294: Mass Transfer from Entrapped DNAPL Sources Undergoing Remediation: Characterization Methods and Prediction Tools. Report available online: https://serdp-estcp.org.

Imhoff, P., A. Frizzell and C.T. Miller. 1997. Evaluation of Thermal Effects on the Dissolution of a Nonaqueous Phase Liquid in Porous Media. Environmental Science & Technology 31(6), 1615-1622. DOI: 10.1021/es960292x

IT. 1992. Remedial Investigation/ Feasibility Study, Williams AFB, Arizona. Final Remedial Investigation Report, Liquid Fuels Storage Area - Operable Unit 2. January

IT. 1999. Installation Restoration Program, Williams Air Force Base, Arizona. Draft Focused Feasibility Study Report, Operable Unit 2. October.

Interstate Technology Regulatory Council (ITRC). 2018. LNAPL-3: LNAPL Site Management: LCSM Evolution, Decision Process, and Remedial Technologies. Accessed 9/27/22: LNAPL Update (itrcweb.org).

Ji W, Brusseau ML. 1998. A general mathematical model for chemical-enhanced flushing of soil contaminated by organic compounds. Water Resources Research. 34(7):1635–1648.

Johnson, R. L. and J. F. Pankow. 1992. Dissolution of dense chlorinated solvents into groundwater, 2, Source functions for pools of solvent, Environ. Sci. Technol., 26, 869–901.

Johnson, P., P. Lundegard, and Z. Liu. 2006. Source zone natural attenuation at petroleum hydrocarbon spill sites - I: Site-specific assessment approach. Ground Water Monitoring and Remediation. 26(4): p. 82-92.

Johnson, R., P. Tratnyek, B. Sleep and M Krol. 2010. Final Report In Situ Thermal Remediation of DNAPL Source Zones. SERDP Project ER-1458. Report available online: https://serdp-estcp.org.

Kavanaugh, M., R. Deeb, J. Nyman, L. Stewart, and M. Widdowson. 2011. ESTCP Project ER200833: Improved Field Evaluation of NAPL Dissolution and Source Longevity. Report available online: https://serdp-estcp.org.

Kokkinaki, A., C. J. Werth, and B. E. Sleep. 2014. Comparison of volume-averaged models for multistage mass discharge from DNAPL source zones, Water Resour. Res., 50, 3187–3205,

doi:10.1002/2013WR014663.

Lebrón, C., D. Major, J. Konzuk, B. Kueper, and J. Gerhard. 2012. ER-200424. Development of a Protocol and a Screening Tool for Selection of DNAPL Source Area Remediation. Report available online: https://serdp-estcp.org.

Lebrón, C.A., Wiedemeier, T.H., Wilson, J.T., Löffler, F.E., Hinchee, R.E., and Singletary, M.A. 2015. ER-201129. Development and Validation of a Quantitative Framework and Management Expectation Tool for the Selection of Bioremediation Approaches (Monitored Natural Attenuation [MNA], Biostimulation and/or Bioaugmentation) at Chlorinated Solvent Sites. Report available online: https://serdp-estcp.org.

Leeth, D. C. 1999. *Hydrogeology of the Surficial Aquifer in the Vicinity of a Former Landfill, Naval Submarine Base Kings Bay, Camden County, Georgia.* Atlanta: U.S. Geological Survey.

Liu, C., Ball, W.P., 2002. Back diffusion of chlorinated solvent contaminants from a natural aquitard to a remediated aquifer under well-controlled field conditions: Predictions and measurements. Groundwater 40, 175-184.

Liu, Y., T. Illangasekare, and P. Kitandis. 2014. Long-term mass transfer and mixing-controlled reactions of a DNAPL plume from persistent residuals, Journal of Contaminant Hydrology. Volume 157, p. 11-24.

Luciano, A., P. Viotti and M.P. Papini. 2012. On morphometric properties of DNAPL sources: Relating architecture to mass reduction. Water, Air, and Soil Pollution 223(5), 2849-2864.

Macbeth, T., M. Truex, T. Powell, and M. Michalsen. 2012. ER-200719: Combining Low-Energy Electrical Resistance Heating with Biotic and Abiotic Reactions for Treatment of Chlorinated Solvent DNAPL Source Areas., Report available online: https://serdp-estcp.org.

MacKinnon, L. K., and N. R. Thomson (2002), Laboratory-scale in situ chemical oxidation of a perchloroethylene pool using permanganate, J. Contam. Hydrol., 56(1), 49–74.

Marble, J.C., E.L. DiFilippo, Z. Zhang, G.R. Tick, and M.L. Brusseau. 2008. Application of a lumped-process mathematical model to dissolution of non-uniformly distributed immiscible liquid in heterogeneous porous media. Journal of Contaminant Hydrology. 100(1-2):1-10.

McCray, J.E., T.B. Boving and M.L. Brusseau. 2000. Cyclodextrin-Enhanced Solubilization of Organic Contaminants with Implications for Aquifer Remediation. Groundwaer Monitoring & Remediation. 20(1) 94-103.

Miller, C., M. M. Poirier-McNeill, and A. S. Mayer. 1990. Dissolution of trapped nonaqueous phase liquids: Mass transfer characteristics, Water Resour. Res., 26, 2783–2796.

Mobile, M., M. Widdowson and D. Gallagher. 2012. Multicomponent NAPL Source Dissolution: Evaluation of Mass-Transfer Coefficients. Environ. Sci. Technol. 46(18):10047-10054.

Molz, F. 2015. Advection, Dispersion, and Confusion. Ground Water. 53(3):348-353.

Mumford, K.G., S. Bryck, B.H. Kueper, S. Mancini, M. Kavanaugh, and D. Reynolds. 2022. Virtual Site Investigation to Evaluate Conceptual Site Model Development at DNAPL-Impacted Sites. Groundwater Monitoring & Remediation 42:44–58. https://doi.org/10.1111/gwmr.12537

Muskus, N. and R.W. Falta. 2018. Semi-analytical method for matrix diffusion in heterogeneous and fractured systems with parent-daughter reactions. Journal of Contaminant Hydrology. 218:94-109.

National Research Council (NRC). 2004. Contaminants in the Subsurface: Source Zone Assessment and Remediation. National Academies Press: Washington, DC.

NRC. 2013. Alternatives for Managing the Nation's Complex Contaminated Groundwater Sites. National Academies Press: Washington, DC.

Parker, B.L., Chapman, S.W., Guilbeault, M.A., 2008. Plume persistence caused by back diffusion from thin clay layers in a sand aquifer following TCE source-zone hydraulic isolation Journal of Contaminant Hydrology 102, 86-104.

Parker, J.C., U. Kim, P. Kitanidis, M. Cardiff, X. Liu, and J. Lee. 2011. SERDP ER-1611: Practical Cost-Optimization of Characterization and Remediation Decisions at DNAPL Sites with Consideration of Prediction Uncertainty. Report available online: https://serdp-estcp.org.

Parker, J.C., U. Kim, B. Borden, and A. Fortune. 2017. SERDP ER-2310: A Practical Approach for Remediation Performance Assessment and Optimization at DNAPL Sites for Early Identification and Correction of Problems Considering Uncertainty. Report available online: https://serdp-estcp.org.

Parker, J. C. and E. Park. 2004. Modeling field-scale dense nonaqueous phase liquid dissolution kinetics in heterogeneous aquifers. Water Resources Research, 40: W05109, doi:10.1029/2003WR002807.

Perina, T. 2022. Semi-analytical model for solute transport in a three-dimensional aquifer with dual porosity and a volumetric source term. Journal of Hydrology 607, 127520.

Phelan, T.J, Linda M. Abriola, Jenny L. Gibson, Kathleen M. Smits, and John A. Christ. 2015. Development and application of a screening model for evaluating bioenhanced dissolution in DNAPL source zones. Journal of Contaminant Hydrology, Volume 183, Pages 1-15.

Popp, S., C. Beyer, A. Dahmke, N. Koproch, R. Kober and S. Bauer. 2016. Temperature-dependent dissolution of residual non-aqueous phase liquids: model development and verification. Environmental Earth Sciences. 75, 953 (2016). https://doi.org/10.1007/s12665-016-5743-x.

Powers S.E., Loureiro C.O., Abriola L.M., Weber W.J. Jr. 1991. Theoretical study of the significance of nonequilibrium dissolution of nonaqueous phase liquids in subsurface systems. Water Resour. Res; 27(4):463–477.

Powers, S. E., L. M. Abriola, and W. Weber. 1994. An experimental investigation of NAPL dissolution in saturated subsurface systems: Transient mass transfer rates, Water Resour. Res., 30, 321–332.

Powers, S.E., I.M. Nambi, and G.W. Curry Jr. 1998. Non–aqueous phase liquid dissolution in heterogeneous systems: mechanisms and a local equilibrium modeling approach, Water Resour. Res. 34 (12) (1998) 3293, https://doi.org/10.1029/98WR02471.

Rao, P.S.C., Jawitz, J.W., Enfield, C.G., Falta Jr., R.W., Annable, M.D., Wood, A.L. 2001. Technology integration for contaminated site remediation: Cleanup goals and performance metrics. Sheffield, UK.: Groundwater Quality: Natural and Enhanced Restoration of Groundwater Pollution, no. 274, p. 571-578.

Rockhold, M., Z. Zhang and Y.-J. Bott. 2016. Scale-Dependent Solute Dispersion in Variably Saturated Porous Media. Richland, WA: Pacific Northwest National Laboratory

Saba, T. and T. Illangasekare. 2000. Effect of ground-water flow dimensionality on mass transfer from entrapped non-aqueous phase liquid contaminants, Water Resour. Res., 36(4), 971–979.

Saba, T., T. Illangasekare, and J. Ewing. 2002. Surfactant enhanced dissolution entrapped NAPLs in multidimensional flow fields. J Contam Hydrol 51(1–2):63–82.

Saenton, S. and T. Illangasekare. 2007. Upscaling of mass transfer rate coefficient for the numerical simulation of dense nonaqueous phase liquid dissolution in heterogeneous aquifers. Water Resources Research, 43: W02428, doi: 10.1029/2005/WR004274.

Saenton, S. and T. Illangasekare. 2013. Effects of incomplete remediation of NAPL-contaminated aquifers: experimental and numerical modeling investigations, Appl Water Sci 3:401–414.

Schnarr, M., C. Truax, G. Farquhar, E. Hood, T. Gonullu, and B. Stickney (1998), Laboratory and controlled field experiments using potassium permanganate to remediate trichloroethylene and perchloroethylene DNAPLs in porous media, J. Contam. Hydrol., 29(3), 205–224. doi:10.1016/S0169-7722(97)00012-0.

Seagren, E.A., B.E. Rittman and A.J. Valocchi. 1994. Quantitative Evaluation of the Enhancement of NAPL-Pool Dissolution by Flushing and Biodegradation. Environmental Science & Technology, Vol. 28, 833–839.

Seagren, E.A. and J.G. Becker. 2015. Predictions of bioenhancement of nonaqueous phase liquid ganglia dissolution using first- and zero-order biokinetic models. Journal of Contaminant Hydrology, Vol. 182, 210–220. http://dx.doi.org/10.1016/j.jconhyd.2015.08.004

Siegrist, R.L., M.A. Urynowicz, O.R. West, M.L. Crimi, and K.S. Lowe. 2001. Principles and Practices of In Situ Chemical Oxidation Using Permanganate. Columbus. Ohio, Battelle Press.

Seigrist, R., M. Crimi, J. Munakata-Marr, and T. Illangasekare. 2006. ER-1290: Reaction and Transport Processes Controlling In Situ Chemical Oxidation of DNAPLs. Report available online: https://serdp-estcp.org.

Siegrist, R.L., M. Crimi, and Th.J. Simpkin (editors). 2011. In Situ Chemical Oxidation for Groundwater Remediation, Springer 678p.

Stewart, L.D., Chambon, J.C., Widdowson, M.A., Kavanaugh, M.C. 2022. Volume-averaged modeling of complex DNAPL dissolution. Journal of Contaminant Hydrology 244, 103920.

USGS, 2022. MODFLOW and Related Programs. https://www.usgs.gov/mission-areas/water-resources/science/modflow-and-related-programs?qt-science_center_objects=0#qt-science_center_objects. Accessed September 2022.

Waddill, D.W., Widdowson, M.A. 2000. SEAM3D: A Numerical Model for Three-Dimensional Solute Transport and Sequential Electron Acceptor-Based Biodegradation in Groundwater. U.S. Army Engineer Research and Development Center Technical Report ERDC/EL TR-00-18, Vicksburg, MS.

Waldemer, R., P.G. Tratnyek, R.L. Johnson and J.T. Nurmi. 2007. Oxidation of Chlorinated Ethenes by Heat-Activated Persulfate: Kinetics and Products. Environ. Sci. Technol. 1010-1015.

Wang XJ, Brusseau ML. 1993. Solubilization of some low-polarity organic-compounds by hydroxypropyl-beta-cyclodextrin. Environmental Science and Technology. 27(13):2821–2825.

Watermark Numerical Computing. 2018. Model-Independent Parameter Estimation. User Manual Part II: PEST Utility Suport Software. Retrieved from https://pesthomepage.org/documentation

White, J.T. 2018. A model-independent iterative ensemble smoother for efficient history-matching and uncertainty quantification in very high dimensions. Environmental Modelling & Software 109:191–201. https://doi.org/10.1016/j.envsoft.2018.06.009

White, J., R. Hunt, M. Fienen, and J. Doherty. 2020. Approaches to Highly Parameterized Inversion: PEST++ Version 5, a Software Suite for Parameter Estimation, Uncertainty Analysis, Management Optimization and Sensitivity Analysis. Reston, Virginia: U.S. Geological Survey. doi:10.3133/tm7C26

Wilson, J. L., S. H. Conrad, W. R. Mason, W. Peplinski, and E. Hagan. 1990. Laboratory investigations of residual organic liquids from spills, leaks, and disposal of hazardous wastes in groundwater, Rep. EPA/600/6-90/004, Environ. Prot. Agency, Washington, D. C.

Wyllie, M. R. J. 1962. Relative permeability, in Petroleum Production Handbook, vol. II, Reservoir Engineering, edited by T. C. Frick and R. W. Taylor, pp. 25.1–25.14, McGraw-Hill, New York.

Wood, L., M. Annable, J. Jawitz, R. Falta, M. Brooks, C. Enfield, P. Rao, and M. Goltz. 2009. SERDP ER-1295: Impacts of DNAPL Source Zone Treatment: Experimental and Modeling Assessment of Benefits of Partial Source Removal. Report available online: https://serdp-estcp.org.

Yang, Y. and P.L. McCarty. 2002. Comparison between donor substrates for biologically enhanced tetrachloroethene DNAPL dissolution. Environ. Sci. Technol. 36 (15), 3400–3404.

Yang, M., Annable, M.D., Jawitz, J.W., 2015. Back Diffusion from Thin Low Permeability Zones. Environ. Sci. Technol. 49, 415-422.

Yang, Luron, Xinyu Wang, Itza Mendoza-Sanchez, Linda M. Abriola. 2018. Modeling the influence of coupled mass transfer processes on mass flux downgradient of heterogeneous DNAPL source zones, Journal of Contaminant Hydrology, Vol. 211, 1-14.

APPENDIX A POINTS OF CONTACT

POINT OF CONTACT Name	ORGANIZATION Name Address	Phone Fax E-mail	Role in Project
Lloyd "Bo" Stewart	Praxis Environmental Technologies 1440 Rollins Road Burlingame, CA 94010	P: 650-548-9288 F: 650-548-9287 Bo@Praxis-Environ.com	PI, volume-averaged modeling, data collection, data evaluation and reporting
Mark Widdowson	Virginia Polytechnic Institute & State University 200 Patton Hall Blacksburg, VA 24061	P: 540-231-7153 F: 540-231-7532 mwiddows@vt.edu	Co-PI, numerical modeling, data collection, data evaluation and reporting
Julie Chambon	Geosyntec Consultants 1111 Broadway Street, 6th floor Oakland, CA 94607	P: 510-836-3034 jchambon@geosyntec.com	Co-PI, analysis of data, review, technology transfer, data evaluation and reporting
Jennifer Nyman	Geosyntec Consultants 1111 Broadway Street, 6th floor Oakland, CA 94607	P: 510-836-3034 jnyman@geosyntec.com	Co-PI, compilation of data, analysis of data, review, technology transfer
Rula Deeb	Geosyntec Consultants 1111 Broadway Street, 6th floor Oakland, CA 94607	P: 510-836-3034 rdeeb@ geosyntec.com	Co-PI, technology transfer
Michael Kavanaugh	Geosyntec Consultants 1111 Broadway Street, 6th floor Oakland, CA 94607	P: 510-836-3034 mkavanaugh@ geosyntec.com	Co-PI, senior review
Mary Scarpetti	Praxis Environmental Technologies 1440 Rollins Road Burlingame, CA 94010	P: 650-548-9288 F: 650-548-9287 Bo@Praxis-Environ.com	Administrative Point of Contact, Editor, Web Manager

APPENDIX B COMPENDIUM OF MATHEMATICAL MODELS FOR NAPL REMEDIATION

1. Enhanced Reductive Dechlorination
2. ISCO with Permanganate

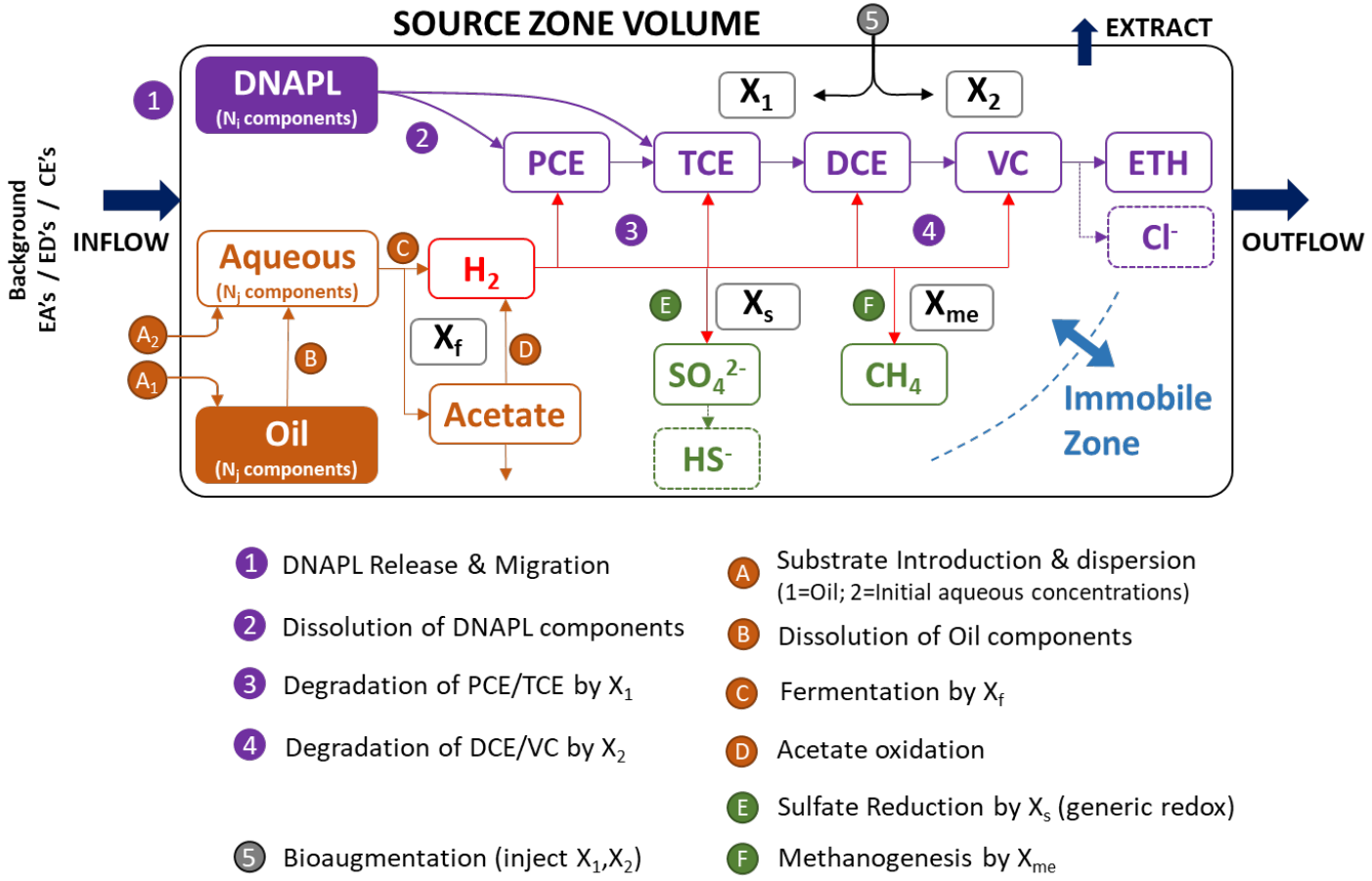

Figure B-1. Schematic of the Processes Occurring during Enhanced Reductive Dechlorination Including Bioaugmentation

Table B-1. Summary of Governing Relationships for Enhanced Reductive Dechlorination

State Variable	Governing Equations & Reaction Terms	Notes
NAPL MASS		
a x i equations: Mass of i in NAPL a	$\frac{dm_{a,i}}{dt} = -V_s K_{a,i}\left(y_{a,i} C_i^* - \bar{C}_{m,i}\right)$	
DISSOLVED MOBILE		
4 equations: PCE, TCE, c12DCE, and VC	$f_m \phi_m R_{m,i} \frac{d\bar{C}_{m,i}}{dt} = \frac{1}{V_s}\left[-Q_{exit}\bar{C}_{m,i} + Q_{bkgd} C_{m,i}^{bkgd} + Q_{inj} C_{m,i}^{inj}\right] - \frac{1}{V_s}\sum_{a=1}^{A} \frac{dm_{a,i}}{dt} + \left(\frac{f_m}{f_{im}}\right)\bar{K}_{im,i}\left(\bar{C}_{im,i} - \bar{C}_{m,i}\right) - f_m \phi_m (1 - \bar{S}_n - \bar{S}_e)\bar{r}_{m,i}$	
PCE Reaction	$\bar{r}_{m,PCE} = X_1 v_1^{max}\left(\frac{\bar{C}_{PCE}}{\bar{C}_{PCE} + K_{PCE}\left[1 + \frac{\bar{C}_{TCE}}{K_{I,TCE}}\right]}\right)\left(\frac{\bar{C}_{H_2} - \bar{C}_{H_2,1}^{min}}{K_{H_2}^1 + \bar{C}_{H_2} - \bar{C}_{H_2,1}^{min}}\right) H\left(\bar{C}_{H_2} - \bar{C}_{H_2,1}^{min}\right)$	
TCE Reaction	$\bar{r}_{m,TCE} = X_1 v_1^{max}\left(\frac{\bar{C}_{TCE}}{\bar{C}_{TCE} + K_{TCE}\left[1 + \frac{\bar{C}_{PCE}}{K_{I,PCE}}\right]}\right)\left(\frac{\bar{C}_{H_2} - \bar{C}_{H_2,1}^{min}}{K_{H_2}^1 + \bar{C}_{H_2} - \bar{C}_{H_2,1}^{min}}\right) H\left(\bar{C}_{H_2} - \bar{C}_{H_2,1}^{min}\right)$	
cis1,2-DCE Reaction	$\bar{r}_{m,DCE} = X_2 v_2^{max}\left(\frac{\bar{C}_{DCE}}{\bar{C}_{DCE} + K_{DCE}\left[1 + \frac{\bar{C}_{VC}}{K_{I,VC}}\right]}\right)\left(\frac{\bar{C}_{H_2} - \bar{C}_{H_2,2}^{min}}{K_{H_2}^2 + \bar{C}_{H_2} - \bar{C}_{H_2,2}^{min}}\right) H\left(\bar{C}_{H_2} - \bar{C}_{H_2,2}^{min}\right)$	
Vinyl Chloride Reaction	$\bar{r}_{m,VC} = X_2 v_2^{max}\left(\frac{\bar{C}_{VC}}{\bar{C}_{VC} + K_{VC}\left[1 + \frac{\bar{C}_{DCE}}{K_{I,DCE}}\right]}\right)\left(\frac{\bar{C}_{H_2} - \bar{C}_{H_2,2}^{min}}{K_{H_2}^2 + \bar{C}_{H_2} - \bar{C}_{H_2,2}^{min}}\right) H\left(\bar{C}_{H_2} - \bar{C}_{H_2,2}^{min}\right)$	
PCE / TCE Degrader Population	$\frac{dX_1}{dt} = -\lambda_1^d (X_1 - X_1^0) + Y_1^{PCE}\bar{r}_{m,PCE} + Y_1^{TCE}\bar{r}_{m,TCE}$	
c12-DCE / VC Degrader Population	$\frac{dX_2}{dt} = -\lambda_2^d (X_2 - X_2^0) + Y_2^{DCE}\bar{r}_{m,DCE} + Y_2^{VC}\bar{r}_{m,VC} + \frac{X_2^{inj} V_{inj}^{X_2}}{f_m V_s}\left[\frac{H(t - t_1^2)H(t_2^2 - t)}{(t_2^2 - t_1^2)}\right]$	
DISSOLVED IMMOBILE		
4 equations: PCE, TCE, c12DCE, and VC	$f_{im}\phi_{im} R_{im,i} \frac{d\bar{C}_{im,i}}{dt} = -\bar{K}_{im,i}\left(\bar{C}_{im,i} - \bar{C}_{m,i}\right) - f_{im}\phi_{im}\bar{r}_{im,i}$	

Table B-1. Summary of Governing Relationships for Enhanced Reductive Dechlorination (Continued)

State Variable	Governing Equations & Reaction Terms	Notes
NAPL SUBSTRATE		
j equations: component of dispersed NAPL	$\frac{dm_{e,j}}{dt} = -V_s K_{e,j}\left(y_j C_j^* - \bar{C}_{m,j}\right) + \frac{V_{inj}^e}{f_m}\left[\frac{m_e y_j^{inj} f_e}{\rho_e} + \frac{C_{m,j}^{inj}}{\phi_m}\right]\left[\frac{H\left(t-t_1^{m_e}\right)H\left(t_2^{m_e}-t\right)}{t_2^{m_e}-t_1^{m_e}}\right]$	Non-uniform dispersion or mixing captured in the K_e; no CE dissolution into NAPL
DISSOLVED SUBSTRATE		
j equations: 1 for each substrate	$f_m\phi_m R_{m,j}\frac{d\bar{C}_{m,j}}{dt} = \frac{1}{V_s}\left[-Q_{exit}\bar{C}_{m,j} + Q_{bkgd}\bar{C}_{m,j}^{bkgd} + Q_{inj}C_{m,j}^{inj}\right] - \frac{1}{V_s}\frac{dm_{e,j}}{dt} - f_m\phi_m(1-\bar{S}_n-\bar{S}_e)\bar{r}_{m,j}$	No transport with immobile zone
Substrate Reactions	$\bar{r}_{m,j} = X_f v_{f,j}^{max}\left(\frac{\bar{C}_{m,j}}{\bar{C}_{m,j} + K_j^f I_e^f}\right) exp\left(-\frac{\bar{C}_{m,H_2}}{C_{H_2}^{scale}}\right)$	Probably ignore inhibition
Substrate Degrader Population	$\frac{dX_f}{dt} = -\lambda_f^d\left(X_f - X_f^0\right) + \sum_{j=1}^{N_j} Y_f^j \bar{r}_{m,j}$	May add more than one population later
HYDROGEN		
1 equation:	$f_m\phi_m R_{m,H_2}\frac{d\bar{C}_{m,H_2}}{dt} = \frac{1}{V_s}\left[-Q_{exit}\bar{C}_{m,H_2} + Q_{bkgd}\bar{C}_{H_2}^{bkgd} + Q_{inj}C_{H_2}^{inj}\right] + f_m\phi_m\sum_{j=1}^{N_j}\left[(1-p_j)\sigma_1^j + p_j\sigma_2^j\right]\bar{r}_{m,j} - f_m\phi_m(1-\bar{S}_n-\bar{S}_e)\left(\bar{r}_{m,H_2}^{dechlor} + \bar{r}_{m,H_2}^{compete}\right)$	No transport with immobile zone
Dechlorinating Reaction	$\bar{r}_{m,H_2}^{dechlor} = \sigma_{PCE}\bar{r}_{m,PCE} + \sigma_{TCE}\bar{r}_{m,TCE} + \sigma_{DCE}\bar{r}_{m,DCE} + \sigma_{VC}\bar{r}_{m,VC}$	
Competing Reaction	$\bar{r}_{m,H_2}^{compete} = \sigma_{su}\bar{r}_{m,SO_4} + \sigma_{me}\bar{r}_{m,meth}$	
AUXILIARY RELATIONSHIPS		
NAPL mole fractions	$y_{a,i} = \frac{n_{a,i}}{n_a} = \frac{n_{a,i}}{\sum_{j=1}^N n_{a,j}} = \frac{1}{M_i}\frac{m_{a,i}}{\sum_{j=1}^N \frac{m_{a,j}}{M_j}}$	
NAPL saturations	$\bar{S}_n = \frac{1}{\rho_n\phi V_s}\sum_{a=1}^{A} m_a$	
NAPL mass transfer coefficients	$K_{a,i} = K_{a,0}\left(\frac{D_i}{D_0}\right)\left(\frac{m_a}{m_{a,0}}\right)^{\delta_a}$	
Water Balance	$-Q_{exit} + Q_{bkgd} + Q_{inj} = 0$	

Table B-2. Summary of Governing Relationships for ISCO with Permanganate

State Variable	Governing Equations & Reaction Terms	Notes
NAPL MASS		
A x N equations: Mass of i in NAPL a	$\frac{dm_{a,i}}{dt} = -V_s K_{a,i}\left(y_{a,i}C_i^* - \bar{C}_{m,i}\right)$	
DISSOLVED CONCENTRATRATIONS in MOBILE ZONE		
N equations: Contaminant i	$f_m\phi_m R_{m,i}\frac{d\bar{C}_{m,i}}{dt} = \frac{1}{V_s}\left[-Q_{exit}\bar{C}_{m,i} + Q_{bkgd}C_{m,i}^{bkgd}\right] - \frac{1}{V_s}\sum_{a=1}^{A}\frac{dm_{a,i}}{dt} + \left(\frac{f_m}{f_{im}}\right)\bar{K}_{im,i}\left(\bar{C}_{im,i} - \bar{C}_{m,i}\right) - f_m\phi_m(1-\bar{S}_n)\bar{r}_{m,i}$	
Permanganate Reaction	$\bar{r}_{m,i} = k_i^{oxi}\bar{C}_{m,i}\left[\frac{f_{inj}}{f_m}C_{MnO_4^-}^{inj} + \left(\frac{f_m - f_{inj}}{f_m}\right)\bar{C}_{MnO_4^-}\right]$	For recirculation, $f_{inj} = 0$
DISSOLVED CONCENTRATRATIONS in IMMOBILE ZONE		
N equations: Contaminant i	$f_{im}\phi_{im}R_{im,i}\frac{d\bar{C}_{im,i}}{dt} = -\bar{K}_{im,i}\left(\bar{C}_{im,i} - \bar{C}_{m,i}\right) - f_{im}\phi_{im}\bar{r}_{im,i}$	
Permanganate Reaction	$\bar{r}_{im,i} = k_i^{oxi}\bar{C}_{im,i}\bar{C}_{im,MnO_4^-}$	
PERMANGANATE in MOBILE ZONE		
	OPTION 1: RECIRCULATION	
Recirculation (1 equation)	$f_m\phi_m(1-\bar{S}_n)\frac{d\bar{C}_{m,MnO_4^-}}{dt} = -\frac{Q_{exit}}{V_s}\bar{C}_{m,MnO_4^-} + \frac{Q_{inj}}{V_s}\bar{C}_{MnO_4^-}^{inj}\left[\frac{H\left(t-t_1^{m_o}\right)H\left(t_2^{m_o}-t\right)}{t_2^{m_o}-t_1^{m_o}}\right] + \left(\frac{f_m}{f_{im}}\right)\bar{K}_{im,MnO_4^-}\left(\bar{C}_{im,MnO_4^-} - \bar{C}_{m,MnO_4^-}\right) - f_m\phi_m(1-\bar{S}_n)\bar{r}_{m,Mg}^{oxi}$	Q_{inj} is assumed to balance Q_{exit} and the natural gradient over the designated period to yield instantaneous, uniform dispersion in mobile zone
Recirculation Reaction	$\bar{r}_{m,Mg}^{oxi} = \bar{r}_m^{oxi} = \sum_{i=1}^{N}\left(Y_i^{oxi}k_i^{oxi}\bar{C}_{m,i}\right)\bar{C}_{MnO_4^-} + \rho_b\left(k_{NOD,f}^{oxi}X_{NOD,f} + k_{NOD,s}^{oxi}X_{NOD,s}\right)\bar{C}_{MnO_4^-}$	

Table B-2. Summary of Governing Relationships for ISCO with Permanganate (Continued)

State Variable	Governing Equations & Reaction Terms	Notes
	OPTION2: DIRECT INJECTION	
Direct Injection (2 equations)	$f_{inj}\phi_m(1-\bar{S}_n)\frac{dC^{inj}_{MnO_4^-}}{dt} = \left[-\frac{Q_{exit}}{V_s}\frac{f_{inj}}{f_m}C^{inj}_{MnO_4^-} - \bar{K}_{mix,ox}\left(C^{inj}_{MnO_4^-} - \bar{C}_{m,MnO_4^-}\right) + \left(\frac{f_{inj}}{f_{im}}\right)\bar{K}_{im,MnO_4^-}\left(\bar{C}_{im,MnO_4^-} - C^{inj}_{MnO_4^-}\right) - f_{inj}\phi_m(1-\bar{S}_n)\bar{r}^{oxi}_{inj,Mg}\right]H\left(t-t^{m_o}_{inj}\right)$ $(f_m - f_{inj})\phi_m(1-\bar{S}_n)\frac{d\bar{C}_{MnO_4^-}}{dt} = -\frac{Q_{exit}}{V_s}\left(\frac{f_m-f_{inj}}{f_m}\right)\bar{C}_{MnO_4^-} + \left(\frac{f_m-f_{inj}}{f_{inj}}\right)\bar{K}_{mix,ox}\left(C^{inj}_{MnO_4^-} - \bar{C}_{MnO_4^-}\right) + \left(\frac{f_m-f_{inj}}{f_{im}}\right)\bar{K}_{im,MnO_4^-}\left(\bar{C}_{im,MnO_4^-} - \bar{C}_{MnO_4^-}\right) - (f_m-f_{inj})\phi_m(1-\bar{S}_n)\bar{r}^{oxi}_{m,Mg}$	Assume instantaneous injection at t=t_{inj} floods a fraction of the source zone volume (f_{inj}) at concentration $C^{inj}_{MnO_4^-,0}$, solely in the mobile zone, and mass transfer disperses the oxidant to the remaining mobile and immobile zones.
Direct Injection Reactions	$\bar{r}^{oxi}_{inj,Mg} = \sum_{i=1}^{N}\left(Y^{oxi}_i k^{oxi}_i \bar{C}_{m,i}\right)C^{inj}_{MnO_4^-} + \rho_b\left(k^{oxi}_{NOD,f}X_{NOD,f} + k^{oxi}_{NOD,s}X_{NOD,s}\right)C^{inj}_{MnO_4^-}$ $\bar{r}^{oxi}_{m,Mg} = \sum_{i=1}^{N}\left(Y^{oxi}_i k^{oxi}_i \bar{C}_{m,i}\right)\bar{C}_{MnO_4^-} + \rho_b\left(k^{oxi}_{NOD,f}X_{NOD,f} + k^{oxi}_{NOD,s}X_{NOD,s}\right)\bar{C}_{MnO_4^-}$	
PERMANGANATE in IMMOBILE ZONE		
1 equation	$f_{im}\phi_{im}\frac{d\bar{C}_{im,MnO_4^-}}{dt} = -\left(\frac{f_m-f_{inj}}{f_m}\right)\bar{K}_{im,MnO_4^-}\left(\bar{C}_{im,MnO_4^-} - \bar{C}_{m,MnO_4^-}\right) - \left(\frac{f_{inj}}{f_{im}}\right)\bar{K}_{im,MnO_4^-}\left(\bar{C}_{im,MnO_4^-} - C^{inj}_{MnO_4^-}\right) - f_{im}\phi_{im}\bar{r}^{oxi}_{im,Mg}$	For recirculation f_{inj} = 0
Permanganate Reaction	$\bar{r}^{oxi}_{im,Mg} = \sum_{i=1}^{N}\left(Y^{oxi}_i k^{oxi}_i \bar{C}_{im,i}\right)\bar{C}_{im,MnO_4^-} + \rho_b\left(k^{oxi}_{NOD,f,im}X_{NOD,f,im} + k^{oxi}_{NOD,s,im}X_{NOD,s,im}\right)\bar{C}_{im,MnO_4^-}$	

Table B-2. Summary of Governing Relationships for ISCO with Permanganate (Continued)

State Variable	Governing Equations & Reaction Terms	Notes
NOD in MOBILE ZONE		
Natural Oxidant Demand, fast	$\frac{dX_{NOD,f}}{dt} = -k^{oxi}_{NOD,f} X_{NOD,f} \left[\left(\frac{f_{inj}}{f_m} \right) C^{inj}_{MnO_4^-} + \left(\frac{f_m - f_{inj}}{f_m} \right) \bar{C}_{MnO_4^-} \right]$	For recirculation $f_{inj} = 0$
Natural Oxidant Demand, slow	$\frac{dX_{NOD,s}}{dt} = -k^{oxi}_{NOD,s} X_{NOD,s} \left[\left(\frac{f_{inj}}{f_m} \right) C^{inj}_{MnO_4^-} + \left(\frac{f_m - f_{inj}}{f_m} \right) \bar{C}_{MnO_4^-} \right]$	For recirculation $f_{inj} = 0$
NOD in IMMOBILE ZONE		
Natural Oxidant Demand, fast	$\frac{dX_{NOD,f,im}}{dt} = -k^{oxi}_{NOD,f,im} X_{NOD,f,im} \bar{C}_{im,MnO_4^-}$	
Natural Oxidant Demand, slow	$\frac{dX_{NOD,s,im}}{dt} = -k^{oxi}_{NOD,s,im} X_{NOD,s,im} \bar{C}_{im,MnO_4^-}$	
AUXILIARY RELATIONSHIPS		
NAPL mole fractions	$y_{a,i} = \frac{n_{a,i}}{n_a} = \frac{n_{a,i}}{\sum_{j=1}^{N} n_{a,j}} = \frac{1}{M_i} \frac{m_{a,i}}{\sum_{j=1}^{N} \frac{m_{a,j}}{M_j}}$	
NAPL saturation	$\bar{S}_n = \frac{1}{\rho_n \phi V_s} \sum_{a=1}^{A} m_a$	
NAPL mass transfer coefficients	$K_{a,i} = K_{a,0} \left(\frac{D_i}{D_0} \right) \left(\frac{m_a}{m_{a,0}} \right)^{\delta_a}$	The mass transfer coefficients for individual compounds are relative to an initial NAPL mass and a reference compound based on diffusivity.
Water Balance	$-Q_{exit} + Q_{bkgd} + Q_{inj} - Q_{ext} = 0$	

APPENDIX C SOURCE CONTROL AND REMEDIAL PERFORMANCE EVALUATION (SCARPÉ), NAPL DISCHARGE TOOL V1.0 (BETA VERSION), USER MANUAL

SOURCE CONTROL AND REMEDIAL PERFORMANCE EVALUATION (SCARPE)

Single-Component NAPL Remediation Tool (SCARPEs v0.1 beta version)

USER MANUAL

1. BACKGROUND

The tool provides an executable file to calculate mass discharge from a non-aqueous phase liquid (NAPL) source zone, based on a volume-averaged approach. Details, background and equations are provided in a recent publication, "Upscaled Modeling of Complex DNAPL Dissolution", JCH, 244(5):103920 (http://dx.doi.org/10.1016/j.jconhyd.2021.103920). This tool was developed as part of the Environmental Security Technology Certification Program (ESTCP) project *Evaluating and Applying Site-Specific NAPL Dissolution Rates during Remediation* (ER19-5223). More information is available at ER19-5223 Project Overview (serdp-estcp.org).

The Single-Component NAPL Remediation Tool (SCARPEs v0.1) is provided as a beta version and can be downloaded from SCARPEmodel.com or obtained by request from **bo@praxis-enviro.com**. Please email feedback, suggestions, or questions to **bo@praxis-enviro.com**. The model has not been reviewed by ESTCP and does not necessarily represent the view of ESTCP.

2. RUN SCARPE NAPL DISCHARGE TOOL

The model is written in python and the executable runs in Windows. Double-click on the executable file to start (note that the executable may take a few minutes to start), then select the input file. An example input file is provided with the model download (example_input.xlsx). Details for preparing input files are described in Section 0. Input and output folders are automatically created in the folder containing the executable file if these folders do not exist.

The interface screen indicates successful import of the data and calculations are performed automatically. When calculations are complete, a message appears on the interface screen and the model generates output (see Figure 1).

Upon completion, a rendering of the input NAPL architecture is displayed on the screen for review. Upon closing the window with this figure, a plot of the discharge concentration versus time is displayed for review. Upon closing this window, a plot of the NAPL mass remaining in the source zone is displayed. Closing this window returns to the interface window as shown in Figure 1.

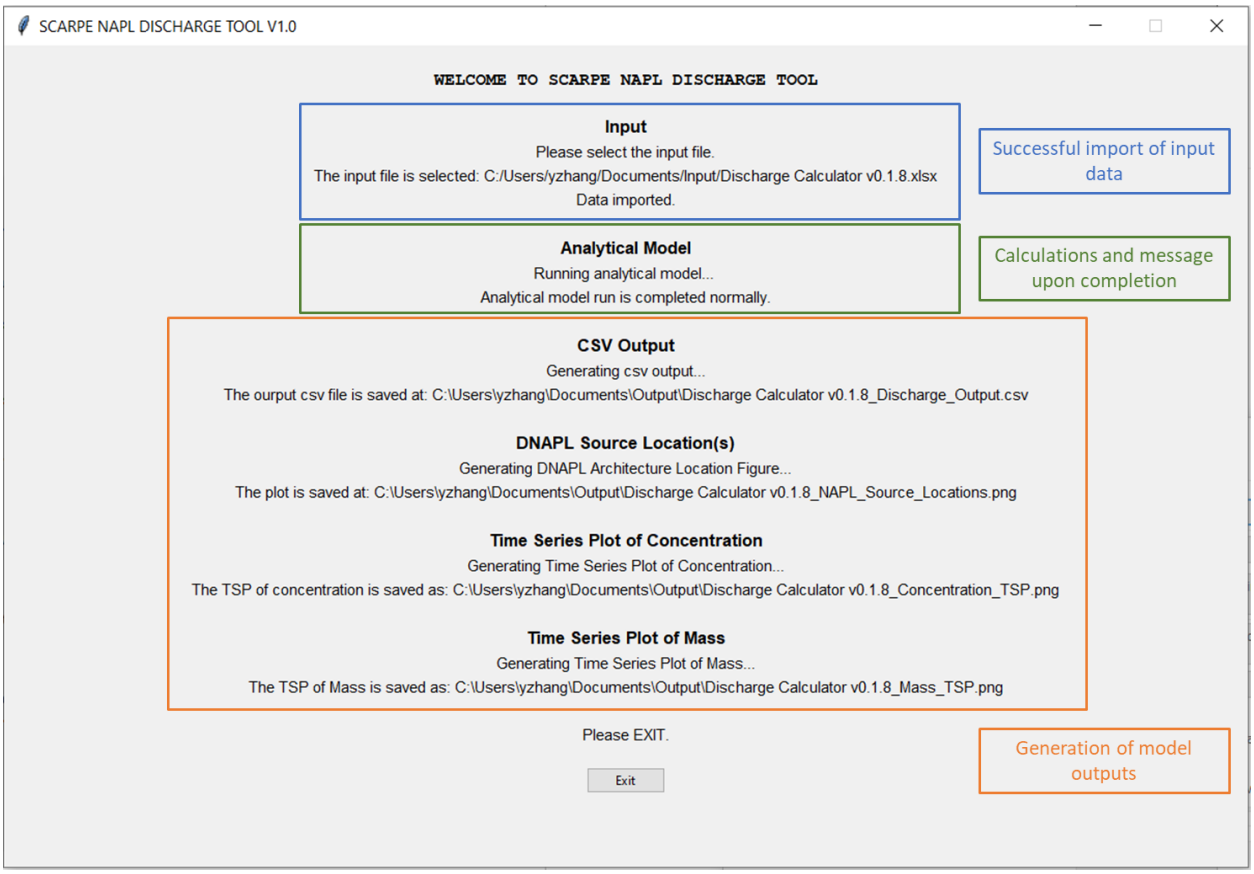

Figure 1 – Interface Screen

Copies of the displayed figures are automatically saved in the output folder. The raw data for discharge concentration and remaining mass are saved in the output folder as a comma-separated value file. The output files are named using the input file name. For example, if the input file name is inputfile1.xlsx, the following output files are saved:

- inputfile1_Output.csv
- inputfile1_NAPL_Source_Locations.png
- inputfile1_Concentration_TSP.png
- inputfile1_Mass_TSP.png

Detailed descriptions of the output files are provided in Section 4.

To perform and save output from multiple runs, the input file name must be changed for each run to save each output file separately, or the output file names must be edited between runs. The model executable automatically writes over an existing output file if the input file name is not changed. In addition, the Excel input file must be closed to enable reading of input data by the executable file. It is recommended to create a separate file for tracking input parameters and associated output file names.

3. TOOL INPUTS

3.1 INPUT DATA FILE

The NAPL Discharge Tool utilizes an excel file for data input and simplifies the formatting process. A template input file (**Example_Input.xlsx)** is provided with the executable and should be placed in the input folder. The template excel file is protected and only displays one tab specifying the input variables (see Figure 2). The yellow highlighted cells are the required user inputs. Other calculated values, e.g., NAPL saturation, are displayed for reference in formulating input data. An approximation for the time for each NAPL mass to be fully depleted is provided in the row titled "Time to Depletion."

Single-Component NAPL Remediation Tool (SCARPEs v0.1) Beta Version

Source Zone Parameters				
Length (X_s)	m	0.4	$X_{s,0}$	0
Width (Y_s)	m	0.0254	$Y_{s,0}$	0
Height (Z_s)	m	0.195	$Z_{s,0}$	0
Darcy Velocity (U_0)	m/day	0.9757149		
Porosity	-	0.4495		
Fraction Mobile (f_m)	-	0.5		
Porosity Immobile	-	0.33		
K_{im}	1/day	2		
$S_{irreducible}$	-	0.15		
k_r exponent	-	3		
Volumetric Flow (Q)	L/day	4.8327158		
Source Volume (V_s)	m^3	0.0019812		

Enter parameters in yellow cells
White cells are calculated automatically
Cells under Mass 1 must be entered; other mass cells can be empty

NAPL Component Parameters		TCE
Density (ρ_l)	g/L	1460
Solubility (C_i*)	mg/L	1100
Molecular Weight	g/mol	131
Diffusion Coefficient	cm^2/day	0.6048
Retardation (R_i) - Mobile		1.1
Retardation (R_{im}) - Immobile		1.1
C inlet ($C_{0,i}$)	mg/L	0
1st Order Decay-Mobile	1/day	10
1st Order Decay-Immobil	1/day	0
Initial Conc - Mobile	mg/L	10
Initial Conc - Immobile	mg/L	0

Solution Settings		
Total Time	days	30
Printing Time Interval	days	0.1

NAPL Architecture		Mass 1	Mass 2	Mass 3	Mass 4	Mass 5	Mass 6	Mass 7	Mass 8	Mass 9	Mass 10
M_{napl} (M_n)	g	9.928	7.3								
Start Location $X_{a,0}$	m	0.17	0.095								
Length X_a	m	0.075	0.35								
Start Location $Y_{a,0}$	m	0	0								
Width Y_a	m	0.0254	0.0254								
Start Location $Z_{a,0}$	m	0.01	0								
Height Z_a	m	0.185	0.005								
Is A_{xy} double-sided?	1 or 2	1	1								
Dispersivity (α_T)	m	0.001	0.001								
Enhancement?	-	1	1								
gamma (γ)	-	0.5	0.5								
a_d ($0 < a_d <= 1$)	-	0	1								
Time to Depletion	days	2.006993	11.938418	0	0	0	0	0	0	0	0
Impacted Volume (V_a)	m^3	0.0003524	4.445E-05	0	0	0	0	0	0	0	0
Saturation (S_n)	-	0.0429	0.2502	0.0000	0.0000	0.0000	0.0000	0.0000	0.0000	0.0000	0.0000

Number of DNAPL Masses	2	Number of DNAPL Components	1	Number of Soil Domains	2

Figure 2 – Excel Input File Interface

Variables are defined in four categories:

- Source Zone Parameters – define the geometry and characteristics of the overall source zone
- NAPL Component Parameters – define the properties and problem-specific characteristics of the NAPL component
- Solution Settings – define the total time for simulation and printing interval for output
- NAPL Architecture – define the mass, geometry and dissolution characteristics of each NAPL accumulation within the source zone (a minimum 1 mass is required)

3.2 DESCRIPTION OF INPUT VARIABLES

The primary characteristic features defining the NAPL dissolution and discharge problem are illustrated in Figure 3. The source zone dimensions (X_S, Y_S, Z_S) fully encompass the NAPL accumulations considered with a height that generally coincides with the height of discharge measurement (e.g., a groundwater monitoring or pumping well screen). The Darcy velocity, U_0, is in the x-direction and defines the total flow, Q, through the source zone where $Q = U_0 Y_S Z_S$. Each NAPL accumulation is assumed to have a relatively uniform saturation defined by its mass (M_a), its characteristic sub-volume ($V_a = X_a Y_a Z_a$) and the total soil porosity. Additional parameters for the NAPL dissolution model (α_T and γ) are described below in Table 1.

Simple estimates for remedial impacts can be generated with technology-specific enhancements and first order reaction rates. An enhancement factor can be specified as indicated in Table 1 and is applied to the NAPL dissolution rate. The potential enhancement is expected to depend on the flow rate compared to the natural gradient, the reaction rate, and NAPL architecture. For example, when groundwater pumping is performed the characteristic velocity through the source zone increases and the ratio to the natural flow provides the enhancement factor. Additional details on estimating flow enhancements and reactive enhancements can be found in the Final Report for ER19-5223 available at ER19-5223 Project Overview (serdp-estcp.org).

The tool also includes optional parameters for including an immobile domain (only applicable if $f_m < 1$) to model diffusion into and out of fine-grained material as a first order process.

Additional information and discussion on the parameters can be found in the previously cited publication, “Upscaled Modeling of Complex DNAPL Dissolution.”

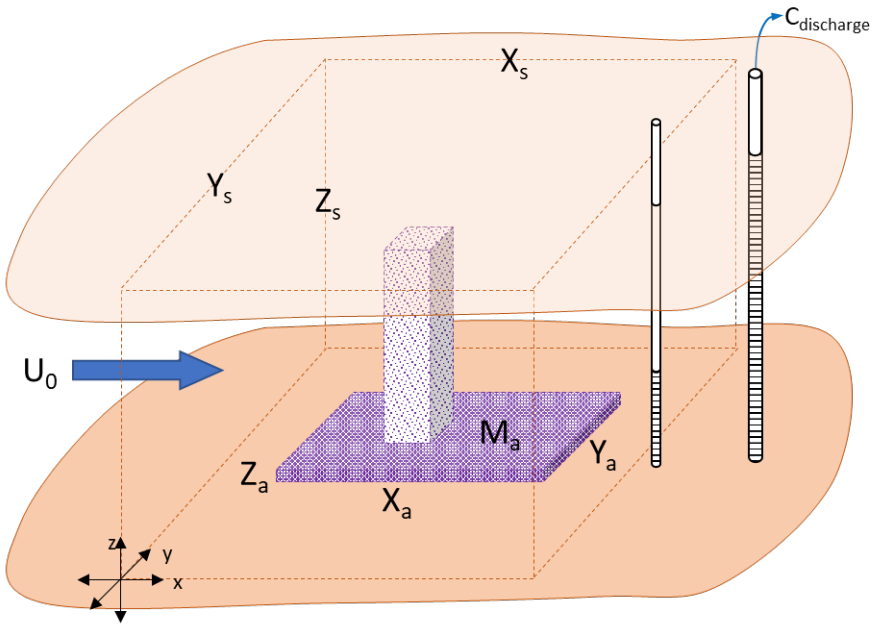

Figure 3 – Characteristic Dimensions of the Source Zone and NAPL Mass Accumulations

3.3 UNITS

The units are specified for the input and output files and cannot be modified, i.e., the user needs to enter the variables in the specified units.

Table 1. Input Variable Descriptions

	Units	Description	Potential Sources of Information and References
Source Zone Parameters			
Length (X_s)	m	Length of the source zone (in groundwater flow direction)	- Estimated longitudinal extent of the complete NAPL footprint based on soil borings, groundwater monitoring data, historical release information, or other characterization tools
Width (Y_s)	m	Width of the source zone (perpendicular to groundwater flow direction)	- Estimated lateral extent of the complete NAPL footprint based on soil borings, groundwater monitoring data, historical release information, or other characterization tools - Can also be based on width of a monitoring transect downgradient of NAPL source zone or the width of the capture zone of a pumping well
Height (Z_s)	m	Height of the source zone	- Estimated NAPL vertical extent based on soil borings, groundwater monitoring data, historical release information, or other characterization tools - Can also be based on downgradient monitoring well screen intervals, monitoring transect vertical extent and/or aquifer thickness
$X_{s,0}$	m	Starting coordinates for NAPL source zone Only use for plotting NAPL source, values do not impact solution	- The origin (0,0,0) is the least confusing option. The values do not impact the solution but non-origin values may be useful for illustration when output is used as transport model input
$Y_{s,0}$	m		
$Z_{s,0}$	m		
Darcy Velocity (U_0)	m/day	Darcy velocity through the NAPL source zone	- Can be estimated based on hydraulic gradient and hydraulic conductivity - Hydraulic gradient can be calculated based on water level contour map(s) - Hydraulic conductivity can be estimated based on aquifer testing data and/or based on soil type and typical range of conductivity values (for example from Freeze and Cherry, Groundwater, 1979 - available at https://fc79.gw-project.org/english/chapter-2/#2.3). If multiple measurements are available, the median or geometric mean can be used to estimate the average within the source zone.
Porosity	-	Porosity of mobile domain (or of entire domain if no immobile domain)	- Can be measured in soil samples - Can be estimated based on soil type and typical range of porosity values (for example from Freeze and Cherry, Groundwater, 1979 - available at https://fc79.gw-project.org/english/chapter-2/#2.5)
Fraction Mobile (f_m)	-	Fraction of mobile domain (between 0 and 1)	- $0 < f_m \leq 1$ (immobile domain fraction is 1- f_m) - Default value is 1; model applicability diminishes with decreasing value unless increasing characterization of immobile zones is available
Porosity Immobile	-	Porosity of the immobile domain	- Can be measured in soil samples - Can be estimated based on soil type and typical range of porosity values (for example from Freeze and Cherry, Groundwater, 1979 - available at https://fc79.gw-project.org/english/chapter-2/#2.5)
K_{im}	1/day	Mass transfer coefficient between mobile and immobile domains	- Various physical interpretations can be applied to this first order parameter[1] - This model assumes uniformly distributed lenses of fine-grained material in the source zone wherein aqueous diffusion dominates the mass transfer process. Hence, lens thickness, porosity and surface sorption parameters determine this first order coefficient.
$S_{irreducible}$	-	Irreducible water saturation	- Used to calculate the relative permeability k_r, based on the Wyllie correlation[2,3] - Typically varies from 0.05 to 0.15 depending upon the soil type[4] - Default value is 0.15
k_r exponent	-	Relative permeability exponent	- Used to calculate the relative permeability k_r, based on the Wyllie correlation[2,3] - Default value is 3
Volumetric Flow (Q)	L/day	Total flow through source zone	- Calculated based on U_0, Ys, Zs
Source Volume (V_s)	m^3	Total source volume	- Calculated based on Xs, Ys, Zs

1 Haggerty, R. and S. Gorelick, 1995. Multiple-rate mass transfer for modeling diffusion and surface reactions in media with pore-scale heterogeneity, Water Resources Research, 31(10) pp 2383-2400, https://doi.org/10.1029/95WR10583

2 Wyllie, M.R.J., 1962. Relative permeability. In: Frick, T.C., Taylor, R.W. (Eds.), Petroleum Production Handbook, Vol. II, Reservoir Engineering. McGraw-Hill, New York, pp. 25.1–25.14.

3 This version of the model assumes a constant relative permeability (k_r), equal to the averaged relative permeability based on the initial mass, which is calculated using the Wyllie correlation.

4 Wilson, J.L., Conrad, S.H., Mason, W.R., Peplinski, W., Hagan, E., 1990. Laboratory Investigations of Residual Organic Liquids from Spills, Leaks, and Disposal of Hazardous Wastes in Groundwater, Rep. EPA/600/6–90/004. Environ. Prot. Agency, Washington, D. C.

Table 1. Input Variable Descriptions (Continued)

	Units	Description	Potential Sources of Information and References
NAPL Component Parameters			
Density (ρ_i)	g/L	NAPL component density	- Can be found in chemical databases (e.g., CompTox Chemicals Dashboard (epa.gov)
Solubility (C_i*)	mg/L	NAPL component solubility	- Can be found in chemical databases (e.g., CompTox Chemicals Dashboard (epa.gov)
Molecular Weight	g/mol	NAPL component molecular weight	- Can be found in chemical databases (e.g., CompTox Chemicals Dashboard (epa.gov)
Diffusion Coefficient	cm^2/day	NAPL component diffusion coefficient in water at appropriate temperature.	- USEPA on-line tools can be used to estimate diffusion coefficients (https://www3.epa.gov/ceampubl/learn2model/part-two/onsite/estdiffusion.html and https://www3.epa.gov/ceampubl/learn2model/part-two/onsite/estdiffusion-ext.html)
Retardation (R_i)	-	Retardation factor in mobile soil domain resulting from water-soil partitioning of the NAPL component	- Can be calculated based on Ri = 1+ρb*Koc*foc/(mobile porosity) ρb is bulk density of mobile domain (can be estimated based on ρb = 2.65*(1-mobile porosity) or measured in soil samples; Koc is octanol-water partition coefficient for the NAPL component; and foc is the organic carbon fraction of soil solids in the mobile domain that can be measured in soil samples - USEPA on-line tools can be used for this calculation (https://www3.epa.gov/ceampubl/learn2model/part-two/onsite/retard.html), which include Koc values for several constituents - Koc values can also be found in CompTox Chemicals Dashboard (epa.gov)
Retardation (R_{im}) -Immobile	-	Retardation factor in immobile soil domain	- As above, although ρb, foc, and porosity can be different in the immobile soil domain, e.g., clayey silt versus sand.
C inlet ($C_{0,i}$)	mg/L	Influent NAPL component concentration upgradient of the source zone	- Can be estimated based on groundwater monitoring data although the value is a constant - Default value is 0
1st Order Decay-Mobile	1/day	First-order degradation rate of dissolved phase in mobile domain	- Can be estimated from monitoring data, literature values based on site-specific redox and geochemical conditions, or remedy assumptions - Default value is 0 although increased values can be used to represent remedial processes decreasing the discharge concentration
1st Order Decay-Immobile	1/day	First-order degradation rate of dissolved phase in immobile domain	- Can be estimated from monitoring data or from literature values based on site-specific redox and geochemical conditions - Default value is 0
Initial Conc - Mobile	mg/L	Initial (average) dissolved concentration in mobile domain in the NAPL source zone	- Can be estimated based on groundwater monitoring data - Default value is 0
Initial Conc - Immobile	mg/L	Initial (average) dissolved concentration in immobile domain in the NAPL source zone	- Can be estimated based on groundwater monitoring data - Default value is 0
Solution Settings			
Total Time	days	Total calculation time for tool outputs	- Not applicable
Printing Time Interval	days	Time interval for tool outputs (output variables will be printed at each time interval through total calculation time)	- Not applicable
NAPL Architecture			
M_{napl} (M_n)	g	Mass of NAPL in the accumulation	- Can be estimated based on release information and/or site-specific measurements or can be back-calculated based on estimated saturation
Start Location ($X_{a,0}$)	m	Starting coordinate for individual NAPL accumulation Only used for illustrating the relative locations of NAPL accumulations, values do not impact solution	- As described below for the Inhibition Factor, a mass accumulation upgradient of a second accumulation will inhibit, or suppress, the dissolution of the downgradient mass by decreasing the driving concentration gradient until the upgradient mass depletes. The start locations and lengths yield an illustration of the relative NAPL locations in the output graph "NAPL_Source_Locations.png"
Length (X_a)	m	Length of the NAPL accumulation (in groundwater flow direction)	- Estimated longitudinal extent of the individual NAPL accumulation footprint based on soil boring, groundwater monitoring data, historical release information, or other characterization tools - See Figure 3
Start Location ($Y_{a,0}$)	m	Starting coordinate for individual NAPL accumulation	- See the description for $X_{a,0}$
Width (Y_a)	m	Width of NAPL accumulation (perpendicular to groundwater flow direction)	- Estimated lateral extent of the individual NAPL accumulation footprint based on soil boring, groundwater monitoring data, historical release information, or other characterization tools - See Figure 3
Start Location ($Z_{a,0}$)	m	Starting coordinate for individual NAPL accumulation	- See the description for $X_{a,0}$
Height (Z_a)	m	Height of NAPL accumulation	- Estimated NAPL accumulation footprint based on soil boring, groundwater monitoring data, historical release information, or other characterization tools - See Figure 3

Table 1. Input Variable Descriptions (Continued)

	Units	Description	Potential Sources of Information and References
NAPL Architecture (continued)			
Is A_{xy} double-sided?	1 or 2	Flow on one side (1) or both sides (2) (i.e., above and below) of the NAPL accumulation	- Expected to be 1 for DNAPL; may be 2 for LNAPL; represents the number of surfaces available for tangential dispersion - Default value is 1
Dispersivity (α_T)	m	Tangential Dispersivity	- Default value is 0.001
Enhancement?	-	Enhancement factor for NAPL mass transfer	- Default value is 1 and represents natural flow conditions - Can be used to represent remediation options (for example enhanced groundwater flow due to extraction, or enhanced dissolution resulting from increased degradation rates, e.g., enhanced biodegradation or chemical oxidation/reduction)
gamma (γ)	-	Exponent of the mass ratio	- $0 \leq \gamma < 1$ - γ expected to fall between theoretical values of 0.5 (pool) and 0.67 (ganglia) - γ can be used as a fitting parameter with discharge concentration measurements - γ has a significant impact on the depletion tail and little influence on early discharge concentrations
a_d ($0 < a_d \leq 1$)	-	Inhibition factor	- a_d is a shape factor accounting for any overlap of projected areas between the two masses, one upgradient to another. In practice masses are assumed independent ($a_d = 0$) or are directly in line with each other ($a_d = 1$). - Default is 0 (no inhibition) - a_d for Mass 1 is always 0, i.e., no mass is allowed to reside upgradient of Mass 1 - For inhibition of a mass by an upgradient mass, the downgradient mass must follow directly in the input table, i.e., Mass a +1 is inhibited by Mass a as indicated by a nonzero a_d - Inhibition is allowed to be sequential, i.e., multiple masses can reside in line along the flow direction - Changes in flow direction resulting from groundwater pumping or injection can be captured with changes in the shape factor, assuming the relative spatial locations of distinct masses are available.
Time to Depletion	days	Time for depletion of NAPL accumulation	- Calculated based on input parameters - This time is for complete removal of the NAPL mass. This is not expected to be achievable in the field, where residual mass may remain in the subsurface, but this number provides information on the order of magnitude of NAPL source lifetime and is useful for comparison between the different masses, and understanding the impact of the NAPL characteristics on NAPL lifetime.
Impacted Volume (V_a)	m^3	Volume impacted by NAPL accumulation	- Calculated based on Xa, Ya, Za - Sum of accumulation volumes must be less than the mobile source zone volume to avoid overlapping NAPL volumes.
Saturation (S_n)	-	NAPL accumulation saturation	- Calculated for the NAPL impacted volume based on NAPL mass, NAPL density and total porosity

4. TOOL OUPUTS

4.1 GRAPHS

The Single-Component NAPL Remediation Tool creates three output graphs saved in the output folder:

- A 3D rendering of the relative locations defining the NAPL source zone (i.e., XXX_ NAPL_Source_Locations.png) – depicts the geometry of the source zone (blue rectangle) and the NAPL accumulations located inside it (black rectangles)

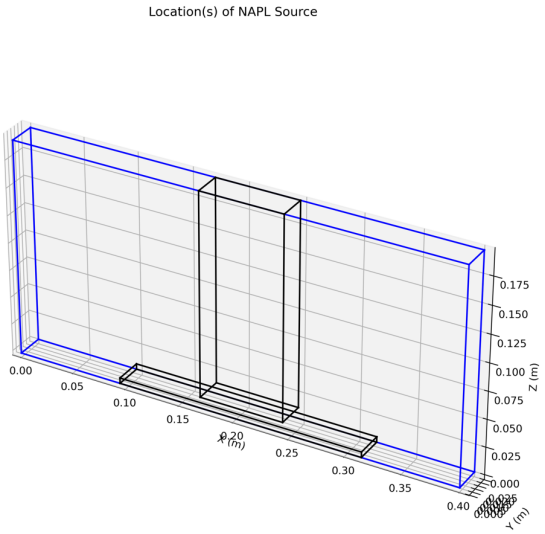

Figure 4 – Output Graph: NAPL Source Locations

- The time series plot of discharge concentration (i.e., XXX_ Concentration_TSP.png) – plots the discharge concentration over time; the mass discharge is calculated from this concentration multiplied by Q

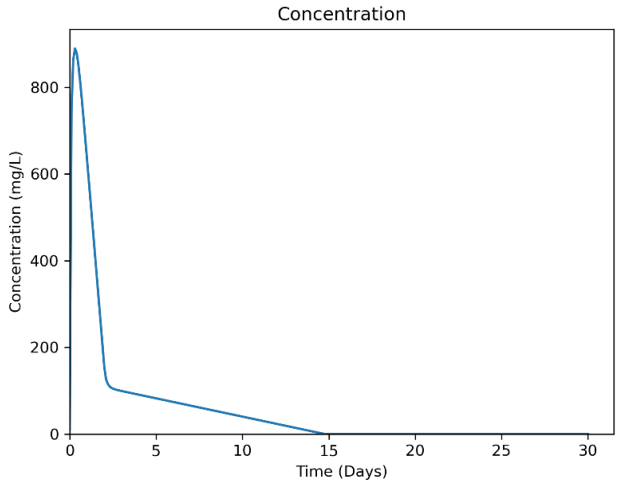

Figure 5 – Output Graph: Time Series Plot of NAPL Concentration in Discharge

- The time series plot of remaining mass (i.e., XXX_ Mass_TSP.png) – plots the remaining NAPL mass in the source zone over time

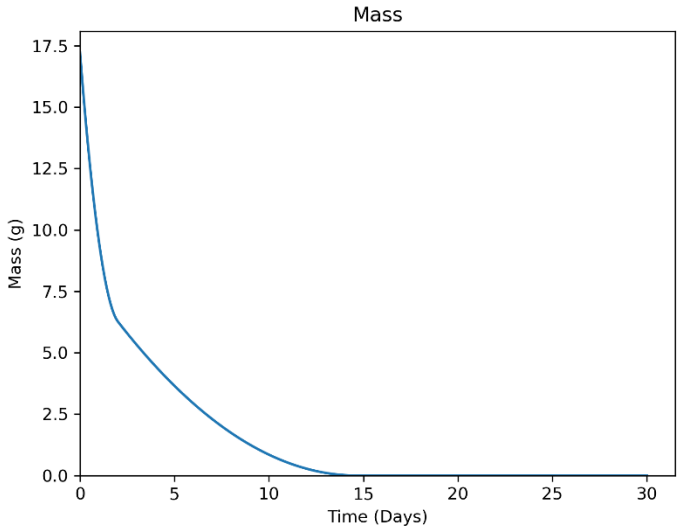

Figure 6 – Output Graph: Time Series Plot of NAPL Mass in the Source

4.2 OUTPUT FILES

The Single-Component NAPL Remediation Tool saves calculation results into a csv file (XXX_Output.csv) in the output folder. As described in Section 2, the program will write over an existing file with the same name without warning. The output data structure is shown in Figure 7 below. The first three rows list the time of depletion for each of the NAPL accumulations. The time of depletion is the time for complete (100%) removal of the NAPL mass in the source zone. This is not expected to be achievable in the field, where residual mass may remain in the subsurface, but this number provides information on the order of magnitude of NAPL source

lifetime and is useful for comparison between the different masses, and understanding the impact of the NAPL characteristics on NAPL lifetime. The user can use the output file (see below) to estimate cleanup time for different end points (for example based on percentage of NAPL mass removal, target mass discharge or target discharge concentration).

From row four, the calculated results are listed by columns and printed at the specified intervals in rows. The columns of calculated variables are:

- Time – cumulative time (days)
- C – source discharge concentration (gram per cubic meter or mg/L)
- Ci – average aqueous concentration in the immobile domain (gram per cubic meter or mg/L)
- Rmass – remaining NAPL mass in the source zone (grams)
- gen – volumetric mass generation term calculated as the mass discharge rate per unit source zone volume (grams per day per cubic meter)
- Mass Rate – mass discharge from the source zone (grams per day)

	A	B	C	D	E	F
1	Time Deplete (days):					
2	Mass 1	Mass 2				
3	2.006993	14.6571				
4	Time	C	Ci	Rmass	gen	Mass Rate
5	days	mg/L	mg/L	g	g/day/m3	g/day
6	0	10	0	17.228	24.39287	0.048327
7	0.100897	747.2883	381.1429	16.25217	1822.851	3.611432
8	0.201794	863.2963	681.0038	15.32109	2105.828	4.172066
9	0.302691	889.2346	816.3656	14.43479	2169.099	4.297418
10	0.403587	878.7042	862.4371	13.59328	2143.412	4.246527
11	0.504484	849.9197	862.629	12.79657	2073.198	4.10742
12	0.605381	811.8035	839.342	12.0447	1980.222	3.923216
13	0.706278	768.8978	804.0341	11.3377	1875.562	3.715864
14	0.807175	723.5208	762.5608	10.67561	1764.875	3.496571
15	0.908072	676.8548	717.9125	10.05846	1651.043	3.271047
16	1.008969	629.501	671.615	9.486327	1535.534	3.042199
17	1.109865	581.7636	624.4452	8.95925	1419.088	2.811498
18	1.210762	533.7949	576.7972	8.477299	1302.079	2.579679
19	1.311659	485.6697	528.8693	8.040543	1184.688	2.347104
20	1.412556	437.4232	480.7597	7.649057	1067.001	2.113942
21	1.513453	389.07	432.5155	7.302922	949.0534	1.880265

Figure 7 – Output CSV File

4.3 USES

In addition to providing information on time to NAPL depletion, mass discharge, discharge concentration, and remaining NAPL mass, the outputs from the NAPL Discharge Tool can be used as input to groundwater transport models for evaluating downgradient plume concentrations. Compatible models include:

- MT3DMS or MT3D-USGS three-dimensional numerical model where the mass rate is a mass loading input to represent dissolution from a NAPL source zone; and

- A soon-to-be-released semi-analytical solute transport model for a three-dimensional aquifer with sequential first order decay and dual porosity[5] provided by the United States Environmental Protection Agency. The volumetric mass generation source term in the Discharge Tool output can be directly read as input by the transport model. The model pairing provides a fast, convenient methodology to assess plume changes in response to transient discharge including first approximations for remedial efforts.

5. MISCEALLENOUS

5.1 LIMITATIONS

The results generated with the NAPL Discharge Tool are based on several simplifying assumptions resulting in limitations to some field applications. These assumptions are discussed in "Upscaled Modeling of Complex DNAPL Dissolution" and include:

- The NAPL is assumed to be immobile and the potential for partial re-mobilization of NAPL mass during dissolution is not considered.
- This version of the model does not allow changes in flow or degradation rates within the source zone; steady conditions are assumed.
- This version of the model assumes constant relative permeability (k_r), equal to the averaged relative permeability based on the initial mass. This approximation overpredicts early discharge and underpredicts later mass discharge but roughly matches the depletion time for the NAPL mass.
- The flow rate through the source zone and resulting dispersion are assumed to be sufficiently large to render aqueous diffusion negligible in NAPL dissolution.
- Increases in local soil heterogeneity are not explicitly included and are expected to limit the applicability of the model to those conditions, although modifications to the dissolution model can provide approximations.
- The model is not intended to match initial breakthrough curves precisely as a result of volume-averaging in the source zone. The averaging in the upscaled model is expected to yield a lesser peak discharge concentration and to lag the time of the actual breakthrough peak.
- As with all models, limitations in available data for characterizing the source zone directly limit the representativeness of the results; however, the NAPL Discharge Tool is designed to be adaptable for accepting an increased resolution of input data, e.g., an increased number of defined mass accumulations and characterization of fine-grained lenses.

5.2 ERROR CHECKING

5 Perina, T., 2022. Semi-analytical model for solute transport in a three-dimensional aquifer with dual porosity and a volumetric source term. Journal of Hydrology 607, 127520. https://doi.org/10.1016/j.jhydrol.2022.127520

Several conditions can prevent the tool executable from running properly. If the user is not able to run the tool successfully, please check for the following potential conflicts:

- If the program window closes automatically or the interface window does not appear after shortly after double clicking the executable file, check to ensure output file with the same prefix as the input file are closed and available for writing. If not, close the .csv and .png output files and launch the executable file again.
- After selecting the input file, if the input file is open, does not exist, or the program cannot find the input file, the following error message will be displayed in the window.

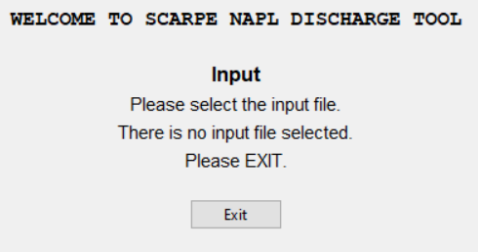

Figure 8 – Error Message 1

- Please troubleshoot the following items:
  - Make sure the input file is closed.
  - Check the location of the input file and make sure the input file is accessible.
  - After selecting a readable input file, if the following error message pops up on the window, it may include error(s) in the input file. Please double check the input parameters in the input file.

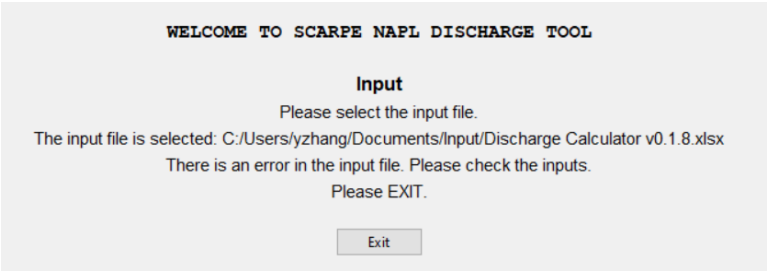

Figure 9 – Error Message 2

- For some parameters, valid input values must fall within the following ranges (or the above error message will be displayed):
- X_s, Y_s, $Z_s > 0$
- $U_0 > 0$
- Porosity > 0 and < 1
- $f_m > 0$ and ≤ 1
- Porosity Immobile > 0 and < 1

- $K_{im} \geq 0$
- Total Time > 0
- $\rho_i > 0$
- $C_i^* > 0$
- $R_i \geq 1$
- $R_{im} \geq 1$
- $C_{0,i} \geq 0$
- 1st Order Decay-Mobile ≥ 0
- 1st Order Decay-Immobile ≥ 0
- Initial Conc – Mobile ≥ 0
- Initial Conc – Immobile ≥ 0
- For each NAPL architecture:
- Number of DNAPL Masses ≥ 1 (Integer)
- $M_n > 0$
- $X_a, Y_a, Z_a > 0$
- Is A_{xy} double-sided? = 1 or 2
- $\alpha_T \geq 0$
- Enhancement > 0
- $0 \leq \gamma < 1$
- $0 < a_d \leq 1$

In addition, calculated dissolution model parameters must be physically consistent. A number of checks are provided within the excel input spreadsheet for the most common issues, as follows:

- $X_a, Y_a, Z_a \leq X_s, Y_s, Z_s$
- Sum of individual impacted volumes ($\sum V_a$) ≤ $V_s * f_m$
- Each accumulation saturation (S_n) ≤ $1-S_{irr}$

An error warning appears in the excel input file (column O) if the conditions above are not met, as shown Figure 10 below.

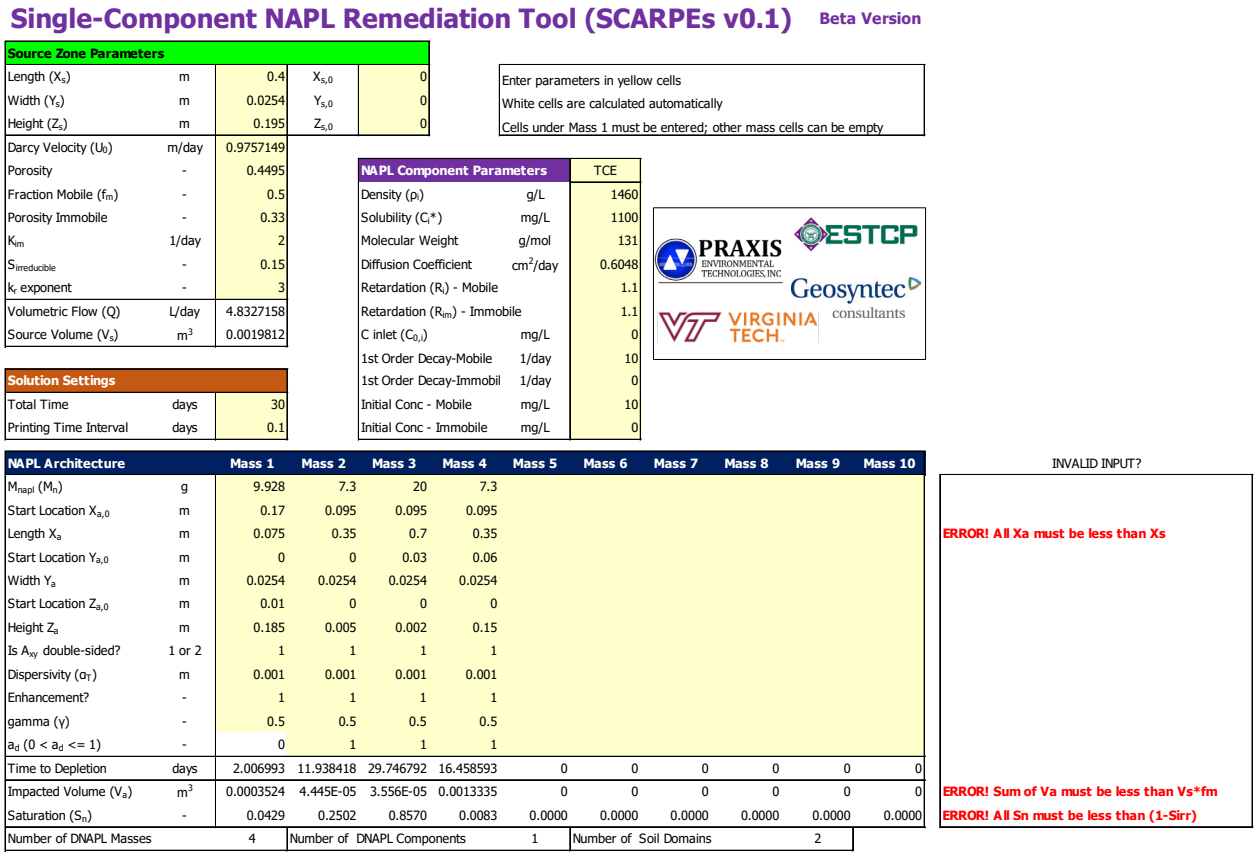

Single-Component NAPL Remediation Tool (SCARPEs v0.1) Beta Version

Source Zone Parameters				
Length (X_s)	m	0.4	$X_{s,0}$	0
Width (Y_s)	m	0.0254	$Y_{s,0}$	0
Height (Z_s)	m	0.195	$Z_{s,0}$	0
Darcy Velocity (U_0)	m/day	0.9757149		
Porosity	-	0.4495		
Fraction Mobile (f_m)	-	0.5		
Porosity Immobile	-	0.33		
K_{im}	1/day	2		
$S_{irreducible}$	-	0.15		
k_r exponent	-	3		
Volumetric Flow (Q)	L/day	4.8327158		
Source Volume (V_s)	m^3	0.0019812		

Enter parameters in yellow cells
White cells are calculated automatically
Cells under Mass 1 must be entered; other mass cells can be empty

NAPL Component Parameters		TCE
Density (ρ_l)	g/L	1460
Solubility (C_i*)	mg/L	1100
Molecular Weight	g/mol	131
Diffusion Coefficient	cm^2/day	0.6048
Retardation (R_l) - Mobile		1.1
Retardation (R_{lm}) - Immobile		1.1
C inlet ($C_{0,l}$)	mg/L	0
1st Order Decay-Mobile	1/day	10
1st Order Decay-Immobil	1/day	0
Initial Conc - Mobile	mg/L	10
Initial Conc - Immobile	mg/L	0

Solution Settings		
Total Time	days	30
Printing Time Interval	days	0.1

NAPL Architecture		Mass 1	Mass 2	Mass 3	Mass 4	Mass 5	Mass 6	Mass 7	Mass 8	Mass 9	Mass 10
M_{napl} (M_n)	g	9.928	7.3	20	7.3						
Start Location $X_{a,0}$	m	0.17	0.095	0.095	0.095						
Length X_a	m	0.075	0.35	0.7	0.35						
Start Location $Y_{a,0}$	m	0	0	0.03	0.06						
Width Y_a	m	0.0254	0.0254	0.0254	0.0254						
Start Location $Z_{a,0}$	m	0.01	0	0	0						
Height Z_a	m	0.185	0.005	0.002	0.15						
Is A_{xy} double-sided?	1 or 2	1	1	1	1						
Dispersivity (α_T)	m	0.001	0.001	0.001	0.001						
Enhancement?	-	1	1	1	1						
gamma (γ)	-	0.5	0.5	0.5	0.5						
a_d ($0 < a_d <= 1$)	-	0	1	1	1						
Time to Depletion	days	2.006993	11.938418	29.746792	16.458593	0	0	0	0	0	0
Impacted Volume (V_a)	m^3	0.0003524	4.445E-05	3.556E-05	0.0013335	0	0	0	0	0	0
Saturation (S_n)	-	0.0429	0.2502	0.8570	0.0083	0.0000	0.0000	0.0000	0.0000	0.0000	0.0000

Number of DNAPL Masses	4	Number of DNAPL Components	1	Number of Soil Domains	2

INVALID INPUT?

ERROR! All Xa must be less than Xs

ERROR! Sum of Va must be less than Vs*fm

ERROR! All Sn must be less than (1-Sirr)

Figure 10 – Example Error Messages in Excel Input File

5.3 EXECUTION TIME

The run time for the model depends upon the number of masses input and the computer processor. For most scenarios, the run time is less than one minute; however, inclusion of an immobile fraction can result in longer (several minutes) execution time.

APPENDIX D SITE 11, NSB KING'S BAY, GA REMEDIATION AND NUMERICAL MODELING REPORT

APPENDIX D

SITE 11, NSB KING'S BAY, GA REMEDIATION AND NUMERICAL MODELING REPORT

Evaluating and Applying Site-Specific NAPL Dissolution Rates during Remediation

ESTCP Project ER19-5223

Version 1.0

Lloyd "Bo" Stewart, Praxis Environmental Technologies, Inc.
Andres Prieto Estrada & Mark Widdowson, Virginia Tech

TABLE OF CONTENTS

LIST OF FIGURES

LIST OF TABLES

LIST OF ACRONYMS

bd	below detection limit
CAP	Corrective Action Plan
CERCLA	Comprehensive Environmental Response, Compensation, and Liability Act
CSM	conceptual site model
DNAPL	dense nonaqueous phase liquid
DoD	Department of Defense
DPT	direct push technology
EA	electron acceptor
EPA	US Environmental Protection Agency
ERD	enhanced reductive dechlorination
ESTCP	Environmental Security Technology Certification Program
ft	feet
ft bgs	feet below ground surface
GMS	Groundwater Modeling System
gpm	gallons per minute
IM	interim measure
ISCO	in situ chemical oxidation
MCL	maximum contaminant level
MIP	membrane interface probe
mg/L	milligrams per liter
MNA	monitored natural attenuation
MODFLOW	modular finite-difference flow model
NAPL	nonaqueous phase liquid
NAS	natural attenuation software

NAVFAC	Naval Facilities Engineering Command
NRC	National Resource Council
NSB	Naval Submarine Base
P&T	Pump-and-treat
PCE	tetrachloroethylene
PEST	Parameter Estimation Software Tool
RCRA	Resource Conservation and Recovery Act
RT3D	Reactive Transport in 3-Dimensions
RW	recovery well
SEAM3D	Sequential Electron Acceptor Model, 3D
SERDP	Strategic Environmental Research and Development Program
Site 11	Site 11 Naval Submarine Base (NSB) King's Bay, GA
TBD	to be determined
TCE	trichloroethylene
US	United States
USGS	United States Geological Survey
VA	volume average
VC	vinyl chloride
VOC	volatile organic compound
µg/L	micrograms per liter

1.0 REMEDIAL ACTIONS

Site 11 Naval Submarine Base (NSB) King's Bay, GA (Site 11) was regulated under the Resource Conservation and Recovery Act (RCRA) program and a pump and treat system was installed and operated from 1994 to 1999 to contain and treat the dissolved plumes. After a period of containment pumping, the estimated time of remediation for the downgradient pump and treat system to achieve remediation goals was lengthy and the results of an evaluation of natural attenuation processes to remediate the site in a reasonable time frame were positive (Chapelle and Bradley, 1998). The remediation focus shifted in 1999 from pump and treat to more targeted source reduction of contaminants with in situ chemical oxidation and monitored natural attenuation (MNA) to polish residual concentrations. Long term monitoring programs have been conducted at Site 11, including monitoring as required by the RCRA Permit and performed by Navy contractors since 1999 and monitoring conducted from 1999 to 2011 by the United States Geological Survey (USGS) in coordination with the Navy to evaluate the effectiveness of MNA (USGS, 2009). Details of the remedial actions relevant to the modeling of the source zone remediation over time are described in the following subsections.

1.1 Pump & Treat

Pump-and-treat (P&T) was the first active remedial action at Site 11 designed as an interim measure (IM) to contain the offsite migration of chlorinated ethene plumes (ABB Environmental Services Inc., 1994). The containment P&T system was installed and tested in 1993 with its first operational phase starting in 1994 (Bechtel Environmental, Inc., 1998). The second phase included the installation of an additional recovery well (RW-6) and ceased in August 1998 before the first ISCO phase (Bechtel Environmental, Inc., 1998; Chapelle et al., 2005). Additional recovery wells (RW-7 and RW-8) were installed during ISCO phase 1 and the system was operated between February and March 1999 (Bechtel Environmental, Inc., 2000). The system was permanently shut down in March 1999 because of fouling of the wells, pumps, and effluent piping (Bechtel Environmental, Inc., 2000). Figure 1-1 indicates the location of the P&T recovery wells and the direction of groundwater flow.

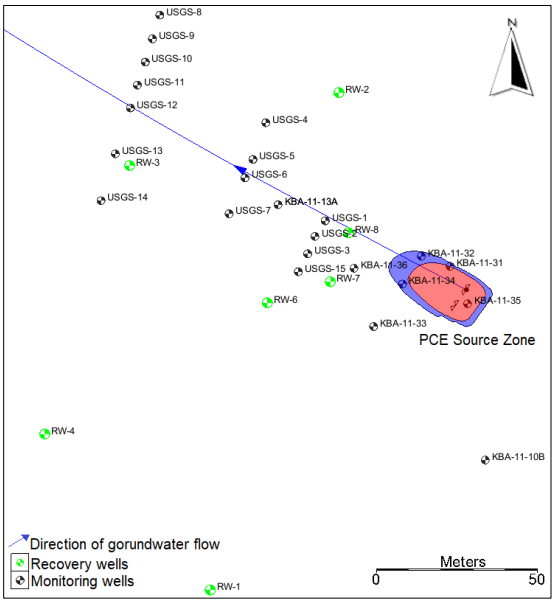

Figure 1-1. Location of Pump-and-Treat Wells

Table 1-1 summarizes the operational history of the P&T containment system. Detailed historical operational schedules of the P&T containment system could not be located in the Naval Facilities Engineering Command (NAVFAC) administrative record files. In addition, reports for the concentrations of contaminants in extracted groundwater were also sparse. The lack of groundwater extraction rates and mass discharge data resulted in uncertainty in numerical model calibration of steady-state natural attenuation conditions prior to ISCO phases and total dense-nonaqueous-phase-liquid (DNAPL) mass estimation. Nonetheless, several historical newsletters and reports provided some information on groundwater extraction rates and contaminant concentrations which were used to estimate contaminant mass and to evaluate the effects of P&T in the source zone with the Volume-Averaged Model. This scattered data is summarized in Tables 1-2 through 1-5 below.

Table 1-1. Chronology of IM System Activities Obtained from NAVFAC Record Files

Date	Action	Information Source^
4/1994-12/1994	Pilot testing of five extraction wells completed	June 1994 EnviroUpdate
12/1995	Five extraction wells pumping at a combined rate of 35 gpm (5 – 9 gpm each well). More than 24 million gallons of groundwater had been extracted and treated by air stripping (Phase 1 IM). System shut down for well redevelopment and pump maintenance.	December 1995 EnviroUpdate March 1996 EnviroUpdate June 1996 EnviroUpdate
4/1996 – 8/1996	System re-started; pulsed pumping pilot testing included two sequences of 8 days on 8 days off	June 1996 EnviroUpdate
12/1996	RW-6 installed, and RW-5 abandoned (Phase 2 IM)	December 1996 EnviroUpdate
3/1997	Total extraction rate increased from 21 gpm to 44 gpm	March 1997 EnviroUpdate
7/1997	Extraction rate at RW-6 increased from 14 gpm to 39 gpm with new pump. Combined extraction rate increased to 58 GPM	July 1997 EnviroUpdate
10/1998	System shut down in 1998 before ISCO phase 1.	Bechtel Environmental, Inc. 1998 CAP
2/1999 – 3/1999	Recovery wells RW-7 and RW-8 added to IM system in 2/1999 and shut down in 3/1999 because of fouling of wells, pumps, and effluent piping (Phase 3 IM)	Bechtel Environmental, Inc. 1998 CAP Bechtel Environmental, Inc. 2000 Completion Report for IM at Site 11

^Information sources are available in the site Administrative Record

Table 1-2. Historical Groundwater Extraction Rates in Gallons Per Minute (gpm) for IM Recovery Wells Interpreted and/or Obtained from NAVFAC Record Files

Well ID	1994	1997[a]	1997[b]
RW-1	7.5[1]	7.4[2,*]	5[2,*]
RW-2	9.4[1,*]	9.3[2,*]	6[2,*]
RW-3	7.5[1]	6[2,*]	4[2,*]
RW-4	7.9[1]	7.3[2,*]	5[2,*]
RW-5 (deep)	3.7[1,*]	0	0
RW-6	0	14[2,*]	35[2,*]
Total	36	44	55

[1] Interim Measure Phase I Activities (Table 2-4): Evaluation and Recommendations Report Addendum (ABB Environmental Services, Inc., 1996)

[2] Operations and Maintenance Manual Groundwater Extractions and Treatment System Revision 1 (Table 3-1): Evaluation and Recommendations Report Addendum (ABB Environmental Services, Inc., 1997)

* Interpreted/modified extraction rates to match composite rates per EnviroUpdate newsletters (see Table 4-1)

Table 1-3. Dissolved Concentrations (µg/L) of Chlorinated Solvents Measured Onsite at End of IM Phase 1 Pilot Testing

(Appendix K1 – ABB Environmental Services, Inc. 1994)

Well ID	PCE	TCE	DCE	VC
RW-1	13.13	19.88	287.31	25.27
RW-2	1	1	130.67	49.11
RW-3	58.35	159.35	1873.3	1
RW-4	1	6.6	25.53	5.5
RW-5	1	1	30	21.11

Table 1-4. Dissolved Concentrations (µg/L) of Chlorinated Solvents Measured at Recovery Wells in March 1997

(Appendix C, Figure 5: Summary of 1997 focused groundwater investigations – ABB Environmental Services, Inc. 1997)

Well ID	PCE	TCE	DCE	VC
RW-1	0	5.7	41	9.1
RW-2	0	1.8	64	20
RW-3	37	38	240	38
RW-4	0	8.3	46	16
RW-6	0	0	9.3	0

Table 1-5. Dissolved Concentrations (µg/L) of Chlorinated Solvents Measured at Recovery Wells in September 1997

(Appendix C, Figure 6: Summary of 1997 focused groundwater investigations – ABB Environmental Services, Inc. 1997)

Well ID	PCE	TCE	DCE	VC
RW-3	12	15	26	27
RW-6	72	90	3.4	3.4

The USGS monitoring wells had not yet been installed when the groundwater extraction system was operating. Therefore, limited groundwater monitoring data is available near the source zone during this period. The well closest and most directly in line with flow from the source during this period was KBA-11-13A as indicated in Figure 1-1. Pumping wells were located downgradient (RW-3) and cross-gradient (RW-6) from KBA-11-13A The groundwater concentrations measured in this well are summarized in Table 1-6.

Table 1-6. Groundwater Concentrations in Monitoring Well KBA-11-13A

	Jan 94*	Apr 94*	Sep 94*	Apr 95^	Mar 97#	Sept 97#	Sept 98#
PCE	<100	580	460	1,300	100	nd	nd
TCE	300	2,400	770	790	890	170	24
cDCE	2,900	1,800	700	440	280	770	160
VC	170	110	<50	53	nd	39	78

*Data from Appendix B Supplemental RCRA Report (ABB Environmental Services Inc., 1997)
^Data from Plan for IM Phase 2 Upgrades (ABB Environmental Services Inc., 1996)
Data from Appendix C Supplemental RCRA Report (ABB Environmental Services Inc., 1997)

KBA-11-13A was sampled in January 1994 (before any extraction started) and in April 1994 (after extraction started in March 1994). The impact of pumping is apparent in the concentrations. cDCE dominated in January 1994 before the pumping started in March 1994 in RW-3. The cDCE then decreased and TCE and PCE increased after extraction pulled upgradient parent concentrations toward the well. When pumping started in RW-6 in March 1997 the plume centerline was apparently pulled southward away from KBA-11-13A.

The pumping rates and measured concentrations were interpreted to provide estimates of the source zone discharge during pumping. The pumping rates cited in Table 3 are not directly applicable to the source zone. Numerical groundwater flow modeling (SEAM3D) was used to estimate the velocity of groundwater flow through source zone before pumping started, during the initial pumping, and after the increased pumping rate associated with the addition of a new pumping well. These calculations are described in Section 2.

1.2 In-Situ Chemical Oxidation

Following the pump-and-treat interim measure, ISCO using catalyzed hydrogen peroxide (CHP) was implemented in four different phases (Figure 1-2). Phase 1 of ISCO included 23 injection points centered around monitoring well KBA-11-34, which was regarded as the primary area of concern at the time but was downgradient from the actual DNAPL source. The injection wells were constructed to a depth of 32 to 45 feet bgs with 3-ft stainless steel screens. Groundwater samples were collected and analyzed from the injection wells prior to the injection activities. KBA-11-34 was included among the injection wells receiving oxidant which compromised its use for monitoring after Phase 1. Phase 1 consisted of two injections events conducted in November 1998 and February 1999 for a total approximate injection volume of 12,063 gallons of 50% hydrogen peroxide and an equivalent amount of ferrous iron catalyst solution. Groundwater samples were collected and analyzed in the subsequent months to asses progress and guide future injections. A cone penetrometer was also advanced at 24 locations to provide vertical and lateral definition to the plume.

Phase 2 ISCO included the installation of 20 additional injection points screened between 32 and 35 ft bgs and between 37 and 40 ft bgs. The new injection wells were sampled prior to the introduction of oxidant. Approximately 11,250 gallons of 50% hydrogen peroxide and an equivalent amount of ferrous iron catalyst solution were delivered in two injections conducted in June and July of 1999. Groundwater sampling followed in the months following the oxidant injections.

Only aqueous and sorbed contaminant were destroyed above and downgradient of the DNAPL source; DNAPL was not located within the target volumes. A Geoprobe investigation to collect groundwater samples with a mobile laboratory for onsite sample analyses was performed in September 1999 to investigate and locate the source of PCE rebounding (increasing concentration) at injector I-14. Groundwater samples were collected at 16 locations, GP-1 through GP-16 at depths of 21-24 ft, 24-27 ft, and 27-30 ft bgs at each location. Additional samples from depths of 11-14 ft, 15-18 ft, 18-21 ft, and 30-33 ft were collected at selected locations. Vertical profiles and lateral distribution of PCE groundwater concentrations are illustrated in Figure 1-3 although the sampling did not extend below 30 ft bgs. The maximum concentration detected was 99 mg/L representing nearly half the solubility limit of PCE. Additional data can be found in Bechtel Environmental, Inc. (1999).

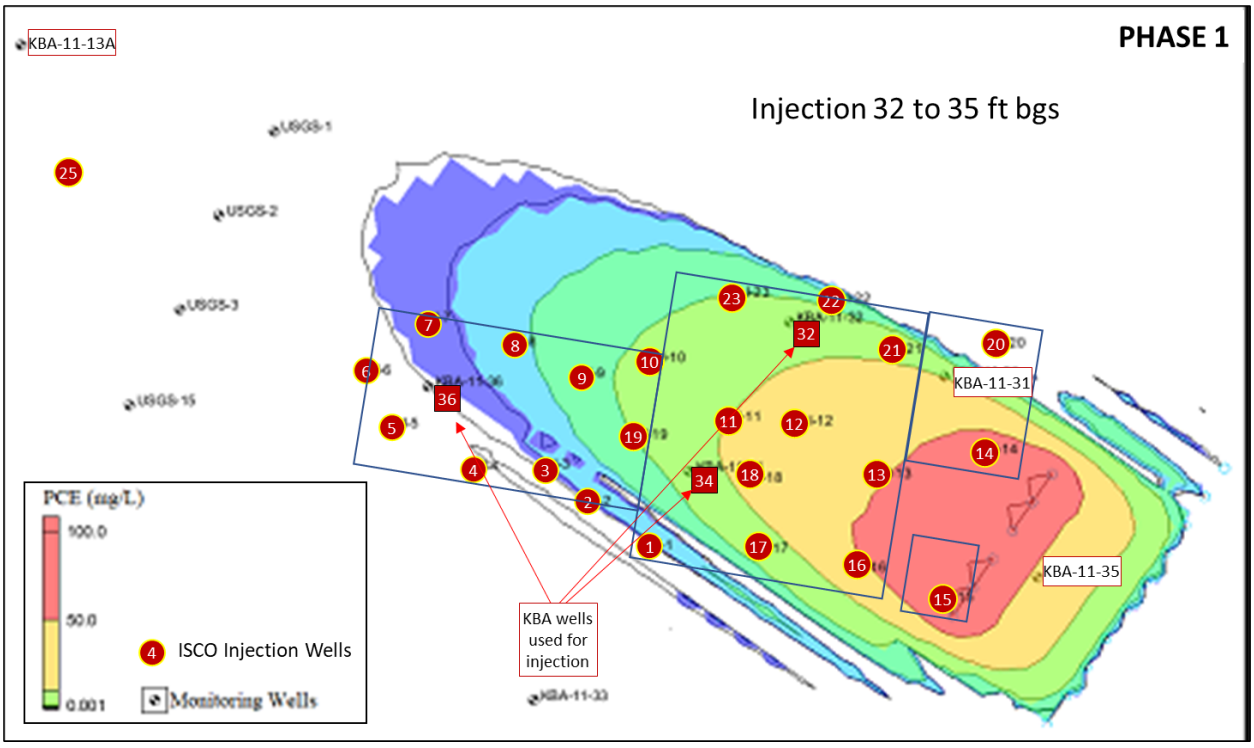

Figure 1-2a. PCE Source Zone and ISCO Injection Locations (Phase 1)

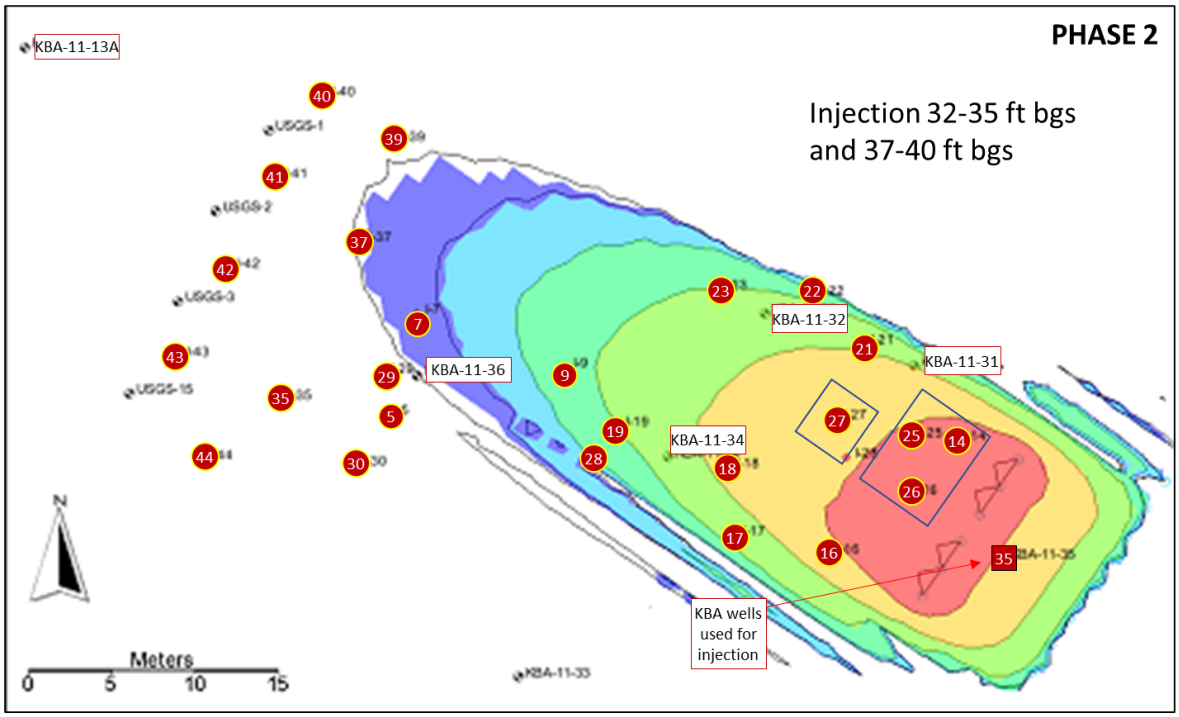

Figure 1-2b. PCE Source Zone and ISCO Injection Locations (Phase 2)

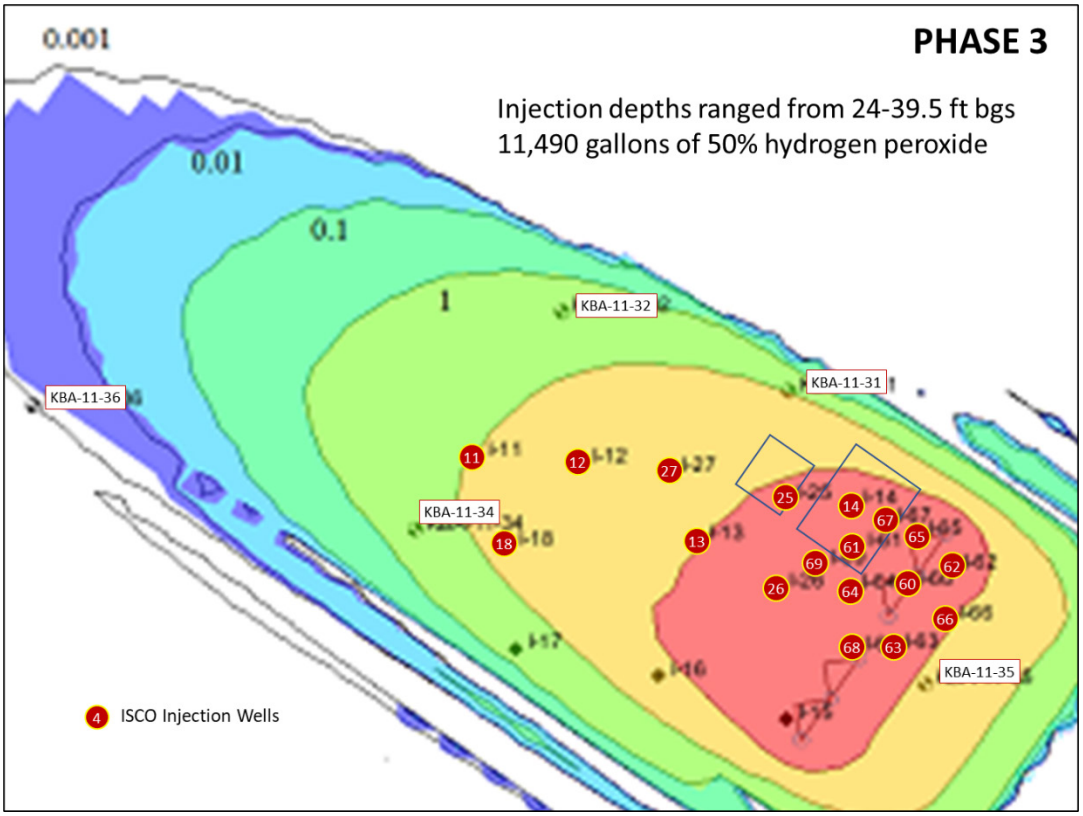

Figure 1-2c. PCE Source Zone and ISCO Injection Locations (Phase 3)

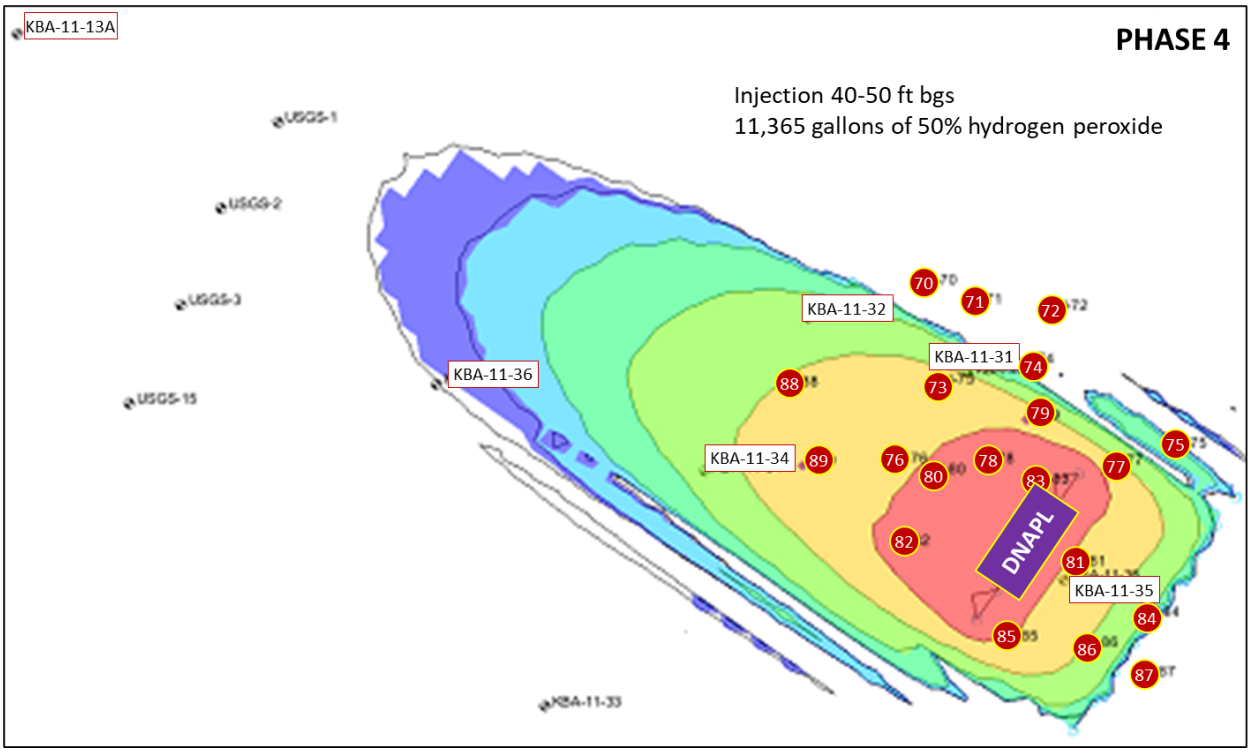

Figure 1-2d. PCE Source Zone and ISCO Injection Locations (Phase 4)

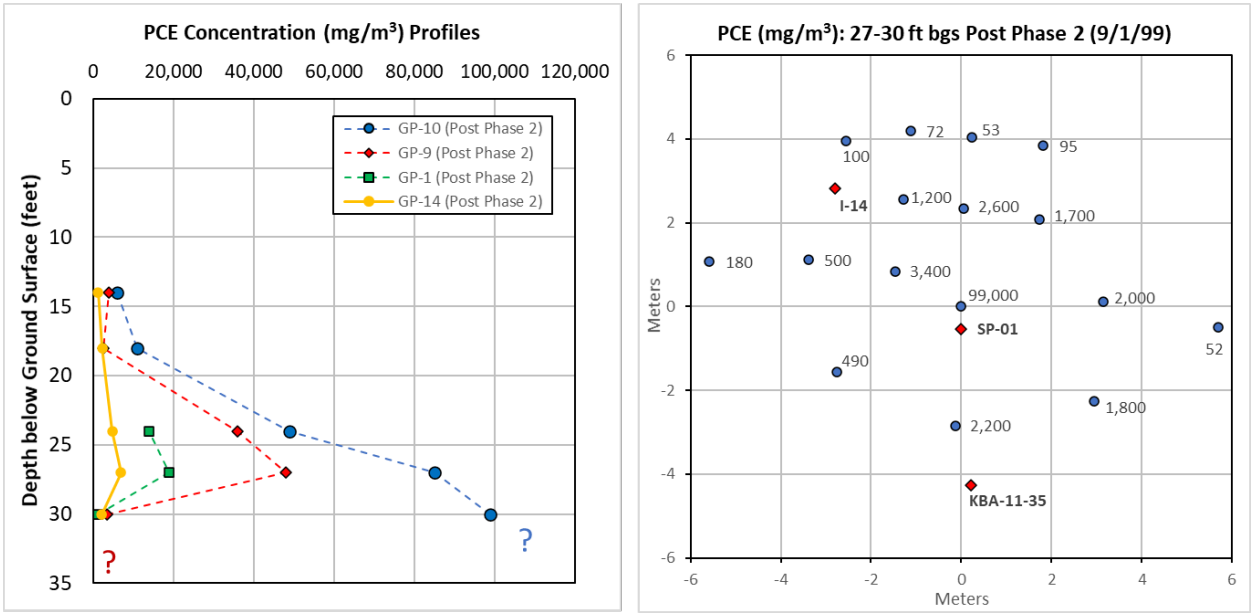

Figure 1-3. Sampling Results Around the DNAPL Source Zone after Phase 2 of ISCO Referenced to the Location of Injector I-60

Phase 3 of ISCO was performed in three injection events between January and April of 2000 and was focused in the DNAPL source zone. This phase included the installation of 10 additional injectors ranging from 24 to 39.5 ft bgs and total approximate injection volume of 11,500 gallons of 50% hydrogen peroxide and an equivalent amount of ferrous iron catalyst solution (Bechtel Environmental, Inc., 1999; 2000). Groundwater sampling followed the Phase 3 injections and rebound was observed as the PCE concentration increased in 15 of the 18 injectors sampled. A significant increase observed at I-60 near the DNAPL source again suggested the presence of a DNAPL source volume below 39 ft bgs. The post-Phase 3 conceptual sketch shown in Figure 1-4 led to an additional high resolution site characterization effort with direct push technology (DPT) to delineate the DNAPL source zone.

In November 2000, a source area delineation was completed utilizing a membrane interface probe (MIP)/DPT rig. The MIP technology was utilized to provide a vertical profile of the subsurface on a horizontal 10-foot grid around Injector I-60. Following completion of the MIP, groundwater samples were collected on a horizontal 10-foot grid from Injector I-60. Groundwater samples were collected from each boring using the DPT rig with peristaltic sampling pump and analyzed onsite. Based on the groundwater sample analytical results collected during this effort, the vertical interval of contamination in the source area was determined to be from 44 to 48 feet below land surface (bls). However, additional groundwater collection sampling and analysis was determined to be necessary to delineate the horizontal extent of contamination. In January 2001 a second source area delineation was completed utilizing a DPT rig with offsite laboratory analyses. Groundwater samples were collected on a 25-foot grid centered 5 feet to the west of Injector I-60, with samples collected from each of nine borings at depths of 36 to 40 feet bls, 40 to 44 feet bls, 44 to 48 feet bls, and 48 to 52 feet bls. The results of the two source area delineation efforts are illustrated in Figure 1-5. The conceptual location of the delineated DNAPL source zone is indicated in Figure 1-2d.

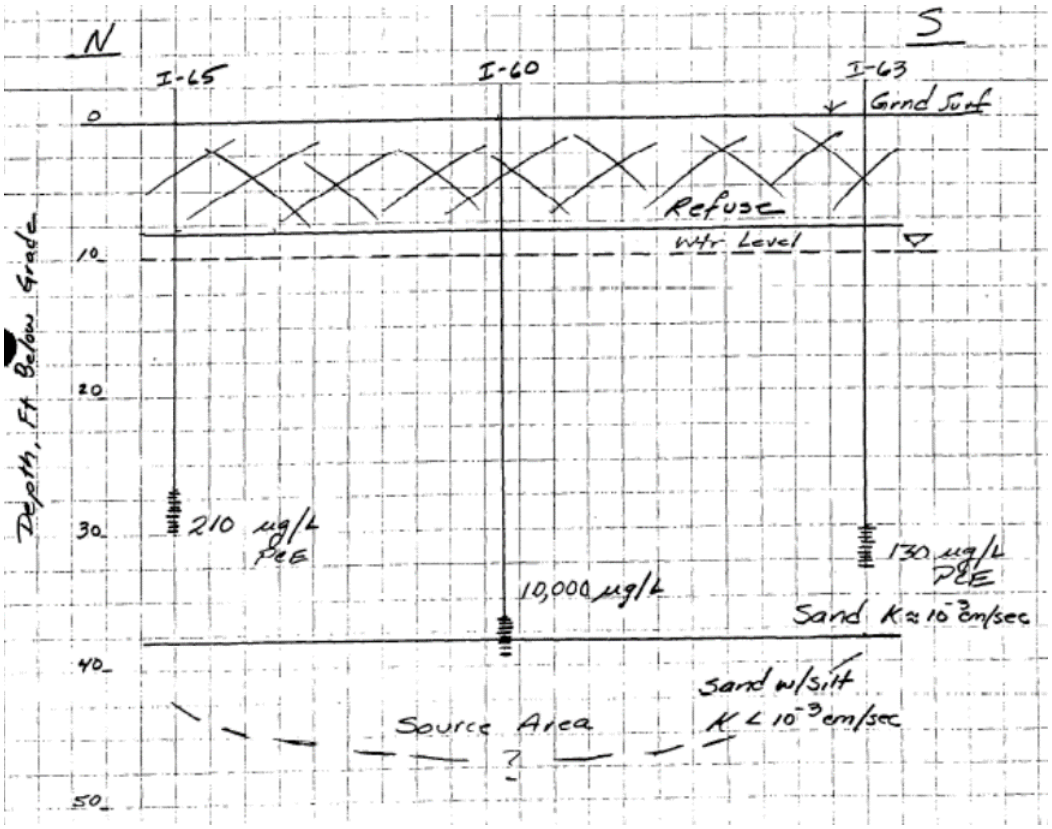

Figure 1-4. Sketch of Suspected DNAPL Source after Phase 3 (CH2M 2002)

Based on the source zone delineation, a fourth ISCO phase was performed between October and November 2001. A total of 20 injectors (numbered I-70 to I-89) with screen intervals from 45 to 48 feet bg were installed centered around I-60 intended to target the depth interval from 40 to 50 ft bgs. This Fenton's reagent chemical oxidation was performed in two phases: a primary injection and a polishing phase for a total injected volume of 23,585 gallons (approximately 12,220 gallons of catalyst and 11,365 gallons of 50% hydrogen peroxide).

1.3. Edible Vegetable Oil Injection for Enhanced Reductive Dechlorination

Following Phase 4 chemical oxidation injection, groundwater pH across the site was less than 5.0. Potassium hydroxide was injected through ISCO injector wells in December 2001 and totaled 5,500 gallons of solution to raise the pH for biological degradation. The potassium hydroxide injection solution was weak (pH of 9.0), but sufficient to overcome the groundwater pH. This action was followed by the injection of 25,208 gallons of emulsified soybean oil containing approximately 35% oil, 65% water, and 100 mg/L iodine (as sodium bromide tracer) into 39 DPT injection points from 28 to 48 feet bg (CH2M Hill Constructors, Inc., 2002). The soybean oil contained 7.5 percent (by weight) lecithin to act as an emulsifier and enhance mixing with water.

Figure 1-5. Lateral and Vertical Delineation of PCE Concentrations in the DNAPL Source Zone after Phase 3

1.4 Monitored Natural Attenuation

Long-term monitoring programs were conducted at Site 11, including monitoring as required by the RCRA Permit and performed by Navy contractors since 1999 and monitoring conducted from 1999 to 2011 by the United States Geological Survey (USGS) in coordination with the Navy to evaluate the effectiveness of MNA (USGS, 2009).

Following the soy bean oil injection, the downgradient plume was extensively monitored. Nearby transects of monitoring wells (USGS-series) were installed to supplement existing long-term monitoring wells (KBA-series) and provided projected areas of contaminant flow and mass fluxes over time. The locations of the monitoring wells are shown in Figure 1-1. A portion of these data are plotted in Figure 1-6 along with an indicator of the ISCO phases. KBA-11-34 was located in close proximity to the source zone, KBA-11-36 was located further downgradient and lateral to the source zone, and KBA-11-13A was located directly downgradient from the source zone as indicated in Figure 1-1. These data were used to assess the residual DNAPL mass and discharge after ISCO and to quantify back diffusion from the source zone.

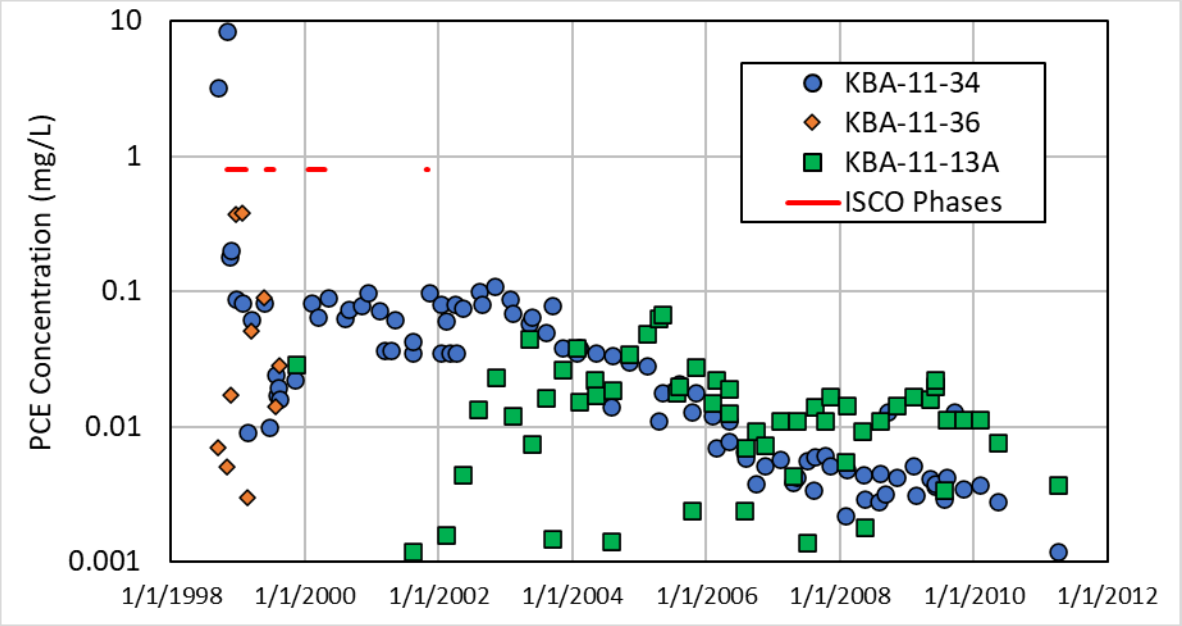

Figure 1-6. Long-Term Monitoring PCE Groundwater Concentrations

2.0 NUMERICAL FATE AND TRANSPORT MODEL DESCRIPTION

2.1 NUMERICAL GROUNDWATER FLOW MODEL

The intermediate semi-confined aquifer unit was simulated as a single layer in GMS using MODFLOW-2005. Groundwater flow was simulated at steady-state upon evaluating a number of hydraulic head datasets ranging from year 1999 through 2010, which suggested a general northwest groundwater flow direction. Specified-head boundary conditions were assigned at the NW and SE end rows with no-flow boundaries at the SW and NE columns of the numerical grid. Three recharge zones were assigned to the model domain based on land coverage (i.e., residential and vegetation areas) and hydraulic conductivity was set uniform throughout the grid. Recharge and hydraulic conductivity parameters were calibrated to water levels observed in August 2004 using PEST software. Model grid dimensions, boundary conditions, and calibrated parameters are detailed in Table 2-1 below.

Table 2-1. Groundwater flow model configuration

Item	Value	Units
Grid type	Cell centered	
X origin	444864.85	m
Y origin	3408834.18	m
Z origin	0	m
Length in X (j)	614	m
Length in Y (i)	488	m
Length in Z (k)	3	m
Rotation angle	325	
No. cells i	244	
No. cells j	307	
No. cells k	1	
No. of cells	74908	
Projection	UTM, Zone: 17 (84°W - 78°W - Northern Hemisphere), NAD83	m
HK	2.35	m/d
Recharge 1	0.0001	m/d
Recharge 2	0.000349	m/d
Recharge 3	0.000021	m/d
NW BC	19.5	m
SE BC	25.5 – 26.0	m
NE/SW BCs	No flow	

2.2. NUMERICAL CONTAMINANT FATE AND TRANSPORT MODEL

A subset of cells (i: 198 cells x j: 87 cells) from the numerical grid described above was selected for the contaminant transport model developed with SEAM3D (Waddill and Widdowson 2000). Two constant-concentration boundary conditions were defined at the ends of the transport model domain, perpendicular to the principal direction of groundwater flow. Constant concentrations were also assigned to areal recharge in the source/sink mixing package. All model parameters are detailed in Table 2-2 to 2-7. The source zone representation is defined in the following section.

Table 2-2. Dispersion Parameters

Dispersion Package		
Item	**Value**	**Units**
Longitudinal dispersivity	1.5	m
Transverse dispersivity	0.075	m

Table 2-3. Initial Conditions, Concentrations at the Landfill Boundary, and Recharge Concentrations for Electron Donors, Electron Acceptors, and Biodegradation End Products

Constituent	Concentrations (mg/L)		
	Initial	Boundary	Recharge
Electron donor	0.1	0.1	0.1
O_2	0	0	0
[(1)]Fe(III)	50	0	0
SO_4	1	0	20
[(2)]Fe(II)	1	0	0
[(2)]CH_4	2	0	0
Cl	0	0	0

[(1)]Concentrations starting at 62 m downgradient from source cells (~ at well KBA-11-13A) through downgradient end of numerical model domain (cell j: 164 through j: 1; all i cells across model domain); unit for Fe(III) is mg/g

[(2)] Source cells only (see table 2-8 for cell locations)

Table 2-4. Definition of Monod Kinetic Parameters Used to Simulate Biodegradation of Dissolved Organic Carbon and Redox Processes with SEAM3D

Symbol	Parameter definition
M_x	Microbial biomass concentration for x = 1,2…NM (number of microcolonies)
$\nu_{x,ls,le}^{max}$	Maximum specific rate of substrate utilization for microbial population *x* growing on substrate *ls* and electron acceptor *le*
$\bar{K}_{x,ls,le}^{s}$	Half-saturation constant for substrate *ls* for utilization of electron acceptor *le*
$\bar{K}_{x,le}^{e}$	Effective half-saturation constant for electron acceptor *le*
$Y_{x,ls,le}$	Biomass yield coefficient of microcolony *x* produced per unit mass of substrate *ls* while utilizing EA *le*
$\gamma_{x,ls,le}$	Electron-acceptor use coefficient
ς_x	Product generation coefficient
$\kappa_{le,li}$	Electron-inhibition coefficient representing inhibition of electron acceptor *le* by electron acceptor *li*

Table 2-5. Initial Concentration of Microbial Populations and Biodegradation Parameters for Four Terminal Electron-Accepting Processes

Microbial population	M_x	$\nu_{x,ls,le}^{max}$	$\bar{K}_{x,ls,le}^{s}$	$\bar{K}_{x,le}^{e}$	$Y_{x,ls,le}$	$\gamma_{x,ls,le}$	ζ_x	$\kappa_{le,li}$ [1]		
	g/m^3	1/d	g/m^3	g/m^3	g/g	g/g	g/g	O_2	Fe(III)	SO_4
Aerobes	0.3	0.05	5	1	0	3	N/A	N/A	N/A	N/A
Iron Reducers	0.03	0.05	10	N/A	0	33	0.1	10	N/A	N/A
SO_4 Reducers	0.03	0.48	10	1	0	4.5	N/A	10	50	N/A
Methanogens	0.03	0.01	10	N/A	0	N/A	0.2	10	25	1

[1] Units for inhibition coefficients are in mg/L, except for Fe(III), which is in mg/g.

Table 2-6. Definition of Monod Kinetic Parameters Used to Simulate Chlorinated Ethene Reductive Dechlorination with SEAM3D

Symbol	Parameter definition
M_y	Microbial biomass concentration of chlorinated ethene reducers for x = 1 or 2
$\nu_{lc}^{max,EA}$	Maximum rate of reductive dechlorination for a chlorinated ethene *lc*
$\bar{K}_{lc}^{e}$	Effective half saturation constant for a chlorinated ethene (serving as an electron acceptor) *lc*
$\kappa_{le,li}$	Electron acceptor inhibition coefficient representing inhibition of the use of a chlorinated ethene *lc* (as an electron acceptor) by electron acceptor *li* (where *li* = 1, 2, 3, 4, or 5 only);

Table 2-7. Initial Concentration of PCE/TCE and DCE/VC Degraders and Kinetic Reductive Dechlorination Parameter for the Simulated Chlorinated Ethenes

Microbial population	M_y	$\nu_{lc}^{max,EA}$	$\bar{K}_{lc}^{e}$	$\kappa_{le,li}$ [1]					
	g/m^3	1/d	g/m^3	O_2	Fe(III)	SO_4	PCE	TCE	DCE
PCE	0.03	0.0259	5	0.5	10000	50	N/A	N/A	N/A
TCE		0.0715	10	0.5	10000	25	12.5	N/A	N/A
DCE	0.03	1.755	20	1	15	1.25	1	1.2	N/A
VC		1.512	15	1	1.5	1.5	1000	1000	2

[1] Units for inhibition coefficients are in mg/L, except for Fe(III), which is in mg/g.

2.3 DNAPL SOURCE ZONE

The numerical representation of the source zone consists of 5 contiguous cells with constant concentrations set at 9 mg/L of PCE in each cell (Figure 2-1). Considering an estimate of initial PCE mass of 1,119 kg (Chapelle et al., 2007), PCE density (ρ_{PCE}), porosity (n), and the cell size of the SEAM3D numerical model (2m x 2m x 3m), the source zone was represented with the characteristics indicated in Table 2-8.

The residual DNAPL saturation (S_r) was calculated as: $S_r = V_{DNAPL}/V_{pores} = V_{DNAPL}/nV_{total}$. The location of the 5 source cells was designed as a transect perpendicular to the principal direction of groundwater flow covering the lateral extent of the highest PCE detection points (Figure 2-1).

This numerical representation of the source zone is useful to produce steady-state plumes of chlorinated ethenes which can be calibrated to site pre-ISCO conditions considering the observed redox conditions and natural attenuation capacity of the aquifer system. The volume averaged model will then be used to represent the conceptualized source zone architecture more accurately in order to produce more realistic estimates of mass removal by various remedial scenarios.

Table 2-8. Numerical Model Source Zone Properties

Item	Value	Unit
n	0.3	
DNAPL (PCE) Mass	1,119	(kg)
DNAPL (PCE) Density	1.62	(g/cm^3)
DNAPL (PCE) Volume	0.691	(m^3)
Grid cell volume	2m x 2m x 3m	(m^3)
No. of cells	5	
Cell number j (Y-axis)	194	
Cell number i (X-axis)	106 – 110	
Source Zone Volume	60	(m^3)
S_r	0.008	

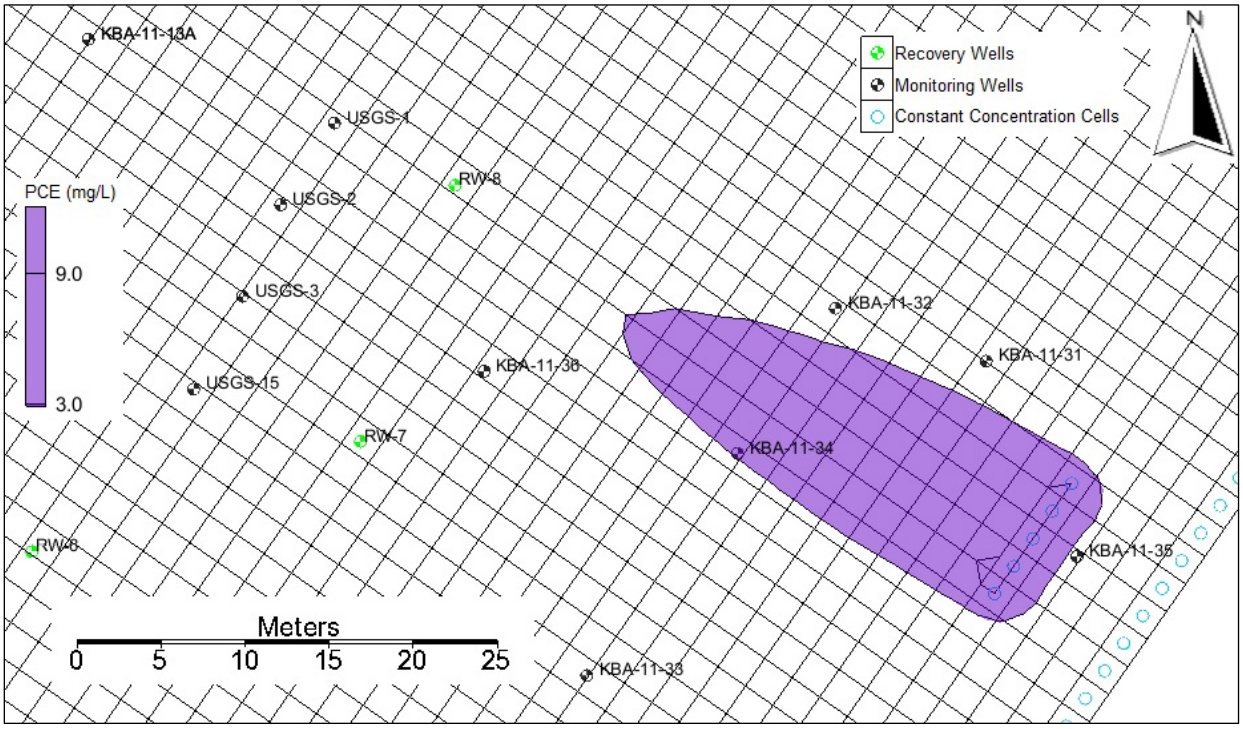

Figure 2-1. Numerical Representation of PCE Source Zone in SEAM3D.

2.4 SEAM3D CALIBRATION TARGETS

Table 2-9 below shows the water-level dataset used to calibrate the MODFLOW model.

Table 2-9. Calibration targets of MODFLOW model

ID	Water Elevation (ft msl)
KBA-11-03B	23.89
KBA-11-08B	25.47
KBA-11-10B	24.77
KBA-11-11A	25.5
KBA-11-13A	23.95
KBA-11-15	23.5
KBA-11-16	23.01
KBA-11-17B	21.47
KBA-11-18	19.88
KBA-11-20	20.24
KBA-11-21	20.17
KBA-11-22B	24.72
KBA-11-34	24.37
KBA-11-36	24.21
KBA-11-37	22.46
PS-2	24.01

A combination of chlorinated-ethene concentration data obtained from monitoring wells and from temporary source-delineation boreholes collected before and during the ISCO phases, respectively, were used to calibrate the SEAM3D model. Data from monitoring wells (USGS and KBA in Table 2-10) corresponds to maximum concentrations detected in 1998 prior to the first ISCO phase. This calibration dataset was used to estimate the steady-state natural attenuation capacity of the intermediate aquifer system and to constrain the location and strength of the DNAPL source zone.

Table 2-10. Concentrations of chlorinated ethenes (mg/L): SEAM3D calibration targets

ID	PCE	TCE	DCE	VC	Sample date	Data source
CPT-02	bd	bd	bd	bd	4/12/1999	1
CPT-11	0.021	bd	bd	bd	4/13/1999	1
CPT-12	0.019	bd	bd	bd	4/13/1999	1
CPT-14	bd	bd	bd	bd	4/13/1999	1
CPT-19	bd	0.185	0.595	0.15	4/14/1999	1
SP-37	0.006	0.00022	0.00058	0.0012	1/8/2001	2
USGS-1	bd	1.14	0.919	0.314	8/6/1998	3
USGS-2	bd	0.681	0.578	0.0626	11/4/1998	3
USGS-3	bd	0.511	1.27	0.112	11/4/1998	3
USGS-4	bd	bd	0.083	0.208	8/6/1998	3
USGS-5	bd	bd	0.074	0.792	8/6/1998	3
USGS-6	bd	bd	0.0718	0.888	8/6/1998	3
USGS-7	bd	bd	0.0266	0.196	8/6/1998	3
USGS-8	bd	bd	0.0145	0.0115	11/4/1998	3
USGS-9	bd	bd	0.497	0.465	8/6/1998	3
USGS-10	bd	0.314	0.683	0.997	8/6/1998	3
USGS-11	bd	bd	0.0584	0.11	8/6/1998	3
USGS-12	bd	bd	0.0294	0.0756	8/6/1998	3
USGS-13	bd	bd	0.305	0.0562	11/24/1998	3
USGS-14	bd	bd	0.0093	0.0289	8/6/1998	3
USGS-15	bd	0.0098	0.0685	0.0102	11/4/1998	3
KBA-11-13A	bd	0.024	0.16	0.078	9/17/1998	4
KBA-11-31	bd	0.009	0.006	0.002	9/17/1998	4
KBA-11-32	0.003	0.091	0.03	0.009	9/17/1998	4
KBA-11-33	bd	bd	bd	bd	9/17/1998	4
KBA-11-34	3.2	0.35	0.008	bd	9/17/1998	4
KBA-11-35	bd	bd	bd	bd	9/17/1998	4
KBA-11-36	0.007	0.44	0.06	0.005	9/17/1998	4
KBA-11-37	bd	bd	0.024	0.0025	8/17/1999	3
108-Cottage-Ct	bd	bd	0.007	bd	3/1/2000	5

[1] Final Construction Completion Report for Groundwater Remediation at Site 11. CH2M Hill, 2002.

[2] Semi-Annual Corrective Action Assessment Interim Measures Progress Report for Site 11. Bechtel Environmental, Inc., 1999.

[3] Appendix B

[4] Completion Report for Interim Measures at Site 11. Bechtel Environmental, Inc., 2000.

[5] Table A-2

2.5 ASSUMPTIONS AND CALIBRATION TO PRE-ISCO CONDITIONS

Calibration of steady-state plumes prior to ISCO phases was achieved by a trial-and-error approach to circumvent uncertainty in the groundwater flow field and contaminant transport patterns derived from containment pumping operations, whose detailed documentation was not available in the

NAVFAC website for the Administrative Record. In addition to the calibration targets shown in Table 2-10 a historical dataset of monitoring well KBA-11-34, located downgradient from the DNAPL source, was used to guide the model calibration process. Specifically, the chlorinated-ethene historical concentration threshold observed in KBA-11-34, shown in Table 2-11, served to adjust the PCE source strength, location of bioavailable ferric iron in the aquifer, and reductive dechlorination rates and inhibition terms. This data was therefore critical in refining the simulation of daughter-product plumes, particularly vinyl chloride, which displayed a complex spatial pattern resulting from aquifer redox zonation and a variety of natural attenuation processes, including VC anoxic mineralization (direct oxidation). The calibrated model is illustrated with calculated plumes of PCE and the daughter products in Figure 2-2.

Table 2-11. Pre-ISCO contaminant concentrations (ug/L) at monitoring well KBA-11-34

Date	Jan 94*	Apr 94*	Sep 94*	Apr 95^	Mar 97**	Sep 94**
PCE	<100	580	460	1300	100	nd
TCE	300	2400	770	790	890	170
DCE	2900	1800	700	440	280	770
VC	170	110	<50	53	nd	39

*Data from Appendix B Supplemental RCRA Report (ABB Environmental Services Inc., 1997)

**Data from Appendix C Supplemental RCRA Report (ABB Environmental Services Inc., 1997)

^Data from Plan for IM Phase 2 Upgrades (ABB Environmental Services Inc., 1996)

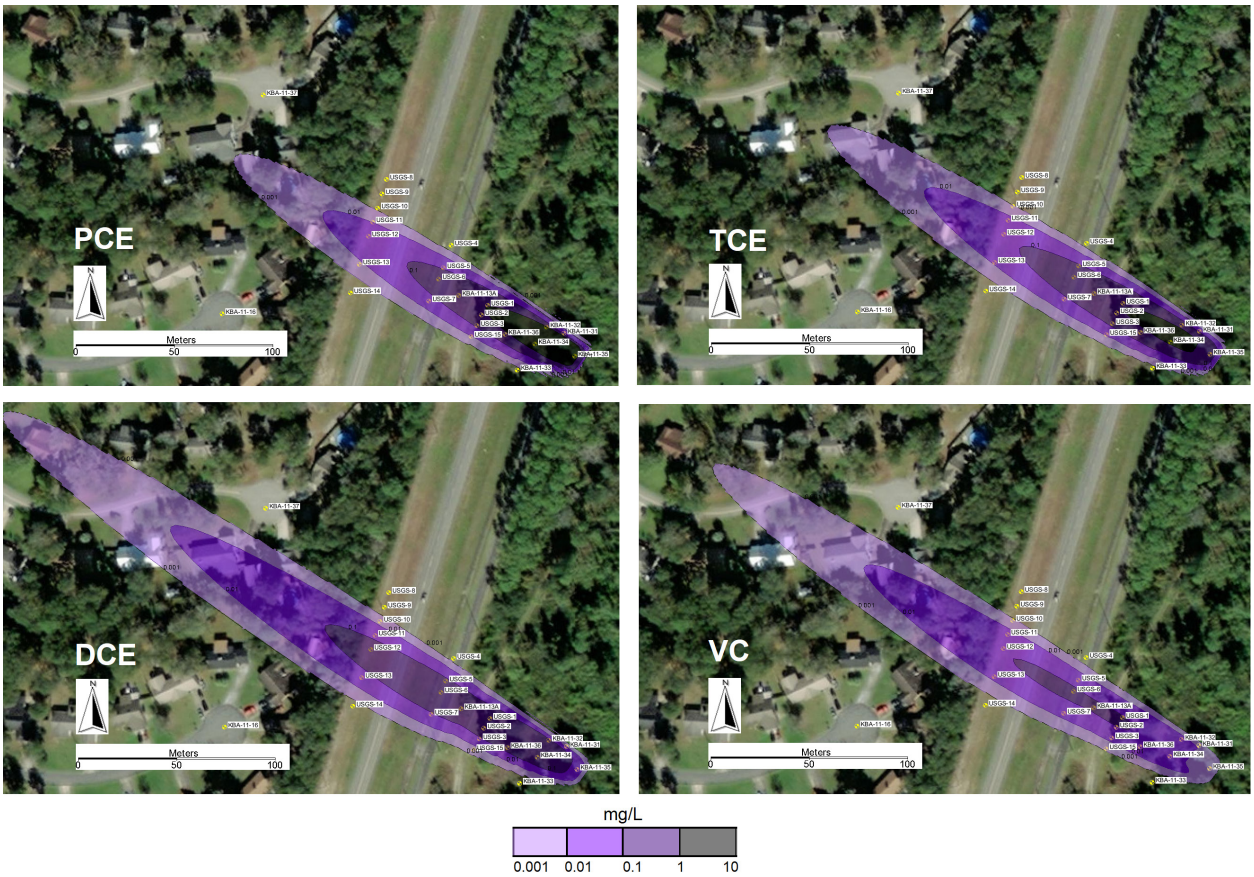

Figure 2-2. Simulated Plumes of Chlorinated Ethenes Prior to ISCO Remediation (1998)

3.0 REFERENCES

ABB Environmental Services Inc., 1995, Technical Memorandum November 1994 Field Program for Site 11 NSB Kings Bay. Administrative Record N42237.AR.000364.

ABB Environmental Services Inc., 1996. Plan for Interim Measure Phase 2 Upgrades at Site 11 NSB Kings Bay. Administrative Record N42237.AR.000402.

ABB Environmental Services Inc., 1997. Draft Final Supplemental RCRA Facility Investigation Report for Site 11. Administrative Record N42237.AR.000436.

Bechtel. 1998. Corrective Action Plan, Site 11, Old Camden County Landfill, Naval Submarine Base Kings Bay, Georgia.

Bechtel. 1999. Groundwater Monitoring Plan for Site 11,Old Camden County Landfill, U.S. Naval Submarine Base, Kings Bay, Georgia, June 1999.

Bechtel. 2000. Completion Report for Interim Measures at Site 11, Old Camden County Landfill, Naval Submarine Base Kings Bay, Georgia.

CH2M HILL. 2002. Construction Completion Report for Groundwater Remediation at Site 11, Old Camden County Landfill, Naval Submarine Base Kings Bay, Georgia.

Chapelle, F.H., and P.M. Bradley. 1998. Selecting remediation goals by assessing the natural attenuation capacity of ground-water systems. Bioremediation Journal 2:227-238.

Chapelle, F.H. and P.M. Bradley. 1999. *Selecting Remediation Goals by Assessing the Natural Attenuation Capacity of Groundwater Systems*. Proceedings of the Technical Meeting Charleston, South Carolina. March 8-12, 1999, Volume 3 of 3 Subsurface Contamination From Point Sources, Water-Resources Investigations Report 99-4018C. U.S. Geological Survey.

Chapelle, F.H., M. Widdowson, J. Brauner, E. Mendez, and C. Casey. 2003. *Methodology for Estimating Times of Remediation Associated with Monitored Natural Attenuation*. USGS Water Resources Investigation Report 03-4057. Available at http://pubs.usgs.gov/wri/wri034057/pdf/wrir03-4057.pdf.

Chapelle, F.H., P.M. Bradley, and C.C. Casey. 2005. Behavior of a chlorinated ethene plume following source-area treatment with Fenton's reagent. Ground Water Monitoring & Remediation. 25(2), 131-141.

Chapelle, F.H., J. Novak, J. Parker, B.G. Campbell, and M. Widdowson. 2007. *A framework for assessing the sustainability of monitored natural attenuation*. USGS Circular 1303, 35 pp.

USGS, 2009. Monitoring the Efficiency of Natural Attenuation at the Old Camden County Landfill, Kings Bay Naval Submarine Base, Georgia. U.S. Geological Survey Administrative Report, Water Resources Division, Columbia, SC.

Waddill, D.W. and M.A. Widdowson. 2000. *SEAM3D: A Numerical Model for Three-Dimensional Solute Transport and Sequential Electron Acceptor-Based Biodegradation in Groundwater*. U.S. Army Engineer Research and Development Center Technical Report ERDC/EL TR-00-18, Vicksburg, MS.

APPENDIX E DESCRIPTION OF SITE ST012, FORMER WILLIAMS AIR FORCE BASE, AZ

APPENDIX E

DESCRIPTION OF SITE ST012, FORMER WILLIAMS AIR FORCE BASE, AZ

Evaluating and Applying Site-Specific NAPL Dissolution Rates during Remediation

ESTCP Project ER19-5223

Version 1.0

Lloyd "Bo" Stewart, Praxis Environmental Technologies, Inc.
Julie Chambon & Jennifer Nyman, Geosyntec

TABLE OF CONTENTS

1.0 NAPL COMPOSITION AND COMPONENT TRANSPORT PROPERTIES

Measured mass contents in NAPL samples collected from multiple wells at Site ST012 in 2006, 2010, 2018, and 2021 are provided in **Table E-1**.

Table E-1. Measured Mass Content of NAPL Samples

		2006	2010				2018			2021			
Compound	**Aqueous Solubility** (mg/L)	**LSZ Model**	**W01**	**MWN-3B***	**W03**	**RB-2C**	**LSZ 16***	**LSZ 50**	**W37**	**W12**	**LSZ-46**	**LSZ-50**	**LSZ-49**
			(% mass)										
Benzene	**1780**	**0.83**	**0.60**	**0.22**	**0.83**	**0.44**	**<0.02**	**0.31**	**0.19**	**<0.017**	**0.27**	**0.23**	**0.42**
Toluene	515	2.90	1.80	1.50	2.90	3.00	0.17	2.84	1.76	<0.016	1.84	0.18	0.34
Ethylbenzene	152	1.40	1.40	1.10	1.30	1.70	1.18	1.70	1.66	0.89	1.62	1.59	1.60
m&p-Xylenes	162	2.20	2.20	1.80	2.10	2.40	2.88	4.56	3.77	1.28	3.80	1.24	2.25
o-Xylene	175	0.83	0.70	0.67	0.83	1.10	1.31	1.49	1.34	0.19	1.31	0.78	1.01
Naphthalene	32	0.50	0.60	0.22	0.83	0.44	0.30	0.11	0.17	0.08	0.13	0.23	0.15

* within SEE or TEE treatment zones

The measured mass contents were converted to mole fractions using the molecular weights of each model compound, or family of compounds in a previously derived NAPL model for the LSZ (BEM 2011) listed in **Table E-2**. The equilibrium groundwater concentration for each compound was then estimated using Raoult's Law from the calculated mole fraction and aqueous solubility as provided in **Table E-2**.

Table E-2. Model NAPL Composition for the LSZ and Solubility at 25 C

C#	NAPL Component / Surrogate Compound	Mass Fraction, %	Mole Fraction	Aqueous Solubility (mg/L)		Equilibrium Concentration (mg/L)
Aromatic Compounds of Concern						
6	Benzene	0.83	0.0116	1790		20.7
7	Toluene	2.90	0.0342	526		18.0
8	Ethylbenzene	1.40	0.0143	169		2.42
8	m&p-Xylenes	2.20	0.0225	161		3.63
8	o-Xylene	0.83	0.0085	178		1.51
10	Naphthalene*	0.50	0.0042	31		0.13
Other Aromatic Constituents						
9	1,2,4-Trimethylbenzene	1.10	0.0100	57		0.57
9	1,3,5-Trimethylbenzene	0.37	0.0033	48		0.16
9	1-Methyl-3-ethylbenzene	1.15	0.0104	35		0.37
9	Isopropylbenzene	0.28	0.0025	61		0.16
9	n-Propylbenzene	0.37	0.0033	52		0.17
10	1,2,3,5-Tetramethylbenzene	3.98	0.0323	28		0.90
11	1-Methylnaphthalene	1.59	0.0122	25		0.30
Isoalkanes						
6	2-Methylpentane	3.03	0.0382	14		0.54
7	2-Methylhexane	6.10	0.0662	4.4		0.29
8	3-Methylheptane	11.77	0.1120	1.5		0.16
9	2-Methyloctane	6.68	0.0567	0.48		0.027

Table E-2. Model NAPL Composition for the LSZ and Solubility at 25 C (Continued)

C#	NAPL Component / Surrogate Compound	Mass Fraction, %	Mole Fraction	Aqueous Solubility (mg/L)		Equilibrium Concentration (mg/L)
Cycloparaffins						
6	Cyclohexane	10.30	0.1331	55		7.32
7	Methylcyclohexane	10.00	0.1108	17		1.88
8	Dimethylcyclohexane	2.25	0.0219	8.4		0.184
9	Isopropylcyclohexane	4.28	0.0369	3.1		0.114
n-Alkanes						
5	n-Pentane	1.40	0.0211	38		0.802
6	n-Hexane	2.95	0.0372	9.5		0.354
7	n-Heptane	4.90	0.0531	3.4		0.181
8	n-Octane	4.20	0.0400	0.41		0.0164
9	n-Nonane	3.00	0.0255	0.22		0.0056
10	n-Decane	2.88	0.0220	0.052		0.0011
11	n-Undecane	3.09	0.0215	0.0044		9.48E-05
12	n-Dodecane	2.67	0.0170	0.0037		6.30E-05
13	n-Tridecane	2.03	0.0120	0.0029		3.47E-05
14	n-Tetradecane	0.97	0.0053	0.0022		1.17E-05
TOTAL		100	1.0000			60.9

*Naphthalene has a fugacity ratio of 3.3 (solid at 25 C)

The results of recent groundwater sampling and analyses are listed in **Table E-3** for wells that currently exist along with the calculated equilibrium concentration. The reasonable correlation between the calculated and measured groundwater concentrations, considering the potential for dilution in monitoring wells, corroborates the calculated mole fractions of benzene. The corroboration between NAPL content and groundwater analyses also indicates that groundwater concentrations can be used to infer the proximity of NAPL to wells even when NAPL does not appear in the well. The NAPL analyses also indicate a vast majority of the benzene mass remaining at ST012 is part of the NAPL hydrocarbon mixture rather than dissolved in groundwater or sorbed to soil solids. In the modeling to follow, the initial mole fractions of components of concern are assumed equal to the 2006 model mole fractions listed in **Table E-2**.

Table E-3. Calculated Benzene Mole Fractions, NAPL-Equilibrium Water Concentrations, and Recent (2021) Measured Groundwater Concentrations

LSZ Benzene Data		Mole Fraction	Equilibrium Concentratio (µg/L)	Recent GW Concentration (µg/L)
2018	LSZ16*	0.00028	<500	-
	LSZ50	0.00422	7,550	2,980
	W37	0.00297	5,320	7,250
2021	W12	0.00024	<430	17
	LSZ46	0.00379	6,780	1,860
	LSZ50	0.00344	6,160	2,980
	LSZ49	0.00578	10,300	5,490

* within the TEE or SEE treatment zones

Properties of components of concern of the JP4 mixture relevant to dissolution and transport are provided in **Table E-4**. These properties are utilized as input to the dissolution and remediation model. The retardation coefficient, *R*, was calculated from the equation below and utilized the site-wide soil properties listed in **Table E-5**.

$$R = 1 + \frac{\rho_b f_{oc} K_{oc}}{\phi}$$

Table E-4. NAPL Component Properties

Property	Unit	Benzene	Toluene	Naphthalene
Molecular Weight, *MW*	g/mol	78.114	92.141	198.394
Solubility, C^*	mg/L	1806.6	556.2	111.7
Cleanup Concentration, C_{MCL}	mg/L	0.005	1	0.027[a]
MCL Mole Fraction, y_{MCL}	-	2.768E-06	0.0017979	0.0002417
Initial Mole Fraction, y_0	-	0.011557	0.034234	0.004243
NAPL Equil Solubility, $y_0 C^*$	mg/L	20.8794	19.0410	0.4739
Octanol-Carbon Coeff, K_{oc}		56.234133	117.48976	912.01084
Retardation, R		1.0830	1.1735	2.3465

[a] Naphthalene does not have an MCL but the site ROD specifies a cleanup goal of 27 ug/L.

Table E-5. Site ST012 Soil Properties

Property	Unit	Value
Total Soil Porosity,	-	0.35
Soil Bulk Density,	kg/L	1.723
Organic Carbon Fraction, f_{oc}	-	0.0003

2.0 NAPL EXTENT AND SATURATION ESTIMATES

The data employed to develop the estimated NAPL extent, architecture and saturation in each LSZ target volume shown in **Figure 5.5.12** of the main text included:

- 40 geologic logs;
- Discrete testing for NAPL presence using dye tests;
- Benzene and total petroleum hydrocarbon concentrations in monitoring wells;
- Detection and removal of NAPL from wells across the LSZ;
- Laboratory analyses on NAPL samples;
- Design and operation of the SEE system; and
- Historical rise in the water table and consequent changes in NAPL appearance across the site since 1990 (IT, 1992; IT 1999; BEM Systems, 2011; Amec Foster Wheeler, 2018).

2.1 CHARACTERIZATION OF NAPL LATERAL AND VERTICAL EXTENTS

The total volume released and current distribution of NAPL in the saturated zone are not known; however, field evidence suggests NAPL is smeared across all but the lower 10 to 15 feet of the LSZ (~210 to 242 feet below ground surface[bgs]). The concept of vertical migration leaving residual NAPL and lateral spreading of pooled NAPL atop the water table is supported by the 1990 delineation of extent shown in **Figure E-1**. The areal extent of pooled NAPL shrunk as the water table rose above the LSZ, as indicated by the 1997 NAPL delineation and the 2022 estimated isoconcentration contour of benzene in the LSZ groundwater at the maximum contaminant level (MCL).

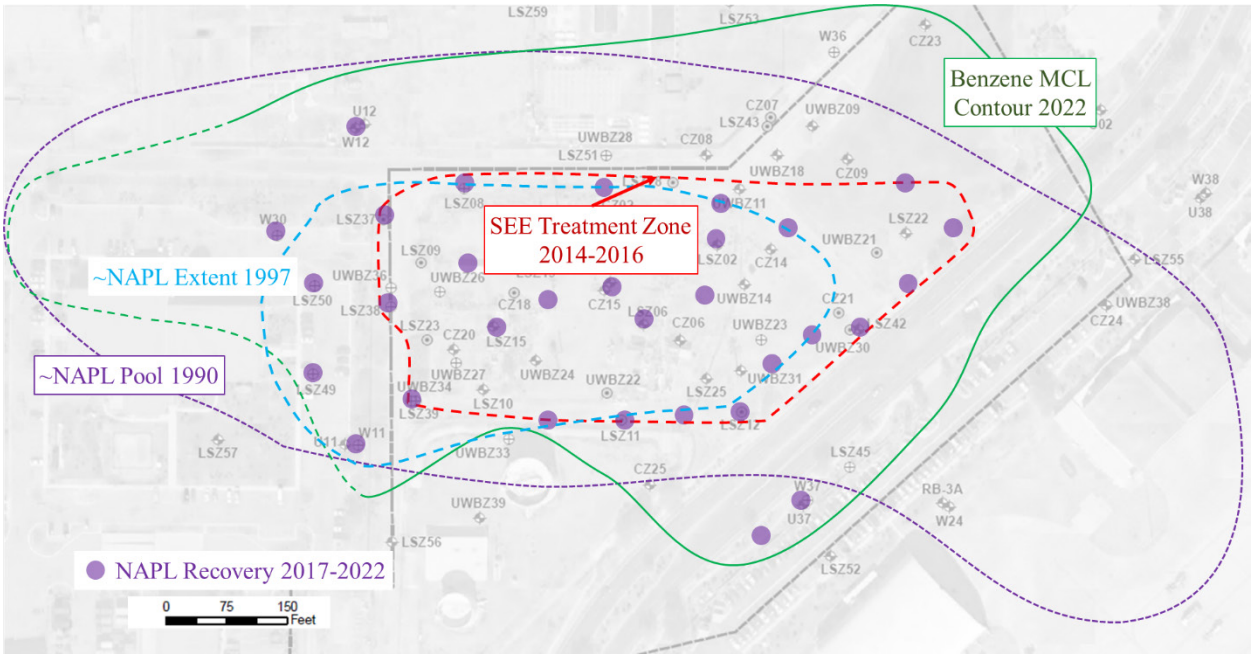

Figure E-1. Estimates of NAPL Lateral Extent in the LSZ in 1990 and 1997, Area of Steam Enhanced Extraction (SEE) Treatment, and Wells with Recoverable NAPL after SEE

As illustrated in **Figure E-1**, the benzene contour aligns closely with the historical extent of NAPL detected in 1990 except in the southeast area. The 2022 extent suggests residual NAPL remained in some outer areas while the area to the southeast had a thin pool which was depleted of benzene as the water table changed direction to the northeast. Similar smearing and mobilization occurred in the overlying UWBZ and CZ as the water table rose but this effort focuses solely on the LSZ.

The implementation of SEE in the CZ, UWBZ and LSZ substantially reduced the mass of NAPL in targeted volumes of each zone. The target volume for the LSZ is indicated by the dashed red line in **Figure E-1**. The estimate for the NAPL recovered from the three zones during SEE is equivalent to about 450,000 gallons of JP-4. Of this volume, about half was recovered in the volatile and dissolved phases and about half as pumped NAPL. Based on this recovered volume and current estimates of the remaining NAPL mass, SEE is assumed to have removed roughly 50% of the NAPL mass in place at the start of SEE. **Figure E-1** also indicates the locations and recovery of NAPL in the LSZ after SEE was terminated. These observations indicate residual NAPL remains within the treated volume but the benzene content is significantly depleted.

Geologic logs from wells shown on **Figure E-2** were evaluated and collected into groups coinciding with six LSZ treatment areas shown in **Figure 5.5.12** of the main text. Logs from the SEE perimeter were emphasized and multiple cross-sections were developed as shown in **Figure E-2**.

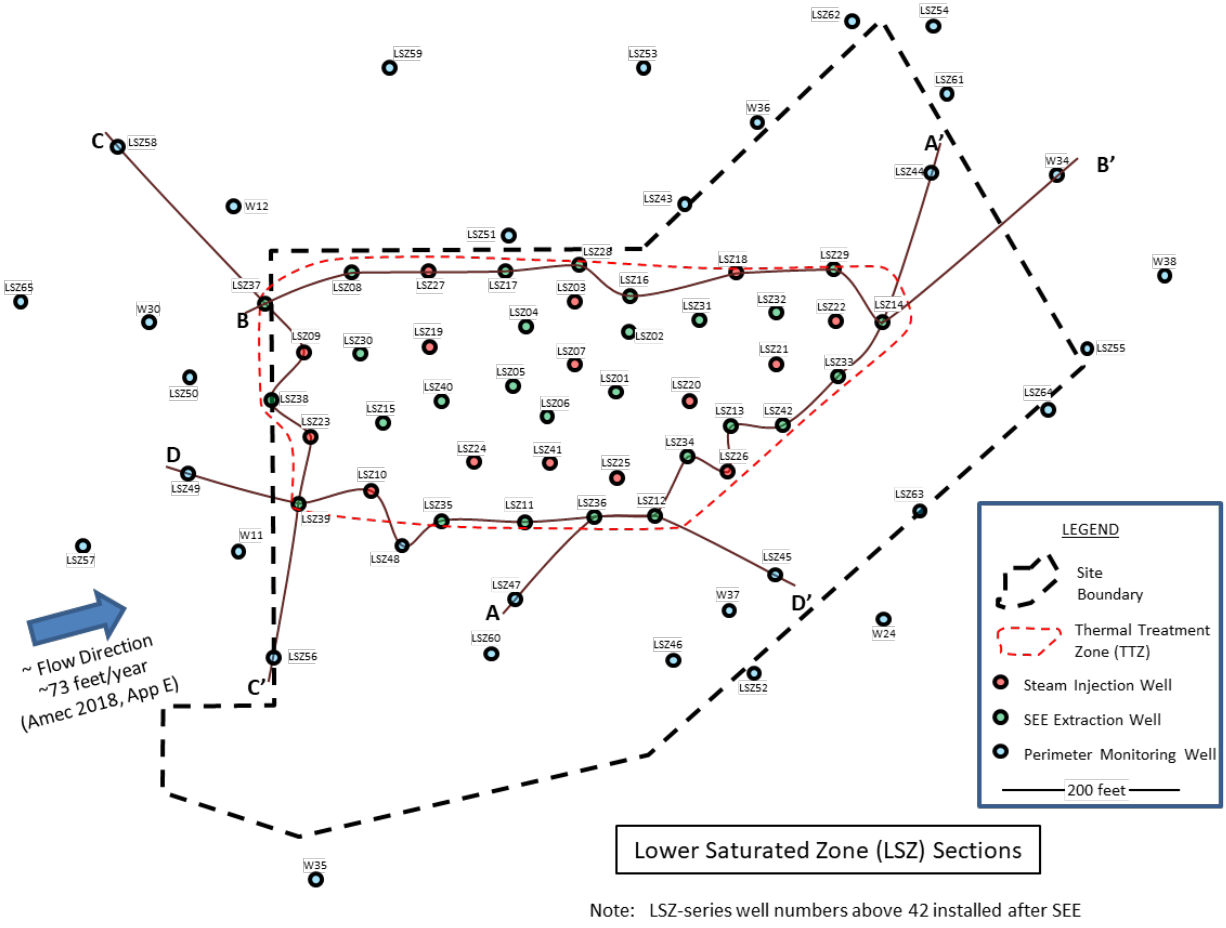

Figure E-2. Location of Boring Logs and Sections

Example geologic input for developing the conceptual source models is illustrated in **Figure E-3** for Pool 1 coinciding with section C-C'. The geologic logs included positive/negative NAPL dye detections and elevated handheld photoionization detector readings from soil cores. The geologic designations for soil are based on the reported boring logs and follow USGS standards. Similar logs were collected and evaluated in developing the models of the other NAPL treatment zones.

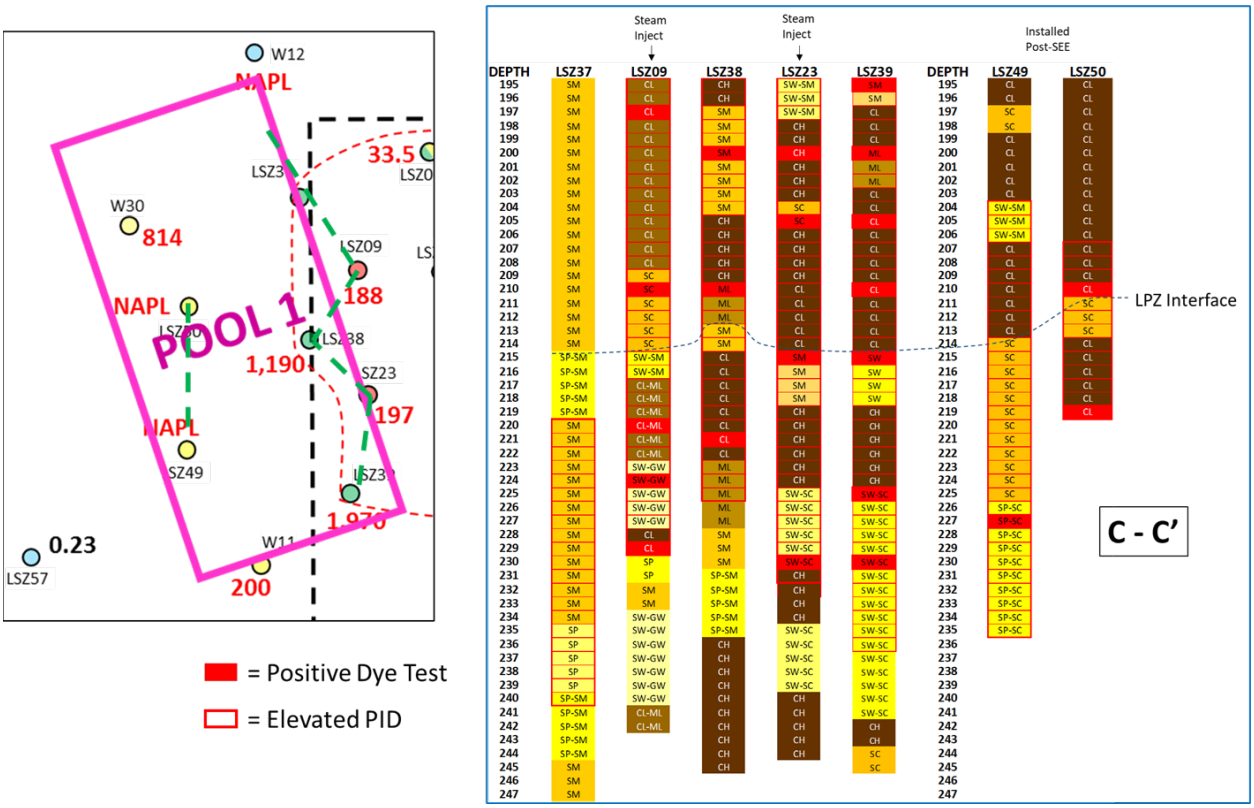

Figure E-3. Boring Logs Defining the Pool 1 Volume

A consistent geologic feature of the site is the continuous existence of a low permeability zone (LPZ), characterized as clay, providing a semi-confining layer above the LSZ. The approximate bottom of the clay is indicated by a blue dashed line in **Figure E-3**. The bottom of this clay interval is typically found from 205 to 215 feet bgs. The red blocks in the logs indicate positive tests for the presence of NAPL and red outlines indicate elevated photoionization detector readings. As indicated in the logs, discrete detections of NAPL tended to coincide with the interface of finer grained material overlying coarser material. This phenomenon is consistent with pooled NAPL floating on the water table in 1990 at a depth of approximately 232 feet bgs and rising approximately 90 feet over the past 30 years. As the water table came up, light NAPL was trapped underneath the finer grained material in discrete pools dictated by the shape of the interface.

The geologic logs and NAPL detections in **Figure E-3** suggest pools may reside on two horizons, at the low-permeability zone interface around 215 feet bgs and in the deeper sand interval around 225 feet bgs. With lateral groundwater flow, pools on these two horizons would dissolve independently. These observations resulted in the designation of the treatment area as Pool 1 to indicate the architecture is dominated by pools. Conceptual source models for the NAPL architecture in the other accumulations were developed similarly.

The conceptual model parameters defining the characteristic length scales for each target volume in the LSZ depicted in **Figure 5.5.12** of the main text and the estimated flow through the volumes are listed in **Table E-6**. The flow through the volume is based on an estimated groundwater Darcy velocity of 73 feet/year (22.3 m/yr) and the soil porosity is estimated to be 0.35 (BEM 2007).

Table E-6. Characteristic Source Zone Dimensions for ST012 LSZ Target Treatment Volumes

Parameter	Unit	Pool 1	Pool 2	Pool 3	Pool 4	Ganglia 1	Ganglia 2	Source
Length (X_s)	m	48.8	56.4	56.4	51.5	104.9	69.1	Figure 4
Width (Y_s)	m	103.6	56.9	37.5	36.8	30.1	31.6	
Height (Z_s)	m	9.14	9.14	9.14	9.14	9.14	9.14	LSZ monitor well screen length
Soil Volume (V_s)	m^3	46,203	29,288	19,315	28,895	19,967	17,290	Calculated
Volume Flow (Q)	L/d	57,769	31,684	20,895	16,798	17,617	20,485	Calculated

2.2 NAPL SATURATION AND MASS ESTIMATES

Two approaches are available for calculating the total NAPL volume in the designated treatment volumes: a uniform residual saturation throughout the volume and a pool saturation in discrete, narrow horizons.

Uniform Residual Average Saturation

An overall NAPL mass balance from the SEE operations yields a minimum, aggregate, average NAPL saturation of about 0.025 over the entire SEE treatment volume. Another estimate was developed based on representative average NAPL saturations for each hydrostratigraphic layer in the LSZ as found in Adamski et al. (2005) and Charbeneau (2007). The estimated NAPL saturations for each hydrostratigraphic layer are provided in **Table E-7**. This method yields an average NAPL saturation in the LSZ of 0.047. A reasonable estimate within this range (0.025 to 0.047) is assumed to be 0.03 for ganglia saturation. The vertical extent for this average in the LSZ is estimated to be 20 feet (6.7 m) representing the interval from 210 to 230 feet bgs (see **Figure 4.3.2** in the main text).

Table E-7. NAPL Saturation Assumptions for the LSZ from Literature

Hydrostratigraphic Unit	Layer Average Thickness (feet)	Soil Type	Total Soil Porosity	NAPL Saturation
LSZ + 1	9.3	Sand w/Fines (SM)	0.32	0.059
LSZ + 2	4.3	Silt/Clay (CL)	0.35	0.028
LSZ + 3	5.3	Sand w/Fines (SM)	0.32	0.059
LSZ + 4	5.3	Silt/Clay (CL)	0.35	0.028
LSZ Average NAPL Saturation				0.047

Pool Saturation

Estimates for fuel saturation when pooled atop a water table are available from Interstate Technology and Regulatory Council (ITRC, 2018). Examples of measured saturations in homogeneous soils and heterogeneous soils like the LSZ are illustrated in **Figure E-4** and are reproduced from ITRC (2018). Based on the NAPL saturation in **Figure E-4**, a reasonable estimate for pool saturation at ST012 is 0.30 and the vertical extent is assumed to be 1 foot (0.3 m) based on the geologic logs and NAPL detections.

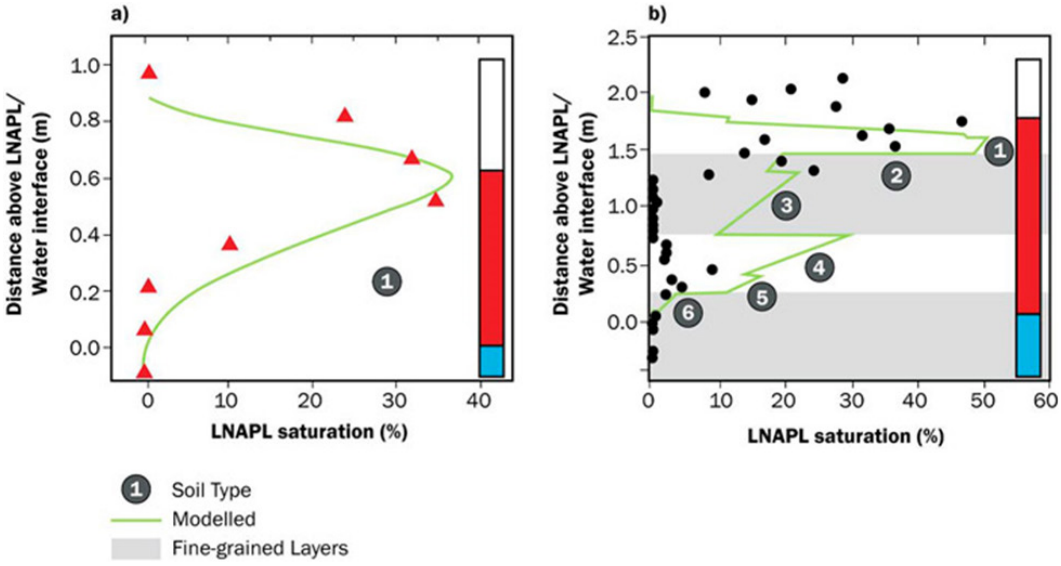

Figure E-4. Measured NAPL Saturations for Fuel Floating on the Water Table in Homogeneous and Heterogeneous Soils (reproduced from ITRC, 2018)

The resulting calculated NAPL volumes in each treatment zone are provided in **Table E-8** along with the cumulative total volume in the LSZ. The total NAPL volume for a uniform saturation of 0.03 was 1.24 million liters (327,000 gallons) and the total assuming one distinct pool interval in each volume was 554,000 liters (146,000 gallons).

Table E-8. NAPL Volume Estimates for each Site ST012 Target Treatment Volume

Parameter	Unit	Pool 1	Pool 2	Pool 3	Pool 4	Ganglia 1	Ganglia 2
Length (X_n)	m	48.8	56.4	56.4	51.5	104.9	69.1
Width (Y_n)	m	103.6	56.9	37.5	36.8	30.1	31.6
Porosity	-	0.35	0.35	0.35	0.35	0.35	0.35
Ganglia Scenario							
NAPL Saturation	-	0.03	0.03	0.03	0.03	0.03	0.03
Zone Height, Z_n	m	6.71	6.71	6.71	6.71	6.71	6.71
NAPL Volume	L	355,761	225,517	148,725	133,130	222,491	153,746
Total NAPL Volume	L	1,239,370					
Pool Scenario							
NAPL Saturation	-	0.3	0.3	0.3	0.3	0.3	0.3
Pool Height, Z_n	m	0.3	0.3	0.3	0.3	0.3	0.3
NAPL Volume	L	159,161	100,892	66,537	59,560	99,539	68,783
Total NAPL Volume	L	554,472					
Combination Scenario							
NAPL Saturation	-	0.3	0.3	0.3	0.3	0.03	0.03
NAPL Interval Height	m	0.3	0.3	0.3	0.3	6.71	6.71
NAPL Volume	L	159,161	100,892	66,537	59,560	222,491	153,746
Total NAPL Volume	L	762,387					

3.0 REMEDY INPUT PARAMETERS AND DURATION ESTIMATES

Site- and technology-specific NAPL dissolution enhancement factors were calculated with (2-39) for pump-and-treat, (2-42) to (2-44) for biological degradation, and (2-45) for ISCO, all in Section 2.2.6 of the main report. Enhanced biological degradation and ISCO also assumed recirculation cells for implementation resulting in flow enhancements additional to reactive enhancements. The flow enhancement for ISCO is somewhat tenuous theoretically based on maintenance of a defined bulk oxidant concentration and deserves further study.

The results of applying these theoretical first order reactive enhancements to MNA and enhanced biological degradation to each target treatment zone in the LSZ are provided in **Table E-9**. Small differences in values result from differing assumed pool lengths. For MNA, the estimated background degradation rate provides a small but significant enhancement to the dissolution rate of pools. As described above, little enhancement is expected for the ganglia architecture.

Table E-9. Remedy Enhancement Factors for each ST012 Target Treatment Volume

Parameter	Unit	Pool 1	Pool 2	Pool 3	Pool 4	Ganglia 1	Ganglia 2
NAPL Zone Length (X_n)	m	48.8	56.4	56.4	51.5	104.9	69.1
Monitored Natural Attenuation							
E_f	-	1	1	1	1	1	1
λ_r	1/day	0.001	0.001	0.001	0.001	0.001	0.001
Da	-	2.29	2.64	2.64	2.41	4.91	3.24
E_r	-	1.63	1.71	1.71	1.66	1	1
Enhanced Bioremediation							
E_f	-	2	2	2	2	2	2
λ_r	1/day	0.005	0.005	0.005	0.005	0.005	0.005
Da	-	11.43	13.21	13.21	12.06	24.57	16.19
E_r	-	3.13	3.34	3.34	3.20	1	1
Pump-and-Treat							
E_f	-	10	10	10	10	10	10
λ_r	1/day	0.001	0.001	0.001	0.001	0.001	0.001
E_r	-	1.63	1.71	1.71	1.66	1	1
In Situ Chemical Oxidation							
E_f	-	2	2	2	2	2	2
λ_r	1/day	0.1	0.1	0.1	0.1	0.1	0.1
E_r	-	15	15	15	15	15	15

The implementation of enhanced anaerobic degradation via the introduction of sulfate salt to promote sulfate reduction involves both flow and reactive enhancements to dissolution. The pilot study of enhanced sulfate reduction as currently operated at ST012 is not expected to enhance dissolution. Large quantities of sulfate were injected in wells and have been left to drift across the site. Given the slow groundwater velocity and the lack of mixing, the sulfate is not expected to be well dispersed. Therefore, in the modeling demonstration, a recirculation cell is assumed to be operated in each of the treatment zones. A constant, low level of flow provides a flow enhancement dissolution, estimated to be a factor of 2 over the natural gradient, while also dispersing the sulfate more uniformly across the cell and re-supplying the sulfate as it is utilized. The recirculation system is assumed to have the capability to monitor the effluent and add amendments as necessary, e.g., nutrients, to maintain the degradation rate until cleanup goals are achieved. An increase in the sustained degradation rate by a factor of five was estimated from Monod kinetics. The Damkohler number increased accordingly and the theoretical enhancement for the pool dissolution calculated with (2-42) yielded an increase of approximately 3, in line with estimates from other sites (Seagren and Becker 2015), and as indicated in **Table E-9**. If an order-of-magnitude increase in the degradation rate could be generated, the enhancement factor increased to about 4.5 for the pools, nearly tripling the dissolution rate as compared to MNA.

The implementation of pump-and-treat was very straightforward and only involved a flow enhancement factor linearly proportional to the increase in characteristic velocity through the target zone. The increased flow may accelerate the introduction of background electronic acceptors to promote increased degradation rates but this increase is offset by the decreased residence time

of water in the volume. Hence, no reactive enhancement over natural conditions is assumed as indicated in **Table E-9**. The assumed value of 10 was based on a practical limit for drawdown in extraction wells and surface treatment capacity. The total groundwater extraction rate for implementing pump-and-treat in the LSZ was on the order of 300 gallons per minute.

ISCO provides rapid reaction rates for the dissolved contaminants when the oxidant is well dispersed and constantly supplied. Therefore, in the modeling demonstration, it is assumed a partial recirculation cell is created in each of the treatment zones. The oxidant is introduced and moves through saturated soil depleting reactive carbon from the soil solids and, when this sink is satisfied, reacts effectively with dissolved contaminants. The oxidant demand of the soil solids was not included in this modeling. The partial recirculation system provides a flow enhancement to the dissolution and mixing with the oxidant. The rapid reaction rate makes this process closer to second order than first order; therefore, the reactive enhancement factor was calculated using the second order estimate of Cussler (1992) provided in Eqn (2-45). For the modeling demonstration, the selected oxidant is presumed to be persulfate with a stoichiometric molar mass ratio of about 18 with a mixture of aromatics from JP-4. A byproduct of the oxidation reaction is sulfate which can then migrate downgradient and be utilized by sulfate reducing bacteria to promote aqueous degradation in other areas of the site. A second order reactive enhancement factor for persulfate ISCO was calculated from Eqn (2-45) assuming a bulk oxidant concentration of 10,000 milligrams per liter,

$$E_{r,2} = 1 + \frac{1}{Y_{react}}\left(\frac{C_{react}}{\sum y_i C_i^*}\right)\left(\frac{D_i}{D_{react}}\right) = 1 + \frac{1}{18}\left(\frac{10,000}{40}\right)(1) \approx 15$$

The enhancement factor is based on the total equilibrium concentration of NAPL components and is therefore assumed to be identical for all compounds. This relationship is transient during the remediation process for a multi-component NAPL with changing mole fractions of soluble compounds during NAPL depletion. Theoretically, the enhancement will increase with decreasing equilibrium concentrations. Based on the NAPL component model provided in **Table E-2**, a reasonable cumulative concentration for the modeling is 40 milligrams per liter representing a mid-point concentration between the initial equilibrium concentration and the substantial depletion of benzene from the NAPL.

The input data for calculating the duration of treatment for each target volume and each technology using **Eqn (14)** of the main text are provided in the tables above. The dimensions of each target zone and the flow moving through under natural gradients are provided in **Table E-6**. The volume of NAPL and its assumed architecture for each target are described in **Table E-8**. The initial mole fraction of each of the relevant NAPL components and their transport properties are listed in **Tables E-2** to **E-4**. The calculated target-specific dissolution enhancement factors and technology-specific reactive enhancements for each remedial alternative are listed in **Table E-9**.

Calculations for the benzene discharge concentrations from Pool 1 are illustrated in **Figures E-5 to E-7** for each remedial alternative compared to MNA. The plots on the right-hand side of each figure are calculated mole fractions of benzene remaining in the pool. The mole fraction corresponding to an aqueous equilibrium concentration equal to the benzene MCL (MCL-equivalent) represents NAPL depletion. Attaining this level of depletion ensures meeting cleanup criteria on any measurement scale.

For these figures, the remedial activity was terminated at discharge MCL rather than MCL-equivalent mole fraction. The benzene discharge concentration on the left-hand side is also function of the target zone height and width. Recall, for this site demonstration a height of 30 feet (9.14 m) was assumed for all target source zones as this height corresponds to the length of monitoring well screen intervals in the LSZ.

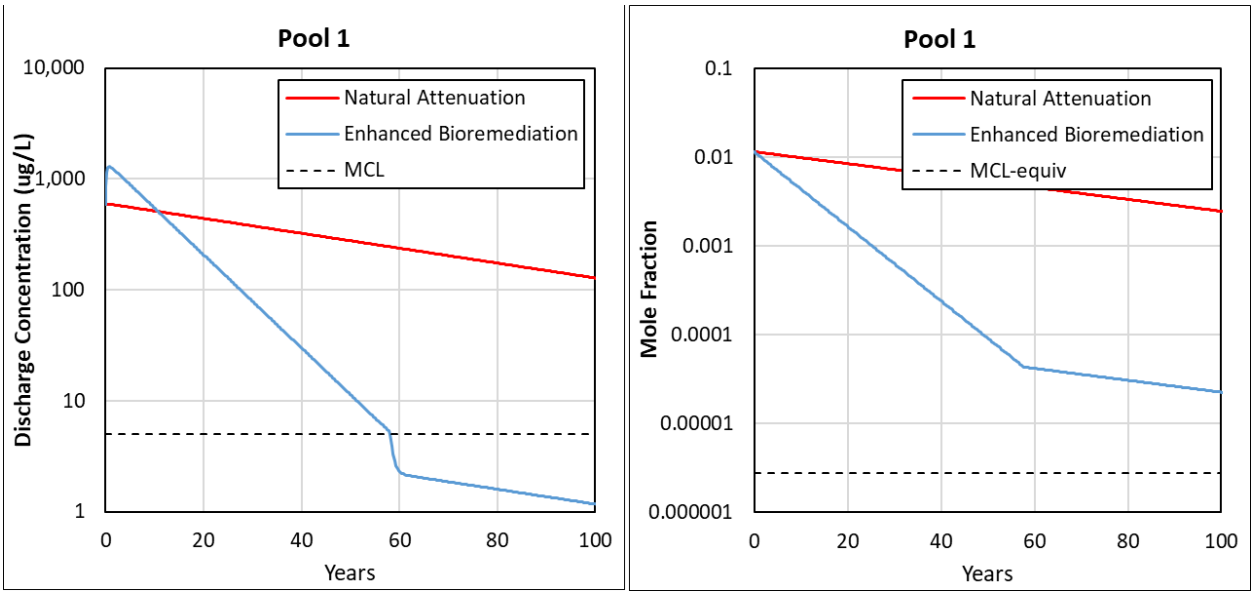

Figure E-5. Model Output for Enhanced Bioremediation with Recirculation in Pool 1

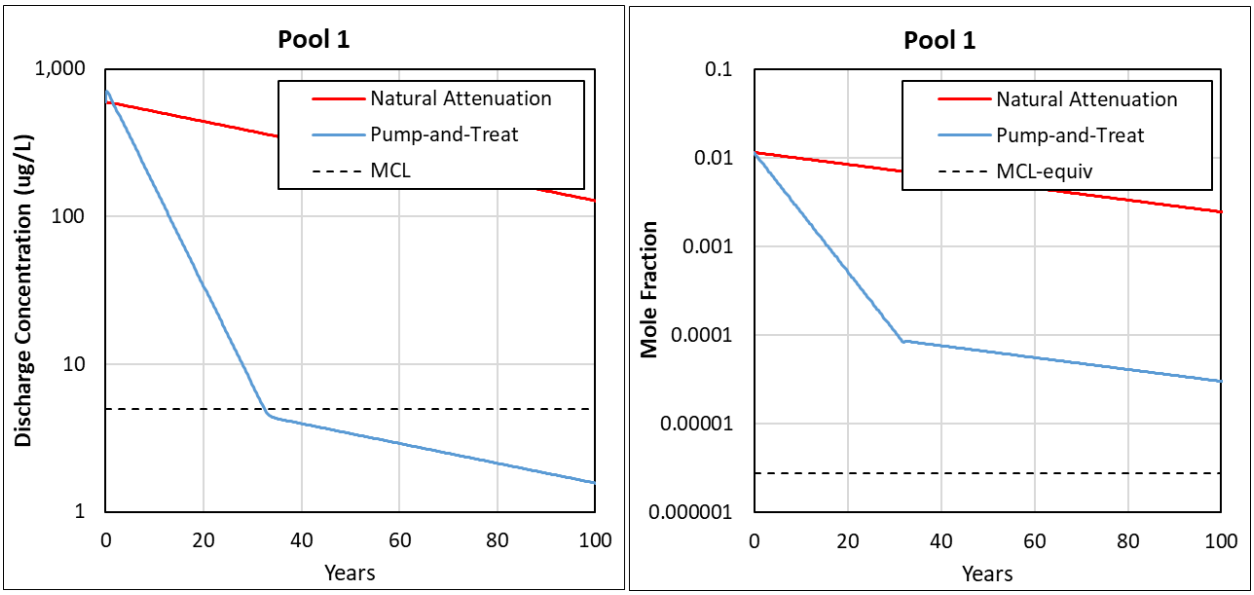

Figure E-6. Model Output for Pump-and-Treat in Pool 1

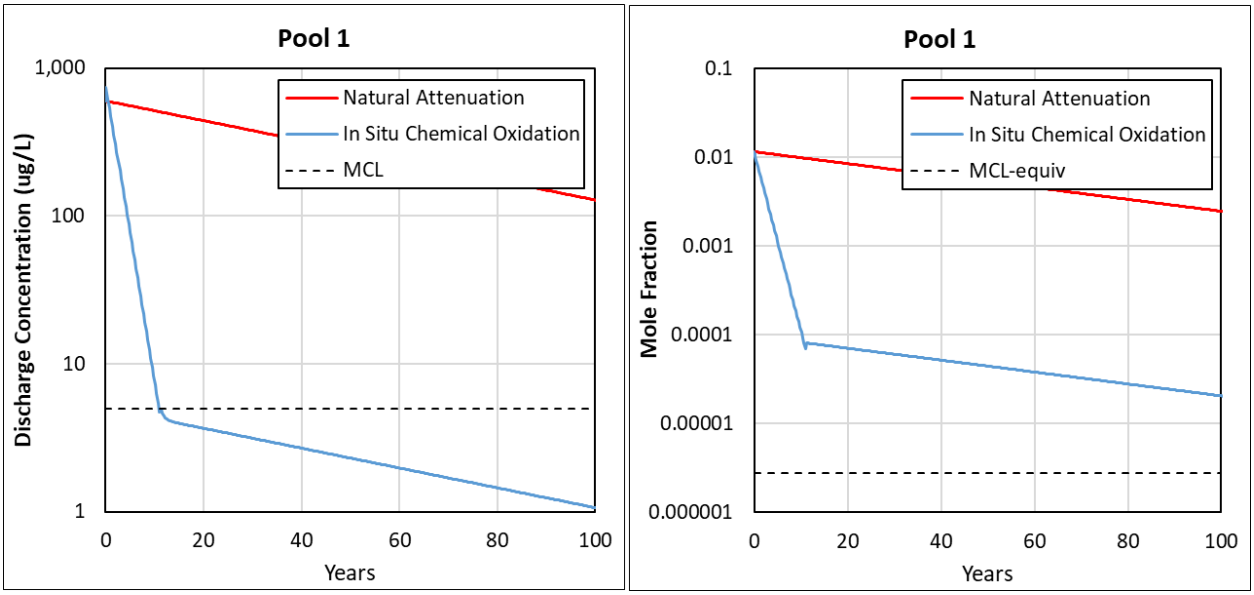

Figure E-7. Model Output for ISCO with Recirculation applied to Pool 1

The calculated durations of treatment for each technology in each target volume are summarized in **Table E-10**.

Table E-10. Summary of Operational Years for Remedy Alternatives to Attain Cleanup Goals

Parameter	Pool 1	Pool 2	Pool 3	Pool 4	Ganglia 1	Ganglia 2
Monitored Natural Attenuation						
MCL at discharge plane	310	351	322	325	122	82
MCL in source zone	540	609	556	565	136	90
Enhanced Bioremediation						
MCL at discharge plane	58	66	60	61	21	14
MCL in source zone	85	97	89	90	22	15
Pump-and-Treat						
MCL at discharge plane	32	37	34	34	13	8
MCL in source zone	54	61	55	56	13	9
In Situ Chemical Oxidation						
MCL at discharge plane	11	12	11	11	4	3
MCL in source zone	18	20	19	19	4	3

4.0 SENSITIVITY AND UNCERTAINTY ANALYSES

Predictive uncertainties associated with the calculated source zone remediation scenarios summarized in **Table E-10** were quantified on the basis of parameter uncertainty bounds (**Table E-11**).

Parameter bounds reflect plausible variability of source zone properties and remedial variables derived from site characterization data and expert knowledge, propagating uncertainties of system properties into model predictions.

Table E-11. Parameter Range for Uncertainty Analysis

Parameter	Unit	Base Value	Low Value	High Value
Height of the Source Zone	m	9.14	3	9.14
Groundwater Velocity	m/day	0.06096	0.03	0.075
Porosity	-	0.35	0.3	0.4
Retardation Coefficient	-	1.083	1	1.2
Initial Mole Fraction	-	0.012	0.004	0.015
Length of NAPL zone	m	30	15	60
Height of NAPL zone	m	0.3	0.15	0.6
NAPL Saturation	-	0.3	0.15	0.6
Tangential Dispersivity	m	0.001	0.0005	0.002
Local Flow Variation Factor	-	1	0.5	2
MNA				
Natural 1st Order Degradation Rate	1/day	0.001	0.0003	0.003
Flow Enhancement Factor	-	1	1	1
Pump-and-Treat				
1st Order Degradation Rate	1/day	0.002	0.001	0.01
Flow Enhancement Factor	-	5	2	20
Enhanced Bio				
Enhanced 1st Order Degradation Rate	1/day	0.02	0.002	0.2
Flow Enhancement Factor	-	2	2	2
ISCO				
Flow Enhancement Factor	-	2	2	2
Oxidant Bulk Concentration	mg/L	10,000	1,000	20,000

The height of the source zone corresponds to the measurement scale for the groundwater concentration. Current well screens span an interval of 30 feet (9.14 m) but calculations are also performed assuming a 10-foot (3.05 m) interval.

Darcy velocity is based on field measures of hydraulic gradient and pumping test values for hydraulic conductivity. Measured gradients across the site are small (0.004 to 0.006) and hydraulic conductivity estimates range from 18 to 40 ft/day yielding the minimum and maximum values.

Initial mole fraction high value is an average for analyses performed on fuel samples collected from the LSZ near the center of the site and preceding any significant remedial actions other than natural attenuation. The low value for the mole fraction (0.004) is the average value of five NAPL samples analyzed in 2018 and 2021 (range from 0.003 to 0.006). These mole fractions are described in SI Section 1.

Length and height estimates for the pools are based on the geologic logs, NAPL detections in the borings, and professional judgement. The large lateral spacing of boring logs (on the order of 30 meters) introduces significant uncertainty on the number, extent, and continuity of a pool within an assumed source zone. However, as demonstrated in Stewart et al. (2022), discrete pools in close proximity and residing along the same flow path act as a single pool with a length equivalent to the summed length of the discrete pools. The range for the pool length exceeds an order of magnitude. The pool height is constrained to a narrower range based on the consistency of NAPL detections in the logs at geologic interfaces and published literature on NAPL behavior (ITRC 2018). The pool height is intimately related to the NAPL saturation and therefore the initial NAPL mass within a given pool. For the sensitivity and uncertainty calculations, the initial NAPL saturation is input and the initial NAPL mass is calculated from the pool dimensions, porosity, and saturation. The range in initial saturation values is based on published literature for field observations (ITRC 2018) as described in Section 2.2.

The range of values for transverse dispersivity is based on published values for pool dissolution derived from laboratory experiments and field settings (Klenk and Grathwohl 2002, Carey et al. 2018). An additional factor was included to allow the local groundwater velocity to vary by a factor of two as a result of local heterogeneity.

The estimate for the natural degradation rate was based on previous natural attenuation modeling of the site, including background electron acceptors, groundwater velocity, published benzene utilization rates, and published estimates for anaerobic degradation rates. However, large uncertainties accompany the application of a first order degradation rate uniformly within the NAPL source zone and the assumption of a constant value over order-of-magnitude changes in the dissolved concentrations. Hence, the range of degradation rates spans two orders of magnitude.

The assumptions and calculations for the remaining remedy-specific parameters are described in Section 4. The ISCO enhancement factor varied almost linearly with the assumed bulk oxidant concentration.

The remaining model input parameters had little impact on results or were measured properties. These fixed parameters are listed in **Table E-12**.

Table E-12. Fixed Input Parameters for Uncertainty Analysis

Source Zone Parameters		
Pool Width, Y_n	m	10
Source Zone Width, W_s	m	10 (= Y_n)
Source Zone Length, L_s	m	= X_n
Porosity, ϕ	-	0.35
Benzene Properties		
Molecular Weight, MW_b	g/mol	78.114
Aqueous Solubility, C_{sat}	m	1,800
Aqueous Diffusion Coefficient, D_b	m^2/day	0.000077
Drinking Water Standard, C_{MCL}	mg/L	0.005
JP4 Properties		
Density, ρ_{JP4}	kg/L	0.7787
Molecular Weight, MW_{JP4}	-	108.77
Relative Permeability Parameters		
Irreducible Water Saturation, S_{irr}	-	0.15
Relative Permeability Exponent, n_r	-	3

Predictions of interest correspond to model outputs including time of remediation (TOR, time to NAPL depletion in years), time to reach the maximum contaminant levels (MCL, in years), and the amount of NAPL mass (Mass, in kg) entrapped in the source zone. The contribution of input parameters to predictive uncertainties was quantified with first-order second-moment (FOSM) analysis facilitated by PEST software and the linear analysis utilities GENLINPRED and PREDUNC (Doherty, 2015; Watermark Numerical Computing, 2018). Predictive uncertainties were quantified using the prior-based Monte Carlo functionality of the iterative ensemble smoother PESTPP-iES (White, 2018; White et al., 2020), with 20 randomized model realizations per adjustable parameter. While FOSM analysis relies on the model linearity assumption to investigate causality of predictive uncertainties through Jacobian sensitivity matrices (Doherty, 2015), model realizations (ensembles) drawn from parameter bounds with PESTPP-iES allowed to approximate the nonlinear distribution of model predictions.

Figure E-8 shows the contribution of model parameters to the uncertainty variance of TOR, MCL, and NAPL Mass for different remedial scenarios, expressed as percentages of the standard deviations (σ) indicated in **Table E-13**. In all remedial scenarios, all predictive uncertainties were influenced by the uncertainty of saturation (S^n), length (X_n), and height (Z_n) of the NAPL zone. While the dissolution enhancement factor (E_f), enhanced reaction rate (λ_r), and oxidant concentration (C_{ox}) acted as primary uncertainty drivers of TOR and MCL in the P&T, EBR, and ISCO scenarios, respectively, the local flow velocity parameter, E_k, also impacted the uncertainty of TOR and MCL in all remedial cases.

Table E-13. Mean (μ) and Standard deviation (σ) Values of TOR, MCL, and NAPL Mass of Remedial Alternatives.

	MNA		P&T		EBR		ISCO	
Prediction	base	σ	base	σ	base	σ	base	σ
TOR (yr)	328.67	231.14	67.34	60.80	125.39	89.66	11.50	11.45
MCL (yr)	191.10	126.89	39.15	34.17	72.91	49.30	6.68	6.48
Mass (kg)	22076	13349	22076	13349	22076	13349	22076	13349

Figure E-9 depicts the distribution of TOR and MCL timeframes approximated with randomized model realizations. Predictive uncertainty distributions, including NAPL Mass (not shown), are positively skewed with 95% confidence intervals encompassing the base model output (**Table E-13**) values calculated with the base-case parameter sets (**Table E-11**). The non-overlapping confidence limits, depicted as boxplot notches in **Figure E-9**, indicate significantly different median values of TOR and MCL across remedial alternatives.

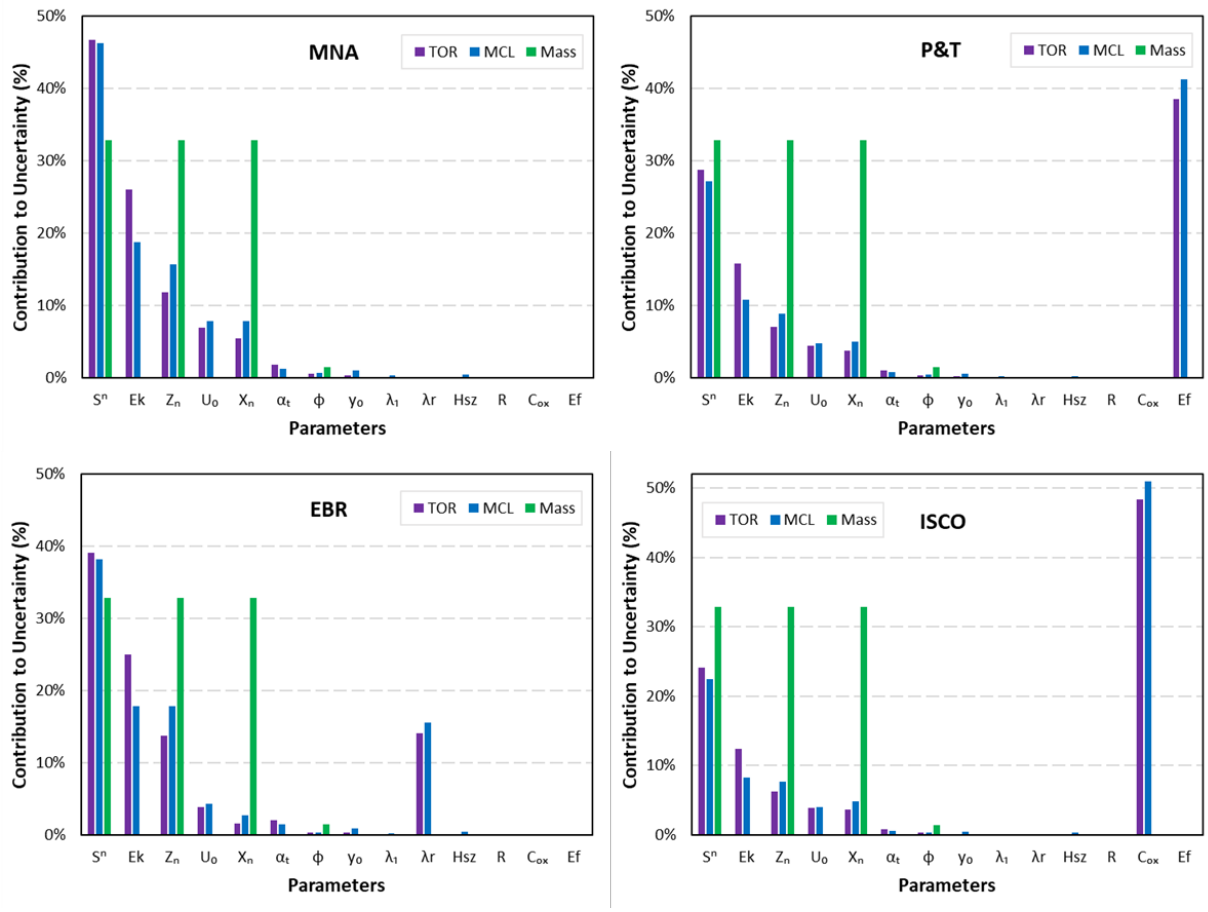

Figure E-8. Contribution of Input Parameters to Predictive Model Uncertainties for Remedial Scenarios.

Contributions are expressed in percentages of total uncertainty variances, corresponding to σ values indicated in Table S-11.

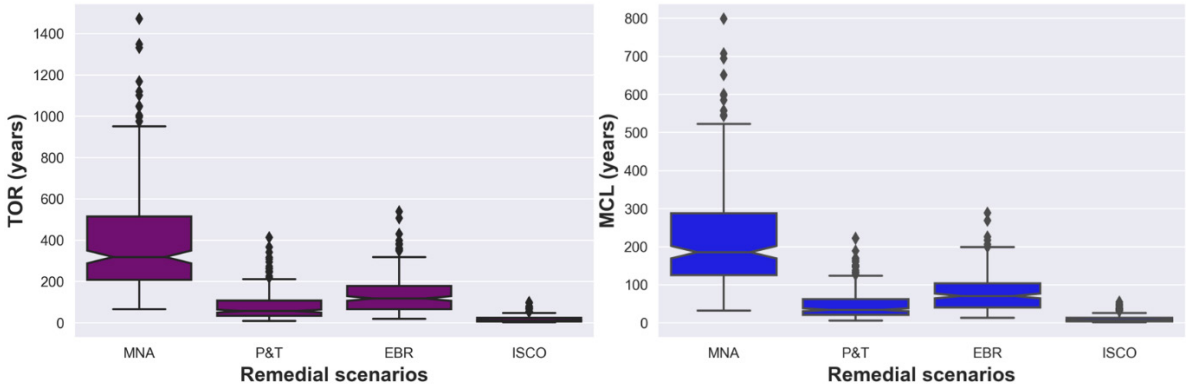

Figure E-9. Boxplots of Nonlinear Uncertainty Distribution of TOR and MCL for All Remedial Alternatives.

Notches indicate 95% confidence intervals around median values.

Uncertainty quantification results reflect source zone conceptual assumptions and uncertainty of remedial variables. The contribution of NAPL dimensions and S^n to all predictive uncertainties suggest value in additional site characterization efforts, including direct (e.g., exploratory boreholes and MIP) and indirect (e.g., DPT groundwater sampling) NAPL delineation technologies. Site investigation including hydraulic profiling tool (HPT) and cone penetrometer testing (CPT) (Horst et al., 2018) could reduce MCL and TOR predictive uncertainties through direct constraining of the E_k parameter (**Figure E-8**), representing soil permeability contrasts. Furthermore, previous studies have indicated the worth of consistent monitoring profiles of mass discharge for significantly reducing the uncertainty of NAPL mass, and thereby, TOR and MCL uncertainties. In this case, a monitoring dataset indicating decreasing mass discharge concentrations would prove useful for indirect constraining of NAPL mass entrapped as pool(s). Overall, the ISCO scenario resulted in the lowest remedial timeframes for a range of C_{ox} values (**Table E-13**), contrasting with the MNA scenario, where uncertainty limits of remedial timeframes extended close to 1,000 years (**Figure E-9**).

5.0 REFERENCES

Adamski, M., V. Kremesec, R. Kolhatkar, C. Pearson, and B. Rowan, 2005, "LNAPL in Fine-Grained Soils: Conceptualization of Saturation, Distribution, Recovery, and Their Modeling," Ground Water Monitoring & Remediation, Vol. 25, No. 1, pp. 100-112.

Amec Foster Wheeler. 2018. Final Pilot Study Work Plan for Operable Unit 2, Revised Groundwater Remedy, Site ST012, Former Williams Air Force Base, Mesa, Arizona. April.

BEM Systems, Inc. 2007. Final ST012 Phase 1 Thermally Enhanced Extraction (TEE) Pilot Test Work Plan. Former Williams Air Force Base, Mesa, Arizona. United States Air Force. November.

BEM Systems, Inc. 2011. Final Phase 1 Thermal Enhanced Extraction (TEE) Pilot Test Performance Evaluation Report. Former Williams Air Force Base, Mesa, Arizona. United States Air Force. March.

Carey, G.R., E.A. McBean and S. Feenstra. 2018. Estimating transverse dispersivity based on hydraulic conductivity. Environmental Technology & Innovation, 10: 36-45.

Charbeneau, Randall, 2007. LNAPL Distribution and Recovery Model (LDRM) Volume 1: Distribution and Recovery of Petroleum Hydrocarbon Liquids in Porous Media. API Publication 4760, January.

Christ, J.A., and L.M. Abriola. 2007. Modeling metabolic reductive dechlorination in dense non-aqueous phase liquid source zones. Advances in Water Resources 30 no. 6–7: 1547–1561. http://dx.doi.org/10.1016/j.advwatres.2006.05.024

Cussler, E.L. 1997 . Diffusion: Mass Transfer in Fluid Systems, 2nd edition. Cambridge University Press.

Demiray, Z., N.H. Akyol and N.K. Copty. 2021. Experimental Assessment and Modeling of Enhanced Solubilization of Pool-dominated Tetrachloroethene Source Zone in Heterogeneous Porous Media, Water Air Soil Pollut, 232:516. https://doi.org/10.1007/s11270-021-05454-z

Doherty, J. 2015. Calibration and Uncertainty Analysis for Complex Environmental Models. Brisbane, Australia: Watermark Numerical Computing.

Horst, J., Welty, N., Stuetzle, R., Wenzel, R., & Germain, R. (2018). Fluorescent dyes: A new weapon for conquering DNAPL characterization. Groundwater Monitoring & Remediation, 38(1), 19-25. doi:10.1111/gwmr.12261

IT. 1992 , Final Remedial Investigation Report, Liquid Fuels Storage Area - Operable Unit 2, Williams Air Force Base, Arizona, prepared for the USAF Air Training Command, Randolph Air Force Base, Texas. January.

IT. 1995. Final Feasibility Study Report, Operable Unit 3, Williams Air Force Base, Arizona, prepared for Air Force Base Conversion Agency, Williams Air Force Base, Arizona. May.

Interstate Technology Regulatory Council (ITRC). 2018. LNAPL-3: LNAPL Site Management: LCSM Evolution, Decision Process, and Remedial Technologies. Accessed 9/27/22: LNAPL Update (itrcweb.org).

Klenk, I.D., and P. Grathwohl. 2002. Transverse vertical dispersion in groundwater and the capillary fringe. Journal of Contaminant Hydrology, 58: 111-128.

McCray, J.E., T.B. Boving and M.L. Brusseau. 2000. Cyclodextrin-Enhanced Solubilization of Organic Contaminants with Implications for Aquifer Remediation. Ground Water Monitoring and Remediation, 20(1): 94-103.

Molz, F. 2015. Advection, Dispersion, and Confusion. Groundwater, 53(3): 348-353.

Phelan, T.J., L.M. Abriola, J.L. Gibson, K.M. Smits, and J.A. Christ. 2015. Development and application of a screening model for evaluating bioenhanced dissolution in DNAPL source zones. Journal of Contaminant Hydrology, 183: 1-15.

Saba, T., T. Illangasekare and J. Ewing. 2001. Surfactant enhanced dissolution entrapped NAPLs in multidimensional flow fields. J Contam Hydrol 51(1–2):63–82.

Seagren, E.A., B.E. Rittmann, and A.J. Valocchi. 1994. Quantitative evaluation of the enhancement of NAPL-pool dissolution by flushing and biodegradation. Environmental Science and Technology 28:833–839.

Seagren and Becker. 2015. Predictions of bioenhancement of nonaqueous phase liquid ganglia dissolution using first- and zero-order biokinetic models, Journal of Contaminant Hydrology, 182: 210–220.

Suchomel E.J., C.A. Ramsburg and K.D. Pennell. 2007. Evaluation of trichloroethene recovery processes in heterogeneous aquifer cells flushed with biodegradable surfactants, Journal of Contaminant Hydrology, 94: 195–214.

Wang, X. and M.L. Brusseau. 1993. Solubilization of some low-polarity organic compounds by hydroxypropyl-β-cyclodextrin. Environmental Science and Technology, 27(12): 2821-2825.

Watermark Numerical Computing. 2018. Model-Independent Parameter Estimation. User Manual Part II: PEST Utility Suport Software. Retrieved from https://pesthomepage.org/documentation

White, J.T. 2018. A model-independent iterative ensemble smoother for efficient history-matching and uncertainty quantification in very high dimensions. Environmental Modelling & Software 109:191–201. https://doi.org/10.1016/j.envsoft.2018.06.009

White, J., R. Hunt, M. Fienen, and J. Doherty. 2020. Approaches to Highly Parameterized Inversion: PEST++ Version 5, a Software Suite for Parameter Estimation, Uncertainty Analysis, Management Optimization and Sensitivity Analysis. Reston, Virginia: U.S. Geological Survey. doi:10.3133/tm7C26

APPENDIX F LIST OF TECHNOLOGY TRANSFER ACTIVITIES

SERDP & ESTCP Webinar Series

"Upscaled Modeling Tools for Residual DNAPL Remediation" took place on January 26, 2023

Journal Publications

Stewart, L. D., Chambon, J. C., Widdowson, M. A., & Kavanaugh, M. C. 2022. Upscaled modeling of complex DNAPL dissolution. *Journal of Contaminant Hydrology, 244*. https://doi.org/10.1016/j.jconhyd.2021.103920

Prieto-Estrada, A.E., M.A. Widdowson and L.D. Stewart. 2022. Quantifying DNAPL source zone longevity with upscaled modeling: practical insights from flow-cell experiments and uncertainty analyses. Submitted to *Water Resources Research* in November 2022.

Stewart, L.D., J. Nyman, A.E. Prieto-Estrada, J.C. Chambon, M.A. Widdowson and M.C. Kavanaugh. 2022. Modeling of Complex, Multi-component NAPL Remediation for Decision Support. Invited manuscript for a special issue of *Ground Water Monitoring & Remediation* on complex sites submitted in December 2022.

Stewart, L. D., J.C. Chambon and J. Rossabi. 2022. Upscaled modeling of complex DNAPL remediation. to be submitted to *Journal of Contaminant Hydrology,* January 2023.

Prieto-Estrada, A.E., M.A. Widdowson and L.D. Stewart. 2022. Numerical modeling and data-worth analysis for characterizing the architecture and dissolution rates of a multicomponent DNAPL source. Submitted to *Water Resources Research* in December 2022.

Project Website and Beta Models

www.SCARPEmodel.com

- SCARPEs_0.1: Single component model of NAPL dissolution and remediation with mixed architecture (python executable)
- SCARPEm_0.1: Multicomponent model of NAPL dissolution and remediation applied to a single NAPL mass (Excel spreadsheet)
- SCARPE User Manual 0.1
- 2021 Workshop Video

Workshops

RemTEC Virtual Workshop March 11, 2021

- "Volume-Averaged Modeling of Complex NAPL Dissolution and Remediation" 45-minute video of the workshop is available at www.SCARPEmodel.com

RemTEC In-Person Workshop October 5, 2022

- "Volume-Averaged Modeling of Complex NAPL Dissolution and Remediation" Models demonstrated at the workshop are available at www.SCARPEmodel.com

Conference Presentations

Battelle 12th International Conference on Remediation of Chlorinated and Recalcitrant Compounds May 22-26, 2022 Palm Springs, CA

- Platform Presentation: "Remediation Modeling of Complex NAPL Sites using Technology-Specific Dissolution Rates"
- Poster Presentation: "Mass Discharge and Cleanup Timeframe Estimates at Complex DNAPL Sites Using Upscaled Modeling of DNAPL Dissolution"
- Poster Presentation: "Modeling Approaches to Support Remedial Decisions at NAPL Sites"
- Poster Presentation: "Evaluating Field Measurements for Characterizing Properties and Predicting Dissolution Rates of DNAPL Source Zones"

RemTEC & Emerging Contaminants Summit, October 4-6, 2022 Westminster, CO

- Poster Presentation: "Quantifying DNAPL source zone longevity with upscaled modeling: practical insights from flow-cell experiments and uncertainty analyses"

SERDP & ESTCP Annual Symposium

- 2019 Poster Presentation
- 2020 Poster Presentation
- 2021 Poster Presentation
- 2022 Poster Presentation